

MIT/WHOI 97-28

**Massachusetts Institute of Technology
Woods Hole Oceanographic Institution**



**Joint Program
in Oceanography/
Applied Ocean Science
and Engineering**



DOCTORAL DISSERTATION

*The Role of Biological Production in Pleistocene
Atmospheric Carbon Dioxide Variations and the
Nitrogen Isotope Dynamics of the Southern Ocean*

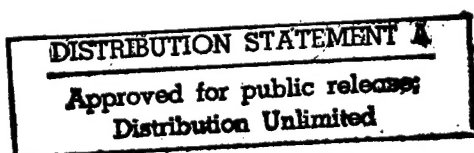
by

Daniel M. Sigman

September 1997

DTIC COLLECTED INFORMATION

19980505 055



MIT/WHOI

97-28

**The Role of Biological Production in Pleistocene Atmospheric Carbon Dioxide
Variations and the Nitrogen Isotope Dynamics of the Southern Ocean**

by

Daniel M. Sigman

Massachusetts Institute of Technology
Cambridge, Massachusetts 02139

and

Woods Hole Oceanographic Institution
Woods Hole, Massachusetts 02543

September 1997

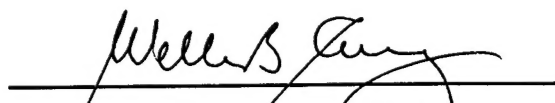
DOCTORAL DISSERTATION

Funding was provided by National Science Foundation Grant OCE-9201286, National Science Foundation Graduate Fellowship Program, and the JOI/USSAC Ocean Drilling Graduate Fellowship Program.

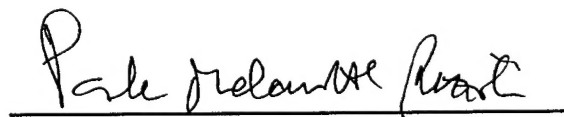
Reproduction in whole or in part is permitted for any purpose of the United States Government. This thesis should be cited as: Daniel M. Sigman, 1997. The Role of Biological Production in Pleistocene Atmospheric Carbon Dioxide Variations and the Nitrogen Isotope Dynamics of the Southern Ocean. Ph.D. Thesis. MIT/WHOI, 97-28.

Approved for publication; distribution unlimited.

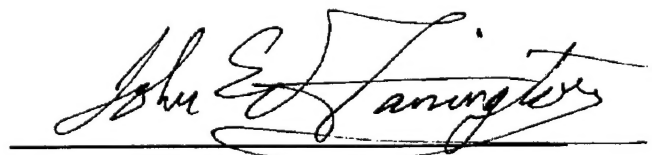
Approved for Distribution:



William B. Curry, Chair
Department of Geology and Geophysics



Paola Malanotte-Rizzoli
MIT Director of Joint Program



John W. Farrington
WHOI Dean of Graduate Studies

The Role of Biological Production in
Pleistocene Atmospheric Carbon Dioxide Variations
and the Nitrogen Isotope Dynamics of the Southern Ocean

by
Daniel M. Sigman

B.S., Stanford University
(1991)

Submitted in partial fulfillment of the requirements for the degree of

Doctor of Philosophy

at the

Massachusetts Institute of Technology

and the

Woods Hole Oceanographic Institution

September 1997

© Daniel M. Sigman

The author hereby grants to MIT and to WHOI permission to reproduce
and to distribute copies of this thesis document in whole or in part.

Signature of Author.....*Daniel M. Sigman*.....
Joint Program in Marine Geology and Geophysics
Massachusetts Institute of Technology
Woods Hole Oceanographic Institution

Certified by.....*Daniel C. McCorkle*.....
Daniel C. McCorkle
Thesis Supervisor

Accepted by.....*Deborah K. Smith*.....
Deborah K. Smith
Chair, Joint Committee for Marine Geology and Geophysics
Massachusetts Institute of Technology
Woods Hole Oceanographic Institution

The Role of Biological Production in
Pleistocene Atmospheric Carbon Dioxide Variations
and
the Nitrogen Isotope Dynamics of the Southern Ocean

by

Daniel M. Sigman

Submitted to the Department of Earth, Atmospheric, and Planetary Sciences and the Woods Hole Oceanographic Institution Joint Program in Oceanography/Applied Ocean Science and Engineering on September 5, 1997 in partial fulfillment of the requirements for the Degree of Doctor of Philosophy

ABSTRACT

This dissertation contributes to the search for a cause of glacial/interglacial variations in atmospheric carbon dioxide. The hypotheses addressed involve changes in low and high-latitude biological export production.

A modelling exercise demonstrates that the paleoceanographic record of calcite preservation places constraints on hypothesized changes in low latitude biological production. The model results indicate that large, production-driven changes in the depth of the calcite saturation horizon during the last ice age would have caused a similar deepening of the calcite lysocline, even when the effect of sediment respiration-driven dissolution is considered. Such a large glacial lysocline deepening is not evident on an ocean-average basis. The results indicate very few mechanisms by which low latitude production could have driven Pleistocene carbon dioxide variations, generally arguing against a low latitude cause for these variations.

The use of N isotopes as a paleoceanographic proxy for nitrate utilization in Southern Ocean was investigated. In order to examine the generation of the link between nitrate utilization and N isotopes in the surface ocean, the isotopic composition of nitrate was studied. The first step in this work was the development of a new method to measure the isotopic composition of nitrate which is amenable to the generation of large, precise data sets. Results from the Southern Ocean demonstrate that the Antarctic and Subantarctic represent distinct regimes of N isotope dynamics. The findings support the use of N isotopes as a proxy for nitrate utilization in the Antarctic.

A study of diatom microfossil-bound N in sediments suggests that this N is native to the diatoms, that it is invulnerable to early diagenesis, and that its isotopic composition varies with that of the sinking flux. Paleoceanographic records of diatom-bound N isotopic composition corroborate the conclusion, previously based on bulk sediment isotopic data,

that nitrate utilization was elevated in the glacial Antarctic, representing a major cause of lower glacial atmospheric carbon dioxide levels.

Thesis Supervisor: Daniel C. McCorkle

Title: Associate Scientist with Tenure, Woods Hole Oceanographic Institution

Acknowledgements

Each of the members of my committee has played an important role in my thesis work. I have too many good things to say about Dan McCorkle and the effort he put into his role as my advisor. Much of this thesis is the brain-child of Mark Altabet and Roger Francois. I thank them both for allowing me to take part in their scientific journey and for their instruction and insight along the way. Lloyd Keigwin has been a tremendous source of ideas and enthusiasm. Since Dan gave me Ed Boyle's "nutrient deepening" papers to read when I was a summer student fellow, Ed has been an inspiration. I have relied on his ideas and advice throughout my time in the Joint Program. Jean Whelan selflessly shared both her expertise and her time over the home-stretch of my thesis work (Thanks also to Lorraine Eglinton in this regard).

The caliber of the technicians and research specialists at WHOI and their willingness to help make it easy for Joint Program students to initiate research. As I have been helped by virtually everyone on the Quissett campus, I will single out only Eben Franks and Jim Broda, who have been generous with their time and wisdom over the years.

Thanks to Bill Martin for giving me a laboratory home and for his help on a variety of subjects. Thanks to Scott Lehman for an exciting collaboration from which I continue to learn. Thanks to Michael Bender for his encouragement and for his help in framing a plan of future research. Thanks also to Jess Adkins, who has shared the scientific teething process with me. Now we need braces.

Having spent the night trying to paginate my thesis, I find myself unable to find the right words to thank my family and friends. I am grateful for what you have given, taken, and shared. I owe my deepest thanks to Ellyn Ito. Her love of life and her boundless curiosity inspire me.

This research was supported by the National Science Foundation Graduate Fellowship Program, the JOI/USSAC Ocean Drilling Graduate Fellowship Program, and by NSF grant OCE-9201286 to D.C. McCorkle.

Biography

Daniel Sigman was born in Los Angeles on June 5, 1969, son of Marian and David Sigman and brother of Hilary Sigman. He attended Stanford University from 1987 to 1991, majoring in Geology. After spending the summer of 1990 at WHOI as a Summer Student Fellow, he entered the MIT/WHOI Joint Program in 1991. More to come...

Table of Contents

Abstract	3
Acknowledgements	5
Table of Contents	6
Chapter 1. Introduction	11
The Role of Low Latitude Biological Production	12
The Role of the Southern Ocean	14
The Nitrogen Isotopic Composition of Nitrate and Its Link to Nitrate Utilization	15
The Isotopic Composition of Diatom Microfossil-Bound Nitrogen	17
Toward a Consistent Picture of the Glacial Southern Ocean	18
References	20
Chapter 2. The Calcite Lysocline as a Constraint on Glacial/Interglacial Low Latitude Production Changes	23
Abstract	24
Introduction	25
Model Description	29
Circulation	29
Export Production/Regeneration Cycle	30
Models of CaCO_3 Input/Output Dynamics	31
Results	37
Part 1: Comparison of Closed, Compensated, and Open System Responses Changes in Low Latitude Production	37
Model Experiment #1: Increasing the Oceanic Phosphate Reservoir by 30%	37
Model Experiment #2: Halving the Warm Surface $\text{CaCO}_3/\text{C}_{\text{org}}$ Rain Ratio	41
Model Experiment #3: Deepening the C_{org} Regeneration Profile	43

Sensitivity of the Model Response to Production/Regeneration Parameters	45
Part 2: the Effect of Chemical Erosion	47
Part 3: the Effect of Sedimentary Respiration-Driven Dissolution	50
Part 4: Coupled Changes in the Quantity and Characteristics of Low Latitude Production	56
Conclusions	58
Appendix 1: Comparison of Standard Case with CYCLOPS and GEOSECS	60
Appendix 2: Parameterizing Calcite Dissolution in the Mixed Layer Sediment Model	63
Acknowledgements	66
References	67
Tables	72
Figures	78

Chapter 3. Natural Abundance-Level Measurement of the Nitrogen Isotopic Composition of Oceanic Nitrate: an Adaptation of the Ammonia Diffusion Method	127
Abstract	128
Introduction	129
Protocol	131
Explanation of Protocol	134
Nitrate Reduction by Devarda's Alloy	136
Ammonia Diffusion	139
Blanks	144
Results	148
Conclusions	150
Acknowledgements	151
References	152
Tables	154
Figures	160

Chapter 4. The Nitrogen Isotopic Composition of Nitrate in the Southern Ocean	187
Abstract	188
Introduction	189
Sample Sets and Methods	193
$\delta^{15}\text{NO}_3$ measurements	194
Nitrate concentration measurements	196
Results	198
Interpretation and Discussion	201
Antarctic Zone	203
Deep Water Variations	203
Upper Water Column Variations	204
Subantarctic Zone	211
Deep Water Variations	211
Upper Water Column Variations	213
Conclusions	218
Acknowledgements	219
References	220
Tables	225
Figures	228
Data Tables	282
 Chapter 5. The Isotopic Composition of Diatom-Bound Organic Nitrogen in Southern Ocean Sediments	 301
Abstract	302
Introduction	303
Materials and Methods	306
Protocol for the Isolation of Diatom-Bound N	307
Isotopic and N Content Analyses	310
Results	312
1. Characteristics of the diatom microfossil-bound N fraction	312
2. Depth variations in the $\delta^{15}\text{N}$ of diatom-bound and bulk sedimentary N	318

3. Latitudinal variations in the $\delta^{15}\text{N}$ of diatom-bound and bulk sedimentary N	321
4. Paleoceanographic records of the $\delta^{15}\text{N}$ of diatom-bound and bulk sedimentary N	325
Conclusions	330
Acknowledgements	331
References	332
Tables	337
Figures	342
Data Tables	362
 Appendix The Isotopic Homogeneity of Deep Ocean Nitrate: a Comparison with Dissolved Inorganic Carbon	 371
References	375
Tables	377
Figures	378

Chapter 1:

Thesis Introduction

This thesis describes four separate research efforts. Chapter 2, "The calcite lysocline as a constraint on glacial/interglacial low latitude production changes", describes the use of an ocean carbon cycle model to constrain hypotheses regarding the cause of glacial/interglacial atmospheric CO₂ variations, focusing on the calcium carbonate cycle. Chapter 3, "Natural-abundance level measurement of the Nitrogen isotopic composition of oceanic nitrate: an adaptation of the ammonia diffusion method," describes the development of a new method for the extraction and isotopic analysis of oceanic nitrate. Chapter 4, "The Nitrogen isotopic composition of nitrate in the Southern Ocean", describes the application of this new method to investigate the Nitrogen isotopic composition of nitrate in that region. Chapter 5, "The isotopic composition of diatom microfossil-bound organic Nitrogen in Southern Ocean sediments", describes the use of this sedimentary N fraction to overcome the problems associated with diagenesis in paleoceanographic N isotope studies of the Southern Ocean.

These chapters are unified by the goal of providing an explanation for glacial/interglacial variations in atmospheric CO₂. Measurements of the gas composition in air bubbles from ice cores have shown that the partial pressure of atmospheric CO₂ was ~80 ppm lower at the peak of the last ice age, a change of almost one-third of its preindustrial concentration (Berner et al., 1979; Delmas et al., 1980; Neftel et al., 1982). The link between atmospheric CO₂ and glacial cycles is also observed in previous interglacials and glacial periods (Barnola et al., 1987). Since CO₂ is an important greenhouse gas, the glacial/interglacial variation of atmospheric CO₂ is a key example of the interaction of geochemical cycles with climate. Nevertheless, the cause of the CO₂ variations is not understood.

Broecker (1981, 1982) first pointed out that atmospheric CO₂ changes must have had their origin in the ocean, since most of the inorganic carbon in the hydrosphere/biosphere system resides in the ocean, and surface ocean pCO₂ controls atmospheric CO₂ on the time scale of ≥ 1 ky. Broecker noted that glacial/interglacial changes in surface ocean temperature are too small to explain the amplitude of atmospheric CO₂ variations. For this reason, he hypothesized an increase in the strength of the “biological pump”, the sequestration of dissolved inorganic carbon in the deep sea by the biogenic rain of particles out of the surface ocean. This original suggestion has led to a number of proposed mechanisms by which biological production could drive glacial/interglacial atmospheric CO₂ variations.

The Role of Low Latitude Biological Production

One set of hypotheses calls upon changes in biological production in the low and mid-latitude regions, where the major nutrients, nitrate and phosphate, ultimately limit the extraction of CO₂ by biological production. Broecker (1981) and McElroy (1983) described possible mechanisms by which the major nutrient reservoirs might increase during glacial times, which would allow enhanced low latitude biological production to lower atmospheric CO₂. However, it was recognized that this basic mechanism would require large changes in nutrient reservoirs to produce the entire observed amplitude of CO₂ change (Boyle, 1988a; Boyle, 1988b; Broecker, 1982). Boyle (1988a) and Broecker and Peng (1987) recognized that the CO₂ effects of some changes in the low latitude biological production would be intensified by the cycling of CaCO₃. Archer and Maier-Reimer (1994) showed that the role of organic matter decomposition in seafloor calcite dissolution greatly increases the capacity of certain low latitude biological production changes to lower atmospheric CO₂. The mechanism proposed by Archer and Maier-Reimer is supported by paleo-pH studies based on Boron isotopes in foraminifera (Sanyal et al., 1995).

As I discuss in Chapter 2, oceanic biological production affects atmospheric CO_2 via several different aspects of inorganic carbon chemistry: (1) the redistribution of dissolved inorganic carbon and alkalinity within the ocean, (2) the transient response of deep sea calcite preservation to this redistribution, and (3) the steady state balance between riverine input of alkalinity and the burial of calcite on the seafloor. I have incorporated a range of models of sedimentary calcite preservation into a time-dependent geochemical box model, in order to estimate the importance of these different responses to hypothesized glacial/interglacial changes in biological production.

I conclude that the potential for low latitude biological production to explain glacial/interglacial atmospheric CO_2 variability is strongly limited by constraints from paleoceanographic data on seafloor sediment calcite content. These constraints arise despite the effects of sediment respiration-driven dissolution considered by Archer and Maier-Reimer (1994). A much deeper calcite saturation horizon during the last ice age, as hypothesized by Archer and Maier-Reimer (1994), would have been accompanied by a similar deepening of the lysocline (the transition from calcite-rich to calcite-poor sediments). Since such an ocean-average lysocline deepening is not observed in glacial sediments (Catubig et al., 1994), we still lack a simple low latitude mechanism by which to lower atmospheric CO_2 during glacial times.

An increase in low latitude biological production, driven by an increase in the ocean nutrient reservoir, coupled to a decrease in the $\text{CaCO}_3/\text{C}_{\text{org}}$ ratio of that production can lower atmospheric CO_2 without causing a change in the depth of the steady state lysocline (Chapter 2). However, a 50% increase in low latitude export production would be required to explain an 80 ppm decrease in atmospheric CO_2 . While there is growing evidence that the Nitrogen cycle is adequately dynamic to allow for a large change in the oceanic nitrate reservoir on glacial/interglacial time scales (Ganeshram et al., 1995), no one has yet envisioned a way by which to cause a 50% increase in the oceanic phosphate reservoir on

these time scales. Without such a phosphate reservoir increase, it is difficult to invoke a large glacial increase in low latitude biological production. The impact of high latitude biological production on atmospheric CO₂ is not similarly constrained by seafloor sediment calcite content, because relatively little calcite is produced in high latitude surface waters today. Thus, the high latitude ocean deserves special consideration as a potential cause of observed glacial/interglacial atmospheric CO₂ variability.

The Role of the Southern Ocean

More than a decade ago, several groups demonstrated that an increase in the biological utilization of surface nutrients by Southern Ocean phytoplankton could explain lower atmospheric CO₂ concentrations during the last ice age (Knox and McElroy, 1984; Sarmiento and Toggweiler, 1984; Sieganthaler and Wenk, 1984). However, paleoceanographic studies suggesting no ice age increase in Southern Ocean biological production caused the hypothesis to lose favor (Mortlock et al., 1991). More recently, Francois et al. (1992) reported sedimentary N isotopic evidence which suggests that the efficiency of nitrate extraction in Antarctic surface waters was higher during the last ice age. This finding does not contradict the previous studies suggesting lower Antarctic production rates, since the efficiency of nutrient consumption involves the rate of nutrient supply as well as the rate of nutrient uptake. When coupled with Th and Pa-based estimates of particle flux, the N isotope data suggest that nitrate was more completely consumed in the glacial surface Antarctic, despite lower rates of export production at that time, because of a decrease in the supply of nitrate-rich water to the surface (Francois et al., 1997). Since the vertical supply of nitrate to the surface is associated with the atmospheric ventilation of subsurface waters, a decrease in nitrate supply, like an increase in N export production, would lower atmospheric CO₂ (Sieganthaler and Wenk, 1984). This hypothesized decrease in the vertical nutrient supply is consistent with previous research suggesting enhanced

surface layer stability in the Antarctic due to an increase in the seasonal extent of sea ice (Burckle, 1984; Morley and Hays, 1983).

The paleoceanographic records of bulk sedimentary N isotopic composition provide a potentially important insight into the nutrient status of the glacial Southern Ocean (Francois et al., 1992; Francois et al., 1997). However, there are major questions involving the link between nitrate utilization and N isotopes and its application to paleoceanography (Altabet and Francois, 1994b). These questions involve both the generation of the nitrate utilization/N isotope link in the water column and the survival of the isotopic signal in the sedimentary record. Chapters 3 through 5 describe the development and application of methods to investigate these questions.

The Nitrogen Isotopic Composition of Nitrate and Its Link to Nitrate Utilization

I have developed a new method to extract nitrate from seawater for N isotopic analysis (Chapter 3). This method allows for better precision and higher throughput than the previously available "distillation" method (Cline and Kaplan, 1975), making the generation of large oceanic data sets of nitrate isotopic composition possible for the first time. The method is based on previous methods from the soil sciences (Keeney and Nelson, 1982). It involves nitrate reduction to ammonia using a conventional reagent, followed by passive diffusion of the ammonia out of the alkaline seawater sample, through a sealed envelope composed of two porous Teflon membranes, and onto an acidified glass fiber filter. The extracted N is then combusted to N_2 by standard methods, and the N_2 is introduced into a stable isotope mass spectrometer for isotopic analysis.

With this method, I have analyzed the isotopic composition of nitrate from latitudinal transects of water column depth profiles and surface samples in the Indian and Pacific sectors of the Southern Ocean (Chapter 4). From measurement of subsurface nitrate, I have characterized the isotopic composition of the nitrate supply to the surface

Antarctic. The isotopic similarity of this nitrate with deep nitrate from the different ocean basins suggests that possible changes in deep water circulation during the last ice age are unlikely to have changed the isotopic value of this supply term. The data demonstrate a relatively simple link between the degree of nitrate uptake by phytoplankton and the isotope systematics of nitrate in Antarctic waters (i.e., south of the Polar Frontal Zone). A Rayleigh fractionation model of nitrate utilization approximately describes surface ocean nitrate isotopic data in the Antarctic. The isotopic and nitrate concentration data allow for an estimation of the fractionation factor associated with nitrate uptake, a crucial variable in the paleoceanographic use of N isotopes. The results suggest a fractionation factor of $5 \pm 1\text{‰}$ for the Antarctic region, in agreement with recent culture studies of diatoms and coccolithophorids (Waser et al., 1997a; Waser et al., 1997b). These findings, taken together, are encouraging with regard to the use of N isotopes as a proxy for nitrate utilization in the Antarctic region.

However, the results include some unexplained features which demonstrate gaps in our understanding of Antarctic nitrate supply and uptake. These uncertainties center around the role of the "Tmin" layer, a cold, fresh layer that is isolated from the surface by summer melting and warming. This layer separates the summer mixed layer from Upper Circumpolar Deep Water, which is the apparent long term source of nitrate to the surface Antarctic. In some cases, the $\delta^{15}\text{NO}_3$ of the Tmin layer falls significantly off the Rayleigh fractionation trend linking Upper Circumpolar Deep Water to the surface layer. Although I have hypotheses for the origin of this effect, such as a $\leq 1\text{‰}$ seasonal variation in the nitrate uptake fractionation factor, a complete understanding will probably require a seasonal study of the Antarctic upper water column.

My transects extend from the Antarctic, across the Polar Frontal Zone, and into the more nutrient-depleted Subantarctic waters. In the Subantarctic region, much of the nitrate supply appears to be by northward transfer of nitrate in the surface layer, although vertical

mixing may also play a role near the Polar Frontal Zone in some regions. Although the possibility of two nitrate sources complicates the estimation of the nitrate uptake fractionation factor for the Subantarctic, the data suggest that the same value found in the Antarctic region ($5 \pm 1\%$) applies in the Subantarctic region as well.

These findings indicate that N isotopes in the Subantarctic cannot be interpreted strictly in terms of nitrate utilization at a given site. Rather, the net northward advection of a surface nitrate pool requires that we consider the nitrate utilization history of that pool. In addition, an advective system is expected to show a greater sensitivity of sinking flux $\delta^{15}\text{N}$ to nitrate utilization than a system in which nitrate is supplied vertically (Altabet and Francois, 1994a). These results have important implications for the interpretation of surface sediment data and paleoceanographic studies in the Subantarctic (Francois et al., 1992; Francois et al., 1993). For instance, a lateral supply model explains the observation of a large ($6\text{--}8\%$) latitudinal gradient in surface sediment $\delta^{15}\text{N}$ in the east Indian sector, where the Subantarctic Zone is expanded (Francois et al., 1997); this $\delta^{15}\text{N}$ gradient is larger than can be generated by a vertical model of nitrate supply and our best estimate for the fractionation factor. The reduced importance of lateral nitrate supply in the central Indian, where the Subantarctic Zone is diminished, similarly explains the smaller latitudinal sediment $\delta^{15}\text{N}$ gradient observed in that region (Chapter 5).

The Isotopic Composition of Diatom Microfossil-Bound Nitrogen

The last component of my N isotope work has involved the development and application of a method for the isotopic analysis of diatom microfossil-bound organic N in Southern Ocean sediments (Chapter 5). The diatom-bound N fraction is operationally defined as the N associated with diatom microfossils which survives a chemical oxidation treatment to remove free and adsorbed organic N. This protocol is intended to isolate N which is native to the diatoms (i.e., which is incorporated into the opal during growth of

the diatom frustules). The isotopic analysis of diatom-bound N provides a potential avenue to assess whether the glacial/interglacial change in bulk sediment N isotopic composition records a true change in the isotopic composition of the sinking flux, or whether diagenetic or sedimentary processes are responsible.

In order to test the paleoceanographic utility of diatom microfossil-bound N, I have measured the isotopic composition of diatom microfossil-bound N and bulk sedimentary N from multicores in Southern Ocean surface sediments and carried out a preliminary study of the chemical composition of diatom-bound N. The results strongly suggest that the diatom microfossil-bound N fraction is invulnerable to early diagenesis and applicable as a proxy to track $\delta^{15}\text{N}$ changes of the sinking flux in the past.

I have measured depth profiles of diatom-bound $\delta^{15}\text{N}$ from paleoceanographic-scale cores in the Atlantic and Indian sectors of the Southern Ocean, south of the modern Polar Front. The downcore records of diatom-bound $\delta^{15}\text{N}$ show a 3-4‰ change across the last glacial/interglacial transition, supporting the previous conclusion derived from bulk sediment data that the $\delta^{15}\text{N}$ of the sinking flux was higher during the last glacial maximum (Francois et al., 1992; Francois et al., 1997). Given our current understanding of Southern Ocean N isotope dynamics, the simplest explanation for such a change is that the degree of nitrate utilization in Antarctic waters was higher during the last ice age.

Toward a Consistent Picture of the Glacial Southern Ocean

While unanswered questions remain, my thesis work provides strong support for the hypothesis that nitrate utilization was higher in the glacial Antarctic. The paleoceanographic N isotope data suggest that nitrate utilization in the glacial Antarctic was >60%, more than twice the modern extent of nitrate extraction. If this result is directly incorporated into a carbon cycle box model of the ocean, it suggests that the Southern Ocean was potentially the sole cause for the lower level of atmospheric CO_2 during the last

ice age (Keir, 1988; Knox and McElroy, 1984; Sarmiento and Toggweiler, 1984; Sieganthaler and Wenk, 1984).

However, these results do not provide the final word regarding the nutrient status of the glacial Southern Ocean. My thesis work has revealed a number of questions which remain to be addressed regarding the N isotope dynamics of the modern Southern Ocean. In addition, seasonal time-series studies and studies in other high latitude environments will be required before we will know how Southern Ocean N isotope dynamics would respond to the environmental changes associated with an increase in the importance of sea ice. Finally, other paleoceanographic proxies have their own story to tell about the ice age Southern Ocean, and the ultimate theory of glacial/interglacial atmospheric CO₂ variations must satisfy all of them.

References

- Altabet, M.A. and Francois, R., 1994a. Sedimentary nitrogen isotopic ratio as a recorder for surface ocean nitrate utilization. *Global Biogeochemical Cycles*, 8(1): 103-116.
- Altabet, M.A. and Francois, R., 1994b. The use of nitrogen isotopic ratio for reconstruction of past changes in surface ocean nutrient utilization. In: R. Zahn, M. Kaminski, L. Labeyrie and T.F. Pederson (Editors), *Carbon Cycling in the Glacial Ocean: Constraints on the Ocean's Role in Global Change*. NATO ASI series. Springer Verlag, Berlin, Heidelberg, New York, pp. 281-306.
- Archer, D. and Maier-Reimer, E., 1994. Effect of deep-sea sedimentary calcite preservation on atmospheric CO₂ concentration. *Nature*, 367: 260-263.
- Barnola, J.M., Raynaud, D., Korotkevich, Y.S. and Lorius, C., 1987. Vostok ice core provides 160,000-year record of atmospheric CO₂. *Nature*, 329: 408-414.
- Berner, W., Stauffer, B. and Oeschger, H., 1979. Past atmospheric composition and climate, gas parameters measured on ice cores. *Nature*, 275: 53-55.
- Boyle, E.A., 1988a. The role of vertical chemical fractionation in controlling late quaternary atmospheric carbon dioxide. *Journal of Geophysical Research*, 93(C12): 15,701-15,714.
- Boyle, E.A., 1988b. Vertical oceanic nutrient fractionation and glacial/interglacial CO₂ cycles. *Nature*, 331: 55-56.
- Broecker, W.S., 1981. Glacial to Interglacial Changes In Ocean and Atmospheric Chemistry. In: A. Berger (Editor), *Climatic Variations and Variability: Facts and Theory*, D. Reidel Publishing, pp. 111-121.
- Broecker, W.S., 1982. Glacial to Interglacial Changes In Ocean Chemistry. *Progress In Oceanography*, 2: 151-197.
- Broecker, W.S. and Peng, T.-H., 1987. The role of CaCO₃ compensation in the glacial to interglacial atmospheric CO₂ change. *Global Biogeochemical Cycles*, 1(1): 15-29.
- Burckle, L.H., 1984. Diatom distribution and paleoceanographic reconstruction in the southern ocean: Implications for late Quaternary paleoceanography. *Marine Micropaleontology*, 9: 241-261.
- Catubig, N.R., Archer, D.E., Howard, W.R., deMenocal, P.B. and Froelich, P.N., 1994. an atlas of LGM calcium carbonate concentrations in deep sea sediments and implications for the deep sea burial rate. *EOS*, 75(44): 367.
- Cline, J.D. and Kaplan, I.R., 1975. Isotopic fractionation of dissolved nitrate during denitrification in the eastern tropical North Pacific Ocean. *Marine Chemistry*, 3: 271-299.
- Delmas, R.J., Ascencio, J.-M. and Legrand, M., 1980. Polar ice evidence that atmospheric CO₂ 29,000 yr BP was 50% of the present. *Nature*, 284: 155-157.

- Francois, R., Altabet, M.A. and Burkle, L.H., 1992. Glacial to interglacial changes in surface nitrate utilization in the Indian sector of the Southern Ocean as recorded by sediment $\delta^{15}\text{N}$. *Paleoceanography* 7: 589-606.
- Francois, R., Bacon, M.P., Altabet, M.A. and Labeyrie, L.D., 1993. Glacial/interglacial changes in sediment rain rate in the S.W. Indian sector of Subantarctic waters as recorded by ^{230}Th , ^{231}Pa , U, and $\delta^{15}\text{N}$. *Paleoceanography*, 9(5): 611-630.
- Francois, R.F., Altabet, M.A., Yu, E.-F., Sigman, D.M., Bacon, M.P., Frank, M., Bohrmann, G., Bareille, G. and Labeyrie, L.D., 1997. Water column stratification in the Southern Ocean contributed to the lowering of glacial atmospheric CO_2 . *Nature*, in press.
- Ganeshram, R.S., Pedersen, T.F., Calvert, S.E. and Murray, J.W., 1995. Large changes in oceanic nutrient inventories from glacial to interglacial periods. *Nature*, 376(6543): 755-758.
- Keeney, D.R. and Nelson, D.W., 1982. Nitrogen -- inorganic forms. In: A.L. Page, R.H. Miller and D.R. Keeney (Editors), *Methods of Soil Analysis*. American Society of Agronomy, Inc., Madison, pp. 643-693.
- Keir, R.S.P., 3, 413-445, 1988, 1988. On the late Pleistocene ocean geochemistry and circulation. *Paleoceanography*, 3: 413-445.
- Knox, F. and McElroy, M., 1984. Changes in atmospheric CO_2 influence of the marine biota at high latitude. *J. Geophys. Res.*, 89: 4629-4637.
- McElroy, M.B., 1983. Marine biological controls on atmospheric CO_2 and climate. *Nature*, 302: 328-329.
- Morley, J.J. and Hays, J.D., 1983. Oceanographic conditions associated with high abundances of the radiolarian *Cycladophora davisiana*. *Earth and Planetary Science Letters*, 66: 63-72.
- Mortlock, R.A., Charles, C.D., Froelich, P.N., Zibello, M.A., Saltzman, J., Hays, J.D. and Burckle, L.H., 1991. Evidence for lower productivity in the Antarctic during the last glaciation. *Nature*, 351: 220-223.
- Neftel, A., Oeschger, H., Schwander, J., Stauffer, B. and Zumbunn, R., 1982. Ice core sample measurements give atmospheric CO_2 content during past 40,000 yr. *Nature*, 295: 220-223.
- Sanyal, A., Hemming, N.G., Hanson, G.N. and Broecker, W.S., 1995. Evidence for a higher pH in the glacial ocean from Boron isotopes in foraminifera. *Nature*, 373: 234-236.
- Sarmiento, J.L. and Toggweiler, J.R., 1984. A new model for the role of the oceans in determining atmospheric pCO_2 . *Nature*, 308: 621-624.
- Sieganthaler and Wenk, 1984. Rapid atmospheric CO_2 variations and ocean circulation. *Nature*, 308: 624-626.

Waser, N.A.D., Needoba, J., Calvert, S.E. and Harrison, P.J., 1997b. Nitrogen isotope fractionation by 4 groups of marine microalgae during batch culture growth on nitrate, ASLO Aquatic Sciences Meeting, Santa Fe, NM, pp. 337.

Waser, N.A.D., Turpin, D.H., Harrison, P.J., Nielsen, B. and Calvert, S.E., 1997a. Nitrogen isotope fractionation during the uptake and assimilation of nitrate, nitrite, and urea by a marine diatom. *Limnology and Oceanography*, in press.

Chapter 2:

The Calcite Lysocline as a Constraint on Glacial/Interglacial Low Latitude Production Changes

Daniel M. Sigman^{1*}, Daniel C. McCorkle¹, William R. Martin²

¹Department of Marine Geology and Geophysics, Woods Hole Oceanographic Institution,
Woods Hole, MA 02543, e-mail: dsigman@whoi.edu, fax: (508)-457-2183

*corresponding author

²Department of Marine Chemistry and Geochemistry, Woods Hole Oceanographic
Institution, Woods Hole, MA 02543

Abstract

We investigate the link between calcium carbonate production and the depth of the lysocline in the response of the ocean/atmosphere system to changes in the export production of the low latitude surface ocean (the combined equatorial, tropical, and subtropical regions). We employ different calcium carbonate input/output schemes in a time-dependent ocean carbon cycle model to separate the production/lysocline link from the other components of the model response, and to estimate the effects of chemical erosion and dissolution driven by organic matter decomposition in surface sediments ('respiratory dissolution').

The model predicts that a simple increase in low latitude production will lead to a significant shoaling of the steady state lysocline; this shoaling works to increase atmospheric CO_2 . Our results suggest that chemical erosion and respiratory dissolution are unlikely to decouple the lysocline depth from calcium carbonate production changes in this case. Because the low latitude biogenic rain pumps alkalinity as well as dissolved inorganic carbon into the deep ocean, increasing low latitude production does not drive a transient dissolution event in our model. As a result, "calcium carbonate compensation" [Broecker and Peng, 1987] does not cause a large decrease in atmospheric CO_2 when only low- and mid-latitude export production is increased.

A decrease in the calcium carbonate/organic carbon rain ratio or an increase in the depth to which organic carbon sinks in the deep ocean can lower atmospheric CO_2 considerably, but the changes required to lower CO_2 to glacial levels would also increase the ocean-average depth of the calcite saturation horizon by more than 1.5 km - much more than is suggested by data on the glacial lysocline. The inclusion of respiratory dissolution causes these changes in the characteristics of the low latitude biogenic rain to be more efficient at lowering atmospheric CO_2 by enhancing their deepening of the saturation horizon. However, even with respiratory dissolution, the model predicts that the lysocline deepens significantly when the saturation horizon deepens, so that respiratory dissolution does not prevent the lysocline depth from providing a constraint on low latitude export production. While chemical erosion would play an important role in the timing of lysocline shoaling and its effect on atmospheric CO_2 , it similarly would not prevent the lysocline depth from being a constraint on glacial/interglacial time scales.

These results and previous studies which suggest a fairly constant whole-ocean lysocline depth through glacial/interglacial cycles suggest that a simple increase in low latitude production cannot explain the lower atmospheric CO_2 levels of the last glacial maximum. Likewise, changes in either the calcium carbonate/organic carbon rain ratio or the organic carbon regeneration depth of low latitude production, taken alone, cannot explain last glacial maximum atmospheric CO_2 values without causing unacceptable shifts in the lysocline. However, if a low latitude production increase was accompanied by a decrease in the calcium carbonate/organic carbon rain ratio, these simultaneous changes could lower atmospheric CO_2 to the observed last glacial maximum levels without causing a significant change in the ocean-average depth of the saturation horizon. The required production rate increase is more than 50% of the modern rate.

Introduction

The alkalinity of seawater reflects a balance between the alkalinity input from rivers and the removal of calcium carbonate in sediments and coral reefs [Edmond, 1974; Keir, 1995; Milliman, 1974; Milliman, 1993; Opdyke and Walker, 1992]. This balance is maintained by the distribution of calcium carbonate accumulation in the deep sea, which is largely controlled by the depth of the "lysocline", the transition separating shallower seafloor sediments in which calcite is preserved from deeper seafloor sediments in which almost all of the calcite dissolves [Archer, 1991a; Berger, 1970]. One of the primary controls on the depth of the lysocline is the calcite saturation depth, which is set by the carbonate ion concentration of bottom water and the pressure dependence of calcite solubility [Broecker and Takahashi, 1978]. A change in either the river input rate of alkalinity or the seafloor burial rate of calcium carbonate would change the whole ocean alkalinity inventory. This alkalinity change would shift the ocean-average calcite saturation depth and thus the depth of the lysocline. Changing the depth of the lysocline causes a change in the calcium carbonate burial rate, so that the output of alkalinity changes to balance the new input rate of alkalinity by rivers.

Open ocean biological production is one potential driver of changes in the oceanic alkalinity balance. For example, an increase in the open ocean calcium carbonate (CaCO_3) rain rate would increase the rate of CaCO_3 burial on the seafloor above the lysocline. As a result, the whole ocean inventories of alkalinity (ALK) and dissolved inorganic carbon (DIC) would decrease in a 2:1 ratio (the stoichiometry of "dissolved" CaCO_3). This inventory change would cause a decrease in the deep ocean carbonate ion concentration, which would, in turn, cause a shoaling of the calcite saturation horizon. This shoaling of the saturation horizon would cause a shoaling of the lysocline, which would decrease the area of seafloor over which CaCO_3 is buried, restoring the CaCO_3 input/output balance.

This link between open ocean CaCO_3 production and the lysocline is significant for two reasons. First, if river input and shelf burial remain constant, variability in the lysocline depth would reflect changes in the rate and chemical nature of surface ocean export production. Second, the whole ocean changes in ALK and DIC which drive the lysocline changes also affect the concentration of atmospheric CO_2 [Keir, 1995], which was ~80 ppm lower during the last glacial period [Barnola *et al.*, 1987].

Much paleoceanographic work has addressed the role of biological production in observed glacial/interglacial atmospheric CO_2 variability. The low latitude ocean (the combined equatorial, tropical, and subtropical regions) is responsible for most deep sea calcite burial [Catubig *et al.*, 1994; Milliman, 1993]. Therefore, a change in low latitude production may cause a significant lysocline response. Any hypothesis regarding changes in low latitude production must be consistent with paleoceanographic data regarding the lysocline, and the expected CO_2 impact of a production change must include the effect of the oceanic alkalinity input/output balance.

The actual change in the ocean-average lysocline depth over the last glacial/interglacial cycle is not well known. The Atlantic lysocline was apparently about 1 km shallower during the last glacial [Crowley, 1983; Crowley, 1985; Curry and Lohmann, 1986], and Howard and Prell [1994] estimate that the glacial lysocline was 0.5 km shallower in the Atlantic and Indian sectors of the Southern Ocean. No clear change in lysocline depth is observed in the Indian Ocean, although preservation and dissolution events have occurred on glacial/interglacial transitions [Peterson and Prell, 1985]. While equatorial and northeast Pacific data suggest that the glacial lysocline was 0.6 km deeper [Farrell and Prell, 1989; Karlin *et al.*, 1992], there is an active debate as to whether this deepening was due to a local increase in CaCO_3 production or to an increase in the saturation depth and lysocline of the entire low latitude Pacific [Anderson *et al.*, 1995; Archer, 1991b]. Compiling a global ocean data set, Catubig *et al.* [1994] find that the

whole ocean-averaged lysocline depth of the last glacial was the same or shallower than that of the Holocene.

In this study, we investigate the response of the lysocline to changes in low latitude production, to learn if and by what mechanisms low latitude biological production changes can lower atmospheric CO_2 to observed glacial levels while being consistent with available data on glacial/interglacial changes in the ocean-average lysocline depth. Using a time-dependent ocean-atmosphere carbon cycle model (with architecture after *Keir* [1988]), we have run three model experiments which involve changes in low latitude biological production: (1) an increase in low latitude export production, (2) a decrease in the calcium carbonate/organic C ($\text{CaCO}_3/\text{C}_{\text{org}}$) ratio of low latitude export production, and (3) an increase in the fraction of C_{org} export production which reaches the deep ocean. Similar experiments have been carried out previously, with a variety of assumptions being made about the role of deep sea CaCO_3 preservation [*Archer and Maier-Raimer*, 1994; *Boyle*, 1988; *Broecker and Peng*, 1987; *Broecker et al.*, 1984; *Dymond and Lyle*, 1985; *Keir*, 1988]. In our study, the model experiments are carried out under a set of CaCO_3 input/output models which cover the range of models used by earlier workers. Using these different CaCO_3 input/output models, we compare the steady state lysocline response with the other components of the carbon cycle response. In addition, we incorporate parameterizations for the processes of chemical erosion [*Keir*, 1984] and sediment respiration-driven dissolution [*Emerson et al.*, 1980] in order to evaluate the potential roles of these processes. We address the following questions:

- 1) How much of a change in the steady state lysocline depth occurs for various changes in the rate and nature ($\text{CaCO}_3/\text{C}_{\text{org}}$ ratio, and C_{org} regeneration depth) of biological production, and how is this lysocline change distributed in a global ocean model? How important is this

lysocline change to atmospheric $p\text{CO}_2$, relative to other components of the carbon cycle response?

2) How effectively can chemical erosion retard shoaling of the saturation depth? Can it decouple the saturation depth (and lysocline depth) from carbonate production on glacial/interglacial time scales?

3) Does the inclusion of sediment respiration-driven dissolution greatly alter the response of the saturation horizon to a change in low latitude export production? Does this porewater-driven dissolution decouple the lysocline from the saturation horizon, so that migration of the saturation horizon would not be evident in lysocline behavior?

None of the model experiments, when performed individually, lower atmospheric CO_2 to glacial levels without causing large (> 1 km) changes in the ocean-average lysocline depth. Chemical erosion retards shoaling of the lysocline, but not enough to prevent the production/lysocline link from being a constraint on glacial/interglacial time scales. While sediment respiration-driven dissolution does not significantly modify the carbon cycle response to a simple increase in low latitude production, it enhances the effect of a rain ratio decrease or a deepening of C_{org} regeneration on the calcite saturation depth [Archer and Maier-Raimer, 1994]. However, this enhancement is accompanied by a migration of the steady state lysocline, so that the potential for these production changes is still constrained by observations of the glacial/interglacial change in lysocline depth. Given these model results and the available data on glacial/interglacial lysocline variability, the only low latitude production mechanism which could explain lower atmospheric $p\text{CO}_2$ during the last glacial involves the coupling of oceanographic changes which have opposite effects on the lysocline. As an example, we consider an increase in low latitude export production, which would cause the steady state lysocline to shoal, coupled with a decrease in its $\text{CaCO}_3/C_{\text{org}}$ rain ratio, which would cause it to deepen.

Model Description

The results presented in this study are from a time-dependent box model of the ocean-atmosphere system which simulates the cycles of carbon, alkalinity, phosphate, molecular oxygen, ^{13}C and ^{14}C . Architecture, circulation, and production/remineralization parameters are taken from the CYCLOPS model of *Keir* [1988]. We focus on the CaCO_3 input/output dynamics and the production/regeneration cycles, as these aspects of the model are most important to this study. The model treatment of gas exchange processes and isotope systematics will be described in *Sigman and Lehman* [in prep.]. In appendix I, we show a comparison of the model standard "interglacial" distributions of phosphate, DIC, and ALK with those of *Keir* [1988] and with averaged GEOSECS data [*Takahashi et al.*, 1981].

Circulation (figure 1):

Water is provided to the warm surface boxes via mixing with, and advection from, the intermediate ocean boxes. The intermediate boxes are fed largely from the Antarctic surface. Water is advected into the deep Atlantic box from the warm surface box and the intermediate Atlantic box by way of the high North Atlantic boxes. This "NADW" source advects into the Antarctic Circumpolar box, where it mixes with water from other deep boxes and is upwelled into the surface Antarctic, from which it is advected into the intermediate boxes. The Antarctic Circumpolar box has large mixing terms with the surface Antarctic and with the low latitude deep boxes, so that model deep water has effectively both North Atlantic and Southern Ocean sources. This circulation scheme is discussed by *Keir* [1988].

Export Production/Regeneration Cycle (figure 2):

We calculate new production for the warm surface ocean by forcing production to occur until phosphate is completely consumed. New production in the warm surface ocean is thus controlled by (1) the phosphate concentration of subsurface waters and (2) the amount of water exchanged between subsurface and surface waters.

For the model experiments described in this study, high latitude production is held constant, so that the phosphate concentration of the high latitude surface ocean may vary. There are two justifications for this choice. First, production in most high latitude regions does not appear to be limited by phosphate or nitrate, so that high latitude production should not respond to a change in phosphate supply [e.g., *Cullen, 1991; Mitchell et al., 1991*]. Second, high latitude production affects the ocean carbon cycle by several mechanisms; allowing high latitude production to change obscures the effects of low latitude production. All experiments have also been run with other rules for high latitude production. From these runs, we know that the choice of high latitude production rule is significant only for model experiment 1; this concern is addressed in the model experiment 1 discussion.

The $\text{CaCO}_3/\text{C}_{\text{org}}$ rain ratio of export production is different for the model's low and high latitude surface boxes. The export production of the warm surface boxes has a rain ratio of 0.4 (ALK/DIC rain ratio = 0.46), while that of the high latitude boxes has a rain ratio of 0 (ALK/DIC rain ratio = -0.15). The production-normalized whole ocean rain ratio is 0.31 (ALK/DIC rain ratio = 0.36).

The C_{org} and CaCO_3 water column regeneration schemes are also different for the low and high latitude surface boxes. Of the C_{org} raining out of the low latitude boxes, 84% is degraded in the intermediate boxes, and the remaining 16% is degraded in the deep boxes, so that no C_{org} is buried. The calcite rain associated with the model's low latitude

production penetrates more deeply into the ocean interior, with 20% of the rain dissolving at intermediate depths and the remaining 80% raining onto the seafloor. Given a rain ratio of 0.4 and the above regeneration schemes, the $\text{CaCO}_3/\text{C}_{\text{org}}$ flux ratio into the low latitude deep ocean is 2, which is consistent with, but perhaps in the upper range of, observations from deep sediment traps and seafloor studies [Archer, 1991a; Honjo, 1996; Honjo *et al.*, 1995; Honjo and Manganini, 1992]. The high latitude subsurface is not separated into intermediate and deep, so that C_{org} production from the high latitude surface is completely regenerated in a single deep box, which mixes actively with other deep boxes.

The use of different production/regeneration parameters is one potential cause for disagreements between different models. In order to check the sensitivity of our results to the production/regeneration parameters, we have also carried out the model experiments using different values for these parameters. The results from these sensitivity cases are described in a section following the closed system/compensated/open system comparison of the model experiments.

Models of CaCO_3 Input/Output Dynamics (figure 3)

The model experiments are carried out under three different schemes of CaCO_3 input/output dynamics: (1) "closed system", (2) "compensated", and (3) "open system". These different CaCO_3 input/output schemes allow us to resolve three different components of the carbon cycle response: (1) the closed system redistribution of ALK and DIC within the ocean, (2) the transient compensation by deep sea calcite dissolution/preservation of the closed system effect on deep ocean $[\text{CO}_3^{2-}]$, and (3) the migration of the lysocline to a new steady state depth due to a change in CaCO_3 rain rate.

In the closed system case, there is neither river input of DIC and ALK nor seafloor burial of biogenic CaCO_3 . As a result, production changes simply redistribute DIC and

ALK within the ocean/atmosphere system; there are no whole ocean reservoir changes in these components.

In the compensated and open system cases, whole ocean reservoir changes in DIC and ALK occur via loss or gain of "dissolved CaCO_3 ", which represents one unit of DIC and two units of ALK. The compensated case estimates the potential for production changes to drive a transient preservation or dissolution event in the deep sea [Boyle, 1988; Broecker and Peng, 1987]. In the compensated case, any change in the deep ocean carbonate ion concentration ($[\text{CO}_3^{2-}]$) is removed by a transient dissolution event (increasing whole-ocean ALK and DIC in a 2:1 ratio) or a transient preservation event (decreasing ALK and DIC in a 2:1 ratio). The compensated case does not explicitly model the feedbacks among river input, CaCO_3 rain, and deep sea calcite preservation which lead to the oceanic alkalinity balance. As a result, this case does not capture the link between CaCO_3 production and the steady state lysocline depth.

In the open system case, deep ocean $[\text{CO}_3^{2-}]$ is explicitly controlled by the balance between river input of dissolved CaCO_3 and the seafloor burial of biogenic CaCO_3 . As a result, the open system case includes the steady state lysocline effect as well as the transient lysocline effect of the compensated case. The steady state lysocline response alone can thus be estimated by the difference between the open and compensated cases.

Finally, we have developed and experimented with two open system CaCO_3 models: the "rain-based open" case and the "mixed layer open" case. The rain-based open system runs yield a hypothetical end-member case for the lysocline response, in which bottom water saturation state alone controls the dissolution of biogenic CaCO_3 . This case has no sediment memory, with only the yearly CaCO_3 rain being vulnerable to dissolution. It thus includes neither chemical erosion nor sedimentary respiration-driven dissolution. The goal of the rain-based case is to provide a simplified view of the basic lysocline changes which occur in the model experiments.

With the mixed layer open system case, we then consider the more realistic aspects of the lysocline. As described in appendix II, we have developed a parameterization for seafloor dissolution using results from an explicit sediment geochemistry model [Martin and Sayles, 1996]. This parameterization includes the effects of both bottom water-driven dissolution and sediment respiration-driven dissolution. The mixed layer open system case includes sediment mixed layer dissolution and chemical erosion.

In part 1 of the results section, the rain-based model is used for the comparison of open system results with those of the closed system and compensated cases. In the later sections, we then use the mixed layer open system model to address (1) the role of chemical erosion in retarding migration of the lysocline (part 2), and (2) the effect of sedimentary respiration-driven dissolution on the production/lysocline link (part 3, see figure 3).

Calculation Scheme for the Compensated Case

We use the compensated case to quantify the seafloor dissolution/preservation response to changes in deep ocean $[\text{CO}_3^{-2}]$ caused by the redistribution of ALK and DIC within the ocean. Unlike the other cases, it is not an explicit time-dependent model. Instead, it is a calculation performed from the open system steady state results:

- (1) From the open system case final output, the deep ocean average ALK and DIC are calculated. This average is weighted for (a) seafloor area, and (b) the CaCO_3 rain rate in overlying surface waters. The weighting for rain rate is to keep non-carbonate (i.e., high latitude) regions from causing a seafloor compensation response.
- (2) From the average deep ocean ALK and DIC, an average $[\text{CO}_3^{-2}]$ is calculated. This value is slightly different from that which would be calculated by averaging the $[\text{CO}_3^{-2}]$ of all the deep boxes with sedimentary CaCO_3 ; we have found the difference to be insignificant.

(3) ALK and DIC are changed in a 2:1 ratio (i.e., as dissolved CaCO_3) in all boxes equally until the average deep ocean $[\text{CO}_3^{-2}]$ equals that of the standard “interglacial” case.

(4) Atmospheric CO_2 is recalculated given this whole ocean ALK and DIC change.

This protocol is similar to that of *Broecker and Peng* [1987], except that (1) they do not include the Atlantic in their calculation of deep ocean $[\text{CO}_3^{-2}]$ change, and (2) they carry out their compensation from the closed system case. The significance of the first difference is discussed by *Broecker and Peng* [1987]. We have confirmed that the results are not significantly affected by these differences.

Calculation Scheme for the Open System Models

In the rain-based open system model, the only calcite vulnerable to dissolution in the rain-based open case is the yearly calcite rain; the sediments have no memory of previous calcite accumulation. The calcite saturation depth is calculated from the bottom water $[\text{CO}_3^{-2}]$ ($[\text{CO}_3^{-2}]_{\text{bw}}$) using the equation for calcite saturation $[\text{CO}_3^{-2}]$ ($[\text{CO}_3^{-2}]_{\text{sat}}$) of *Broecker and Takahashi* [1978] (as was used by *Keir* [1988]). Below the saturation depth, dissolution occurs as a linear function of undersaturation,

$$\text{Dissolution} = K_{\text{rb}} * ([\text{CO}_3^{-2}]_{\text{sat}} - [\text{CO}_3^{-2}]_{\text{bw}})$$

with the rate coefficient K_{rb} equal to $\sim 1.2 \mu\text{mol CaCO}_3$ per cm^2 per year per $\mu\text{mol/kg} [\text{CO}_3^{-2}]$ undersaturation. K_{rb} (“rb” for rain-based) was calculated from a calcite dissolution rate constant (“ k_d ”) of 30/day [*Keir*, 1980], assuming a linear dependence on undersaturation. The depth at which the dissolution rate equals the CaCO_3 rain onto the seafloor is the rain-based model calcite compensation depth (CCD). Thus, while the top of the lysocline, the calcite saturation horizon, is determined by only the deep ocean $[\text{CO}_3^{-2}]$, the base of the lysocline, the CCD, is a function of the deep $[\text{CO}_3^{-2}]$, the CaCO_3 rain rate into the deep

ocean, and the kinetics of CaCO_3 dissolution. Under standard conditions, the rain-based lysocline, as defined by the saturation depth and the CCD, is about 800 m thick. We approximate the hypsometry of each basin as a set of ramps, based on *Menard and Smith* [1966].

In the mixed layer open case, CaCO_3 within the sediment mixed layer is vulnerable to dissolution, and the dissolution rate can exceed the CaCO_3 rain rate. If the calculated carbonate dissolution rate exceeds the total sediment flux (the sum of the carbonate and non-carbonate sediment rain rates), sediment from below the 8 cm deep mixed layer is reincorporated into the mixed layer (i.e., chemical erosion occurs). Following *Oxburgh and Broecker* [1993], we account for effect of % CaCO_3 on sediment density, using the expression of *Farrell* [1991] for equatorial Pacific sediments. The % CaCO_3 of the reincorporated sediment is set at that of the mixed layer at the beginning of the model experiment. Thus, our chemical erosion model does not record the entire carbonate burial history at each site.

The dissolution model for the mixed layer open case was derived by generating multivariate polynomial fits to output from an off-line sediment geochemistry model [*Martin and Sayles*, 1996] and using these fits in the ocean box model. In this study, we treat bottom water-driven dissolution and respiration-driven dissolution as additive components of the total dissolution; these two components are parameterized separately, as described in appendix II.

For the mixed layer open system model, the calcite saturation equation of *Ingle* [1975] was used, for consistency with the off-line sediment geochemistry model [*Martin and Sayles*, 1996]. Largely because of the different calcite saturation equations, the rain-based open system results and mixed layer model responses differ slightly (see appendices).

For the experiments employing the mixed layer open system model (parts 2 through 4), the low latitude basin resolution was removed, collapsing the low latitude boxes into a single set of low latitude surface, intermediate, and deep boxes. This was done for two reasons. First, including basin resolution would require that we show the response of at least two low latitude deep boxes, as we have done for the rain-based case. The rain-based case results give an adequate sense of the interbasin differences we observe if basin resolution is included in the experiments using the mixed layer open system model. Second, the interbasin differences which result in our model are based on a deep circulation scheme designed to describe the modern ocean. The significance of these interbasin differences for the glacial ocean is uncertain, given the evidence for major differences in deep circulation during the last Ice Age.

Results

Part 1: Comparison of Closed, Compensated, and Open System Responses to Changes in Low Latitude Production

Using our different CaCO_3 input/output schemes, we perform model experiments in which we change low latitude export production. In model experiment 1, we increase the whole ocean phosphate reservoir by 30%, which represents a simple mechanism for observing the effect of an increase in low latitude production [Broecker, 1982; Broecker and Peng, 1987; Keir, 1988]. In model experiment 2, we model the effects of halving the $\text{CaCO}_3/\text{C}_{\text{org}}$ rain ratio of low latitude production [Archer and Maier-Raimer, 1994; Broecker et al., 1984; Dymond and Lyle, 1985]. In model experiment 3, we model the effect of an increase in the fraction of C_{org} export production which reaches the deep boxes [Archer and Maier-Raimer, 1994; Boyle, 1988].

For each model experiment, we compare the different magnitudes of atmospheric CO_2 response due to (1) the closed system redistribution of ALK and DIC within the ocean, (2) the transient compensation by deep sea calcite dissolution/preservation of the closed system effect on deep ocean $[\text{CO}_3^{2-}]$, and (3) the change in the steady state saturation depth driven by changes in the CaCO_3 rain rate (figure 4). The time-dependent results for the closed and open system cases help to illustrate these three different effects (figure 5). Using the open system results, we assess whether any of our model experiments can lower atmospheric CO_2 to glacial levels while being consistent with observed glacial/interglacial lysocline variability.

Model Experiment #1: Increasing the Oceanic Phosphate Reservoir Size by 30%

Broecker [1982] suggested that one potential driver of increased production is an increase in the phosphate content of the ocean. From our perspective, this hypothesis

represents a mechanism to increase low latitude production without the auxiliary effects associated with changing circulation.

In our experiment, the whole-ocean phosphate reservoir is increased by 30% while allowing low latitude production to increase so as to maintain phosphate-free surface water. We focus here on the model response for the case in which the high latitude productive flux is held constant. However, we also discuss the "constant nutrient utilization" case for the high latitude, which should be comparable to the high latitude "constant residence time" rule used by *Broecker and Peng* [1987].

Increasing the phosphate reservoir by 30% yields a 34 ppm CO₂ decrease for the closed system case, a 29 ppm decrease for the compensated case, and only an 18 ppm decrease for the open system case (figure 4a). Thus, lysocline processes reduce the magnitude of the CO₂ decrease resulting from the model experiment. That is, they tend to raise atmospheric CO₂.

The time-dependent output plotted in figures 5.1 a-d shows the opposing effects of the closed system and open system processes on atmospheric CO₂. Increased production immediately lowers atmospheric CO₂ by pumping DIC out of the surface, leading to the initial drop in atmospheric CO₂ seen for both closed and open system scenarios (figure 5.1 a). However, the increase in the CaCO₃ rain associated with increased low latitude production causes a temporary excess in CaCO₃ burial relative to river input of dissolved CaCO₃ (figure 5.1 b). This represents a loss of ALK and DIC from the ocean in a 2:1 ratio, which raises the pCO₂ of surface water and results in higher atmospheric CO₂ for the open system scenario (figure 5.1 a). The loss of ALK and DIC also causes the deep ocean [CO₃²⁻] to decrease, so that the saturation horizon shoals an average of 540 m throughout the ocean (figures 4b, 5.1 c, d). As the saturation horizon and lysocline shoal, the rate of CaCO₃ burial decreases, driving the burial/river ratio back to unity (figure 5.1 b).

The Atlantic-Pacific difference in lysocline changes is largely due to deep ocean circulation [Keir, 1988]. The deep Atlantic receives surface waters which have a higher $[\text{CO}_3^{-2}]$ than in the standard case, while the old waters of the Pacific have gained more DIC from the oxidation of surface new production. As a result, the difference in the lysocline depths between the Atlantic (figure 5.1 c) and Pacific (figure 5.1 d) increases, although the lysoclines of all deep boxes shoal so as to bring CaCO_3 burial back into balance with river input.

The effect of CaCO_3 production on the depth of the steady state lysocline is illustrated in figure 6, which shows the ocean-averaged depth of the steady state calcite saturation horizon over a range of low latitude production rates (controlled by varying the whole ocean phosphate reservoir while keeping the $\text{CaCO}_3/C_{\text{org}}$ ratio fixed at 0.4). At the standard case production value, the saturation horizon shoals by 175 meters for a 10% increase in CaCO_3 rain rate (or 75 m per $\text{gCaCO}_3/\text{m}^2/\text{yr}$). The sensitivity, or slope, of the relationship becomes greater as the lysocline becomes deeper. This is due both to the ocean's hypsometry and to an increase in lysocline sensitivity at low levels of CaCO_3 production. That is, as the CaCO_3 rain rate approaches zero in the model, the area of seafloor burial required to match the riverine alkalinity input increases in a hyperbolic fashion.

So far we have only discussed the response of the steady state lysocline. CaCO_3 compensation, the transient component of the lysocline response, causes a small (5 ppm) atmospheric CO_2 increase relative to the closed system case for this experiment (figure 4a). The compensation effect is driven by a $1.5 \mu\text{M}$ increase in deep ocean $[\text{CO}_3^{-2}]$ which occurs in the closed system model (figure 4b). In the compensated case, this $[\text{CO}_3^{-2}]$ increase results in excess deep sea preservation, causing the ocean to lose ALK and DIC in a 2:1

ratio. This small transient preservation event is not apparent in the open system time-dependent results because of the dominant effect of the steady state lysocline change.

The CaCO_3 compensation response in our model differs from that observed by *Broecker and Peng* [1987]. They modelled the pCO_2 response to increasing the whole-ocean phosphate reservoir for cases roughly equivalent to our closed and compensated cases. Their results suggested that the transient lysocline response would significantly enhance the pCO_2 drop associated with this experiment, from a 33 ppm decrease in the closed system case to a 52 ppm decrease in the compensated case.

The difference in model response is partially due to our different high latitude production rules. In our model experiment, high latitude production was held constant, while high latitude production in the model of *Broecker and Peng* [1987] is allowed to increase as phosphate supply increases, so as maintain to a constant phosphate residence time in the high latitude surface. Because high latitude production is deeply regenerated, an increase in high latitude production efficiently drives DIC into the deep ocean, so that a transient dissolution event occurs [*Broecker and Peng*, 1987; *Keir*, 1988]. When we run model experiment 1 assuming the same high latitude production rule as *Broecker and Peng* [1987], we find that there is a transient dissolution response, which drives a 10 ppm decrease (rather than a 6 ppm increase). The lack of transient dissolution in our model response to an increase in low latitude export production will be considered further in a later section on the sensitivity of the model results to production/regeneration parameters.

We have also carried out a model experiment in which low latitude production is increased by increasing the mixing (or “upwelling” rate) between the intermediate boxes and the low latitude surface boxes [*Boyle*, 1988; *Broecker and Peng*, 1987]. While the closed system response to this model experiment is different from that of the experiment described here, the lysocline responses, both transient and steady state, are quite similar to

those of model experiment 1. That is, the lysocline responses to an increase in low latitude production do not seem to be sensitive to the mechanism of the production increase. In our model, a simple increase in low latitude export production, regardless of the mechanism, cannot lower atmospheric CO_2 to observed glacial levels without causing >1 km shoaling of the ocean-average steady state lysocline.

Model Experiment 2: Halving the Warm Surface $\text{CaCO}_3/C_{\text{org}}$ Rain Ratio

As is apparent from model experiment 1, a major limitation on the capacity of low latitude production to lower atmospheric CO_2 is the CaCO_3 component of the biogenic rain. In experiment 2, we lower the $\text{CaCO}_3/C_{\text{org}}$ rain ratio of the low latitude biogenic flux from 0.4 to 0.2 (molar ratio) without changing the rate of biological production, which results in a halving of the CaCO_3 rain rate. Such a change has previously been examined by *Broecker et al.* [1984] for the compensated case, *Dymond and Lyle* [1985] for the closed system case, and *Archer and Maier-Raimer* [1994] for the open system case.

Atmospheric CO_2 is much more sensitive to the rain ratio of low latitude export production in the open system scenario than in the compensated or closed system scenarios (figures 4a, 5.2a). Decreasing the rain ratio from 0.4 to 0.2 in the open system model produces an atmospheric CO_2 decrease of 63 ppm, compared to the 35 ppm and 22 ppm decreases which occur in the compensated and closed system cases, respectively. Thus, the steady state lysocline response represents a CO_2 sink of 28 ppm, while CaCO_3 compensation accounts for 13 ppm of the atmospheric CO_2 decrease.

The steady state lysocline deepening is driven by the decrease in the CaCO_3 rain rate associated with halving the rain ratio. This decrease in rain rate causes the burial rate of CaCO_3 to fall below the river input rate of dissolved CaCO_3 (figure 5.2 b), and the whole ocean reservoirs of ALK and DIC increase in a 2:1 ratio. In response, the deep sea $[\text{CO}_3^{2-}]$

increases, causing the lysocline to deepen and the area above the lysocline to increase (figure 5.2 c,d). A new steady state deep ocean lysocline depth is achieved when enough new area above the lysocline is provided for CaCO_3 burial to balance the river input once again. Meanwhile, the whole ocean increase in ALK and DIC has caused atmospheric CO_2 to decrease (figure 5.2 a).

The CaCO_3 compensation response to this model experiment is a dissolution event. When the $\text{CaCO}_3/\text{C}_{\text{org}}$ rain ratio is lowered, there is a decrease in the ratio of ALK to DIC being pumped into the deep ocean. In the closed system case, this redistribution of DIC and ALK causes a $4 \mu\text{M}$ decrease in the $[\text{CO}_3^{2-}]$ of average deep water. In the compensated and open system cases, this increased undersaturation drives a dissolution event. The open system time dependent results show this dissolution event as a transient shoaling of the calcite saturation horizon in the North Pacific (figure 5.2 d).

While the lysocline in the North Pacific (and the other Indo-Pac basins) shoals due to CaCO_3 compensation and then deepens to a new steady state depth, the lysocline in the Atlantic begins to deepen almost immediately (fig 5.2 c). This effect is related to the similar increase in Atlantic-to-Pacific gradient observed in model experiment 1. It can be thought of as the result of an increase in the ALK/DIC ratio of the surface water which is fed into the deep ocean in the North Atlantic. This response is contrary to observations of a shallower glacial Atlantic lysocline [Crowley, 1985]. However, evidence for a weaker interbasin nutrient gradient during the last glacial [Boyle and Keigwin, 1982], perhaps due to reduced North Atlantic Deep Water formation, prevents this disagreement from being a strong constraint.

In total, a halving of the $\text{CaCO}_3/\text{C}_{\text{org}}$ rain ratio lowers atmospheric CO_2 by more than 60 ppm, which approaches the observed ~ 80 ppm glacial/interglacial variability of atmospheric CO_2 [Barnola *et al.*, 1987]. The magnitude of the atmospheric CO_2 response to

saturation horizon deepening varies among models [Keir, 1995], and among experiments, due to changes in interbasin $[\text{CO}_3^{2-}]$ gradient. In another model, the CO_2 change due to the deepening of the steady state lysocline may be 10 ppm or so higher, so that the total CO_2 decrease would be >70 ppm, on the order of the observed last glacial/Holocene difference. However, the CO_2 decrease is associated with a 1.5 km deepening of the saturation horizon. This appears to violate % CaCO_3 data for the last glacial, suggesting that this mechanism alone cannot explain lower atmospheric CO_2 levels during the last glacial maximum.

What is needed to explain glacial/interglacial CO_2 variability is a mechanism to lower atmospheric CO_2 without causing a large deepening of the steady state lysocline. This could involve oceanographic changes which drive a large closed system or CaCO_3 compensation response [Keir, 1988; Knox and McElroy, 1984], or which decouple the saturation horizon from the lysocline [Sanyal *et al.*, 1995]. Model experiment 3, an increase in the fraction of C_{org} export production which reaches the deep ocean, represents a low latitude production change which might do both of these things [Archer and Maier-Raimer, 1994; Boyle, 1988].

Model Experiment 3: Deepening the C_{org} Regeneration Profile

Deepening the C_{org} regeneration profile reorganizes the DIC distribution of the ocean, increasing the DIC/ALK ratio of the deep ocean and thus causing a transient dissolution event [Boyle, 1988]. This scenario for the glacial ocean is viable if new production increased or became more seasonal during glacial periods, since a larger proportion of new production sinks through the intermediate ocean when the production rates are high and/or sporadic [Billet *et al.*, 1983; Bishop *et al.*, 1980].

A change in the organic matter regeneration profile from 84%/16% (intermediate/deep) to 60%/40% causes CO₂ decreases of 15 and 19 ppm in the compensated and open system scenarios, respectively, but no CO₂ change in the closed system scenario (figure 4a, figure 5.3 a). Thus, this pCO₂ decrease noted here is almost entirely due to CaCO₃ input/output processes. The CaCO₃ compensation response (a dissolution event) dominates the CO₂ response, so that the compensated case CO₂ decrease is nearly the same as the open system case CO₂ decrease.

Deepening the C_{org} regeneration profile increases the amount of DIC (relative to ALK) which is transported to the deep ocean. As a result, the [CO₃⁻²] in the deep ocean decreases by 7 μM in the closed system model. In the compensated and open system cases, this [CO₃⁻²] decrease drives a transient dissolution event, evident as a minimum in lysocline depth at 2 kyrs in the North Pacific (figure 5.3 d). This lysocline shoaling decreases the seafloor area over which CaCO₃ burial occurs, which leads to a deficit in burial relative to river input (figure 5.3 b). The deficit in burial causes the ocean to gradually increase in the components of dissolved CaCO₃. The whole ocean change both lowers atmospheric CO₂ (figure 5.3 a) and causes deep ocean [CO₃⁻²] to increase back to its initial value (figures 5.3 c,d).

Deepening of the regeneration of organic matter causes a net transfer of phosphate from the intermediate boxes to the deep boxes [Boyle, 1988]. As a result, low latitude export production and its associated CaCO₃ rain decrease by 10%. This leads to a whole-ocean lysocline deepening of 0.2 km. Because of the route of deep circulation, the Atlantic lysocline deepens much more than this, while the North Pacific lysocline shoals slightly (figures 5.3 c,d). As with the other model experiments, in a glacial ocean with less NADW production, this interbasin gradient would be weaker or absent.

While the CO_2 decrease in this experiment is not associated with a significant change in the steady state saturation depth, the CO_2 decrease itself is less than 20 ppm. Thus, it appears that this model experiment alone cannot lower atmospheric CO_2 levels to observed glacial levels. However, we will see that the open system pCO_2 response for this experiment is much greater when sedimentary respiration is included in the model of CaCO_3 dissolution [Archer and Maier-Raimer, 1994]. In a later section, we will address whether this consideration transforms this model experiment or the previous two experiments into viable mechanisms for lowering atmospheric CO_2 to glacial levels.

Sensitivity of the Model Response to Production/Regeneration Parameters

We have carried out the model experiments using different values for these parameters, as there are disagreements about what values should be used [e.g., Anderson and Sarmiento, 1994]. The alternative parameter sets used for the model experiments, referred to as "sensitivity tests", are summarized in table 1. These cases are not to be thought of as model experiments themselves. Rather, each provides a new initial steady state on which the model experiments are carried out. Sensitivity case 1 assumes a much higher proportion of C_{org} oxidation in the deep box (60%) than in the standard case (14%). Sensitivity case 2 assumes a low latitude $\text{CaCO}_3/\text{C}_{\text{org}}$ rain ratio of 0.2, rather than 0.4. Note for this case that the assumed river input must also be halved; otherwise, the "interglacial" steady state lysocline would be far too deep and atmospheric CO_2 far too low. Sensitivity case 3 combines cases 1 and 2. We have not attempted to tune the model to interglacial conditions using these different parameter sets (the change in the river input rate for sensitivity case being the one exception). The initial atmospheric CO_2 concentration for each of the sensitivity cases is given in table 2. The atmospheric CO_2 changes which occur for the model experiments have been run for each of the three sensitivity cases, for the closed, compensated, and open system cases (table 3). Because the standard interglacial

conditions vary among the sensitivity test cases, small (≤ 5 ppm) differences should not be considered significant.

For none of the sensitivity cases do we observe CaCO_3 compensation to significantly enhance the CO_2 decrease associated with model experiment 1, the simple increase in low latitude export production. The main reason for the modest CO_2 decrease in model experiment 1, as described above, is the atmospheric CO_2 effect of shoaling of the steady state lysocline. However, an equally important limitation on the CO_2 decrease is the lack of a dissolution event following a low latitude production increase. That is, an increase in low latitude production does not drive a major transient dissolution event in our model, over a wide range of assumed production/regeneration parameters.

In our experience, the lack of a significant dissolution event associated with enhanced low latitude production is a robust result for any model including intermediate-depth boxes. We have previously obtained similar results to those described here using a model of much simpler architecture [Lyle and Pisias, 1990]. By contrast, we and other workers do observe a transient dissolution event when high latitude production is increased simultaneously with the low latitude production increase [Boyle, 1988; Broecker and Peng, 1987]. Taken together, these results suggest that high latitude production is the major driver of the dissolution event observed in previous model experiments of enhanced productivity [e.g., Broecker and Peng, 1987].

Part 2: the Effect of Chemical Erosion

The lysocline response to productivity changes on glacial/interglacial time scales depends in part on the importance of chemical erosion, the reincorporation of buried CaCO_3 into the sediment mixed layer due to the dissolution-driven contraction of the mixed layer [Broecker *et al.*, 1991; Keir, 1984; Oxburgh and Broecker, 1993]. The dissolution of the exhumed CaCO_3 at the base of the lysocline would counteract an increase in the amount of burial above the lysocline, so that the net seafloor burial may remain in balance with the river input of dissolved CaCO_3 , and there may be no whole ocean reservoir change in ALK and DIC.

The compensated and rain-based open system cases encompass the range of possible lysocline effects of chemical erosion. If, in the real ocean, chemical erosion prevents changes in the steady state lysocline on glacial/interglacial time scales, then the compensated case is a good representation of how the ocean carbonate system will behave over glacial/interglacial cycles. If, on the other hand, chemical erosion does not have a strong buffering effect, then the open system case is a better representation. For changes in low latitude production, the difference between these two cases can be large. Furthermore, if chemical erosion prevents migration of the lysocline, then the lysocline depth cannot be used as a constraint on inferred CaCO_3 production rate changes.

To assess the importance of chemical erosion, we have carried out our three model experiments using the mixed layer open system model described above (respiratory dissolution not included here). We discuss only the time-course of lysocline shoaling which occurs upon the transition from the steady state of model experiment 2 to the standard interglacial case (figures 7, 8, 9). This is the most relevant experiment because (1) it involves lysocline shoaling, which can be affected by chemical erosion, and (2) it represents a transition into an interglacial period, which has a shorter typical duration than glacial periods. As explained in the Model Description section, we carry out these

experiments on a version of our ocean model in which the low latitude basins are combined, so that concentrations and fluxes of particles are the same in each basin¹.

A key parameter with regard to the importance of chemical erosion is the non-carbonate deposition rate. The deposition of non-carbonate material limits the importance of chemical erosion by producing a carbonate-poor sediment column under conditions of low preservation [Keir, 1984]. Therefore, the approach of the saturation horizon to a shallower steady state depends on the assumed non-carbonate deposition rate (figure 7). The case of 20 g/m²/yr is an unrealistically high deposition rate and is shown here to approximate the "no chemical erosion" case. A non-carbonate deposition rate of 2 g/m²/yr, which corresponds to about 0.25 cm/kyr, is in the range of observations [Archer, 1996]. For this deposition rate, the saturation horizon change is two-thirds complete after 10 kyrs (figure 7). Assuming a lower value of 0.2 g/m²/yr for the non-carbonate flux, chemical erosion slows the shoaling of the lysocline enough that the shoaling would not be complete on glacial-interglacial time scales. For this case, the saturation horizon change is <50% complete after 10 kyrs. As most estimates of non-carbonate deposition rate are in the range of 2 g/m²/yr, it appears that chemical erosion would not prevent the observable shoaling of the saturation horizon on glacial-interglacial time scales, although it would play a clear role in the timing of this shoaling.

Figure 8 gives a more detailed view of the effect of chemical erosion. It shows the ratio of CaCO₃ dissolution to CaCO₃ rain rate at different depths in the deep ocean for the transition from experiment 2 steady state back to the standard interglacial case, assuming non-calcite sedimentation rates of 20, 2 and 0.2 g/m²/yr. The rain is being completely dissolved at a ratio of 1. Note that the zone of chemical erosion is about 0.5 km below the

¹The river input rate for CaCO₃ was adjusted to put the steady state interglacial saturation depth at 3.5 km. In this case, the river input rate is identical to that of Keir (1988), 1.78×10^{13} moles Ca/yr. Because of differences in the rain-based and mixed layer open system cases, the lysocline responses are of slightly different amplitudes and thus not directly comparable.

saturation horizon; the exact depth is set by the combined effects of undersaturation and the fraction of CaCO_3 in the sediment mixed layer. A mixed layer that is composed mostly of non-carbonate sediment will allow for very little chemical erosion regardless of the fraction of CaCO_3 in underlying sediments, because the mixed layer cannot be condensed further by dissolution. Assuming a non-carbonate rain rate of $2 \text{ g/m}^2/\text{yr}$, the zone of $(\text{dissolution}/\text{rain}) > 2$ is less than 500 m thick and occurs only within the first 10 kyr. In contrast, the doubling of the CaCO_3 rain rate leads to a doubling of CaCO_3 burial rates over the entire depth interval above the lysocline. Thus, the excess dissolution due to chemical erosion is not comparable in area to the increase in CaCO_3 burial rate. As a result, the saturation horizon shoals despite the effect of chemical erosion.

CaCO_3 data from the equatorial Pacific suggest that the modern sediment column from this region is far from steady state, with mixed layer $\%\text{CaCO}_3$ decreasing gradually over the present interglacial [Oxburgh and Broecker, 1993]. This does not require that the alkalinity budget of the modern ocean is similarly far from steady state. For the same model experiment described above, we compare the time course of $\%\text{CaCO}_3$ change at three depths in the deep ocean with the time course of saturation horizon shoaling (figure 9). The $\%\text{CaCO}_3$ content of seafloor sediment at 4.6 km decreases rapidly as the saturation horizon shoals above this depth, reaching steady state in ~ 10 kyrs. At 3.6 km, near the depth to which the saturation horizon eventually shoals, $\%\text{CaCO}_3$ increases because of the increase in calcite rain rate. At 4 km depth, the time course of $\%\text{CaCO}_3$ combines these two changes, at first increasing, then decreasing. This results in a very gradual approach to steady state. Thus, the time scale over which a sediment column reaches its steady state calcite content depends strongly on its position relative to the migration of the saturation horizon. The degree of imbalance in the sedimentary CaCO_3 budget at any one depth provides little information about the degree to which the alkalinity budget of the ocean is out of steady state.

Part 3: the Effect of Sedimentary Respiration-Driven Dissolution

The model of CaCO_3 dissolution used in the comparison of closed and open system processes follows the traditional picture of bottom water undersaturation-driven dissolution [Broecker and Takahashi, 1978]. However, recent research on seafloor dissolution has made two major observations which call for a different picture [e.g., Archer *et al.*, 1989; Berelson *et al.*, 1994; Emerson and Bender, 1981; Hales *et al.*, 1994; Jahnke *et al.*, 1994; Martin and Sayles, 1996; Sayles, 1985]. First, the calcite dissolution rate constant appears to be slower than previously thought. Second, porewater undersaturation due to sediment respiration appears to be a significant driver of calcite dissolution.

In this section, we consider how these findings, when incorporated into the dissolution model, affect the response to our three model experiments. Each model experiment is repeated for the open system case, with two changes: (1) the dissolution rate constant is changed from 30/day to 1/day², and (2) a simple parameterization for sediment respiration-driven dissolution (respiratory dissolution) is included (see appendix 2). These two changes must be made together to produce a realistic model of the lysocline [Emerson and Archer, 1990]. Our comparison of model experiment responses for two dissolution models, one with respiratory dissolution and one without it, is analogous to that of Archer and Maier-Reimer [1994]. However, we focus on the relationship between the saturation horizon and the lysocline.

For our parameterization for respiration-driven dissolution, we have chosen a C_{org} oxidation profile within the sediments which tends to emphasize the importance of respiratory dissolution in the open ocean (see appendix 2). On the other hand, the CaCO_3

²We use a dissolution rate constant k_d of 1/day for consistency with Archer and Maier-Reimer (1994). However, we use 30/day for the case without respiratory dissolution rather than their value of 100/day, which generates an unrealistically sharp lysocline in our model.

rain rate of $18.5 \text{ g/m}^2/\text{yr}$ may be in the high end of estimates for CaCO_3 rain rate [Honjo, 1996]. Perhaps the most pertinent point is that 32% of the CaCO_3 rain dissolves at the saturation horizon in our standard interglacial case. This value is in the ranges of estimates from open ocean studies and modelling work, although it is probably in the lower end of the range in both of these regards [Archer, 1991a; Martin and Sayles, 1996].

One of the major determinants of the saturation horizon/lysocline relationship is the depth dependence of the C_{org} rain within the deep ocean. Sediment trap data and benthic oxygen flux data show a decrease with depth in the supply of C_{org} to the sediments, both in the open ocean [Berger *et al.*, 1988; Martin *et al.*, 1987; Suess, 1980] and on continental slopes [Smith, 1978]. This depth dependence of the C_{org} rain explains the weakness of the depth dependence in measured rates of respiratory dissolution [e.g., Hales *et al.*, 1994] (appendix 2, figure AII-3). We first show the model experiments under the assumption that the C_{org} rain is independent of depth within the deep boxes (1.5-6.5 km). Then we show the result of including a relatively minor C_{org} rain depth dependence, focussing on model experiment 3.

The atmospheric CO_2 and saturation depth changes are shown in figure 10. Experiment 1, the ~30% increase in low latitude production, is essentially unaffected when respiratory dissolution and a slower rate constant are incorporated into the model, with the saturation depth shoaling by 400 m and atmospheric CO_2 decreasing by 16 ppm. Experiment 2, halving the low latitude $\text{CaCO}_3/C_{\text{org}}$ rain ratio, results in a 14 ppm greater CO_2 decrease (68 ppm rather than 54 ppm) and a 600 m greater deepening of the saturation horizon when respiratory dissolution and a slower rate constant are incorporated into the model. Experiment 3, deepening the C_{org} water column regeneration profile, results in a 55 ppm CO_2 decrease when respiratory dissolution and a slower rate constant are incorporated into the model, as opposed to a 16 ppm decrease without these changes. This large enhancement is driven by a 1.4 km increase in the ocean-average saturation depth.

These results are consistent with those of *Archer and Maier-Raimer* [1994] for similar experiments. Because of the large CO_2 decreases which model experiments 2 and 3 cause when respiratory dissolution is included, *Archer and Maier-Raimer* [1994] suggest that these types of changes represent viable mechanisms for lowering atmospheric CO_2 levels during the last glacial.

While information about the glacial lysocline is incomplete, the bulk of the data suggests no large difference in the ocean-average lysocline depth between the modern and glacial oceans [*Catubig et al.*, 1994]. Given the large increases in the saturation depth associated with experiments 2 and 3, a key implication of the *Archer and Maier-Raimer* [1994] hypothesis is that an increase in the importance of respiratory dissolution would decouple the glacial saturation horizon from the lysocline, so that the saturation horizon could deepen by a degree that would not be evident in the $\%\text{CaCO}_3$ distribution for the last glacial. We address this prediction by comparing the changes in saturation depth with the coincident changes in the $\%\text{CaCO}_3$ of surface sediments on the deep seafloor.

Figure 11 shows the change in surface sediment $\%\text{CaCO}_3$ and CaCO_3 burial rate for each of the three model experiments, with respiratory dissolution active. For model experiments 2 and 3, the lysocline deepens by 800 m or more. This lysocline deepening can be understood as a result of the importance of bottom water saturation state to both bottom water-driven dissolution and respiration-driven dissolution [*Archer*, 1991a]. In these experiments, respiration-driven dissolution has not become so great as to dissolve all CaCO_3 above the saturation horizon.

The lysocline deepening that occurs in model experiments 2 and 3 can also be understood from the perspective of the river/burial CaCO_3 balance. These experiments enhance the relative importance of respiratory dissolution, making CaCO_3 burial rates less depth-dependent, with proportionally more of the dissolution occurring on the shallow seafloor (figure 11e, 11f). With less CaCO_3 burial in the shallow ocean, there must be an

increase in CaCO_3 burial rates in the deeper ocean. As the fraction of CaCO_3 in open ocean sediments does not drop off significantly until the burial rate is $\leq 25\%$ of the CaCO_3 rain rate to the seafloor, the "smearing out" of CaCO_3 burial, with lower burial rates over a larger depth range, results in a significant deepening of the lysocline. For instance, in model experiment 3, the amount of the CaCO_3 rain that dissolves at the saturation horizon increases from 30% to 80% (figure 11 f). The depth dependence of CaCO_3 burial is greatly reduced in this case, leading to about 0.8 km of lysocline deepening (figure 11 c).

Once CaCO_3 dissolution is controlled primarily by organic matter respiration, it is possible to deepen the saturation horizon without causing a significant deepening of the lysocline. Model experiment 3', in which the fraction of C_{org} reaching the deep box is increased to 60% (rather than to 40% in experiment 3), causes only a 0.3 km greater deepening of the lysocline than occurs in experiment 3, although the saturation horizon deepens by an additional 1.2 km (figure 11 c). The depth dependence of CaCO_3 burial is already very gradual in model experiment 3. The higher rate of respiratory dissolution in model experiment 3' does not significantly change this pattern (figure 11 f), so that there is no additional mass balance feedback driving the lysocline to deepen further. As a result, the increase in the C_{org} rain rate from experiment 3 to experiment 3' counteracts the effect of an increase in the saturation depth, resulting in little net change in the depth of the lysocline.

The conditions of model experiment 3' are fairly extreme. The $\text{CaCO}_3/C_{\text{org}}$ ratio of the rain onto the seafloor (to be distinguished from the rain out of the surface ocean) is 0.5 in experiment 3', whereas typical values for this ratio in the greater part of the modern subtropical ocean appear to range between 1 and 2 [Archer, 1991a; Honjo, 1996; Honjo *et al.*, 1995; Honjo and Manganini, 1992]. The transition from modern conditions to those conditions require a major deepening of the whole ocean lysocline.

While decreasing the CaCO_3 rain rate (model experiments 2 and 2') has the same general effect on the saturation depth as increasing the C_{org} rain rate (model experiments 3

and 3'), these two mechanisms do not have identical effects on the lysocline/saturation horizon relationship. Model experiment 2', a decrease in the $\text{CaCO}_3/\text{C}_{\text{org}}$ rain ratio out of the surface ocean from 0.4 to 0.15 (rather than to 0.2 for experiment 2), still has not managed to separate the lysocline from the saturation horizon. The low latitude CaCO_3 rain cannot be less than 0.15 in our model; below this value, there is not enough CaCO_3 rain to balance the riverine input of alkalinity. Thus, in our model, a simple decrease in the CaCO_3 rain rate cannot cause a separation of the lysocline from the saturation horizon.

We have assumed to this point that the amount of C_{org} being oxidized in sediments is independent of depth below 1.5 km (i.e., in the deep boxes). Here, we repeat model experiments 3 and 3', in this case assuming a depth dependence of the C_{org} rain to deep sea sediments. We use the C_{org} rain depth dependence of *Archer and Maier-Raimer* [1994], adjusted for the depth dependence in the CaCO_3 rain assumed in their model and normalized to give the same C_{org} rain rate at 3.5 km as in the case of no C_{org} rain depth dependence (appendix 2 figure AII-2). The C_{org} rain depth dependence yields a 30% lower C_{org} rain rate at 6.5 km than at 1.5 km (the top of the deep boxes), which is gradual in comparison to the decrease defined by the equations of *Suess* [1980], *Martin et al.* [1987], and *Berger et al.* [1988].

Even with this relatively subtle depth dependence of the C_{org} rain, we see a significant change in the model response. When this depth dependence is included, the lysocline deepening for both model experiments 3 and 3' is only slightly less than the deepening of the saturation horizon (figure 12a). This stronger coupling between the lysocline and the saturation horizon compared with the results without the C_{org} depth dependence is due to the increase in the fraction of calcite dissolution on the shallow sea floor relative to deeper dissolution, near and below the saturation horizon (figure 12b). Respiratory dissolution well above the saturation horizon causes both the saturation horizon and the lysocline to deepen because it increases the area of seafloor burial required to match

the river inputs of ALK and DIC. In contrast, respiratory dissolution at and below the saturation horizon tends to shoal the lysocline relative to the saturation horizon. By adding a depth dependence to C_{org} rain in the deep boxes, we increase the amount of dissolution on the shallow sea floor relative to dissolution near the saturation horizon. This reduces the tendency for respiratory dissolution to decouple the saturation horizon and the lysocline. This effect would be particularly important for the hypothetical case in which the saturation horizon is shifted to very great depths [Sanyal *et al.*, 1995].

In summary, our model experiments suggest that deepening of the saturation horizon due to an increase in respiratory dissolution leads to a significant deepening of the lysocline as well. For what we consider to be our most realistic model of respiration-driven dissolution (i.e., including a depth-dependent C_{org} rain in the deep boxes), the lysocline/saturation horizon decoupling is insignificant relative to the overall lysocline deepening (figure 12). Even under the most favorable conditions, the lysocline deepens by at least a kilometer in the hypotheses explored by Archer and Maier-Raimer [1994] and Sanyal *et al.* [1995].

Part 4: Coupled Changes in the Quantity and Characteristics of Low Latitude Production

Neither an increase in low latitude production, a change in its $\text{CaCO}_3/\text{C}_{\text{org}}$ rain ratio, nor a deepening of C_{org} regeneration, when occurring alone, could have lowered atmospheric CO_2 to glacial levels without causing unobserved changes in the depth of the steady state lysocline. As we have shown, increasing low latitude production causes the steady state lysocline to shoal (model experiment 1), while decreasing the rain ratio of this production causes a lysocline deepening (model experiment 2). Here, we combine enhanced production with a decreased rain ratio to address whether the combination of these different changes causes a significant CO_2 decrease without violating the paleoceanographic observation of a constant lysocline depth.

Such a simultaneous change is certainly possible given current knowledge of the controls on the characteristics of export production. The $\text{CaCO}_3/\text{C}_{\text{org}}$ ratio of the biogenic flux is anticorrelated with production rates in the modern ocean [Tsunogai and Noriki, 1991]. As a result, an increase in low latitude production, such as that resulting from model experiment 1, may be associated with a decrease in the $\text{CaCO}_3/\text{C}_{\text{org}}$ rain ratio [Keir and Berger, 1983].

It appears that the coupling of an increase in low latitude production with changes in production characteristics could lower atmospheric CO_2 to observed glacial levels without leading to large changes in the ocean-average depth of the saturation horizon (figure 13). A halving of the rain ratio and a whole ocean phosphate increase of ~50% cause atmospheric CO_2 to decrease by 80 ppm, without any change in the ocean's average saturation depth. If the glacial saturation horizon were taken to be shallower or deeper than the modern horizon, the range of acceptable parameter values would shift accordingly. One unrealistic aspect of the model response to these combined changes is the strengthening of Atlantic-to-

Pacific $[\text{CO}_3^{2-}]$ gradient, given the standard case circulation scheme. However, as was mentioned for previously, a weakening of NADW formation during glacial times would weaken this interbasin gradient [Boyle and Keigwin, 1982].

Figure 13 was generated assuming no respiratory dissolution. Both sets of contours would change if respiratory dissolution were included. Specifically, a given decrease in the rain ratio would cause both a larger CO_2 decrease and a greater deepening of the saturation horizon, so that there would be a change in the balance between production rate and rain ratio giving a constant saturation depth. While the quantitative aspects of the balance depend on the processes included, the basic requirement of a balance remains.

Conclusions

The effect of a low latitude biological production change on the ocean carbon cycle is separable into its closed and open system components. The open system component is composed of (1) the transient compensation of deep sea CaCO_3 preservation to an externally forced change in deep ocean $[\text{CO}_3^{-2}]$ and (2) the adjustment of deep ocean $[\text{CO}_3^{-2}]$ to achieve a steady state balance between riverine input and seafloor burial of CaCO_3 . This second process leads to a link between biological CaCO_3 production and the depth of the lysocline.

The CaCO_3 production/lysocline link is strong enough that a significant change in low latitude production with an accompanying change in CaCO_3 production should be recognizable in paleoceanographic records of lysocline depth. On the other hand, an increase in low latitude production alone does not drive a transient dissolution event, because the biogenic rain pumps ALK as well as DIC into the deep ocean. As a result, a simple increase in low latitude production cannot explain lower atmospheric CO_2 levels during the last glacial. Such an increase would have had a limited impact on atmospheric CO_2 and would have resulted in a lysocline shoaling, contrary to paleoceanographic data suggesting a fairly constant lysocline through time. Changes in the nature of low latitude export production, specifically, a decrease in its $\text{CaCO}_3/C_{\text{org}}$ ratio or a deepening of the C_{org} water column regeneration profile, can lower CO_2 significantly. However, they cannot lower atmospheric CO_2 to glacial levels without causing a large (>1 km) deepening of the steady state lysocline.

Our model study of chemical erosion suggests that it would not prevent changes in the steady state lysocline on glacial/interglacial time scales; the first two thirds of the whole ocean alkalinity change would probably have occurred within 10 kyrs. As a result, the production/lysocline link applies to these time scales, as does its effect on atmospheric

CO₂. Steady state is more slowly achieved for the calcite content of surface sediments, at least at some depths.

The inclusion of respiratory dissolution and a slower dissolution rate constant does not significantly change the lysocline effect of a low latitude production increase. Respiratory dissolution does enhance the CO₂ decrease due to a rain ratio decrease, and it greatly enhances the effect of a deepening in the C_{org} regeneration profile, as found by *Archer and Maier-Raimer* [1994]. However, respiratory dissolution does not generally decouple the lysocline from the saturation horizon. As a result, %CaCO₃ data for the last glacial remains an important constraint, arguing against large changes in the depth of the saturation horizon.

Assuming no change in the steady state lysocline between glacial and interglacial periods, our results suggest that the only suitable low latitude production mechanism to lower atmospheric CO₂ without violating glacial %CaCO₃ data involves the coupling of oceanographic changes, such as an increase in export production and a decrease in its CaCO₃/C_{org} rain ratio. Because of the very low CaCO₃/C_{org} rain ratio of high latitude production, hypotheses about changes in high latitude production are not similarly constrained by the history of the steady state lysocline.

Appendix 1:

Comparison of Standard Case with CYCLOPS and GEOSECS

The standard conditions of our interglacial case for the rain-based model are given in table AI-1. In the figures which accompany this appendix, we compare these standard conditions to the Standard Ocean Circulation (SOC) of CYCLOPS ([Keir, 1988], figure AI-1) and to basin-wide averages based on averaging of GEOSECS data by [Takahashi *et al.*, 1981] (figures AI-2, AI-3). For this study, the most relevant components are DIC, ALK, and phosphate. The ^{13}C and ^{14}C distributions will be discussed in [Sigman and Lehman, in prep.]. The CYCLOPS values used here are based on the standard case without the evaporation/precipitation cycle built into the model of [Keir, 1988], because we do not include this cycle.

Figure AI-1 is a DIC and ALK comparison of CYCLOPS SOC to our standard interglacial case. The agreement for the two models with respect to phosphate is exact, so no comparison plot is shown. The clear ALK and DIC offset between the two standard cases is due to a slight difference in the whole ocean reservoir of “dissolved CaCO_3 ” ($5.6 \mu\text{mol/kg}$ DIC, $11.2 \mu\text{eq/kg}$ ALK). Disagreements of this level are to be expected among models including deep sea calcite preservation; there are many potential sources for this disagreement, for instance, slight hypsometric differences.

For the rain-based model, we adopt the calcite saturation equation of [Broecker and Takahashi, 1978], as used by [Keir, 1988]. At one point, we attempted to change over to the calcite saturation equation of [Ingle, 1975], for consistency with the mixed layer model (see below). However, we found that our model reached input/output balance at a much higher whole ocean alkalinity than in [Keir, 1988]. In order to match [Keir, 1988], we were forced to lower the river input rate by 40%, from $1.78 \times 10^{13} \text{ molCa}^{+2}/\text{yr}$ [Keir, 1988] to $1.06 \times 10^{13} \text{ molCa}^{+2}/\text{yr}$. These two values bracket the range of estimates for the river input of dissolved CaCO_3 used in carbon cycle models [Archer and Maier-Raimer, 1994;

Sundquist, 1990]. With some important exceptions, the model results using the calcite saturation equation of [*Ingle*, 1975] and a lower river input were insignificantly different from the results using that of [*Broecker and Takahashi*, 1978]. However, for the sake of consistency with [*Keir*, 1988], we have decided to show the model results using the calcite saturation equation of [*Broecker and Takahashi*, 1978] for the rain-based open system case, assuming the same river input rate as [*Keir*, 1988], 1.78×10^{13} molCa⁺²/yr.

Figure AI-2 is a DIC and ALK comparison of GEOSECS averages [*Takahashi et al.*, 1981] to our standard interglacial case. Note that the GEOSECS averages do not have exactly the same boxes as our model or CYCLOPS, so that trends, rather than individual points, should be compared. While the agreement is generally good, our model surface boxes (and those of CYCLOPS) have a lower DIC and ALK than the GEOSECS averages. A plot of DIC vs. phosphate (figure AI-3) shows that much of this disagreement is due to the model assumption of zero phosphate in the low latitude surface, which stretches to roughly 50° latitude in both hemispheres.

In the mixed-layer open system model, we made several changes away from the rain-based open system case. First, the calcite saturation equations of [*Ingle*, 1975] were used, for consistency with the off-line sediment geochemistry model which was used to parameterize bottom water-driven and sediment respiration-driven dissolution for the mixed layer model (see appendix II). Second, the low latitude basins were combined into one, to simplify explanation of the model results. The river input was increased from that of [*Keir*, 1988] by 1% to give an average low latitude deep ocean saturation depth of 3.5 km. Under these conditions, atmospheric CO₂ is 283.7 ppmV, and deep ocean ALK and DIC are 2428 µeq/kg and 2305 µmol/kg, respectively. When respiratory dissolution and a lower dissolution rate constant were added into the mixed layer model, the river input had to be lowered by 12% from Keir's value to to give an average low latitude deep ocean saturation depth of exactly 3.5 km. Under these conditions, atmospheric CO₂ is 285.7 ppmV, and

deep ocean ALK and DIC are 2428 $\mu\text{eq/kg}$ and 2304 $\mu\text{mol/kg}$, respectively. The river input rate or calcite rain rate must be “tuned” significantly in any modelling exercise which compares different CaCO_3 input/output models (e.g., [Archer and Maier-Raimer, 1994]). This situation underscores the importance of measured carbonate parameters (eg., the river input rate of Ca^{+2} , the calcite solubility constant) to models of the oceanic CaCO_3 balance.

Appendix II:

Parameterizing Calcite Dissolution in the Mixed Layer Sediment Model

Rather than incorporating an explicit model of dissolution into an ocean model (as in [Archer and Maier-Raimer, 1994]), we have generated multivariate polynomial fits to output from a sediment geochemistry model [Martin and Sayles, 1996] and used these fits in the ocean box model. As we wish to run the model both with and without the effects of sediment respiration-driven dissolution, we treat sediment respiration-driven dissolution and bottom water-driven dissolution as additive components of total dissolution [Martin and Sayles, 1996], with independent parameterizations for these two types of dissolution. Bottom water-driven dissolution is the dissolution which occurs if there is no C_{org} respiration within the sediments. Sediment respiration-driven dissolution is defined as the difference between the total dissolution and bottom water-driven dissolution.

The variables incorporated into the parameterization for sediment respiration-driven dissolution are (1) the bottomwater saturation state, (2) the C_{org} rain rate, and (3) the fraction of $CaCO_3$ in the sediment. Variables which were considered in our study but which are not included in the multivariate fit are (1) the calcite dissolution rate constant, k_d [Keir, 1980], and (2) the oxidation profile of C_{org} within the sediment column. The same variables, except for those relating to C_{org} , are considered in the parameterization for bottom water-driven dissolution. The explicit sediment geochemistry model is discussed in [Martin and Sayles, 1996].

For bottom-water driven dissolution, we assume an equation of the form

$$Dissolution = K_{bw} * ([CO_3^{-2}]_{sat} - [CO_3^{-2}]_{bw})^n * F_{ca}^m \quad [Keir, 1988]$$

where: K_{bw} is the coefficient relating bottom water undersaturation to dissolution rate,

$[CO_3^{-2}]_{sat}$ is carbonate ion at saturation for calcite [Ingle, 1975],

$[CO_3^{-2}]_{bw}$ is the carbonate ion concentration of the bottom water,

n is the exponent relating bottom water undersaturation to dissolution rate,

F_{ca} is the weight fraction of calcite in the sediment mixed layer,

m is the exponent relating the weight fraction of calcite to dissolution rate.

By running the sediment geochemistry model over a range of undersaturation (for ~100% CaCO_3), we solve for n and K_{bw} . Running the model over a range of % CaCO_3 (by varying the CaCO_3 rain rate) for several degrees of undersaturation, we find that $m \approx 0.5$. This appears to be roughly independent of variation in other parameters. The same square root dependence of dissolution rate on % CaCO_3 was used in [Keir, 1988].

The bottom water dissolution rate appears to be logarithmically dependent on the calcite dissolution rate constant, k_d . As we consider two different dissolution rate constants, 30/day and 1/day, in our investigation of respiration-driven dissolution, we must design bottomwater-driven dissolution equations for both of these cases. For a k_d of 1/day, with $[\text{CO}_3^{-2}]$ in units of mol/kg, the equation is

$$\text{Dissolution} = 3.76 * 10^{12} * ([\text{CO}_3^{-2}]_{\text{sat}} - [\text{CO}_3^{-2}]_{\text{bw}})^{2.35} * F_{ca}^{0.5}$$

For a k_d of 30/day, the equation is

$$\text{Dissolution} = 20.36 * 10^{12} * ([\text{CO}_3^{-2}]_{\text{sat}} - [\text{CO}_3^{-2}]_{\text{bw}})^{2.35} * F_{ca}^{0.5}$$

The value of 2.35 derived for n is similar to the value of 2.75 used by [Keir, 1988] in his CYCLOPS model. This is encouraging, as we have determined these values independently.

To parameterize respiratory dissolution, we have run the dissolution model over a range of (1) saturation state and (2) C_{org} rain rate. The dissolution rate constant used is 1/day (after [Archer and Maier-Raimer, 1994]) and % CaCO_3 is ~100% (see below). The C_{org} oxidation profile is taken from a site of relatively deep C_{org} oxidation in the Ceara Rise study of [Martin and Sayles, 1996] (site H). A deep C_{org} oxidation profile places DIC production far enough below the sediment surface to prevent carbonate ion from diffusing

in from bottom water, so that our use of a deep oxidation profile represents a significant bias toward higher respiration-driven dissolution rates (W. Martin, unpublished).

From these results, we subtract the dissolution rate output calculated assuming no C_{org} rain. This difference is taken as the respiration-driven dissolution component (figure AII-1) and is fitted to a 15-term polynomial function of saturation state and C_{org} rain rate. When this parameterization is incorporated into the ocean box model, dissolution at the saturation horizon is 32% of the calcite rain (figure AII-2).

We find that the respiratory dissolution rate, unlike the bottom water-driven dissolution, is essentially independent of % $CaCO_3$ until % $CaCO_3$ is below ~10%. Thus, no dependency on % $CaCO_3$, $CaCO_3$ rain rate, or non-carbonate rain rate is needed for the sediment respiration-driven component of dissolution.

The polynomial fit was made for the range of saturation states from +40 to -10 $\mu\text{mol/kg}$ (figure AII-1). For more supersaturated and undersaturated conditions, the model results are extrapolated using the first derivative of the polynomial fits at the boundary.

In our study of respiratory dissolution, we consider two cases for the C_{org} rain rate to the seafloor. In the first case, we assume no depth dependence for the amount of C_{org} which rains onto the seafloor (within the deep boxes). In the second case, we use the C_{org} rain depth dependence of [Archer and Maier-Raimer, 1994], adjusted for a depth dependence which they include for the $CaCO_3$ rain rate, and normalized to give the same C_{org} rain rate at 3.5 km as the case without depth dependence (figure AII-3). The resultant C_{org} rain depth dependence yields a 30% lower C_{org} rain rate at 6.5 km than at 1.5 km. This C_{org} rain decrease is gradual in comparison to the decrease defined by the equations of [Suess and Muller, 1980], [Martin et al., 1987], and [Berger et al., 1988]. Its effect on the depth dependence of seafloor $CaCO_3$ dissolution in the standard case is shown in figure AII-2.

Acknowledgements

We thank R. Keir for his help with the CYCLOPS model conditions. This work benefited from discussions with E. Boyle and D. Archer. D. Sigman was supported by the NSF Graduate Fellowship Program and the JOI/USSAC Ocean Drilling Graduate Fellowship Program.

References

- Anderson, L.A., and J.L. Sarmiento, Redfield ratios of remineralization determined by nutrient data analysis, *Global Biogeochemical Cycles*, 8 (1), 65-80, 1994.
- Anderson, R.F., Y. Lao, M.Q. Fleisher, and F. Marcantonio, New evidence for dissolution control of carbonate cycles in equatorial Pacific sediments, in *5th International Conference on Paleoceanography*, pp. 120, Halifax, 1995.
- Archer, D., Modeling the calcite lysocline, *Journal of Geophysical Research*, 96, 17037-17050, 1991a.
- Archer, D., A data-driven model of the global calcite lysocline, *Global Biogeochemical Cycles*, 10 (3), 511-526, 1996.
- Archer, D., S. Emerson, and C.R. Smith, Dissolution of calcite in deep-sea sediments: pH and O₂ microelectrode results, *Geochimica et Cosmochimica Acta*, 53 (11), 2831, 1989.
- Archer, D., and E. Maier-Raimer, Effect of deep-sea sedimentary calcite preservation on atmospheric CO₂ concentration, *Nature*, 367, 260-263, 1994.
- Archer, D., Equatorial Pacific calcite preservation cycles: production or dissolution?, *Paleoceanography*, 6, 561-571, 1991b.
- Barnola, J.M., D. Raynaud, Y.S. Korotkevitch, and C. Lorius, Vostok ice core provides 160,000-year record of atmospheric CO₂, *Nature*, 329, 408-414, 1987.
- Berelson, W.M., D.E. Hammond, J. McManus, and T.E. Kilgore, Dissolution kinetics of calcium carbonate in equatorial Pacific sediments, *Global Biogeochemical Cycles*, 8, 219-235, 1994.
- Berger, W.H., Planktonic foraminifera: selective solution and the lysocline, *Marine Geology*, 8, 111-138, 1970.
- Berger, W.H., K. Fisher, C. Lai, and G. Wu, Ocean carbon flux: global maps of primary production and export production, in *Biogeochemical Cycling and Fluxes Between the Deep Euphotic Zone and Other Realms*, edited by C.R. Agegian, pp. 131-176, Silver Spring, Md., 1988.
- Billet, D.S.M., R.S. Lampitt, A.L. Rice, and R.F.C. Mantoura, Seasonal sedimentation of phytoplankton to the deep-sea benthos, *Nature*, 302, 520-522, 1983.
- Bishop, J.K., R.W. Collier, D.R. Ketten, and J.M. Edmond, The chemistry, biology and vertical flux of particulate matter from the upper 1500 m of the Panama Basin, *Deep Sea Research*, 27, 615-640, 1980.
- Boyle, E.A., The role of vertical chemical fractionation in controlling late quaternary atmospheric carbon dioxide, *Journal of Geophysical Research*, 93 (C12), 15,701-15,714, 1988.

Boyle, E.A., and L.D. Keigwin, Deep circulation of the North Atlantic for the last 200,000 years: geochemical evidence, *Science*, 218, 784-787, 1982.

Broecker, W.S., Ocean chemistry during glacial time, *Geochimica et Cosmochimica Acta*, 46, 1689-1706, 1982.

Broecker, W.S., M. Klas, E. Clark, G. Bonani, S. Ivy, and W. Wolfli, The influence of CaCO_3 dissolution on core top radiocarbon ages for deep-sea sediments, *Paleoceanography*, 6 (5), 593-608, 1991.

Broecker, W.S., and T.-H. Peng, The role of CaCO_3 compensation in the glacial to interglacial atmospheric CO_2 change, *Global Biogeochemical Cycles*, 1 (1), 15-29, 1987.

Broecker, W.S., and T.H. Peng, The climate-chemistry connection, in *Climate Processes and Climate sensitivity*, edited by J.E. Hansen, and T. Takahashi, pp. 327-336, A.G.U., Washington, D.C., 1984.

Broecker, W.S., and T. Takahashi, The relationship between lysocline depth and in situ carbonate ion concentration, *Deep-Sea Research*, 25, 65-95, 1978.

Catubig, N.R., D.E. Archer, W.R. Howard, P.B. deMenocal, and P.N. Froelich, an atlas of LGM calcium carbonate concentrations in deep sea sediments and implications for the deep sea burial rate, *EOS*, 75 (44), 367, 1994.

Crowley, T.J., Calcium carbonate preservation patterns in the central North Atlantic during the last 150,000 years, *Marine Geology*, 51, 1-14, 1983.

Crowley, T.J., Late Quaternary carbonate changes in the North Atlantic and Atlantic/Pacific comparisons, in *The Carbon Cycle: Natural Variations Archean to Present*, edited by E.T. Sundquist, and W.S. Broecker, pp. 271-284, American Geophysical Union, Washington, D.C., 1985.

Cullen, J.J., Hypotheses to explain high-nutrient conditions in the open sea, *Limnology and Oceanography*, 36 (8), 1578-1599, 1991.

Curry, W.B., and G.P. Lohmann, Late Quaternary carbonate sedimentation at the Sierra Leone Rise (eastern equatorial Atlantic Ocean), *Marine Geology*, 70, 223-250, 1986.

Dymond, J., and M. Lyle, Flux comparisons between sediments and sediment traps in the eastern tropical Pacific: Implications for atmospheric CO_2 variations during the Pleistocene, *Limnology and Oceanography*, 30 (4), 699-712, 1985.

Edmond, J.M., On the dissolution of carbonate and silicate in the deep ocean, *Deep-Sea Research*, 21, 455-480, 1974.

Emerson, S., and D. Archer, Calcium carbonate preservation in the ocean., *Philosophical Transactions of the Royal Society of London A*, 331, 29-40, 1990.

Emerson, S., and M.L. Bender, Carbon fluxes at the sediment-water interface of the deep sea: calcium carbonate preservation, *Journal of Marine Research*, 39, 139-162, 1981.

- Emerson, S., R. Jahnke, M. Bender, P. Froelich, G. Klinkhammer, C. Bowser, and G. Setlock, Early diagenesis in sediments from the eastern equatorial Pacific, I. Pore water nutrient and carbonate results, *Earth and Planetary Science Letters*, 49, 57-80, 1980.
- Farrell, J.W., Late Neogene paleoceanography of the central equatorial Pacific: evidence from carbonate preservation and stable isotopes, Ph.D. thesis, Brown University, 1991.
- Farrell, J.W., and W.L. Prell, climate change and CaCO_3 preservation: an 800,000 year bathymetric reconstruction from the central equatorial Pacific Ocean, *Paleoceanography*, 4, 447-466, 1989.
- Hales, B., S. Emerson, and A. David, Respiration and dissolution in the sediments of the western North Atlantic: estimates from models of *in situ* microelectrode measurements of porewater oxygen and pH, *Deep-Sea Research*, 41, 695-719, 1994.
- Honjo, S., Fluxes of particles to the interior of the open oceans, in *Particle Flux in the Ocean*, edited by V. Ittekkot, P. Schafer, S. Honjo, and P.J. Depetris, Wiley Interscience, Munich, 1996.
- Honjo, S., J. Dymond, R. Collier, and S.J. Manganini, Export production of particles to the interior of the equatorial Pacific Ocean during the 1992 EqPac experiment, *Deep - Sea Research Part II - Topical Studies in Oceanography*, 42 (2-3), 831-870, 1995.
- Honjo, S., and S.J. Manganini, Particle fluxes to the interior of the North Atlantic Ocean studied at two JGOFS stations: 34N 21W and 47N 20W, *Deep-Sea Res.*, 40(1/2), 587-607, 1992.
- Howard, W.R., and W.L. Prell, Late Quaternary CaCO_3 production and preservation in the Southern Ocean: implications for oceanic and atmospheric carbon cycling, *Paleoceanography*, 9, 453-482, 1994.
- Ingle, S.E., Solubility of calcite in the ocean, *Marine Chemistry*, 3, 301-319, 1975.
- Jahnke, R.A., D.B. Craven, and J.-F. Gaillard, The influence of organic matter diagenesis on CaCO_3 dissolution at the deep-sea floor, *Geochimica et Cosmochimica Acta*, 58, 2799-2809, 1994.
- Karlin, R., M. Lyle, and R. Zahn, Carbonate variations in the northeast Pacific during the late Quaternary, *Paleoceanography*, 7, 43-61, 1992.
- Keir, R., and W. Berger, Atmospheric CO_2 content in the last 120,000 years: the phosphate extraction model, *J. Geophys. Res.*, 88, 6027-6038, 1983.
- Keir, R.S., The dissolution kinetics of biogenic calcium carbonates in seawater, *Geochimica et Cosmochimica Acta*, 44, 241-252, 1980.
- Keir, R.S., Recent increase in Pacific CaCO_3 dissolution: a mechanism for generating old ^{14}C ages, *Marine Geology*, 59, 227-250, 1984.

- Keir, R.S., Is there a component of Pleistocene CO₂ change associated with carbonate dissolution cycles?, *Paleoceanography*, 10 (5), 871-880, 1995.
- Keir, R.S.P., 3, 413-445, 1988, On the late Pleistocene ocean geochemistry and circulation, *Paleoceanography*, 3, 413-445, 1988.
- Knox, F., and M. McElroy, Changes in atmospheric CO₂ influence of the marine biota at high latitude, *J. Geophys. Res.*, 89, 4629-4637, 1984.
- Lyle, M., and N. Pisias, Ocean circulation and atmospheric CO₂ changes: coupled use of models and paleoceanographic data, *Paleoceanography*, 5, 15-41, 1990.
- Martin, J.H., G.A. Knauer, D.M. Karl, and W.W. Broenkow, VERTEX: carbon cycling in the northeast Pacific, *Deep-Sea Research*, 34 (2), 267-285, 1987.
- Martin, W.R., and F.L. Sayles, CaCO₃ dissolution in sediments of the Ceara Rise, western equatorial Atlantic, *Geochimica et Cosmochimica Acta*, 60 (2), 243-263, 1996.
- Menard, H.W., and S.M. Smith, Hypsometry of ocean basin provinces, *Journal of Geophysical Research*, 71, 4305-4325, 1966.
- Milliman, J.D., *Marine Carbonates*, 375 pp., Springer-Verlag, New York, 1974.
- Milliman, J.D., Production and accumulation of calcium carbonate in the ocean: budget of a nonsteady state, *Global Biogeochemical Cycles*, 7, 927-957, 1993.
- Mitchell, B.G., E.A. Brody, O. Holm-Hansen, C. McLain, and J. Bishop, Light limitation of phytoplankton biomass and macronutrient utilization in the Southern Ocean, *Limnology and Oceanography*, 36 (8), 1662-1677, 1991.
- Opdyke, B.N., and J.C.G. Walker, Return of the coral reef hypothesis: basin to shelf partitioning of CaCO₃ and its effect on atmospheric CO₂, *Geology*, 20, 733-736, 1992.
- Oxburgh, R., and W.S. Broecker, Pacific carbonate dissolution revisited, *Palaeo., Palaeo., and Palaeo.*, 103, 31-40, 1993.
- Peterson, L.C., and W.L. Prell, Carbonate preservation and rates of climate change: An 800 kyr record from the Indian Ocean, in *The Carbon Cycle and Atmospheric CO₂: Natural Variations Archean to Present*, edited by E.T. Sundquist, and W.S. Broecker, A.G.U., Washington, D.C., 1985.
- Sanyal, A., N.G. Hemming, G.N. Hanson, and W.S. Broecker, Evidence for a higher pH in the glacial ocean from Boron isotopes in foraminifera, *Nature*, 373, 234-236, 1995.
- Sarmiento, J.L., and J.R. Toggweiler, A new model for the role of the oceans in determining atmospheric pCO₂, *Nature*, 308, 621-624, 1984.
- Sayles, F.L., CaCO₃ solubility in marine sediments: Evidence for equilibrium and non-equilibrium behavior., *Geochimica et Cosmochimica Acta*, 49, 877-888, 1985.

Smith, K.L., Jr., Benthic community respiration in the N.W. Atlantic Ocean: in situ measurements from 40 to 5200 m., *Marine Biology*, 47, 337-347, 1978.

Suess, E., Particulate organic carbon flux in the oceans- surface productivity and oxygen utilization, *Nature*, 288, 260-263, 1980.

Sundquist, E.T., Geological perspectives in carbon dioxide and the carbon cycle, in *The Carbon Cycle and Atmospheric CO₂: Natural Variations Archean to Present*, edited by E.T. Sundquist, and W.S. Broecker, pp. 5-59, American Geophysical Union, 1985.

Sundquist, E.T., Influence of deep-sea benthic processes on atmospheric CO₂, *Philosophical Transactions of the Royal Society*, in press, 1990

Takahashi, T., W.S. Broecker, and A.E. Brainbridge, The alkalinity and total carbon dioxide concentration in the world oceans, in *Carbon Cycle Modelling*, edited by B. Bolin, pp. 159-199, 1981.

Tsunogai, S., and S. Noriki, Particle fluxes of carbonate and organic carbon in the ocean. Is the marine biological activity working as a sink of atmospheric carbon?, *Tellus*, 43b, 256-266, 1991.

Low latitude Carbon cycle parameters used by different models

	Ca/Corg of Low Latitude Production	%Corg exported to deep boxes	%CaCO ₃ exported to deep boxes
This work, Standard Case (taken from Keir, 1988)	0.4^a	16	80
Broecker and Peng (1986,1987)	0.2 ^b	15	93
Boyle (1988)	0.16 ^b	14	27 or 42
Archer and Maier-Reimer (1994)	0.25 ^a	30	63

Sensitivity Tests			
#1	0.4	60	80
#2 ^c	0.2	16	80
#3 ^c	0.2	60	80

^a About 25% of all calcite production is buried and thus lost from the deep box, so the effective Ca/Corg is lower, about 0.3 for our model.

^b Broecker and Peng (1987) use a higher rain ratio for high latitude production; Boyle (1988) does not separate high and low latitude production.

^c River input of dissolved CaCO₃ must also be halved in these tests to compensate for the lysocline deepening caused by the halving of CaCO₃ production associated with these parameter changes.

atmospheric CO₂ for initial conditions of sensitivity tests

	STANDARD CASE	SENSITIVITY TEST INITIAL CONDITIONS		
		#1	#2	#3
		DEEP Corg REGENERATION = 60%	WARM SURFACE RAIN RATIO = 0.2 (RIVER INPUT HALVED)	#1 AND #2 COMBINED
CLOSED	307.6	307.9	285.7	289.9
COMPENSATED	296.3	264.3	272.7	248.2
OPEN	297	265.5	273.8	249.7

ΔCO_2 for experiment 1 (30% increase in whole ocean phosphate)

STANDARD	CARBON CYCLE SENSITIVITY TESTS		
	#1	#2	#3
	DEEP Corg REGENERATION = 60%	WARM SURFACE RAIN RATIO = 0.2 (RIVER INPUT HALVED)	#1 AND #2 COMBINED
CLOSED	-34.3	-34.2	-37.5
COMPENSATED	-28.8	-34.7	-36.9
OPEN	-17.5	-20.2	-37.2
		-22.7	-21.5

ΔCO_2 for experiment 2 (halving the $\text{Ca}/\text{C}_{\text{org}}$ rain ratio)

	STANDARD	CARBON CYCLE SENSITIVITY TESTS		
		#1	#2	#3
		DEEP C_{org} REGENERATION = 60%	WARM SURFACE RAIN RATIO = 0.2 (RIVER INPUT HALVED)	#1 AND #2 COMBINED
CLOSED	-21.9	-18	-10	-8.4
COMPENSATED	-34.9	-31.2	-19.9	-17.6
OPEN	-63.2	-68.6	-48.2	-50.7

ΔCO_2 for experiment 3 (deepening the C_{org} regeneration profile)

	STANDARD	CARBON CYCLE SENSITIVITY TESTS		
		#1	#2	#3
		DEEP C_{org} REGENERATION = 60% ^a	WARM SURFACE RAIN RATIO = 0.2 (RIVER INPUT HALVED)	#1 AND #2 COMBINED ^a
CLOSED	0.1	0.1	2.4	0.9
COMPENSATED	-14.8	-5.1	-10.7	-3.7
OPEN	-18.6	-7.7	-14.5	-6.4

^a For the sensitivity cases 1 and 3, the fraction of the C_{org} export production which reaches the seafloor is increased from 60% (initial case) to 72%.

Standard Model Conditions													
	physical			components						export production			
	temp.	sal.	°C	DIC	O ₂	PO ₄	ALK	δ ¹³ C	Δ ¹⁴ C	pCO ₂	CO ₃ ²⁻	C _{org}	CaCO ₃
surface	Atl.	18.5	35	1939	234	0.00	2236	1.93	-52	296	202.9	0.68	0.27
	Ind.	18.5	35	1938	234	0.00	2234	1.89	-48	296	202.7	0.63	0.25
	S. Pac.	18.5	35	1945	234	0.00	2243	1.90	-60	295	204.3	0.47	0.19
	N. Pac.	18.5	35	1925	234	0.00	2217	1.83	-66	296	200.0	0.56	0.23
	N. N. Atl.	4	34.7	2073	321	0.55	2271	1.84	-68	279	136.4	0.59	0.00
Ant.	2	33.5	2203	368	1.62	2369	1.68	-147	298	121.2	3.60	0.00	
intermediate	Atl.	2	34.7	2234	195	2.02	2337	0.71	-151	498	83.7		
	Ind.	2	34.7	2274	174	2.32	2351	0.49	-165	609	71.4		
	S. Pac.	2	34.7	2271	161	2.28	2355	0.44	-178	580	74.7		
	N. Pac.	2	34.7	2318	39	2.73	2350	-0.28	-199	870	52.3		
deep													
N. N. Atl.	2	34.7	2136	269	1.13	2294	1.36	-100	328	109.8			
Atl.	2	34.7	2190	237	1.53	2323	1.05	-142	375	96.0			
Ant.	2	34.7	2265	207	2.12	2359	0.68	-177	513	77.9			
Ind.	2	34.7	2291	188	2.25	2385	0.56	-199	497	77.5			
S. Pac.	2	34.7	2313	156	2.38	2404	0.38	-222	514	76.4			
N. Pac.	2	34.7	2336	127	2.51	2421	0.21	-238	539	74.4			
whole ocean			2301.14	171.127	2.118	2364.41	0.41	-182.6					
atmosphere	CO ₂ (ppmV):		297										
	δ ¹³ C (‰):		-7.18										
	Δ ¹⁴ C (‰):		5.5										
terrestrial	Δ ¹⁴ C (‰):		5										

Figure 1

The model architecture and circulation [Keir, 1988]. Water fluxes are in Sverdrups.

Two-way arrows denote fluxes in both directions (i.e., exchange). Volumes are given in [Keir, 1988].

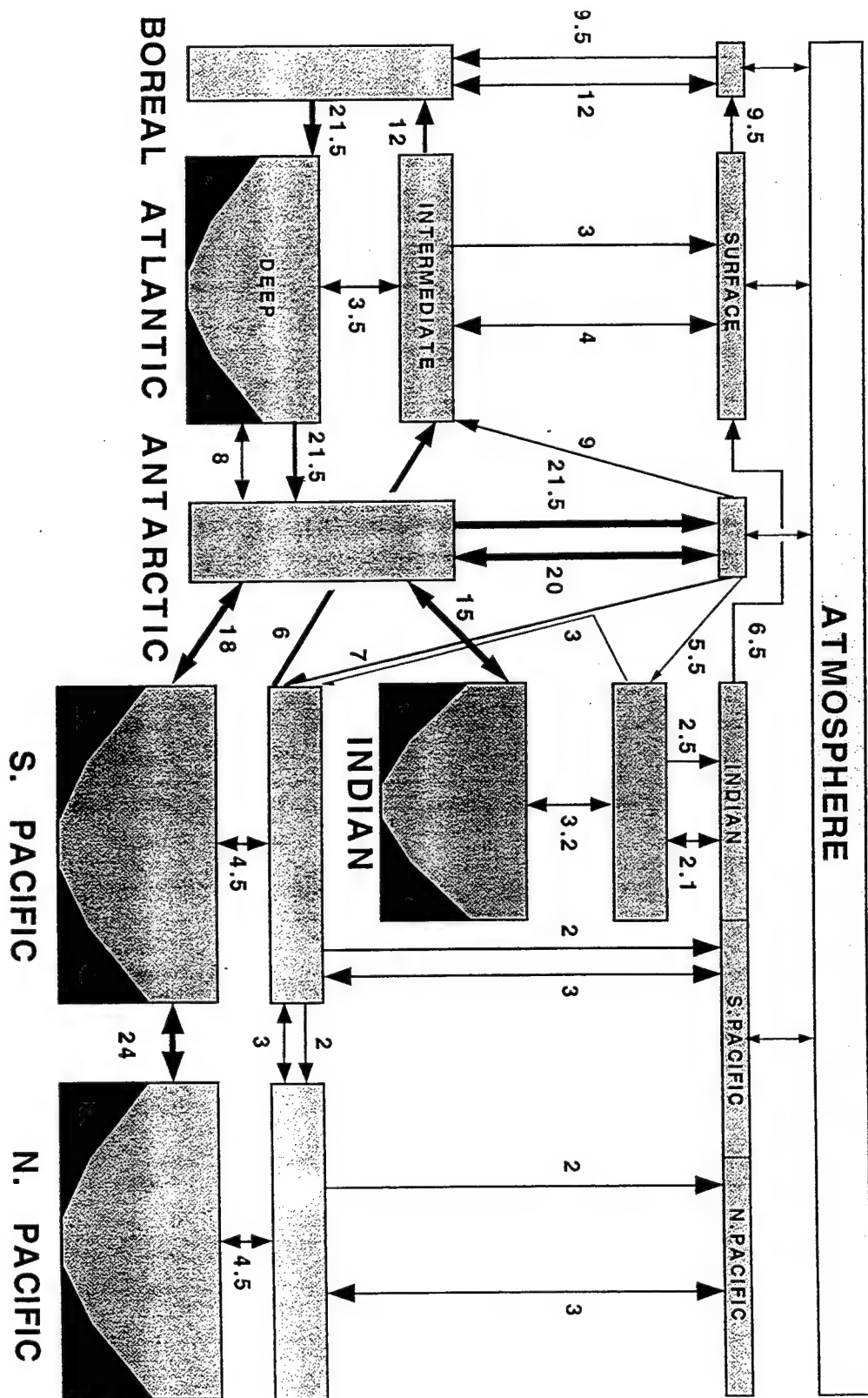


Figure 2

The model production/regeneration cycle [*Keir*, 1988]. See Table 1 for a comparison with other models.

Model Parameters for the Production/Regeneration Cycle

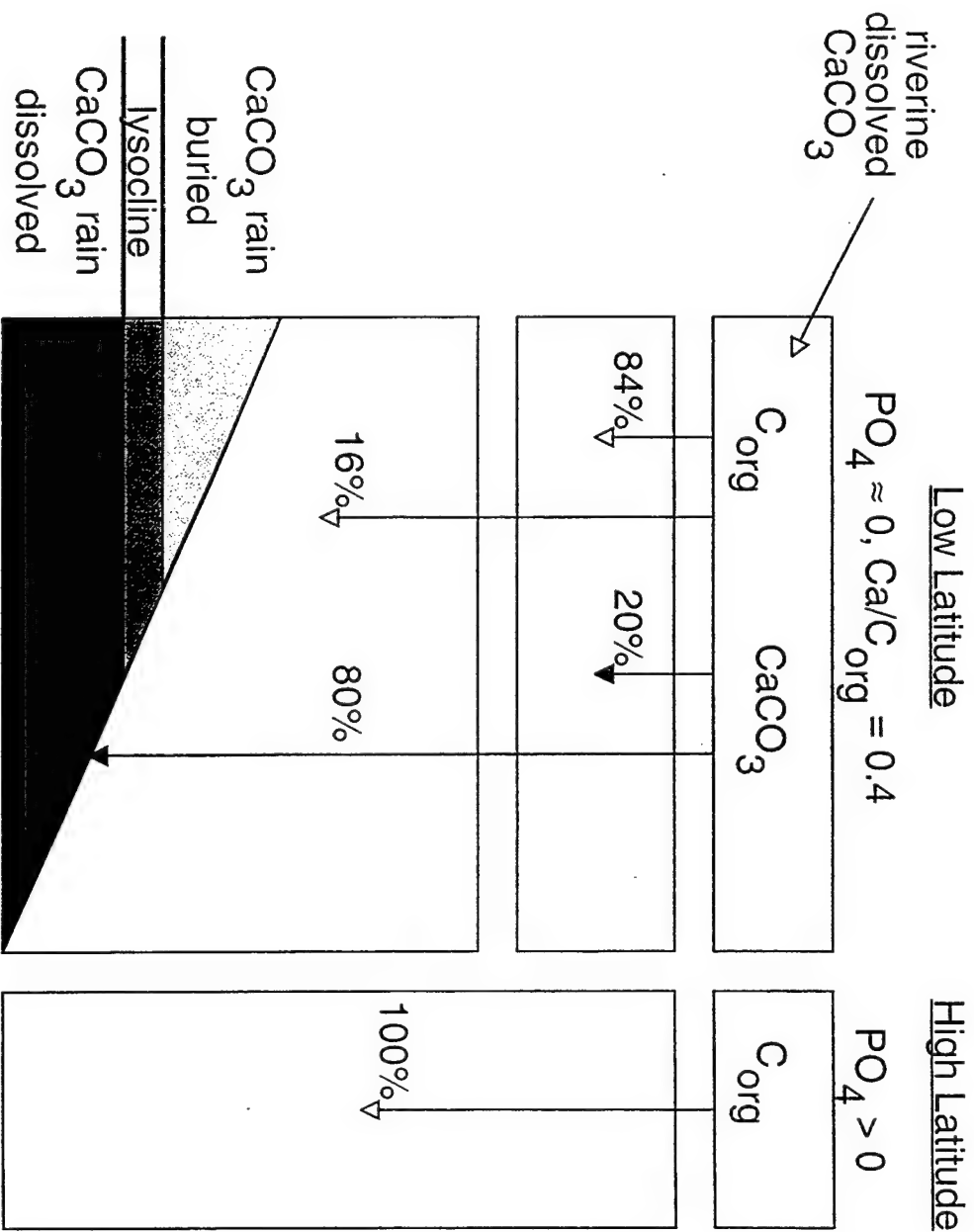


Figure 3

Outline of the the CaCO_3 input/output models used in this study. In part 1, we compare the model experiment responses for the closed system case, the compensated case, and the rain-based open system case. In part 2, the mixed layer open system model without sediment respiration-driven dissolution is used to investigate chemical erosion. In part 3, the mixed layer open system model response is run with and without sediment respiration-driven dissolution, to determine the effect of this process. In addition, two different patterns of C_{org} rain to the seafloor are compared for the case with active sediment respiration-driven dissolution.

CaCO₃ input/output models in this study

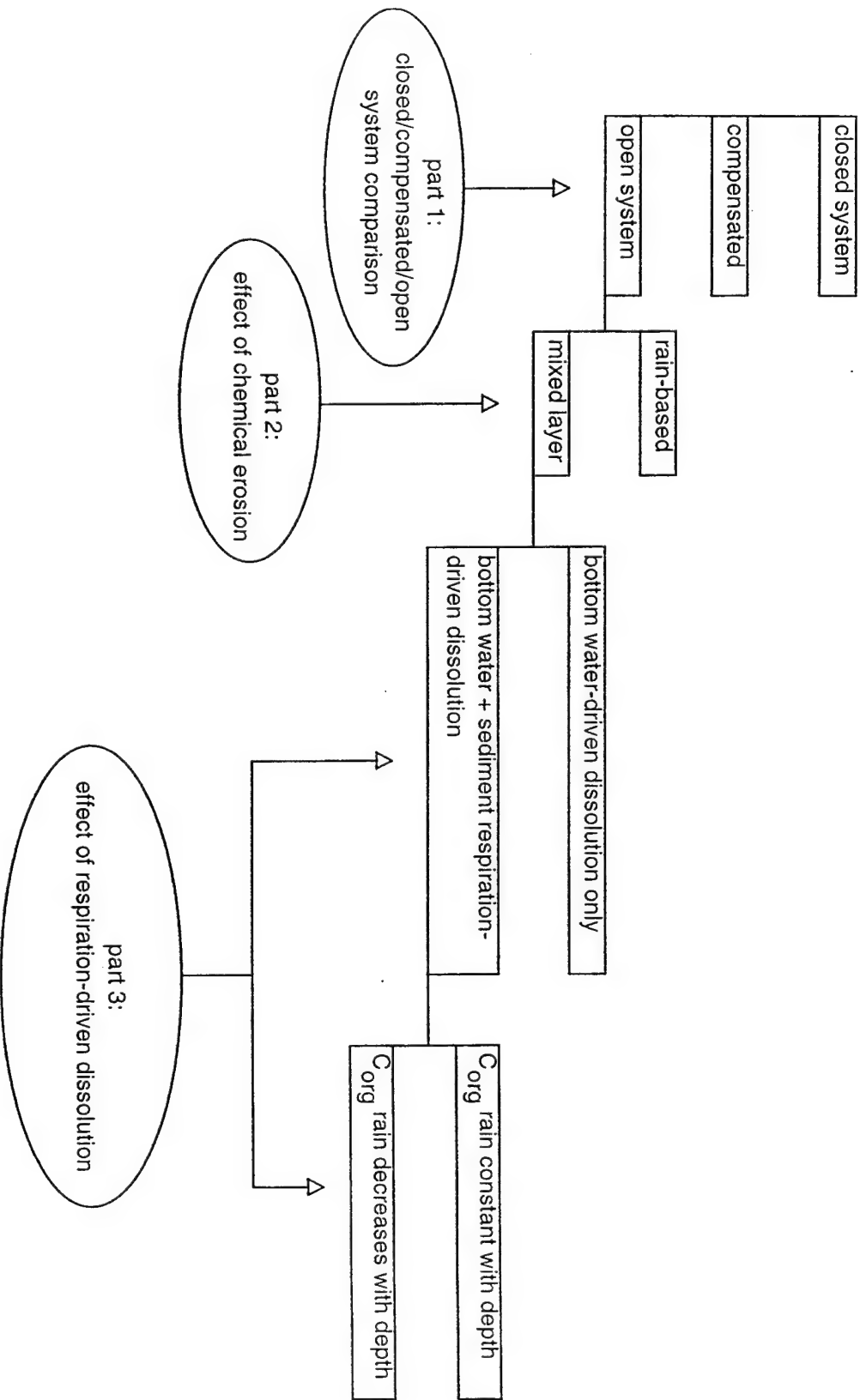


Figure 4a

Comparison of the model experiment steady state responses in the closed system, compensated, and open system cases, for (a) atmospheric CO_2 and (b) ocean-average lysocline depth. Responses are plotted as differences from the standard interglacial case. Model experiment 1 is a 30% increase in the whole ocean phosphate reservoir, which causes a ~30% increase in low latitude export production. Model experiment 2 is a halving of the low latitude $\text{CaCO}_3/\text{C}_{\text{org}}$ rain ratio out of the surface ocean (from 0.4 to 0.2). Model experiment 3 is an increase in the fraction of C_{org} export production which enters the deep boxes (from 16% to 40%). For the experiments shown here, high latitude biological production is held constant.

atmospheric CO₂

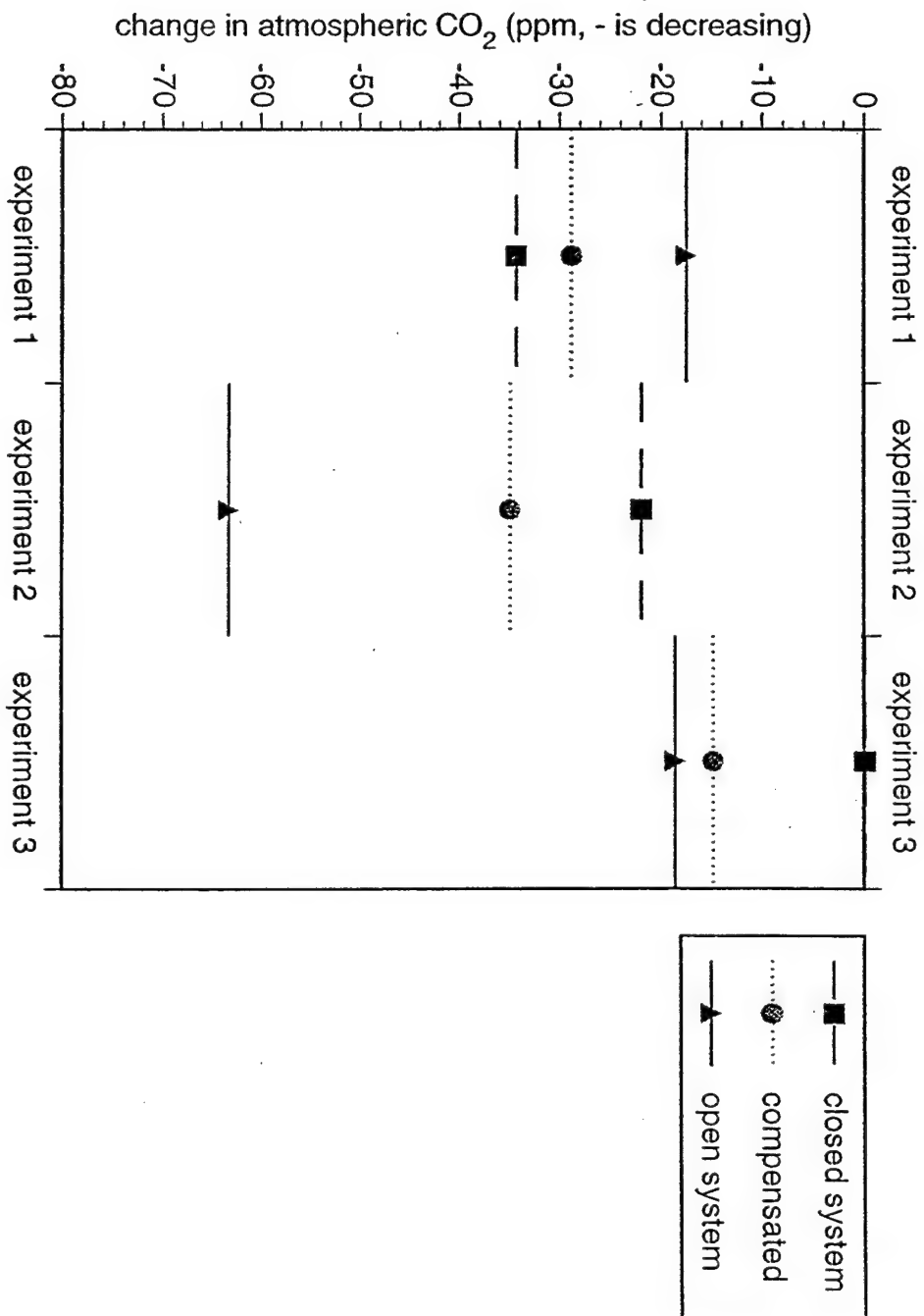


Figure 4b

See Figure 4a caption.

saturation depth

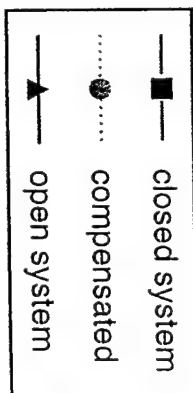
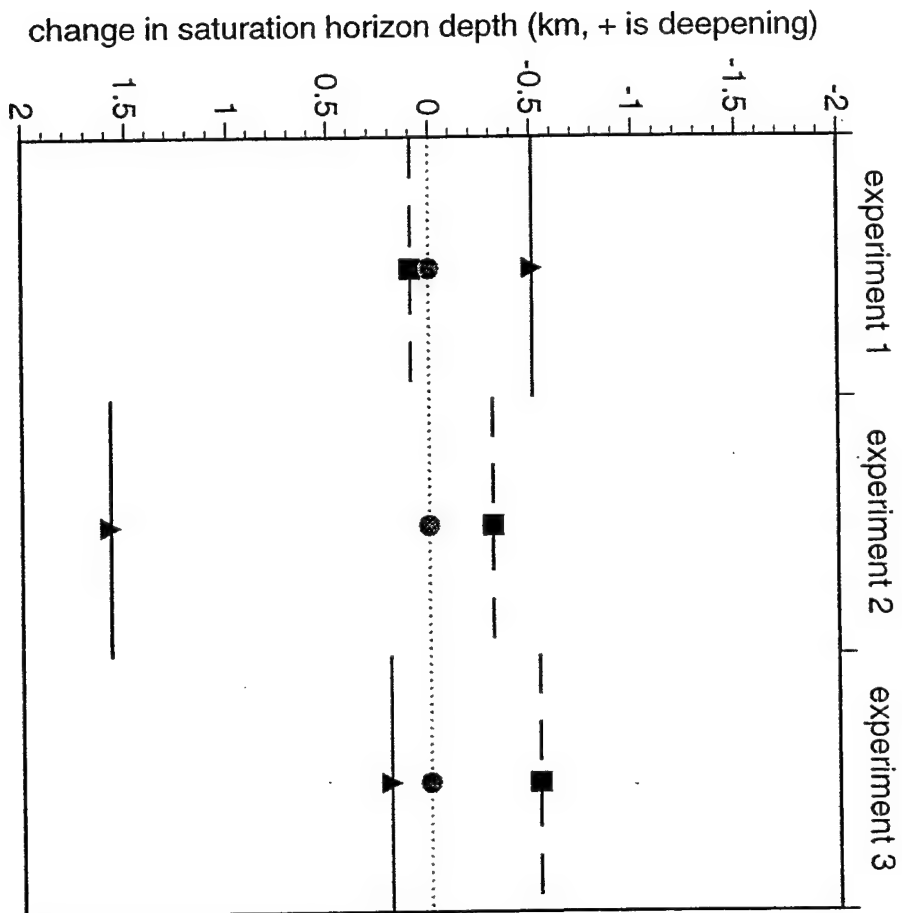


Figure 5-1

Model experiment time dependent results. (a) atmospheric CO_2 , for both closed and open system scenarios. The closed system output has been offset to start at the same initial value as the open system (297 ppm). (b) the instantaneous ratio of CaCO_3 burial to riverine input of dissolved CaCO_3 . If the ratio is <1 , then the ocean is gaining ALK and DIC in a 2:1 ratio. If the ratio is >1 , then the ocean is losing them in the same ratio. (c and d) the calcite saturation horizons in the Atlantic and North Pacific, which have the youngest and oldest waters, respectively.

Experiment 1: Increased CaCO_3 rain associated with the production increase causes CaCO_3 burial to increase above river input (panel b), so that the ocean begins to lose ALK and DIC in a 2:1 ratio. As a result, the pCO_2 of surface water increases, causing atmospheric CO_2 to increase from the closed system case (panel a). The whole ocean loss of ALK and DIC also causes deep ocean $[\text{CO}_3^{2-}]$ to decrease, so that the saturation horizon shoals (panels c and d, note interbasin differences). This shoaling decreases the area of CaCO_3 burial, so that CaCO_3 burial decreases back to equality with river input (panel b). Note that no transient dissolution event is associated with an increase in low latitude production in our model.

model experiment #1: 30% increase in the whole ocean phosphate reservoir

(high latitude constant flux)

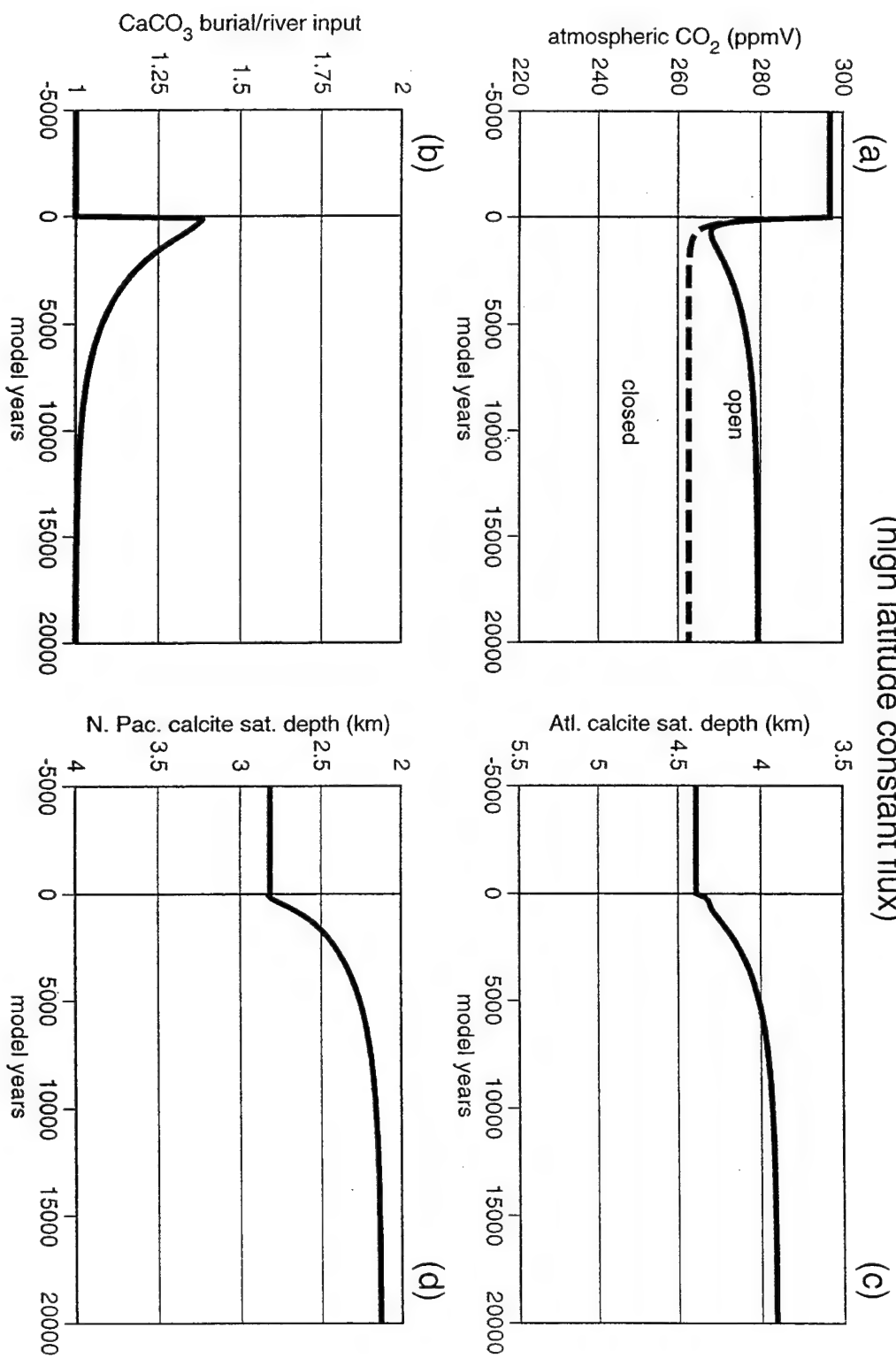


Figure 5-2

See Figure 5-1 caption.

Experiment 2: Decreased CaCO_3 rain associated with the rain ratio decrease causes CaCO_3 burial to decrease below river input (panel b), both because of a transient dissolution event (panel d) and because of a decrease in the rain rate onto seafloor above the saturation horizon. As a result, the pCO_2 of surface water decreases, causing atmospheric CO_2 to decrease from the closed system case (panel a). The whole ocean increase in ALK and DIC also causes deep ocean $[\text{CO}_3^{2-}]$ to steadily increase, so that the saturation horizon deepens (panels c and d, note interbasin differences). This deepening increases the area of CaCO_3 burial until CaCO_3 burial increases back to equality with river input (panel b).

model experiment #2: half the standard warm surface $\text{CaCO}_3/\text{C}_{\text{org}}$ rain ratio

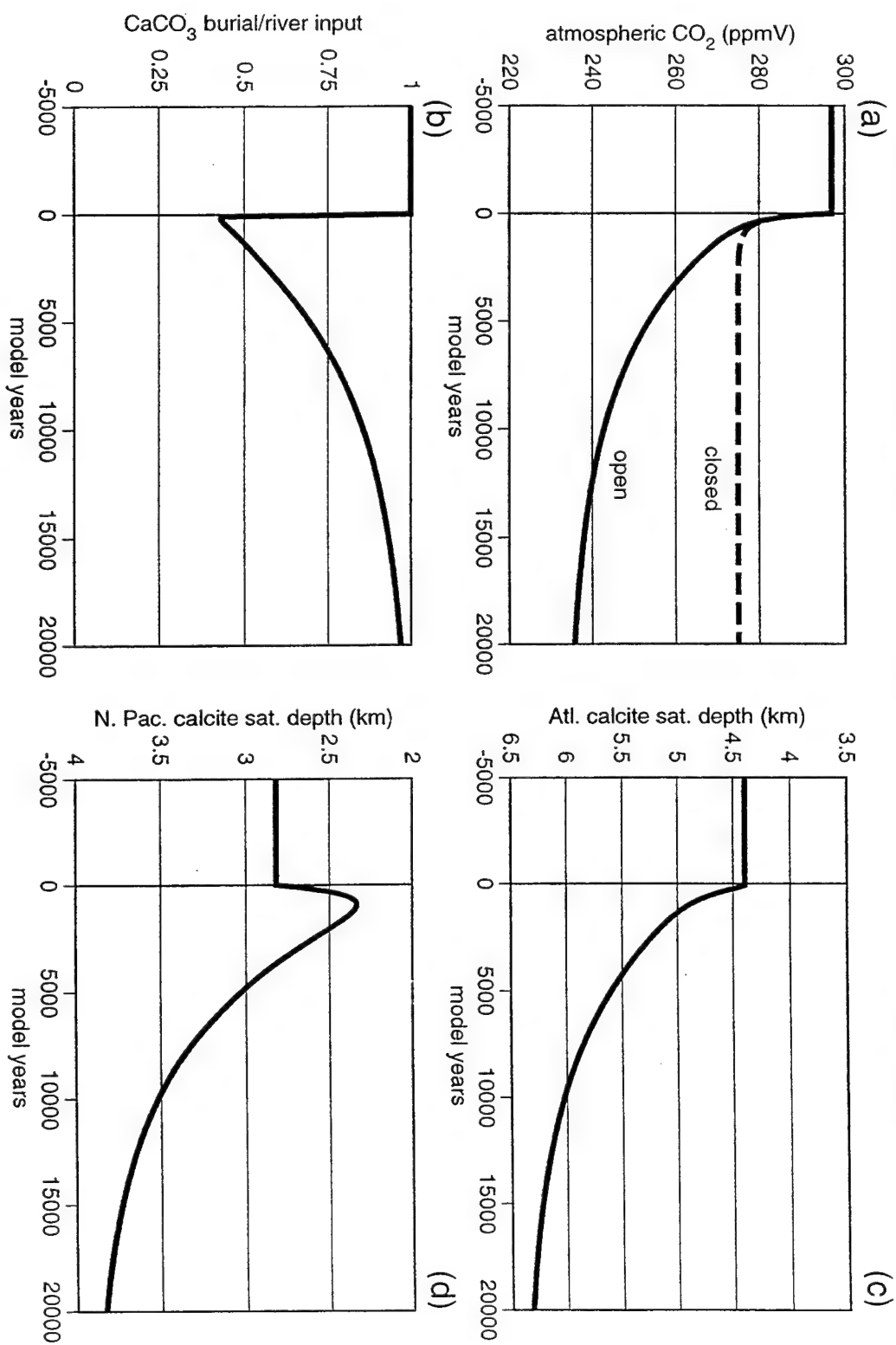


Figure 5-3

See Figure 5-1 caption.

Experiment 3: A transient shoaling of the saturation horizon (panels c, d) causes CaCO_3 burial to decrease below river input (panel b). As a result, the pCO_2 of surface water decreases, causing atmospheric CO_2 to decrease from the closed system case (panel a). The whole ocean increase in ALK and DIC also causes deep ocean $[\text{CO}_3^{2-}]$ back to near its original ocean-averaged depth (panels c and d, note interbasin difference). As the transient dissolution event ends, CaCO_3 burial increases back to equality with river input (panel b).

model experiment #3: increase in fraction of C_{org} reaching the deep boxes

(high latitude constant flux)

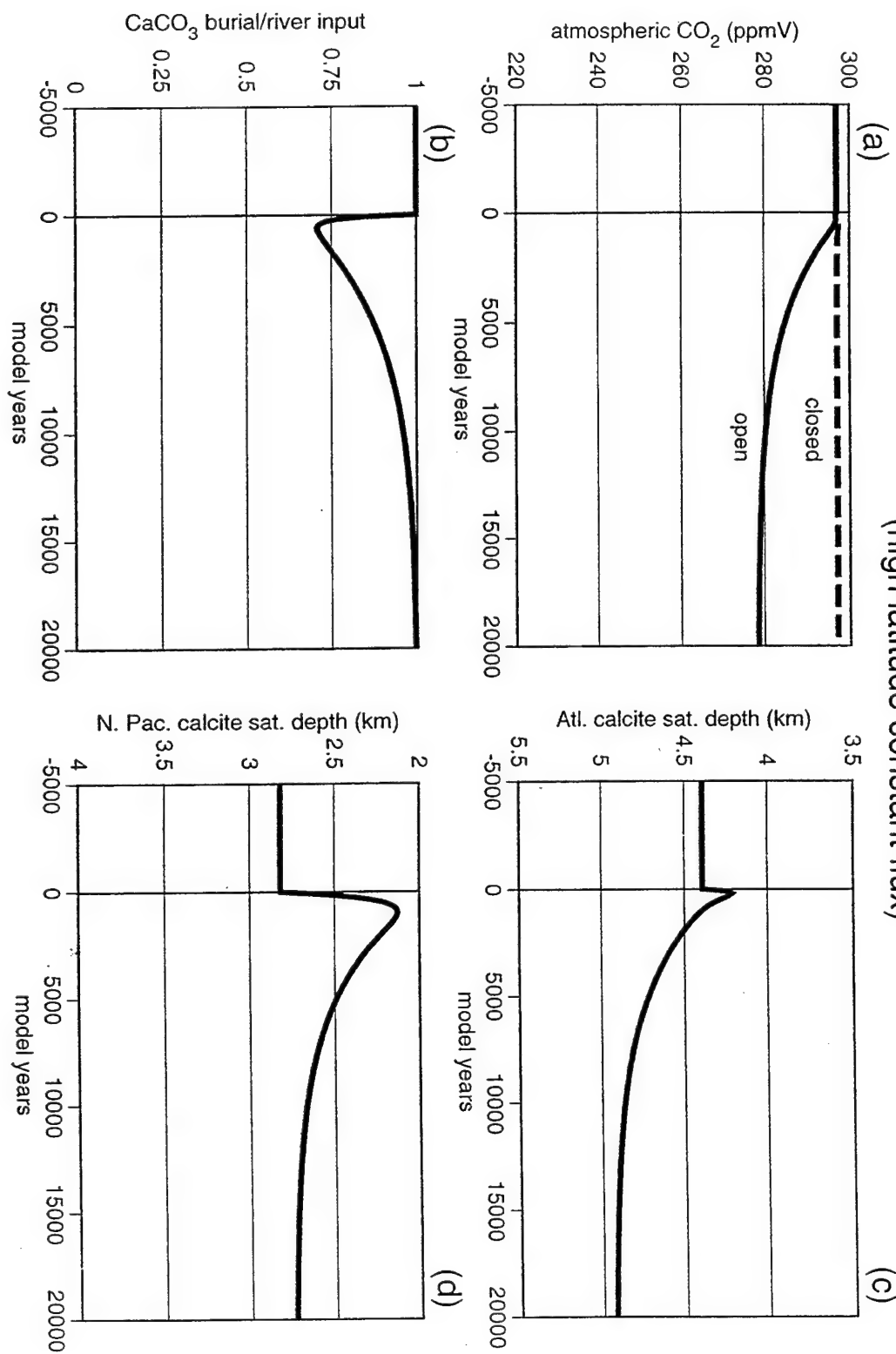


Figure 6

The steady state average saturation depth as a function of the imposed CaCO_3 rain rate (varied by altering the production rate, using the model experiment 1 mechanism). For a higher CaCO_3 rain rate, the saturation horizon must be shallower so that the area of preservation and burial is smaller.

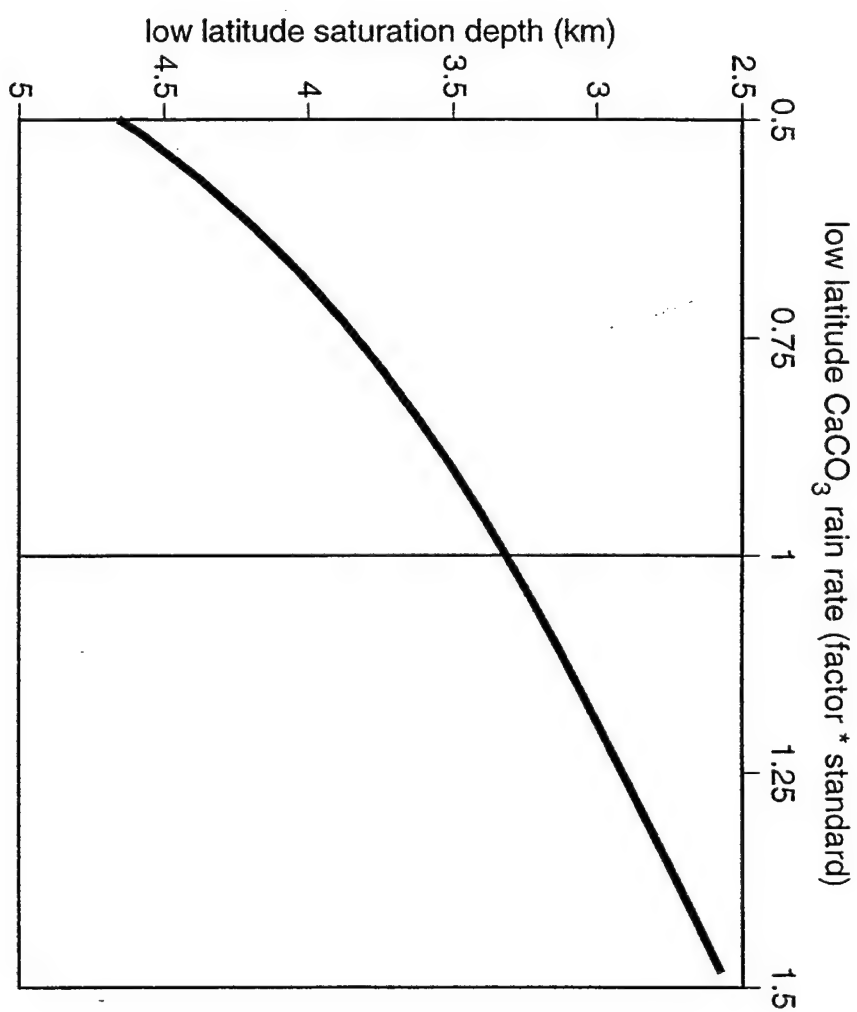


Figure 7

The approach of the saturation horizon to a shallower steady state depth for the return from model experiment 2 back to standard conditions (i.e., from glacial to interglacial), using the mixed layer open system model with a range of different non-carbonate deposition rates. The results have been shifted slightly so that they all start at the same initial saturation depth. Irregularities in the curve shapes are due to limited depth resolution.

reversing model experiment 2:
doubling the $\text{CaCO}_3/\text{C}_{\text{org}}$ rain ratio (from "glacial" to "interglacial")

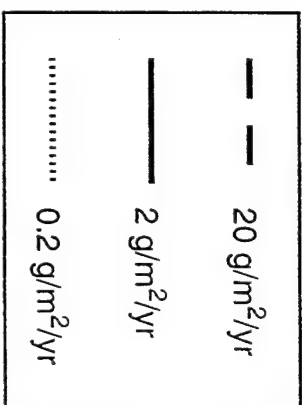
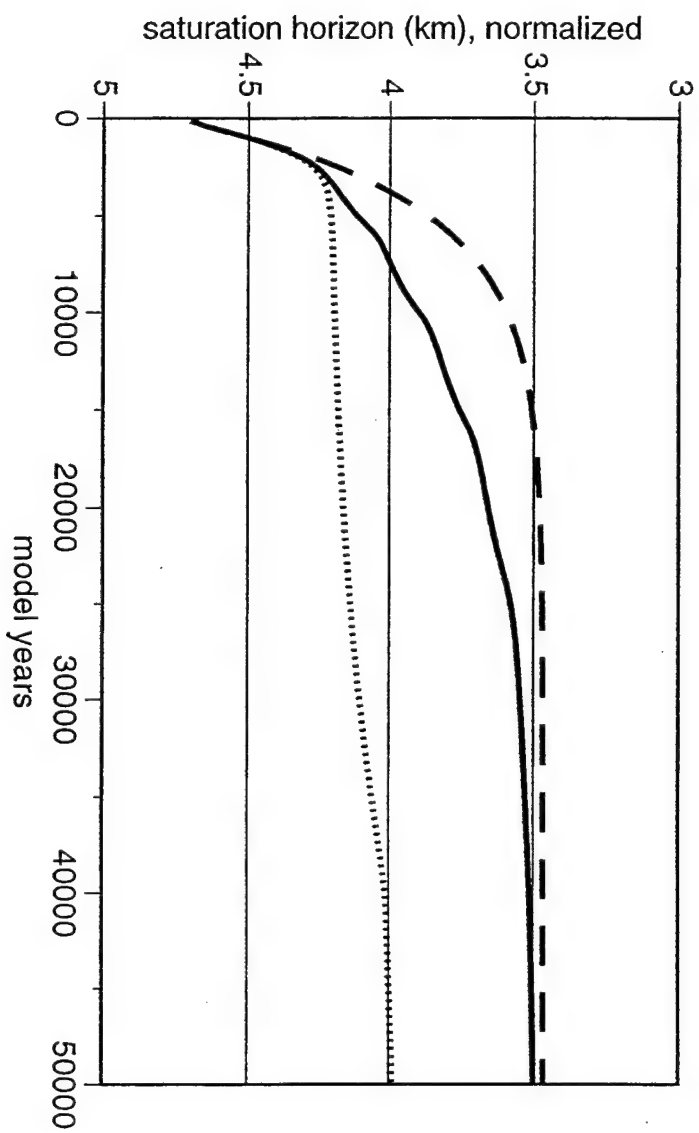


Figure 8

The time dependent ratio of calcite dissolution rate/calcite rain rate at different depths in the low latitude ocean in response to the return from model experiment 2, using the mixed layer open system model with the same range of different non-carbonate deposition rates as in the previous figure. The shaded region shows the zone of chemical erosion. Chemical erosion occurs when the dissolution rate is greater than the total sediment rain rate. For a non-carbonate rain rate of $2 \text{ g/m}^2/\text{yr}$, this occurs when $\text{dissolution/rain} \geq 1.1$. Irregularities in the contours are due to the limited depth resolution of the mixed layer open system model.

non-carbonate flux:

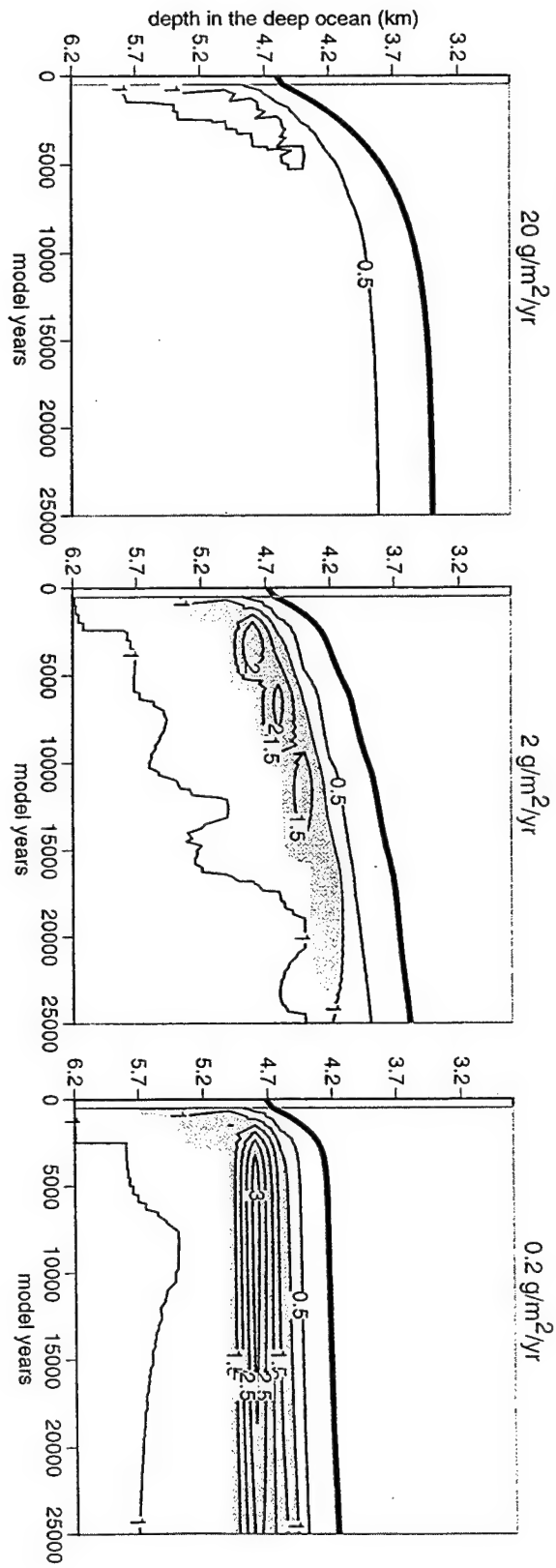


Figure 9

Time dependent changes in the calcite content of mixed layer sediment at three depths in the low latitude deep ocean, in response to the return from model experiment 2 to standard interglacial conditions. The shoaling of the calcite saturation depth is shown for comparison. The rate at which mixed layer sediment reaches a new steady state calcite content depends on its depth relative to the saturation horizon; at 3.6 km depth, it occurs much more slowly than the shoaling of the saturation horizon to its new steady state. The assumed non-carbonate rain rate is $2 \text{ g/m}^2/\text{yr}$.

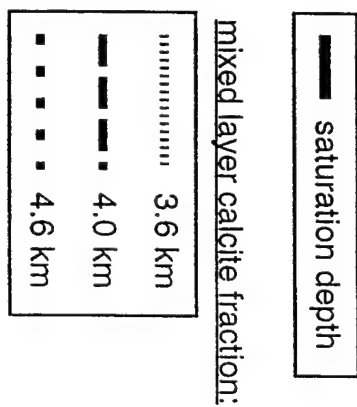
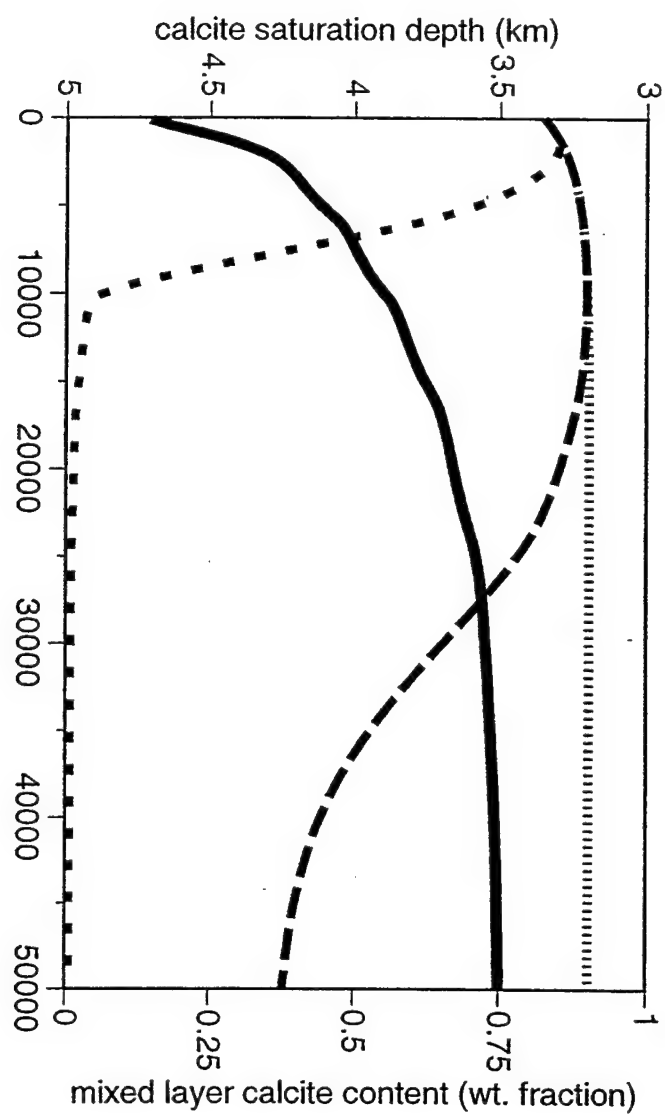


Figure 10a

The effect of respiratory dissolution on changes in (a) atmospheric CO₂ (this figure) and (b) the saturation horizon depth (next page) for each of the model experiments. The two cases shown are (1, square symbols) no respiratory dissolution and a 'fast' dissolution rate constant k_d of 30/day (as has been used to this point), and (2, circles) active respiratory dissolution and a slower dissolution rate constant of 1/day, as used by *Archer and Maier-Reimer* [1994].

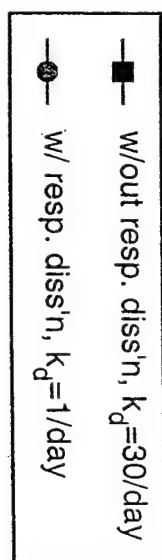
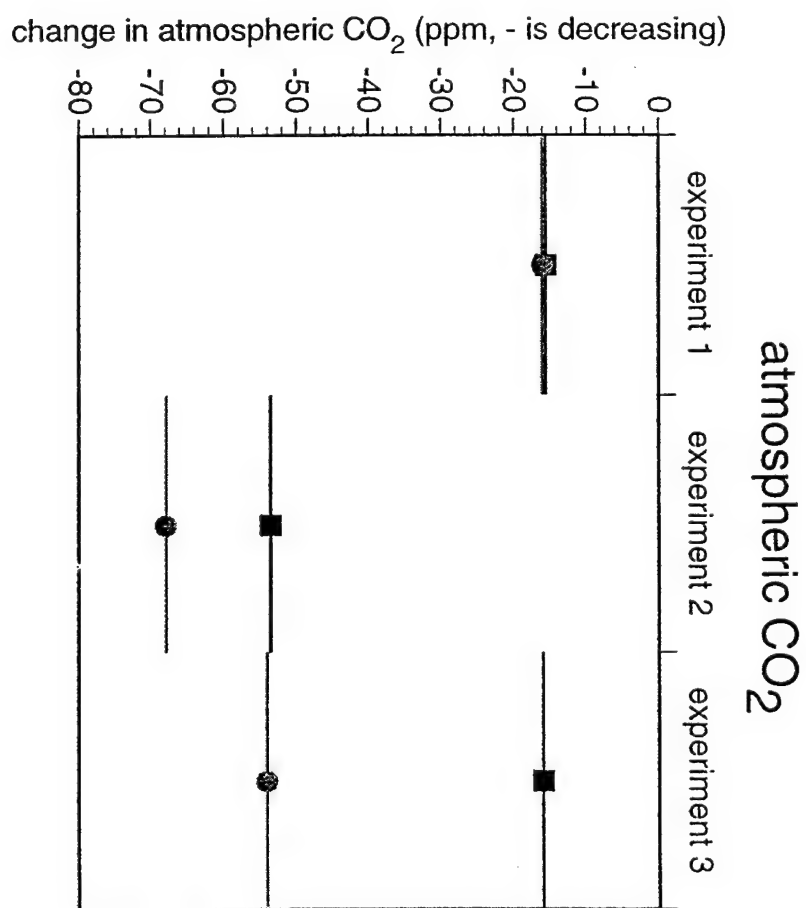


Figure 10b

The effect of respiratory dissolution on changes in (a) atmospheric CO_2 (previous page) and (b) the saturation horizon depth (this figure) for each of the model experiments.

The two cases shown are (1, square symbols) no respiratory dissolution and a 'fast' dissolution rate constant k_d of 30/day (as has been used to this point), and (2, circles) active respiratory dissolution and a slower dissolution rate constant of 1/day, as used by *Archer and Maier-Reimer* [1994].

change in saturation horizon depth (km, + is deepening)

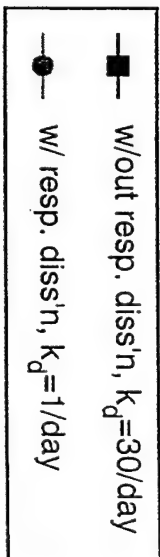
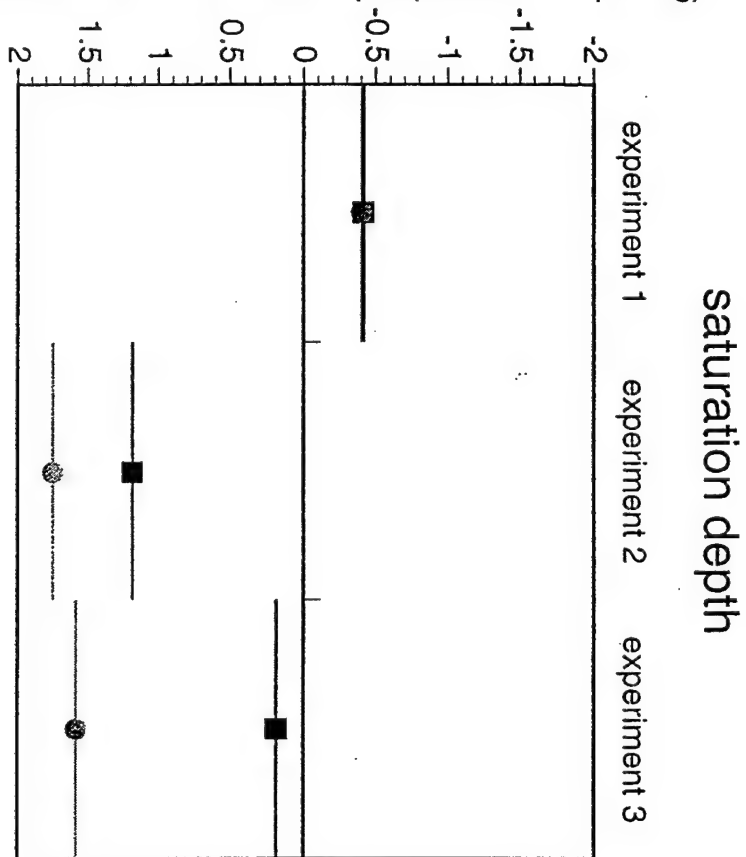
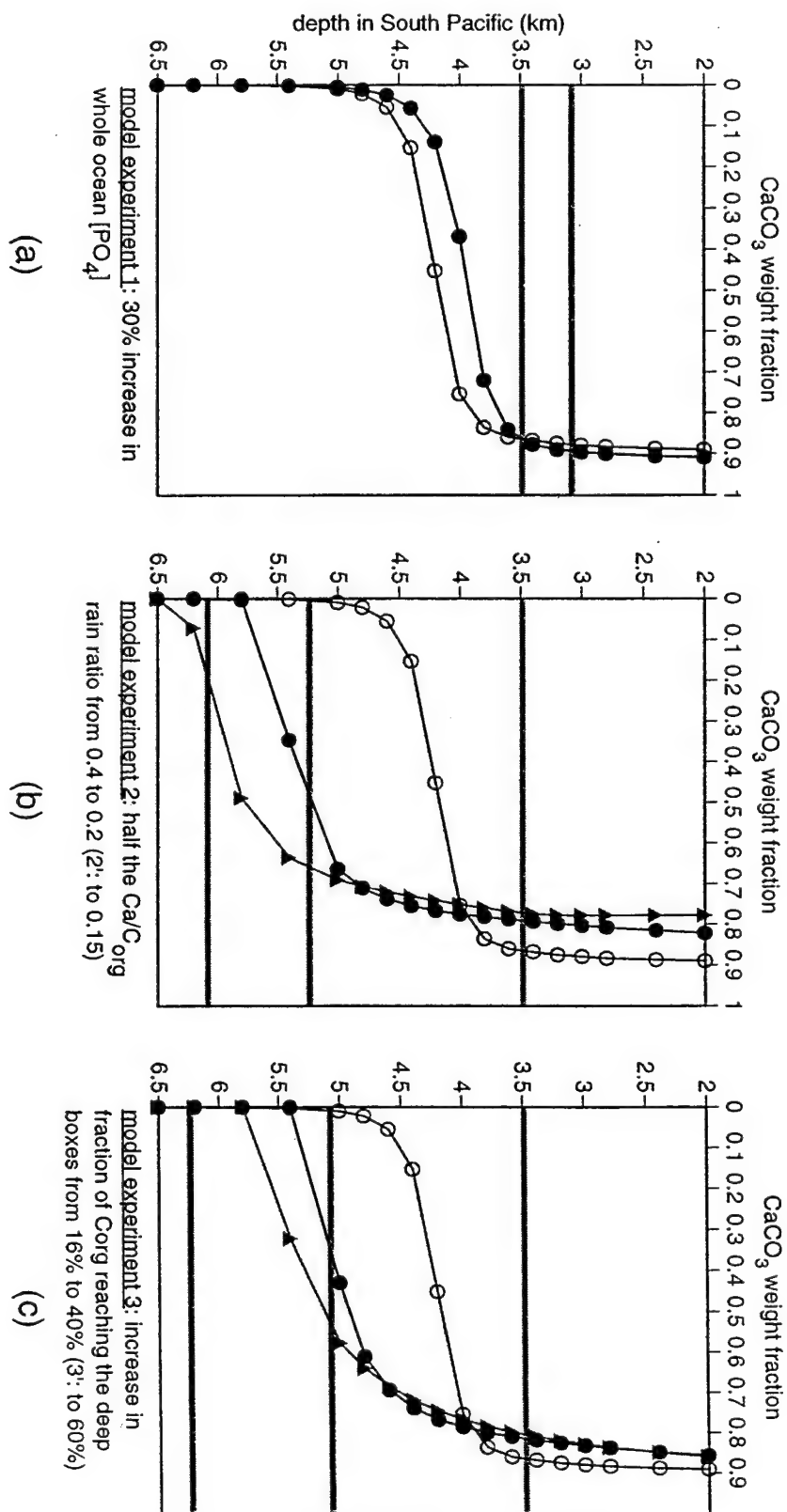


Figure 11a-c

Depth profiles of (a-c) weight fraction CaCO_3 (this figure) and (d-f) CaCO_3 burial rate (next page) for each of the model experiments, using open system mixed layer model with active sediment respiration-driven dissolution and a k_d of 1/day. In each frame, the open symbols and the grey bar at 3.5 km are the depth profile and saturation depth, respectively, for the standard interglacial case. The solid symbols and the additional grey bar are the new profile and saturation depth, respectively, for the model experiment. In the panels of model experiments 2 and 3 (b, c, e, f), the response to experiments 2' and 3' are also shown (solid triangles). Experiments 2' and 3' are more intense versions of experiments 2 and 3, respectively.



○ standard case ● model experiment ▲ model experiments 2,3'

Figure 11d-f

Depth profiles of (a-c) weight fraction CaCO_3 (previous page) and (d-f) CaCO_3 burial rate (this figure) for each of the model experiments, using open system mixed layer model with active sediment respiration-driven dissolution and a k_d of 1/day. In each frame, the open symbols and the grey bar at 3.5 km are the depth profile and saturation depth, respectively, for the standard interglacial case. The solid symbols and the additional grey bar are the new profile and saturation depth, respectively, for the model experiment. In the panels of model experiments 2 and 3 (b, c, e, f), the response to experiments 2' and 3' are also shown (solid triangles). Experiments 2' and 3' are more intense versions of experiments 2 and 3, respectively.

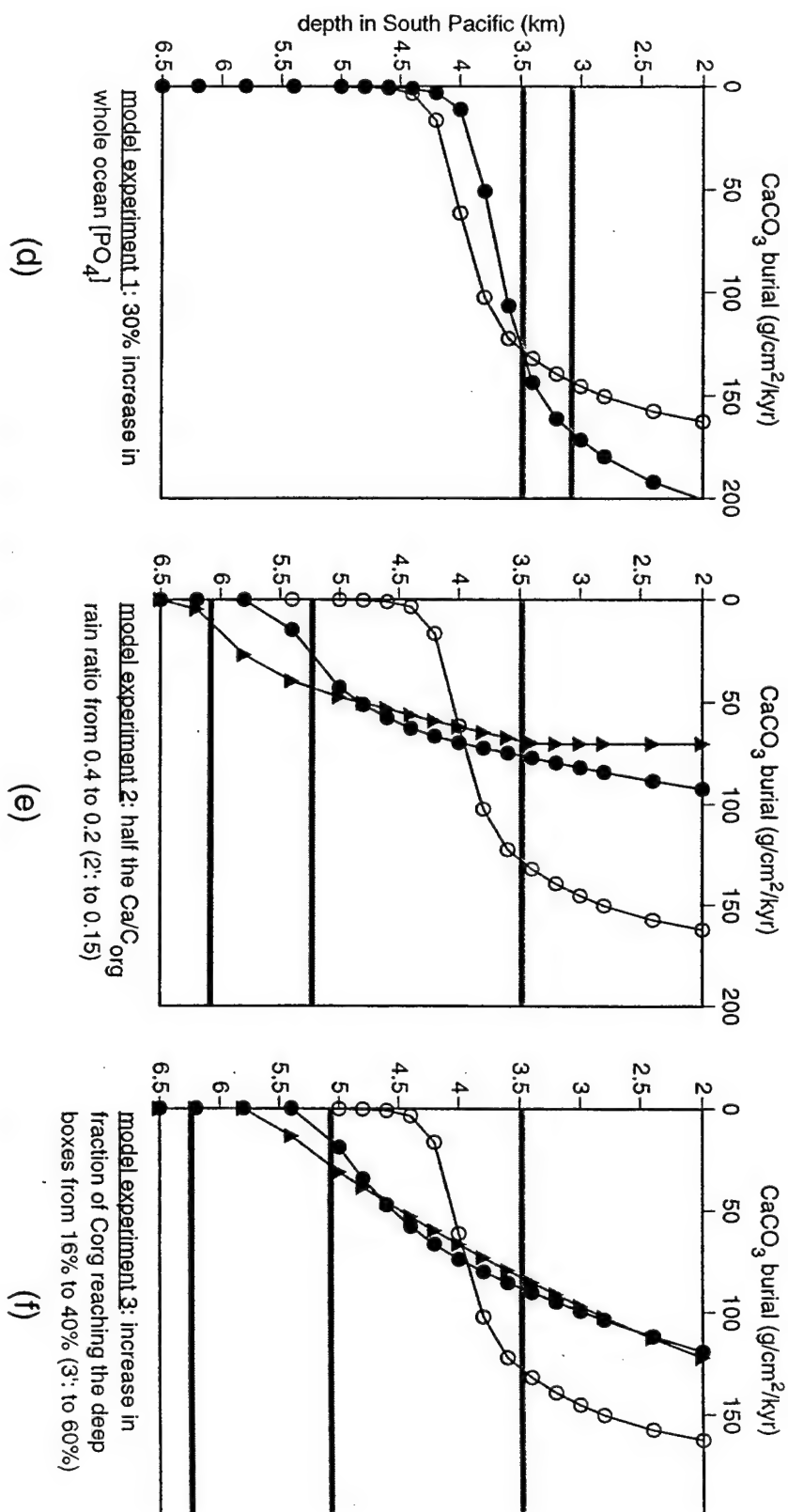


Figure 12

Depth profiles of (a) weight fraction CaCO_3 and (b) CaCO_3 burial rate for the standard interglacial case, experiment 3, and experiment 3', analogous to the output shown in Figures 11 (c) and (f). In this case, we added a depth dependence in the Corg rain to the seafloor. This more realistic treatment results in an even stronger coupling between the saturation horizon and the lysocline.

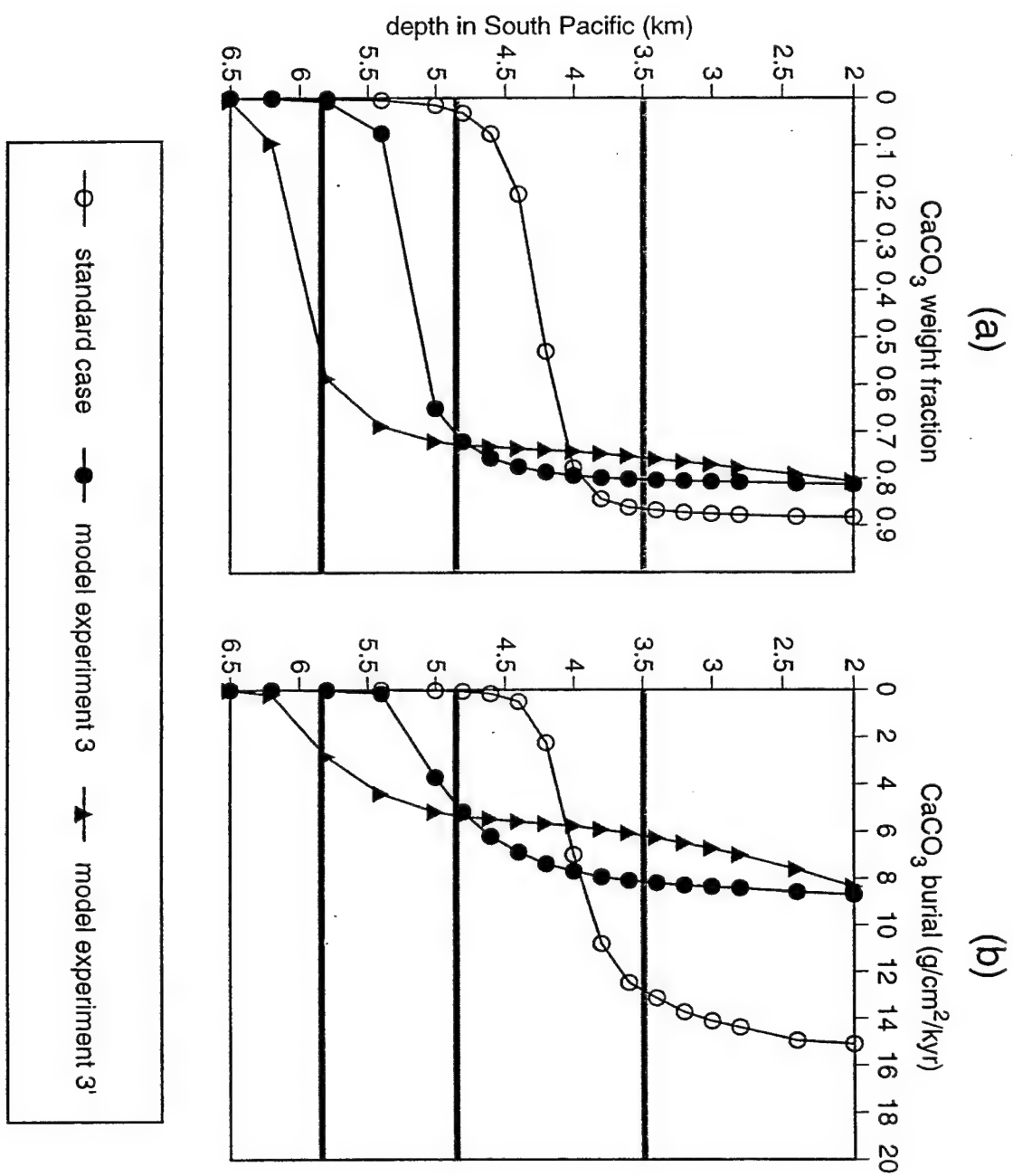


Figure 13

Changes in (1) atmospheric CO_2 (in ppm, black) and (2) the average depth of the saturation horizon (in km, grey) due to combined changes in low latitude production (using the model experiment 1 mechanism) and the low latitude $\text{CaCO}_3/C_{\text{org}}$ rain ratio (model experiment 2), using the rain-based open system model. If we assume that the ocean-average steady state saturation horizon depth does not change on glacial/interglacial transitions, then the combination of these changes which could have lowered atmospheric CO_2 is defined by heavy black line. The grey area denotes a total of ± 300 m uncertainty with regard to this assumption of a constant saturation horizon. These contour plots were generated assuming no respiratory dissolution.

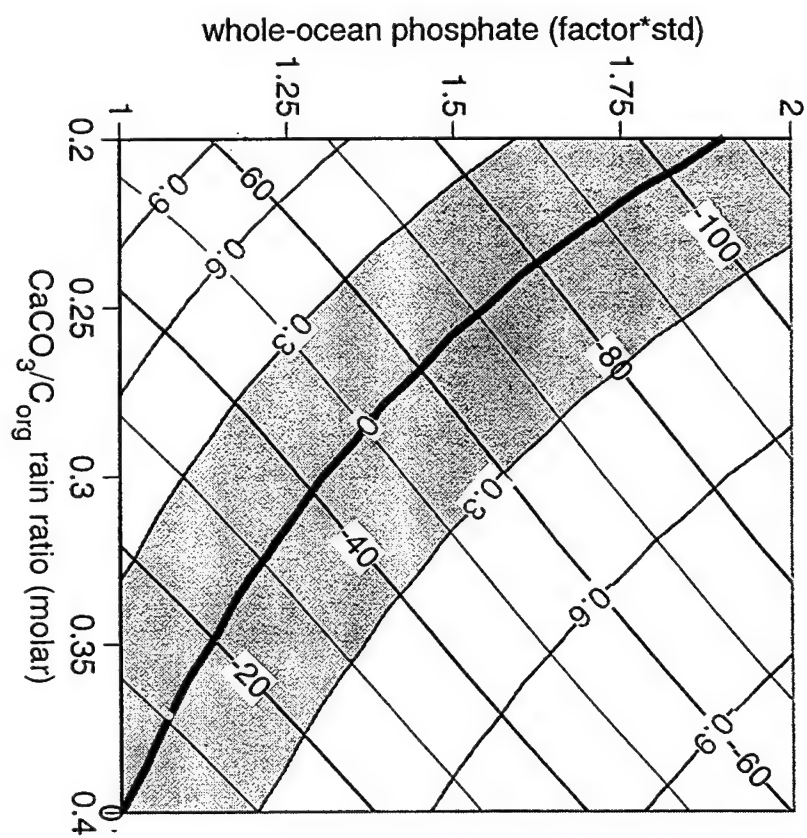


Figure AI-1

A comparison of DIC and ALK output between our standard interglacial conditions and CYCLOPS SOC (without the evaporation/precipitation cycle) [Keir, 1988]. Squares denote surface boxes, triangles denote intermediate boxes, and diamonds denote deep boxes (see the legend). The whole-ocean differences in ALK and DIC are due to differences in the river/burial balance of the two models.

Comparison of DIC and ALK Distributions with CYCLOPS (Keir, 1988)

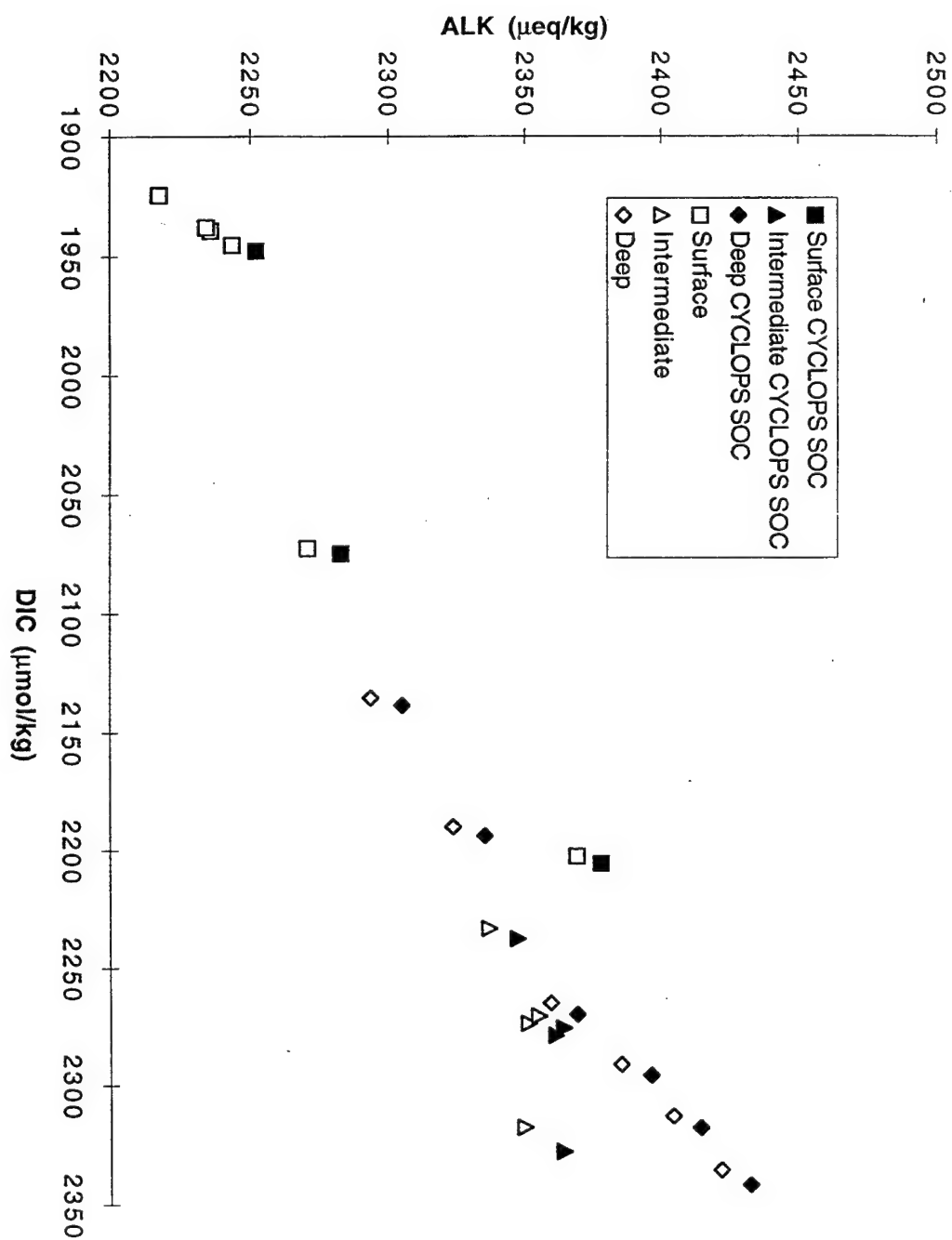


Figure AI-2

A DIC and ALK comparison of GEOSECS basin averages to our standard interglacial case. The GEOSECS averages do not have exactly the same boxes as our model or CYCLOPS, so that trends, rather than individual points, should be compared. The basin averages come from further averaging of depth- and latitude-averaged GEOSECS data [Takahashi *et al.*, 1981].

Comparison of DIC and ALK Distributions with GEOSECS Averages (Takahashi et al., 1981)

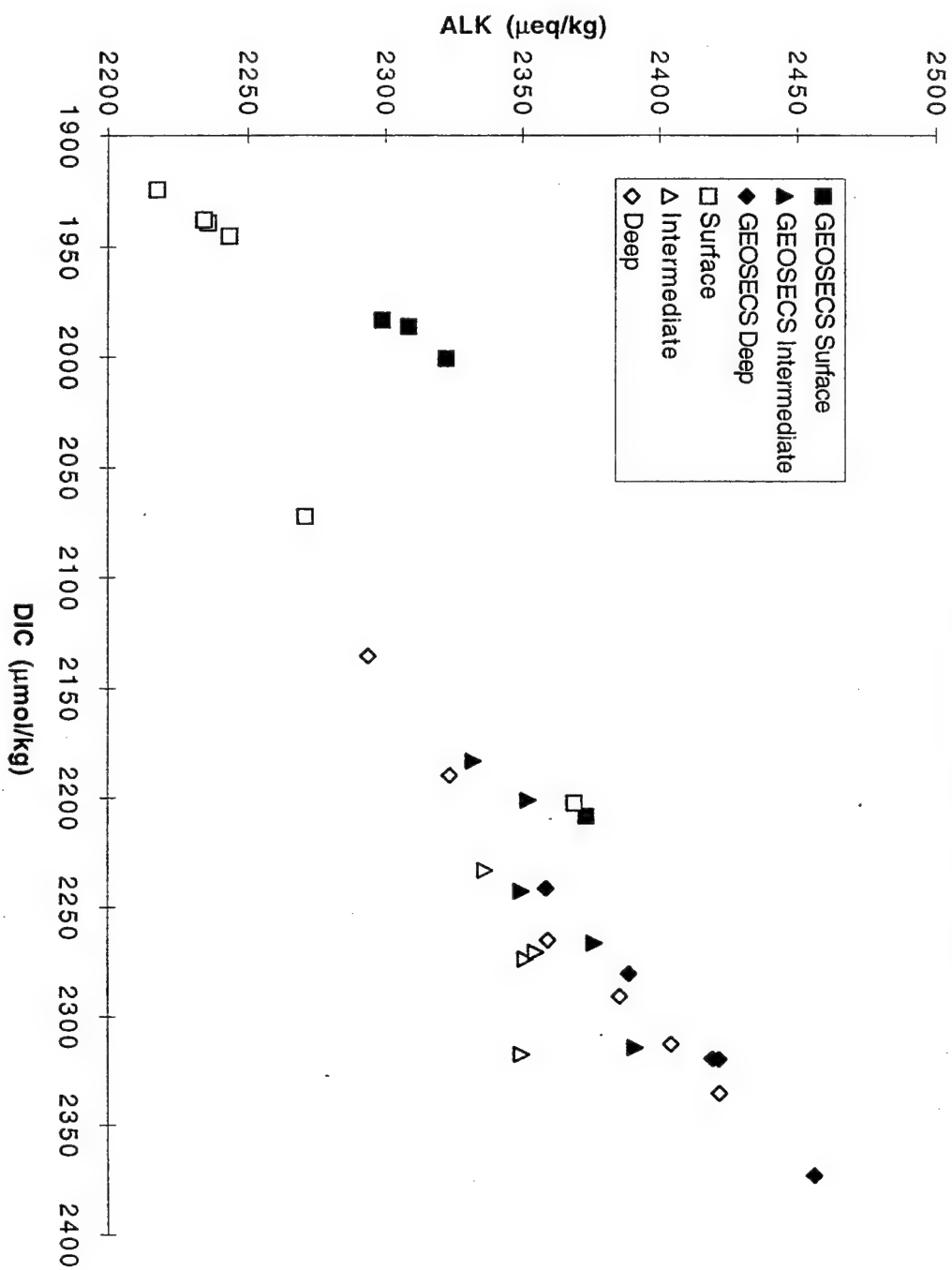


Figure AI-3

A DIC vs. phosphate comparison of GEOSECS basin averages to our standard interglacial case. This comparison suggests that much of the data/model disagreement in surface ALK and DIC is due to the model assumption of no phosphate in the "low latitude" surface box, which extends to 140 m depth and to roughly 50° latitude in both hemispheres.

Comparison of DIC and PO₄ Distributions with GEOSECS Averages (Takahashi et al., 1981)

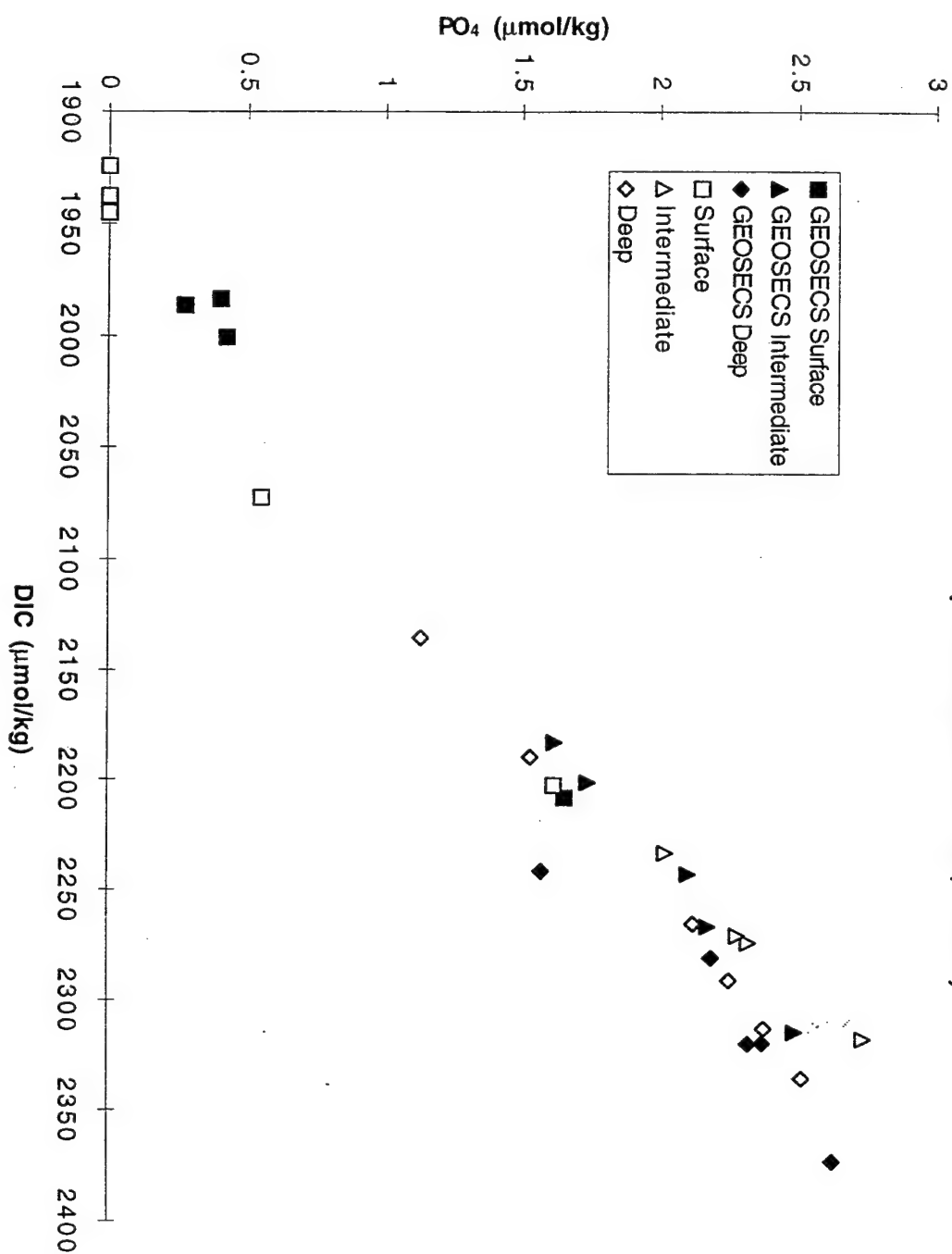


Figure AII-1

The sediment respiration-driven calcite dissolution rate as a function of bottom water saturation state and C_{org} rain rate, calculated using the explicit sediment geochemistry model of [Martin and Sayles, 1995]. In the cases where bottom water is undersaturated with respect to calcite, the model is run both with and without respiration-driven dissolution, and the difference is calculated. The dissolution rate constant k_d is 1/day, and the calcite rain rate is in excess, to keep the calcite fraction at a constant value of ~100%.

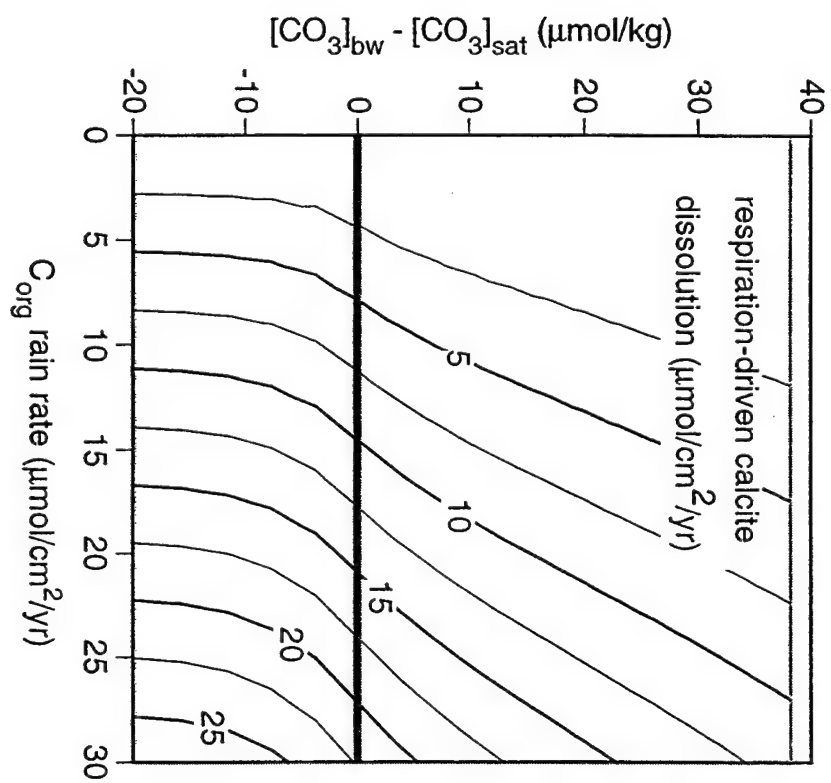
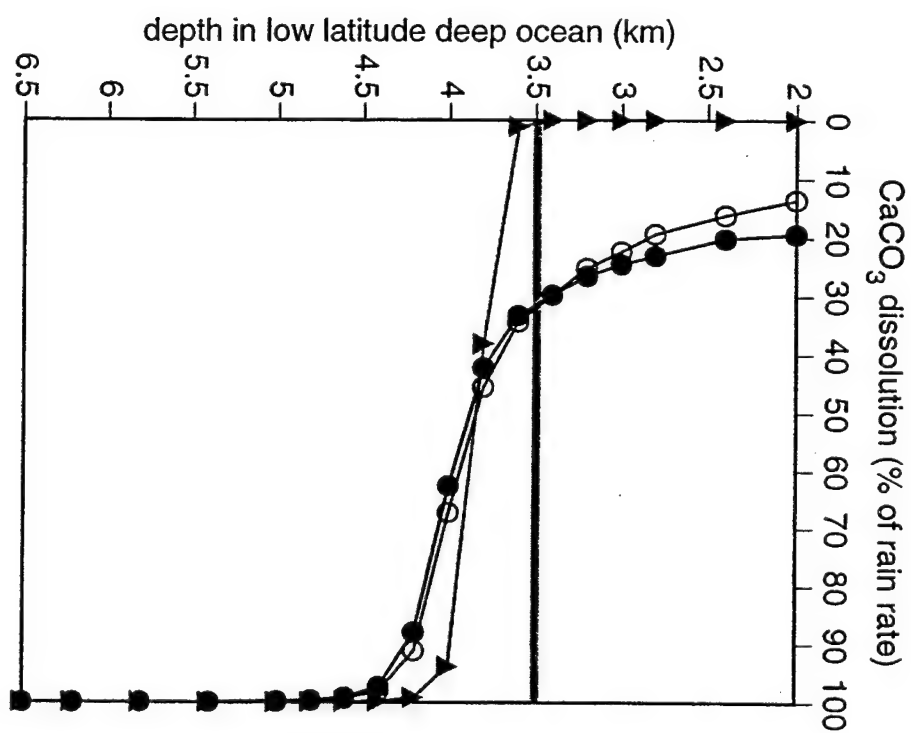


Figure AII-2

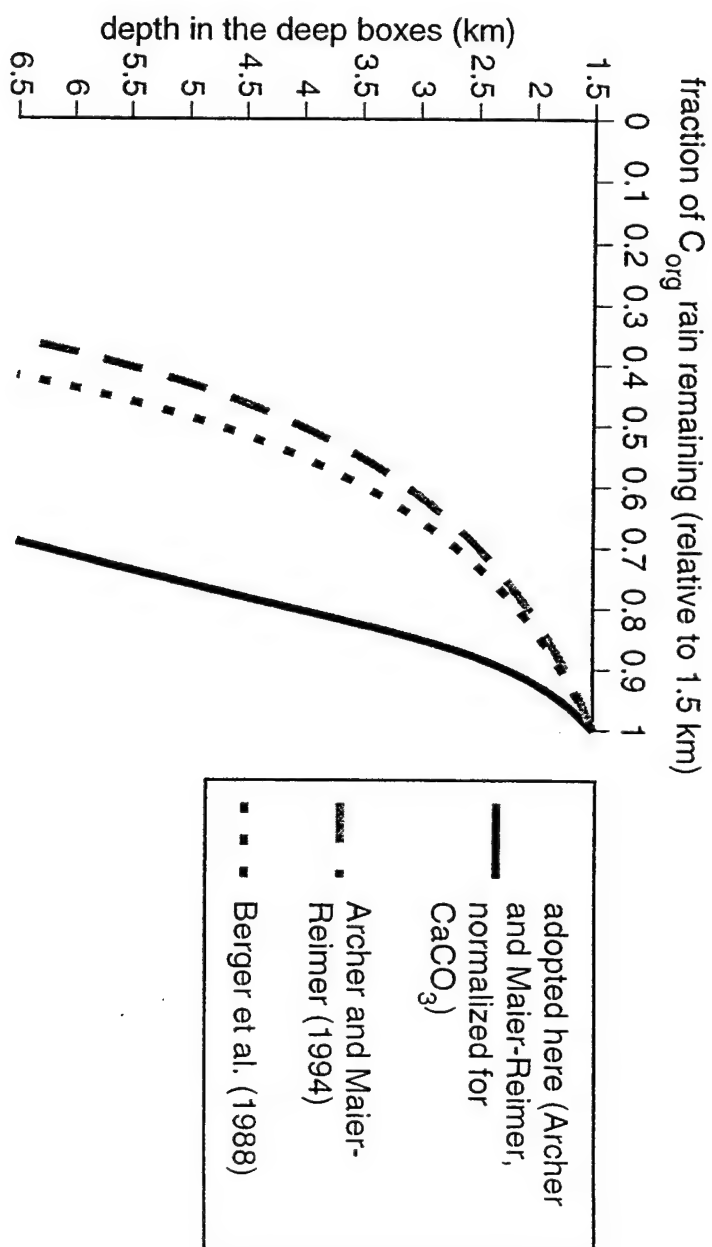
Depth profiles of calcite dissolution (as a percentage of the rain) in the standard interglacial case for the mixed layer open system model with (a) no respiration-driven dissolution and an assumed k_d of 30/day, (b) active respiration-driven dissolution and an assumed k_d of 1/day, with the C_{org} rain to the seafloor independent of water column depth, and (c) the same as (b) but with a C_{org} rain depth dependence adopted from [Archer and Maier-Reimer, 1994] (Figure AII-3).



- w/ resp. diss'n, no C_{org} profile, k_d=1/day
- w/ resp. diss'n, w/ C_{org} profile, k_d=1/day
- ▲ no resp. diss'n, k_d=30/day

Figure AII-3

The depth dependence of the C_{org} rain adopted from [Archer and Maier-Reimer, 1994], before and after adjustment for depth dependence in their $CaCO_3$ rain and normalization to give the C_{org} rain rate at 3.5 km as in the depth-independent case. The depth-dependent case is compared with the depth-independent case in the text. Also shown is the depth dependence defined by the relationship of [Berger *et al.*, 1988].



Chapter 3:
Natural Abundance-Level Measurement of
the Nitrogen Isotopic Composition of Oceanic Nitrate:
an Adaptation of the Ammonia Diffusion Method

D.M. Sigman^{1*}, M.A. Altabet², R. Michener³, D.C. McCorkle¹, B. Fry⁴, R.M. Holmes⁵

¹Department of Marine Geology and Geophysics, Woods Hole Oceanographic Institution,
Woods Hole, MA 02543, e-mail: dsigman@whoi.edu, fax: (508)-457-2183

*corresponding author

²Center for Marine Science and Technology, University of Massachusetts, Dartmouth,
North Dartmouth, MA 02747

³Department of Biology, Boston University, 5 Cummington Street, Boston, MA 02215

⁴Biology Department, Florida International University, University Park, Miami, FL 33199

⁵The Ecosystems Center, Marine Biological Laboratory, 7 MBL Street, Woods Hole, MA
02543

Marine Chemistry
in press

Abstract

We have adapted the "ammonia diffusion" method of nitrate extraction for natural-abundance level nitrogen isotopic measurement of oceanic nitrate. The method involves (1) sample concentration (by boiling or evaporation), (2) conversion of nitrate to ammonia using Devarda's alloy, and (3) the gas-phase diffusion of ammonia onto an acidified glass fiber disk which is sandwiched between two porous Teflon membranes. We have investigated the conditions necessary to effect complete ammonia recovery from natural seawater samples and the use of Devarda's alloy under these conditions. In addition, we have characterized the blanks in this method and designed a protocol to minimize them. Here, we report our protocol for nitrate extraction from seawater and provide an explanation of the protocol based on our method development work. To demonstrate the performance of the method, we present nitrate nitrogen isotopic data from nitrate standard additions to Sargasso Sea surface water and from several Southern Ocean depth profiles.

The nitrate extraction method gives highly reproducible, complete recovery of nitrate and a standard deviation for isotopic analysis of $<0.2\%$ down to $5\text{ }\mu\text{M}$ nitrate (or better). Replicate extractions of a nitrate standard added to Sargasso Sea surface water demonstrate agreement between the isotopic composition of the added and recovered N, with the extraction blank causing a $\leq 0.3\%$ difference at the $5\text{ }\mu\text{M}$ nitrate level.

The blanks inherent in this procedure are from Devarda's alloy and seawater dissolved organic nitrogen ("DON"). The N blank of the Devarda's alloy reagent depends on brand and lot number. The Devarda's alloy which we are currently using results in a blank of $\sim 0.4\text{ nmol N per } 100\text{ ml}$ of seawater (effectively $0.4\text{ }\mu\text{M}$). An isotopic correction is made for this blank. For standard incubation conditions, stored Woods Hole seawater (with $\sim 10\text{ }\mu\text{M}$ DON) gives a $\sim 0.6\text{ }\mu\text{M}$ DON blank, while stored Sargasso Sea surface water gives a DON blank of $0.3\text{--}0.5\text{ }\mu\text{M}$. The DON blank appears to cause a $\leq 0.3\%$ difference between the measured and actual isotopic composition of nitrate added to Sargasso Sea surface water at the $5\text{ }\mu\text{M}$ nitrate level, with a smaller isotopic difference for higher nitrate concentrations. We discuss several ways to lower the DON blank for samples in which the DON concentration is high relative to the nitrate concentration.

The nitrogen isotopic data from several Southern Ocean profiles, in conjunction with the other results presented in this paper, demonstrate the consistency of the data produced by the ammonia diffusion method. The ammonia diffusion-based protocol is more reliable and allows for better precision than the nitrate reduction/ammonia distillation method (Cline and Kaplan, 1975) in our hands. While the samples have an incubation time of four days or longer, we find that the diffusion method allows for higher throughput than the distillation method because samples can be run conveniently in large batches.

Introduction

All published natural abundance-level nitrogen isotopic data for oceanic nitrate have been generated by the Devarda's alloy/ammonia-distillation protocol of Cline and Kaplan (1975). These data have proved invaluable in our understanding of the nitrogen isotopic dynamics of oceanic nitrate (Horrigan et al., 1990; Liu and Kaplan, 1989; Liu et al., 1996). However, many workers find the ammonia distillation component of this method to be labor-intensive and problematic, and there are different reports regarding nitrate recovery, isotopic fractionation, and blanks (e.g., Liu et al., 1996). For this reason, we have investigated the "ammonia diffusion" method (Conway, 1947) as a potential alternative for natural abundance-level measurements on oceanic nitrate.

As developed by previous workers, nitrate extraction via ammonia diffusion involves (1) conversion of nitrate (and nitrite) to ammonia using Devarda's alloy (as in the distillation method), and (2) gas-phase diffusion of ammonia out of the seawater sample and onto an acidified glass fiber disk or into an acidic solution (references in Keeney and Nelson, 1982). These two processes occur within a sealed sample container.

Development work on this method has been done recently for ^{15}N -tracer level work, for soil extracts (Brooks et al., 1989; Downs et al., submitted; Kelley et al., 1991; Lory and Russelle, 1994; Sorenson and Steen-Jensen, 1991) and for seawater (Fisher and Morrissey, 1985; Kristiansen and Paasche, 1989). We have focussed on achieving the level of precision necessary for natural abundance work in seawater, over a nitrate concentration range that would make this method generally applicable in the open ocean. Toward this end, we have investigated the conditions necessary for quantitative nitrate conversion to ammonia by Devarda's alloy and for complete ammonia recovery from a seawater sample. In addition, we have investigated the blanks associated with this method, which are due to (1) N released from Devarda's alloy and (2) N released from the breakdown of a small amount of seawater dissolved organic nitrogen.

In the “Protocol” section, we provide a complete protocol for nitrate extraction via the ammonia diffusion method. In the “Explanation of Protocol” section, we present results from the method development work upon which the protocol is based. In the “Results” section, we present isotopic results for extractions of a nitrate standard added to Sargasso Sea surface seawater and for several nitrate depth profiles from the Southern Ocean, to demonstrate the performance of the method.

Protocol (see Figure 1, Table 1)

This section is intended to provide all of the basic information necessary to carry out nitrate extractions. The section which follows this one, "Explanation of Protocol," provides background and supplemental information which may be useful to some readers. However, all readers planning on using this protocol should refer to the "Blanks" subsection at the end of the "Explanation of Protocol" section.

Figure 1 outlines the major steps of the extraction protocol. Table 1 summarizes recommended extraction conditions for a range of sample nitrate concentrations, targeting a final sample size of 2 $\mu\text{mol N}$ for mass spectrometry.

Step 1: Using a graduated cylinder, measure out an adequate volume of sample to provide enough N for mass spectrometry. Pour the sample into a glass media bottle (Wheaton # 219817, Teflon-coated caps). For samples which are ≤ 200 ml, 250 ml media bottles should be used throughout the protocol. For larger samples, 500 ml or 1 l media bottles can be used. If 1 l bottles are used, the samples should be transferred into 500 ml media bottles after step 6.

Step 2: Add 200-300 mg of MgO (precombusted at 650°C for 4 hours) per 100 mls of sample. This brings the pH to ~ 9.7 for unconcentrated seawater.

Step 3: Preincubate the sample at 65°C for ~ 5 days, in order to decompose labile dissolved organic nitrogen to ammonia. This preincubation step can be carried out under higher pH if the DON blank is likely to be high relative to the nitrate concentration (see "Explanation of Protocol")¹. On the other hand, for samples with high nitrate concentrations and/or low DON concentrations, such as deep ocean water, the preincubation step can be shortened or skipped altogether.

¹ The sample preincubation and boiling can be carried out at higher pH by the addition of ≥ 0.5 ml 10 N NaOH instead of excess MgO. This lowers the N blank from DON breakdown during the nitrate extraction step (see "Explanation of Protocol"), and it also decreases problems with sample bumping if the samples

Step 4: Construct diffusion packets. The diffusion packet is a 1 cm GF/D filter disk (Whatman # 1823 010), acidified with 20-30 μ l of 2 M sulfuric acid, and sandwiched between two 2.5 cm diameter 10 μ m pore-size Teflon membranes (Millipore LCWP 025 00). The protocol for packet construction is as follows:

a) Combust the GF/D disks at 400°C for 4 hours. Transfer the Teflon membranes to a glass beaker. Rinse them once with 10% HCl, then repeatedly with distilled water, and dry at ~65°C.

b) Use a precleaned aluminum foil sheet over several paper towels as the working area. Handle the membranes and glass fiber disks with clean, dull-tipped forceps.

c) Place a glass fiber disk on a Teflon membrane.

d) Pipet 20-30 μ l of 2 M sulfuric acid onto the disk.

e) Place a second membrane over the disk and lower membrane.

f) Seal the two membranes together by hand-pressing with a smooth-edged metal cylinder of about 2 cm diameter and 1 mm wall thickness. A slight rotation of the cylinder ensures that membrane is sealed along the entire circumference.

Packets may be constructed 5 or more at a time, then transferred to and stored in an air-tight container. Following this protocol, 50 packets can be made in an hour or less. We have stored packets in an air-tight container several weeks, with no effect on the N blank (in our case, ~20 nmol for the acidified disk).

Step 5: Boil or evaporate sample down to reduce the sample volume and remove any dissolved ammonia. Recommended volume reduction is to 15-25% of the initial sample volume (see Table 1 and “Explanation of Protocol” below).

are to be boiled (step 5). In this case, the sample pH must be brought below 9 by 50% HCl addition after the boiling step, and then excess MgO should be added.

a) If samples are boiled down, boiling stones should be added, and 50 ml beakers should be placed over the bottle tops. Samples should be stirred periodically before boiling starts, to prevent bumping.

b) Samples may also be evaporated down to dryness at 95°C in a clean laboratory oven². Low-DON deionized water is then added to reach the appropriate volume, and the bottle is swirled to redissolve the salts.

Step 6: Add one diffusion packet to each bottle. Then weigh out the appropriate amount of Devarda's alloy (75 mg per 100 ml initial sample volume, Table 1, see "Explanation of Protocol" below) and add it to the sample bottle. Tighten the cap immediately after the addition of Devarda's alloy.

Step 7: Swirl the bottles and incubate in a laboratory oven at 65°C for 4 days.

Step 8: Remove the bottles from the oven and place on a reciprocating shaker table for up to 7 days, depending on the initial sample volume (see Table 1). Oscillations should be ~1 per second.

Step 9: Remove diffusion packets from the media bottles, dipping each into 10% HCl, then distilled water. Place the packets in a dessicator cabinet with silica gel and an open container of concentrated sulfuric acid (to remove trace ammonia). Leave the packets to dry for 1 to 2 days. Alternatively, samples may be dried for several hours at 65°C in a laboratory oven. Oven drying does not cause ammonium loss or fractionation; however, the samples are more vulnerable to contamination than if dried in a dessicator.

Step 10: For storage, place packets in individual vials with sealing caps. The vials should be stored in an air-tight container, with an open container of glass fiber filter material saturated with sulfuric acid.

² All of the samples for which we show data in this study were boiled to reduce volume. We recently found that oven evaporation can also be used. Evaporation is much less labor intensive and does not suffer from problems such as sample bumping, so that we now consider it our primary method of volume reduction.

Step 11: Shortly before combustion for isotopic analysis, separate the Teflon membranes with dull-tipped forceps and remove the glass fiber disk. If analyzing samples by on-line combustion, pack disks in tin boats on the day of analysis, as the tin reacts with the sulfuric acid in the GF/D disk. Also, the He flow containing the sample N₂ gas should be passed through a liquid N₂ trap after the standard chemical traps, to remove any remaining SO₂. The Teflon membranes may be reused one or two times. They should be separated, soaked for a day in 10% HCl, then washed repeatedly with distilled water and dried at 65°C.

Step 12: The isotopic measurements should be corrected for the effect of the Devarda's alloy blank. This correction will depend on the brand and lot of Devarda's alloy used (see "Explanation of Protocol").

Explanation of Protocol

Below, we discuss results relevant to the protocol described above and to the use of the ammonia diffusion method in general. The explanation is separated into three components: (1) nitrate reduction by Devarda's alloy, (2) ammonia diffusion, and (3) blanks. Because the protocol must be designed considering all of these components together, the separation is somewhat artificial. We list the major questions addressed in each section at the beginning of that section.

Most of the isotopic data presented in this paper were generated using a Europa Roboprep elemental analyzer on-line with a Finnigan MAT 251 stable isotope mass spectrometer. All isotopic values given in this paper are in permil units versus laboratory air, which is checked for consistency with several types of standards. Ammonium sulfate standard solution pipetted onto an acidified glass fiber disk (which is identical to the sample type generated by this nitrate extraction protocol) typically yields a standard deviation of 0.15‰ or better. Isotopic data presented in Figures 5 and 6 were generated at the Marine Biological Laboratory Ecosystems Center stable isotope facility, on a Finnigan Delta-S with an on-line Heraeus elemental analyzer (Fry et al., 1992). As with the MAT 251 system, combusted standards run with the samples also yielded a standard deviation of 0.15‰ or better.

Nitrate concentration measurements presented in Figures 2, 3, 13 were made by nitrate reduction to nitric oxide by V(III), followed by nitric oxide measurement using a NO_x detector (Garside, 1982). We did not attempt to resolve nitrate from nitrite, so the measurements are actually for the sum of these two species. Nitrate concentration data in Figures 11 and 12 were generated on-board by the WOCE science crew during WOCE leg I9.

Nitrate Reduction by Devarda's Alloy

Questions addressed:

- 1) pH/temperature/time conditions necessary for complete nitrate conversion*
- 2) effect of sample volume reduction by boiling on nitrate conversion*
- 3) amount of Devarda's alloy required for optimal isotopic results*

Devarda's alloy, an alloy of Al, Cu and Zn, has a significant N blank associated with the diffusion method (see section below), so that it is optimal to minimize the amount of Devarda's alloy needed to ensure complete nitrate reduction. The conversion of nitrate to ammonia by Devarda's alloy becomes more rapid as the pH and temperature of the incubation are increased. Because pH and temperature also play a role in the size of the N blank associated with the breakdown of dissolved organic nitrogen (see section below), we have experimented with the nitrate reduction step to find the conditions which drive complete nitrate reduction for the smallest amount of Devarda's alloy while minimizing the DON blank.

1) pH/temperature/time conditions necessary for complete nitrate conversion

Nitrate was added to 200 ml samples of Woods Hole seawater, giving a nitrate concentration of 37.5 μM . We then added 200 mg of Devarda's alloy (100 mg per 100 ml seawater) and incubated the samples under four sets of conditions: (1) pH=12.5 (by 10 N NaOH addition), T=65°C, (2) pH=9.7 (by the addition of excess MgO), T=65°C, (3) pH=12.5, T=20°C, (4) pH=9.7, T=20°C. Samples were removed and measured for nitrate+nitrite concentration after 16 hours, 4 days, and 9 days, using different samples for each measurement (Figure 2). It appears that the most rapid nitrate removal occurs in cases (1) and (3), but that nitrate reduction is equally complete for cases (1), (2) and (3) after 4 days. The only inadequate set of conditions for nitrate reduction is case (4): pH=9.7, T=20°C.

We carried out a similar experiment to that described above, except that we added only 50 mg of Devarda's alloy per 100 mls of seawater. In all cases, nitrate reduction was incomplete after 4 days, with the sample incubated at pH=9.7 (using MgO) and 65°C (case 2 above) having the lowest final nitrate concentration of 0.2 μM (~3-4 times the final nitrate concentration for the addition of twice as much Devarda's alloy, Figure 2) and the other samples having more than 1 μM nitrate remaining. Thus, while the speed of nitrate reduction by Devarda's alloy may vary significantly with pH, the total capacity of the reagent to reduce nitrate over a four day period is not greater if run under a higher pH than generated by the MgO buffer.

2) effect of sample volume reduction on nitrate conversion

Reducing the seawater sample volume by boiling or evaporation aids nitrate reduction. This is shown for incubations of 400 ml samples of Woods Hole seawater with 10 μM added nitrate, boiled down to several final volumes (Figure 3). When only 100 mg of Devarda's alloy was added, nitrate reduction was incomplete for all final sample volumes (open symbols, scale on left axis). However, evaporating the sample down to as little as 12% of the initial volume increased the efficiency of nitrate reduction (despite the formation of precipitates). A similar trend is observed for incubations with 200 mg Devarda's alloy, although >99% of the initial nitrate was reduced in all of these samples, with <0.1 μM nitrate remaining in all cases (closed symbols, scale on right axis). Note in Figure 3 that a sample concentrated 16-fold (to 25 ml) showed very poor nitrate reduction. This suggests that 8-fold concentration represents an approximate upper limit on the degree to which seawater nitrate samples should be concentrated.

The poor nitrate reduction efficiency for 16-fold seawater concentration may be due to the observed change in the pH of seawater buffered with MgO as it is concentrated by boiling (Figure 4). Our recommended range of sample concentration is to 15-25% of the initial sample volume. In this range, the sample pH in equilibrium with MgO is between

8.8 and 9.2. For 16-fold sample concentration (~6% of the initial sample volume), the observed pH is ~8.4, very close to that of unbuffered seawater. The reduction of nitrate by Devarda's alloy is facilitated to some degree by elevated pH; it may be that a pH of 8.4 causes an inadequate rate of nitrate reduction.

Na_2CO_3 buffers seawater at a higher pH than MgO , although this pH also decreases as the seawater sample is concentrated, so that a 16-fold concentration of seawater yields a pH of 8.7. A nitrate removal experiment using Na_2CO_3 as the pH buffer did indeed show complete nitrate removal in a seawater sample that had been concentrated 16-fold, consistent with the higher pH of this sample than if it were buffered with MgO . A preliminary test of Na_2CO_3 as a replacement for MgO has given inconsistent results. However, this direction is still worth pursuing, as it may allow for the concentration of samples to smaller final volumes, which is advantageous for the ammonia diffusion step (see "Ammonia Diffusion" below).

3) amount of Devarda's alloy required for optimal isotopic results

In order to determine the amount of Devarda's alloy required to achieve adequate nitrate reduction to produce reliable isotopic data, we made replicate isotopic measurements on 200 ml subsamples of deep water from a western Atlantic station (boiled down to ~30 ml, according to the protocol, Table 1), varying the amount of Devarda's alloy added (Figure 5). Replication of the samples with only 50 mg alloy is poor. However, greater additions of alloy lead to more reproducible results, with a higher measured $\delta^{15}\text{N}$. The $\delta^{15}\text{N}$ values plateau at 100-125 mg Devarda's alloy additions and decrease for greater alloy additions. This $\delta^{15}\text{N}$ decrease with increasing alloy addition is due to the increasing importance of the Devarda's alloy blank (see section below). Thus, if 200 ml samples are boiled down to 15-25% of their initial volume, the optimal amount of alloy to add is roughly 100-125 mg, or 50-60 mg Devarda's alloy per 100 ml of initial sample volume. This result is consistent with the measurements of nitrate removal by Devarda's alloy in

Figure 3, which showed complete nitrate reduction when 200 mg of Devarda's alloy was added to samples with 400 ml initial volume (50 mg/100 ml initial sample volume). The recommended size of Devarda's alloy addition in the protocol is ~75 mg/100 ml initial sample volume, greater than the observed minimum requirement (50 mg/100 ml), to ensure complete nitrate reduction in the case of unforeseen differences in conditions among laboratories or among brands of Devarda's alloy.

Ammonia Diffusion

Questions addressed:

- 1) incubation conditions necessary for complete ammonia extraction*
- 2) effect of sample volume reduction on ammonia extraction*
- 3) incubation time required for optimal isotopic results*

The use of a Teflon container for the acid trap originates with Sorenson and Steen Jensen (1991), who found that an acidified glass fiber filter within an envelope of Teflon tape takes up ammonia efficiently. We have found these packets to be fairly reliable; however, depending on the construction of the envelope, leaks can occur, especially in a vigorously shaken sample. Our diffusion packets, built from porous Teflon membranes (see protocol above), are much more easily and quickly constructed, more leak-tight in a shaken sample, and are more reproducible in construction than the Teflon tape envelopes used previously. The disadvantage of our design is that the Teflon membranes are more expensive (~\$1 per membrane); however, they can be reused, making this less of an issue.

1) incubation conditions necessary for complete ammonia extraction

Ammonia diffusion out of aqueous solution strongly fractionates the nitrogen isotopes, so that yield must be complete. We have investigated the physical conditions (heating, shaking, etc.) necessary to produce quantitative recovery of ammonium and good

reproducibility in the isotopic composition, for 200 ml Woods Hole seawater (not boiled or evaporated down) with 20 μM of added ammonium, incubated for 11 days (Table 2). The Teflon tape envelopes and our Teflon membrane sandwiches give indistinguishable results. We also find that heating (to 65°C) or shaking the diffusing sample give indistinguishable results, while samples incubated at room temperature without shaking did not achieve adequate ammonium uptake. From other experiments, we find that shaking the sample once daily is inadequate, at least for a 200 ml sample volume. Thus, samples must either be heated or shaken continuously to achieve adequate ammonia diffusion on a workable time scale.

There is a 0.4‰ offset between the diffused ammonium samples and the directly measured ammonium standard in this experiment. Ammonium extraction by the distillation method has shown the same offset, giving an average $\delta^{15}\text{N}$ of -0.36‰, with a standard deviation of 0.44‰ (Table 2). The cause for the offset between the extracted ammonium samples and the ammonium standards is unknown. Larger volume diffusions (≥ 500 ml) have shown a systematic negative offset from the ammonium standard isotopic composition associated with incomplete ammonia uptake (Holmes et al., submitted), so that a similar

explanation may apply to the results shown here for 200 ml samples³. This effect for ≥ 500 ml samples is one of the motivations for the sample volume reduction step in the protocol (step 5).

However, the similarity between the diffusion and distillation results may indicate a cause other than fractionation during diffusion. One potential explanation for the offset is an isotopically light N blank. The N blank is $\sim 5\%$ of the ammonium addition for the experiment summarized in Table 2. This blank is due to extraction of background ammonium in stored Woods Hole seawater (typically $0.5\text{--}0.7\ \mu\text{M}$) as well as to the breakdown of some labile DON to ammonia ($\sim 0.3\ \mu\text{M}$, discussed below). For the blank to cause the isotopic offset, it must be lower in $\delta^{15}\text{N}$ than the added ammonium standard (0‰). Unfortunately, we have no reliable isotopic measurements of the DON blank under these conditions. In one set of diffusion experiments, an inverse relationship was observed between measured $\delta^{15}\text{N}$ and yield, which would implicate the blank as a cause as a potential cause for the isotopic offset. However, this relationship is not always observed.

2) effect of sample volume reduction on ammonia extraction

To determine the optimal degree of sample volume reduction, replicate 400 ml samples of surface seawater with $5\ \mu\text{M}$ added nitrate were boiled down to a range of final volumes in preparation for nitrate extraction. All samples were incubated for 4 days in the oven, then 7 days on the shaker table. The isotopic results are shown in Figure 6 for two experiments, experiment 1 using Woods Hole seawater and experiment 2 using Sargasso Sea surface water. Taken together, the two experiments suggest that final volumes between 55 and 80 ml (15–20% of their initial volume) give consistent isotopic results. Both experiments suggest that samples with final volumes >100 ml ($>25\%$ of the initial sample volume) may be lower in $\delta^{15}\text{N}$, with more scatter. In experiment 1, the two samples boiled

³ In another experiment, in which 200 ml samples with $10\ \mu\text{M}$ ammonia (using a different ammonium standard) were extracted while shaking for 2 weeks, the offset between the diffused and directly measured

down to 50 ml give spurious results; however, the results are very reproducible for the 50 ml samples in experiment 2. The disagreement between the two experiments for the 50 ml samples leaves some ambiguity as to the lower limit to which sample volume can be reduced. In the protocol, we recommend that samples be concentrated to 15-25% of their initial volume.

The published pK_a of ammonium is 9.2-9.5, although we have found no data for concentrated seawater (Martell and Smith, 1982). Given the pH range of concentrated seawater (Figure 4), ammonium (rather than ammonia) may be the dominant species for samples concentrated more than 50%. This does not preclude complete ammonium/ammonia recovery, as ammonia is continually leaving solution. Indeed, we have observed isotopically reliable isotopic data for samples concentrated down to 15% of the initial sample volume. However, it may be the low pH that leads to erratic results from samples which are concentrated more than this, either because of the effect on the ammonium/ammonia equilibrium or because of the effect on nitrate reduction discussed above. As mentioned previously, one potential route for circumventing this pH problem involves the use of another pH buffer, such as Na_2CO_3 ; this is a direction for future method development work.

3) incubation time required for optimal isotopic results

We determined the time required for complete nitrate extraction by carrying out the extraction on a nitrate standard added to Woods Hole seawater, stopping the incubation after different amounts of time. Isotope data for 100 ml samples of 20 μM nitrate (boiled down to ~20 ml) suggest adequate extraction after 4 days (Figure 7). The same experiment has also been carried out for 200 ml samples of 10 μM nitrate (boiled down to 30-40 ml). While mass spectrometric problems compromised this experiment, the results suggest that

standard was 0.2-0.25‰. The added three days of diffusion may explain the smaller offset.

the necessary incubation time for a sample of 200 ml initial volume is 6 days (four days in the oven, two on the shaker).

Note in Figure 7 that the $\delta^{15}\text{N}$ of the 100 ml samples may decrease slightly after four days of incubation. This may be due to a growing blank due to DON breakdown, which is evident in the time course of N yield for the 20 μM standards and in blanks run along with the standards (Figure 7)⁴. However, this concern is secondary to ensuring complete nitrate extraction. Because conditions may vary among laboratories for unforeseen reasons, the recommended incubation times given in table 1 are several days longer than we have found to be necessary to generate reproducible isotopic data.

As nitrate reduction occurs relatively rapidly (in ~1-2 days), the main determinant of the necessary incubation time is the ammonium diffusion step. Data for ammonium extraction from sample volumes between 200 ml to 2 l shows that the requisite diffusion time depends on the sample volume (Holmes et al., submitted). The recommended incubations periods for 100 and 200 ml samples in Table 1 are based on time-course experiments. While we have not yet carried out the time course experiment for samples with nitrate concentrations below 10 μM , ammonium extraction experiments suggest that final sample volumes of 200 ml require ~2 weeks for adequate ammonium recovery. Thus, the incubation periods for samples with final volumes >40 ml (initial volumes greater than >200 ml) are conservative estimates, with the constraint that samples with final volumes of 200 ml require incubation times of ~2 weeks to achieve adequate ammonium recovery for reproducible isotopic data.

⁴ The 10% excess in N yield is consistent with the Devarda's alloy being used at the time and a DON-derived blank of ~0.9 μM for Woods Hole seawater without preincubation (see Blanks section). The time series incubations shown in Figure 7 were run with stored Woods Hole seawater, without any preincubation to break down labile DON, so these samples probably represent a worst-case scenario for the blank size.

Blanks

Questions addressed:

- 1) size and isotopic composition of the Devarda's alloy blank*
- 2) size of the DON blank*
- 3) additional methods to reduce the DON blank*

1) size and isotopic composition of the Devarda's alloy blank

Devarda's alloy has a significant N blank associated with our diffusion protocol. The Devarda's alloy blank size can be measured by carrying out the diffusions with a size series of Devarda's alloy in 1M NaCl solution (Figure 8). This blank varies significantly for different brands and lot numbers. Blank estimates for several brands and lots are given in Table 3. We currently use EM Science lot 34194.

While the blanks were measured with the intention of looking at the size data only, we found that the isotopic measurements of the blanks (and standards of similar N amount) often showed good reproducibility and reasonable linearity, despite the small amounts of nitrogen being analyzed. These direct isotopic measurements suggest a $\delta^{15}\text{N}$ between -6 and -7.5‰ for both Reidel-de-Haen and EM Science brands. For Reidel-de-Haen lot 50510, we added a size series of Devarda's alloy to 20 μM nitrate (in 1M NaCl solution), to verify that a sample dilution approach to estimate the $\delta^{15}\text{N}$ of the Devarda's alloy blank gives a similar value. As shown in Figure 9, the $\delta^{15}\text{N}$ of the blank estimated in this way is approximately -6‰, in agreement with the direct isotopic measurements of the blanks.

The calculated offset between the measured $\delta^{15}\text{N}$ of nitrate and its true $\delta^{15}\text{N}$ is shown in Figure 10, for a true $\delta^{15}\text{N}$ of 5‰ and two different sizes of Devarda's alloy blank. If a brand/lot of Devarda's blank with a high blank is used (120 nmol/100mg, e.g., Reidel-de-Haen lot 50510), the offset is less than 1‰ down to ~6 μM nitrate. If a lot of Devarda's alloy with a lower blank is used (45 nmol/100mg, e.g., EM Science lot 34194),

the offset is less than 1‰ down to $\sim 4 \mu\text{M}$ nitrate. In all cases, one can correct for the offset; however, this blank correction and the error associated with it increase as the blank becomes a larger part of the total signal.

We have attempted to lower the Devarda's alloy blank by combusting the alloy, with inconclusive results. In some cases, we observed a decrease in the blank by as much as a half of its initial value; in other cases, no change was observed. Some of our results suggest that combustion of Devarda's alloy in air decreases its nitrate reduction efficiency. A potential direction for future method development work involves removing the N blank from Devarda's alloy or finding a lower-blank reagent to replace it.

2) size of the DON blank

Because of the long period of sample incubation at elevated temperature and pH, a small portion of the DON in the sample breaks down to ammonia, resulting in a "DON blank". For stored Woods Hole seawater⁵, we have observed that the blank associated with this process increases as the pH and temperature of incubation are increased. The speed of nitrate reduction by Devarda's alloy is also enhanced by the same conditions. Therefore, the method must compromise among (1) the speed of nitrate conversion (2) the Devarda's alloy blank, and (3) the DON blank.

Without any pretreatment, we measure a DON/ammonium blank "concentration" in stored Woods Hole seawater of $1.5 \mu\text{M}$ (Table 4, Devarda's alloy and acidified filter blanks already subtracted). Boiling reduces the blank to $0.95 \mu\text{M}$. This $0.6 \mu\text{M}$ decrease in the observed blank is probably mostly due to the loss of ammonium; however, labile organic nitrogen such as amino-sugars would also be removed at this step (Yonebayashi and Hattori, 1980). The same decrease is observed for blanks run without the addition of

⁵ In all cases, Woods Hole seawater was stored in the sunlight for a week to remove trace nitrate before filtering. One DON concentration measurement of stored Woods Hole seawater gave $10.5 \mu\text{M}$. This is higher than the typical DON concentration of $7\text{--}9 \mu\text{M}$ measured in Woods Hole seawater which is filtered immediately after collection.

Devarda's alloy (Table 4). A five-day preincubation with MgO lowers the blank (by an additional $0.3\ \mu\text{M}$) to $0.65\ \mu\text{M}$; this decrease is due solely to the breakdown of labile DON to ammonia.

In this experiment, we found that the DON blank with Devarda's alloy ($0.65\ \mu\text{M}$) was significantly larger than the blank for the ammonium diffusion alone ($0.2\ \mu\text{M}$). This result has varied among different experiments; it cannot be explained by trace nitrate in the surface seawater used for the blank experiments, which was $\sim 0.1\ \mu\text{M}$. The two potential causes for the higher DON blank observed with Devarda's alloy addition are (1) the breakdown of some nitrogenous compounds to nitrate, which is incorporated into the blank only if nitrate is reduced to ammonia, and (2) breakdown of some nitrogenous compounds to ammonia due to the presence of Devarda's alloy. The first of these options has been ruled out by the fact that nitrate concentration did not increase over the course of an incubation without Devarda's alloy. Therefore, we tentatively conclude that Devarda's alloy can facilitate the breakdown of DON to a limited degree.

The DON blank of $0.65\ \mu\text{M}$ in stored Woods Hole seawater, which has a DON concentration of $\sim 10\ \mu\text{M}$, is a likely upper limit for the seawater DON blank if samples are both preincubated with MgO and boiled. Stored Sargasso Sea surface water has a DON blank of $0.3\text{--}0.5\ \mu\text{M}$ (depending on the batch). Several measurements of the diffusion-only blank (no Devarda's alloy addition) for Antarctic surface water gave values of $\leq 0.1\ \mu\text{M}$, lower than that for a 1 M NaCl solution made from combusted NaCl and MilliQ-UV water.

3) additional methods to reduce the DON blank

We have found that the DON blank can be lowered further by preincubation and/or boiling at a pH greater than is generated by excess MgO (Table 5). A batch of Sargasso Sea surface water gave an effective DON blank of $\sim 0.5\ \mu\text{M}$ if preincubated and boiled with MgO. When the preincubation and boiling was carried out at a pH of 11.5, followed by acidification to a pH < 9 and addition of excess MgO, a DON blank of $\sim 0.3\ \mu\text{M}$ was

observed. We have observed similar results for Woods Hole seawater. In surface seawater, with and without 10 μM glycine addition, neither a month-long preincubation nor boiling caused DON (natural or added glycine) to be converted to nitrate. In addition, we find that nitrate is resilient to these pretreatments. As a result, these steps generate no artifacts.

Since the DON breakdown rate increases with temperature, shortening the incubation time at 65°C also lowers the DON blank. We have found for 100 ml samples that the time of incubation at 65°C can be shortened from 4 days to 2 days (adjusting the time on the shaker to give the same total incubation time). This observation needs to be checked for the full range of sample volumes, but it is unlikely to vary. If the incubation time at 65°C is reduced to two days for the same batch of Sargasso Sea surface water described above, the effective DON blank is reduced from $\sim 0.5 \mu\text{M}$ to $\sim 0.25 \mu\text{M}$ (Table 5).

Additional steps for DON removal which may prove useful but which we have not tested are (1) the scavenging of DON by exchange resins, and (2) the conversion of amino N to ammonia by the use of ninhydrin (Kennedy, 1965).

Results

To test our method, stored Sargasso Sea water was amended with nitrate of $\sim 3.7\text{‰}$ and extracted in two separate experiments (Table 6). The standard deviation for all concentrations is better than 0.2‰ ($n=4$). The measured $\delta^{15}\text{N}$ of $5\text{ }\mu\text{M}$ nitrate is $\sim 0.3\text{‰}$ lighter than the added nitrate ($0.4\text{--}0.5\text{‰}$ lighter for samples without preincubation), while higher nitrate concentrations give $\delta^{15}\text{N}$ values closer to the expected value. The isotopic differences between the different concentrations is probably due to the seawater DON blank. Blanks measured for this batch of Sargasso Sea Water give a DON blank of $\sim 0.5\text{ }\mu\text{M}$. This level of blank would give the observed differences among the different nitrate additions if the blank $\delta^{15}\text{N}$ is $\sim 0\text{‰}$. Isotopic measurement of the DON blank in surface waters has given $\delta^{15}\text{N}$ values below 0‰ , but these measurements are unreliable because of the small amount of nitrogen being analyzed. For Kuroshio water, Liu et al. (1996) estimate that the $\delta^{15}\text{N}$ of the DON blank in the distillation method is roughly -3‰ .

In general, samples with $\geq 10\text{ }\mu\text{M}$ nitrate have a precision close to the precision of our isotopic standards. Occasional “fliers” do occur ($\sim 5\text{--}10\%$ of processed samples), with the $\delta^{15}\text{N}$ being anomalously low. These bad extractions are usually obvious, allowing for replication and/or removal from the data set. While anomalously low values are consistent with incomplete ammonia extraction during diffusion, this could occur because of a problem with either the nitrate reduction step or the ammonia diffusion step.

Figure 11 shows a depth profile of $\delta^{15}\text{N}$ data from a WOCE I9 station in the Antarctic sector of the eastern Indian Ocean. Because this station is from south of the Polar Frontal Zone, surface nitrate is reduced only to $24\text{ }\mu\text{M}$ in the surface mixed layer. The $\delta^{15}\text{N}$ data demonstrate the isotopic homogeneity of deep oceanic nitrate in this region. The clear correlation between nitrate concentration and isotopic composition in the upper 500 m of the water column is due to isotopic fractionation during nitrate uptake by phytoplankton (Sigman et al., 1996).

Figure 12 shows a shallow depth profile of nitrate $\delta^{15}\text{N}$ data from a Subantarctic station in the eastern Indian Ocean. In this profile, surface nitrate is reduced to $10\ \mu\text{M}$ in the surface mixed layer. The clear correlation between nitrate concentration and isotopic composition is evident here as well. The $\delta^{15}\text{N}$ measurements of the samples from within the mixed layer are as precise as the mass spectrometry allows.

For a Southern Ocean depth profile from the Kerguelen region, nitrate has been extracted using both the diffusion and distillation methods (Figure 13). The values achieved by the two methods are similar. The $\delta^{15}\text{N}$ data from the diffusion method is more strongly correlated with nitrate concentration within the surface mixed layer. This is consistent with the observation that the diffusion method is more precise than is commonly observed for the distillation method. However, the precision that is possible for the distillation method probably varies among laboratories.

Conclusions

An adaptation of the ammonia diffusion method provides a reliable, accurate, and high-throughput method for the extraction of oceanic nitrate for isotopic analysis. As is evident from the data presented here, the ammonia diffusion-based method represents a major advancement with respect to both the quality and the quantity of $\delta^{15}\text{N}$ data which can be produced for oceanic nitrate. As with the distillation-based extraction method, the diffusion-based method has a lower limit of applicability at 1-2 μM nitrate, largely because of the N blanks. However, we have outlined routes for future method development which may allow for isotopic analyses at and below nitrate concentrations of 1 μM .

Acknowledgements

R. Francois helped to guide the direction of this work. J. Donaghue performed the distillation extractions and aided the progress of this research in many ways. Isotopic analyses at the MBL isotope facility were performed by K. Tholke. Sample collection for the Southern Ocean profiles shown in Figures 11 and 12 was generously performed by the science crew of WOCE I9 (OCE 13167). J. Brandes and J. Montoya provided useful advice. Europa Scientific provided important support and advice. The first author was supported by the NSF graduate research fellowship program and by the JOI/USSAC Ocean Drilling graduate research fellowship program.

References

- Brooks, P.D., Stark, J.M., McInteer, B.B. and Preston, T., 1989. Diffusion method to prepare soil extracts for automated nitrogen-15 analysis. *Soil Science Society of America Journal*, 53: 1707-1711.
- Cline, J.D. and Kaplan, I.R., 1975. Isotopic fractionation of dissolved nitrate during denitrification in the Eastern Tropical North Pacific Ocean. *Marine Chemistry*, 3: 271-299.
- Conway, E.J., 1947. Microdiffusion analysis and volumetric error. Crosby, Lockwood, London.
- Downs, M.R., R.H., M., Fry, B. and Nadelhoffer, K.J., submitted. Routine measurement of dissolved inorganic ^{15}N in streamwater. *Journal of Hydrology*.
- Fisher, T.R. and Morrissey, K.M., 1985. A new method for the recovery of ammonium from natural waters for measurement of ^{15}N composition in isotope dilution experiments. *Marine Chemistry*, 16: 11-21.
- Fry, B., Brand, W., Mersch, F.J. and Garritt, R., 1992. Automated analysis system for coupled $\delta^{13}\text{C}$ and $\delta^{15}\text{N}$ measurements. *Analytical Chemistry*, 64.
- Garside, C., 1982. A chemiluminescent technique for the determination of nanomolar concentrations of nitrate and nitrite in seawater. *Marine Chemistry*, 11: 159-167.
- Holmes, R.M., J. McClelland, D.M. Sigman, B. Fry, B.J. Peterson, Measuring ^{15}N -ammonium in marine, estuarine, and fresh waters: an adaptation of the ammonium diffusion method for samples with low-ammonium concentrations. *Marine Chemistry*, submitted.
- Horrigan, S.G. et al., 1990. Nitrogenous nutrient transformations in the spring and fall in the Chesapeake Bay. *Estuarine Coastal and Shelf Science*, 30: 369-391.
- Keeney, D.R. and Nelson, D.W., 1982. Nitrogen -- inorganic forms. In: A.L. Page, R.H. Miller and D.R. Keeney (Editors), *Methods of Soil Analysis*. American Society of Agronomy, Inc., Madison, pp. 643-693.
- Kelley, K.R., Ditsch, D.C. and Alley, M.M., 1991. Diffusion and automated nitrogen-15 analysis of low-mass ammonium samples. *Soil Science Society of America Journal*, 55(4): 1016-1020.
- Kennedy, I.R., 1965. Release of nitrogen from amino acids with ninhydrin for ^{15}N analysis. *Analytical Biochemistry*, 11: 105-110.
- Kristiansen, S. and Paasche, E., 1989. An improved method for determining relative super(^{15}N) abundance in ammonium regeneration studies by direct diffusion. *Marine Ecology (Progress Series)*, 54(1-2): 203-207.

Liu, K.-K. and Kaplan, I.R., 1989. The eastern tropical Pacific as a source of ^{15}N -enriched nitrate in seawater off southern California. *Limnology and Oceanography*, 34: 820-830.

Liu, K.K., Su, M.J., Hsueh, C.R. and Gong, G.C., 1996. The nitrogen isotopic composition of nitrate in the Kuroshio Water northeast of Taiwan: evidence for nitrogen fixation as a source of isotopically light nitrate. *Marine Chemistry*, 54: 273-292.

Lory, J.A. and Russelle, M.P., 1994. Evaluation of diffusion method for preparing low-nitrogen samples for ^{15}N analysis. *Soil Science Society of America Journal*, 58: 1400-1404.

Martell, A.E. and Smith, R.M., 1982. *Critical Stability Constants*, 5, 604 pp.

Sigman, D.M. et al., 1996. A new method for the nitrogen isotopic analysis of oceanic nitrate and first results from the Southern Ocean. *AGU Ocean Sciences Meeting*, 76(3): 143.

Sorenson, P. and Steen-Jensen, E., 1991. Sequential diffusion of ammonium and nitrate from soil extracts to a polytetrafluoroethylene trap for ^{15}N determination. *Analytica Chimica Acta*, 252: 201-203.

Yonebayashi, K. and Hattori, T., 1980. Improvements in the method for fractional determination of soil organic nitrogen. *Soil Science and Plant Nutrition*, 26(4): 469-481.

Table 1: conditions for nitrate extraction incubations

sample nitrate (μM)	initial sample volume (ml)	final sample volume (ml)	Devarda's alloy (mg)	incubation time at 65°C (days)	total incubation time¹ (days)
20	100	15-20	75 (50-60) ²	4 (2) ³	6 (4)
10	200	30-40	150 (100-120)	4 (2)	8 (6)
5	400	60-80	300 (200-240)	4	12
2.5	800	120-160	600 (400-480)	4	16

¹ The difference between total incubation time and incubation time at 65°C is time that samples are to be incubated on a shaker.

² The values given in the table are recommended amounts. The values in parentheses are minimum amounts that have been shown to give reproducible isotopic data. See "Explanation of Protocol".

³ The values given in the table are recommended times. The values in parentheses are minimum times that have been shown to give reproducible isotopic data, if this information exists.

Table 2: reproducibility of the ammonia diffusion step

packet type	conditions	average $\delta^{15}\text{N}$	std dev (n=3)
tape	shake, room T	-0.40	0.21
membrane	shake, room T	-0.32	0.19
tape	no shake, 65°C	-0.44	0.12
membrane*2	shake, room T	-0.04	0.25
tape	no shake, 65°C, large volume	-0.12	0.12
tape	no shake, room T	-6.52	1.16
distillation results (n=9):		-0.36	0.44
ammonium standard (n=3):		0	0.18

Table 3: N blank of different batches of Devarda's Alloy

Devarda's Alloy	blank size (nmol/100 mg)	effective N¹ (μM)
Fisher (combusted) ²	140	1.05
Malincrodt (combusted) ²	130	0.98
Reidel-de-Haen lot 33300	30	0.23
Reidel-de-Haen lot 50510	120	0.90
Reidel-de-Haen lot 52120	130	0.98
EM Science lot 31012	35	0.26
EM Science lot 33194	85	0.64
EM Science lot 33260	95	0.71
EM Science lot 34194	45	0.34

¹The effective amount N (in concentration units) is calculated assuming that 75 mg of alloy is added per 100 ml of initial sample volume. In cases where this blank is critical, the amount of Devarda's alloy can be reduced (see text).

²These batches were combusted in air at 450°C for 4 hours. The lot numbers of these batches are unknown.

Table 4: Woods Hole seawater DON blank data

type of blank ¹	pretreatment	μM DON release (n=3)
no Devarda's addition	w/ preincubation and boiling	0.22
	w/ boiling only	0.32
	no pretreatment	0.98
with Devarda's addition	w/ preincubation and boiling	0.65
	w/ boiling only	0.95
	no pretreatment	1.52

¹The samples were incubated at 65°C for 5 days, then on a shaker table for 7 days, as would be appropriate for a 5μM nitrate sample.

Table 5: Sargasso Sea surface water DON blank data

	pH of preincubation and boiling	time at 65°C (days) ¹	DON release (μM)	std dev
no Devarda's addition	9.7	5	0.12	0.04 (n=2)
with Devarda's addition	9.7	5	0.48	0.01 (n=2)
	9.7	2	0.25	0.05 (n=3)
	11.5	5	0.29	0.01 (n=2)

¹The samples were all incubated for a total of 11 days, so that the time on the shaker table was 11 days minus the number of days at 65°C

Table 6: recovery of nitrate added to Sargasso Sea surface water

concentration (μM)	average $\delta^{15}\text{N}$ (% vs. air)	std. dev. (n=4)
20 (exp 1)	3.72	0.07
20 (exp 2)	3.62	0.09
10 (exp 1)	3.55	0.14
7.5 (exp 2) ¹	3.56	0.10
5 (exp 2) ¹	3.41	0.11
5 (exp 3) ² (n=6)	3.25	0.15
<u>nitrate standard:</u>		
exp 1 (n=10)	3.73	0.11
exp 2 (n=8)	3.65	0.15

¹These 7.5 μM and 5 μM samples were not boiled down as much as suggested in the protocol (30% of initial volume rather than 15-20%).

²This set of 5 μM samples were not preincubated, so that the DON blank would be greater than in the standard protocol. No direct measurements of the nitrate standard were carried out for experiment 3.

Figure 1

A protocol summary chart for the nitrate extraction method. Information concerning volume reduction, Devarda's alloy addition, and incubation time is given in Table 1.

Overview of the Nitrate Extraction Method

Protocol	Comments
<div>preincubation: add 300 mg MgO per 100 ml seawater; heat at 65°C for 5 days</div>	breaks down labile DON; excess MgO raises seawater pH to 9.7
↓	
<div>boiling or evaporation: reduce sample volume to 15-25% of initial</div>	removes any ammonium; breaks down labile DON; decreases sample volume, which aids in both nitrate reduction and ammonia diffusion
↓	
<div>begin extraction: add "diffusion packets" and 75 mg Devarda's Alloy per 100 ml seawater</div>	
↓	
<div>hot incubation: place in 65°C oven for 4 days</div>	heating facilitates both nitrate reduction and ammonia diffusion
↓	
<div>shaking incubation: remove from oven; place on shaker (60 rpm); see table 1 for times</div>	shaking at room temperature facilitates ammonia diffusion while minimizing DON breakdown

Figure 2

The time-course of nitrate reduction by Devarda's alloy, under four different sets of temperature/pH conditions.

NO₃ reduction by Devarda's Alloy

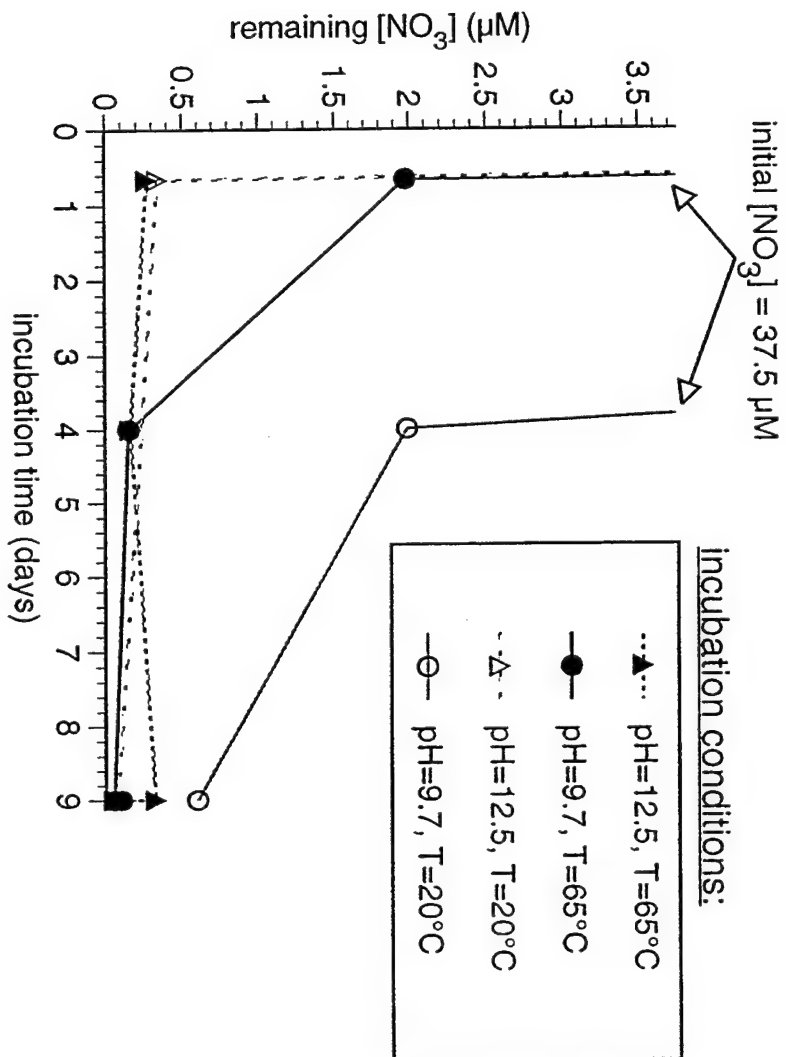


Figure 3

The effect of decreasing the sample volume (by boiling) on the efficiency of nitrate reduction by Devarda's alloy. Two sets of 400 ml samples of Woods Hole seawater with 10 μ M added nitrate and excess MgO were boiled down to a range of final volumes. Either 100 mg (open symbols, scale on left axis) or 200 mg (closed symbols, scale on right axis) of Devarda's alloy was then added to each sample. Samples were incubated with excess MgO and at 65°C for four days; following incubation, the remaining nitrate+nitrite concentration was measured.

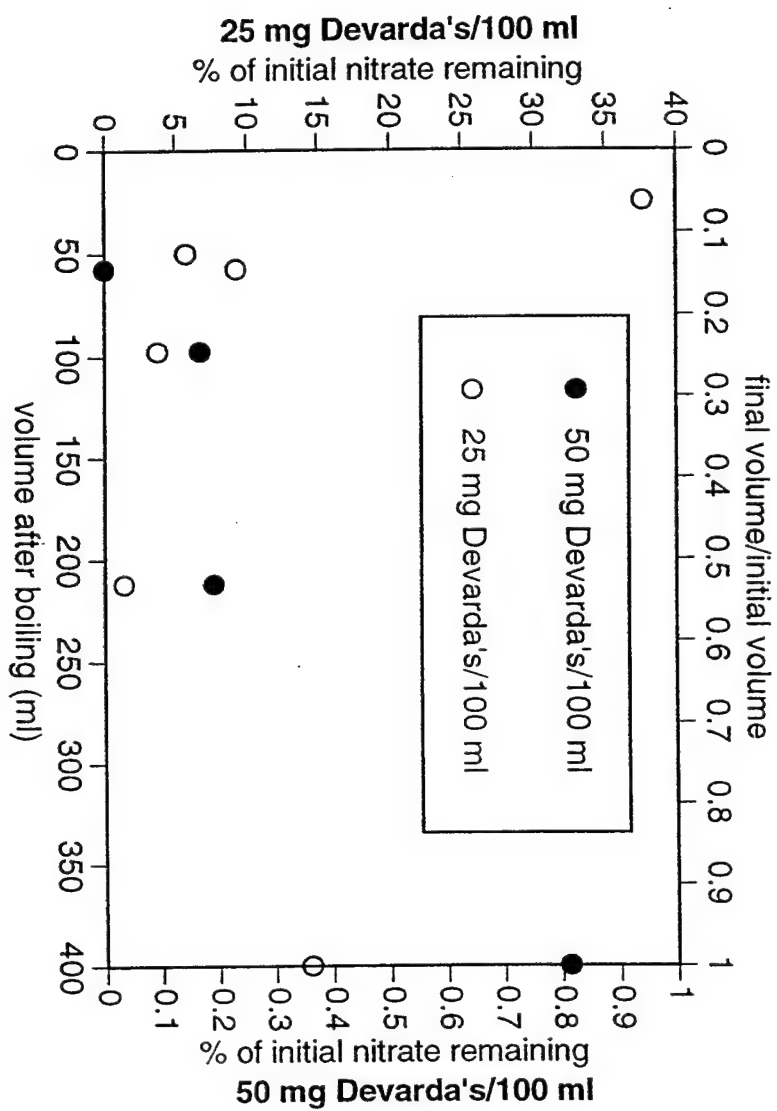


Figure 4

pH measurements on the nitrate removal experiment samples shown in Figure 3. As seawater is concentrated, the pH set by equilibrium with excess MgO decreases. This occurs regardless of the amount of Devarda's alloy used in the incubation.

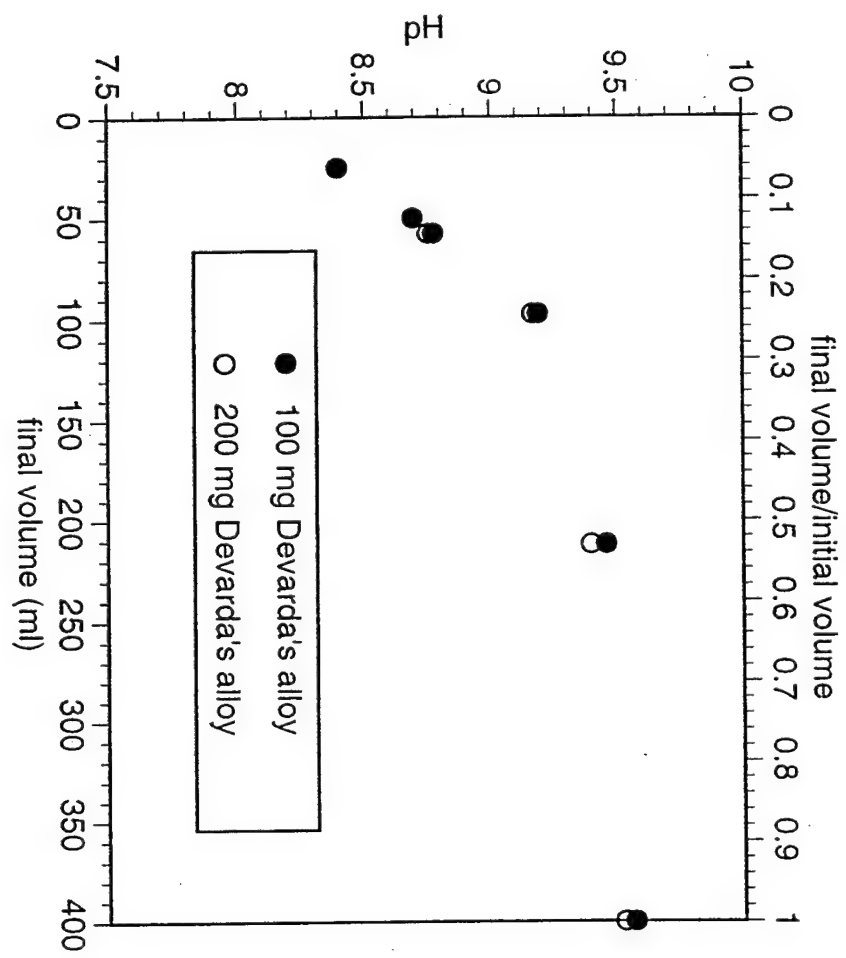


Figure 5

An experiment to determine the amount of Devarda's alloy required to produce reliable isotopic data. Replicate isotopic measurements were made on the nitrate in 200 ml subsamples of deep water from a western Atlantic station, varying the amount of Devarda's alloy added. No Devarda's alloy blank correction was made.

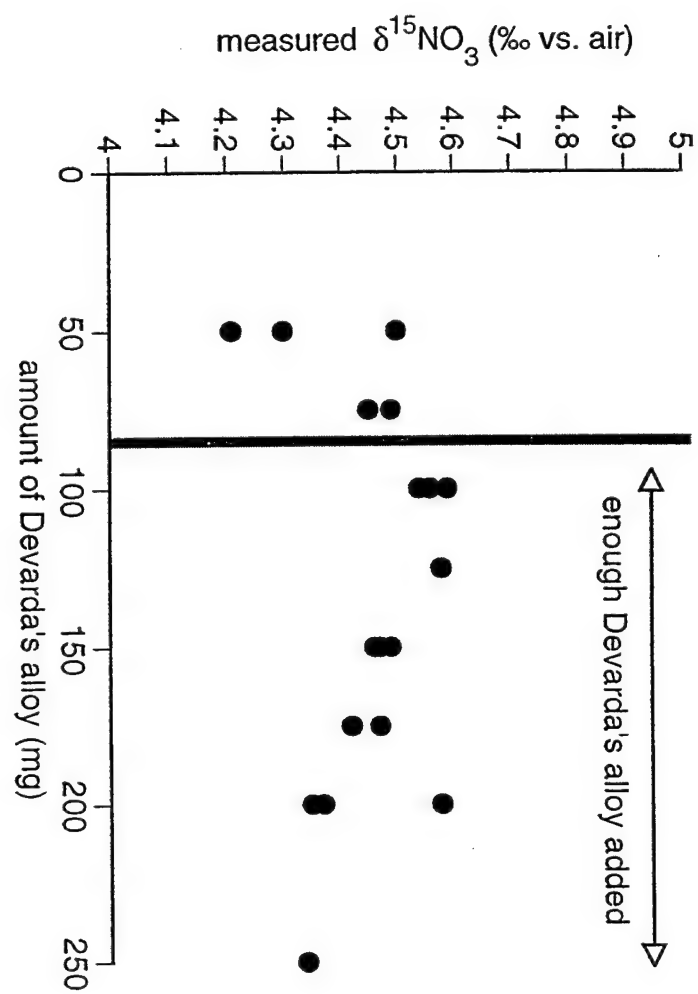


Figure 6

Two experiments to determine the optimal degree of sample volume reduction. 400 ml samples of seawater were amended with 5 μM nitrate, MgO was added, and the samples then boiled down to a range of volumes. Diffusion packets and 280 mg of Devarda's alloy were added to each sample. Samples were incubated at 65°C for four days, then incubated on a shaker for seven additional days, to allow for the longer diffusion time of the largest volume samples.

For experiment 1, the expected $\delta^{15}\text{N}$ of these samples is unknown because the Woods Hole seawater batch used had high ($\sim 3 \mu\text{M}$) initial nitrate before filtration and nitrate standard addition, probably due to several days storage in the dark. Nevertheless, isotopic reproducibility serves as a useful indicator. For experiment 2, zero-nitrate Sargasso Sea water was used. The average $\delta^{15}\text{N}$ of the samples boiled down to ≤ 80 ml gave an average $\delta^{15}\text{N}$ of 3.25‰, 0.4‰ lower than the directly combusted standard (3.6-3.7‰). The DON blank probably accounts for most of this difference; in this experiment, samples were not preincubated to lower the DON blank.

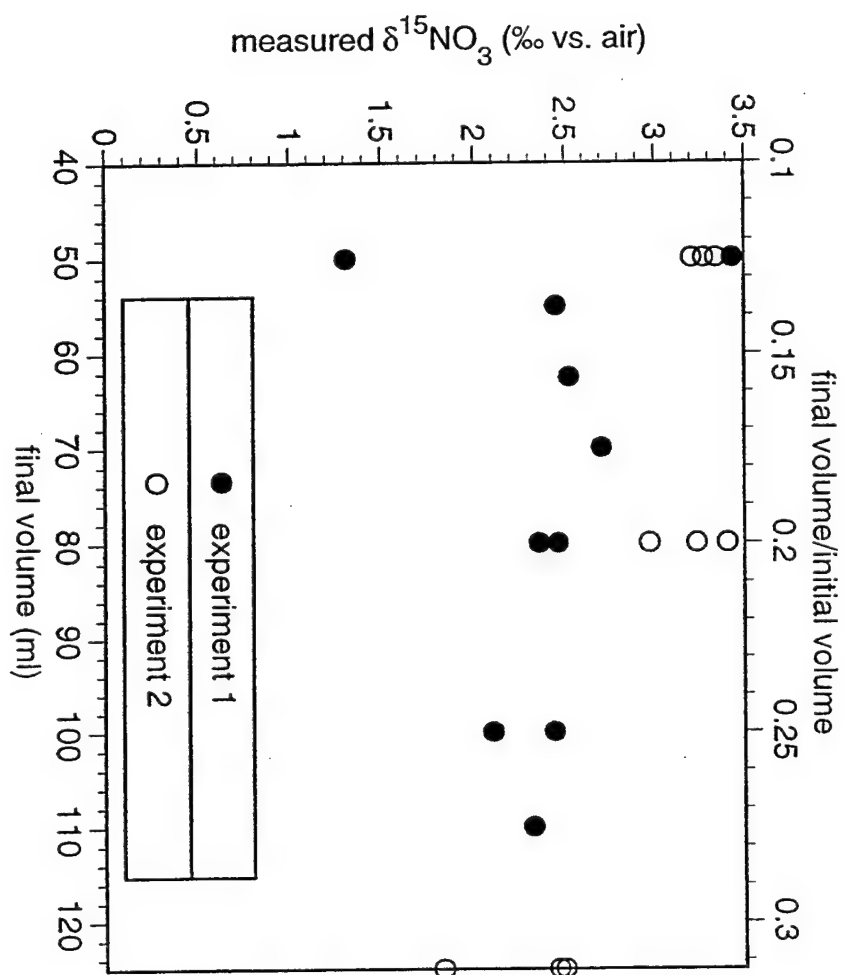


Figure 7

An experiment to determine the time required for complete nitrate extraction. A set of 100 ml samples of Woods Hole seawater were amended with nitrate to 20 μM . MgO was added, and the samples were boiled down to ~25 ml. Diffusion packets and Devarda's alloy were added, and duplicate samples were incubated for 2 to 9 days, removing the samples from the 65°C oven after 5 days and placing them on the shaker for the remaining incubation time.

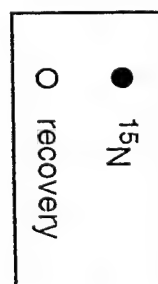
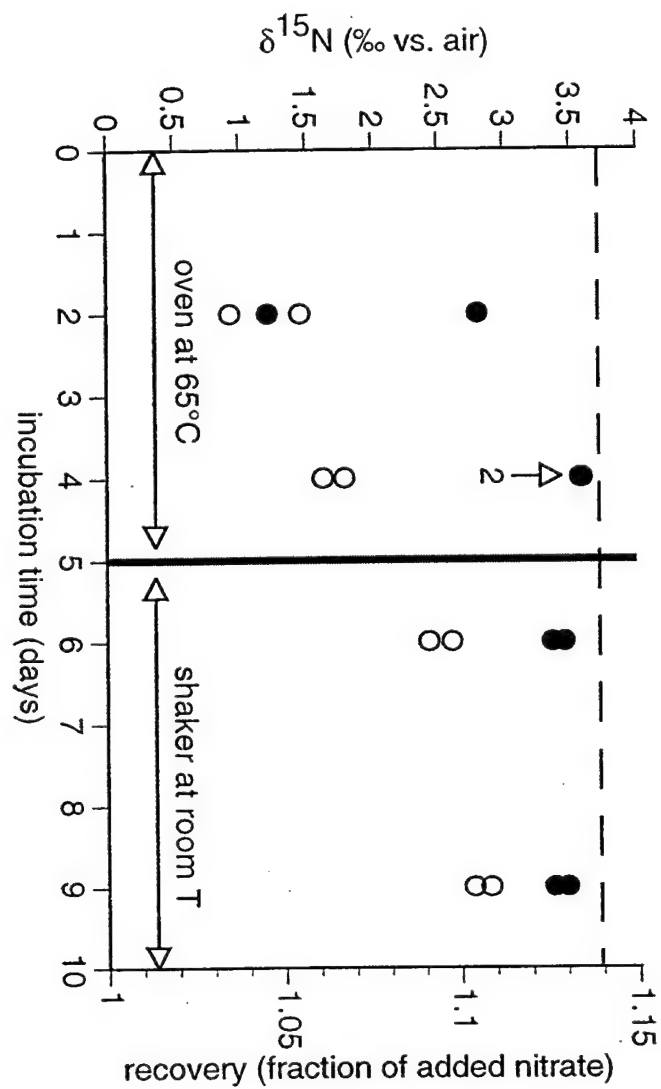


Figure 8

N yield results from a size series of Devarda's alloy in 1 M NaCl solution, for two different lots of alloy (Reidel-de-Haen lot 52120 and EM Science lot 31012). The regression slope of blank size vs. Devarda's alloy addition gives an estimate of the blank size. A given batch gives the same regression slope in zero-nitrate seawater and 1 M NaCl, although the y-intercepts may differ.

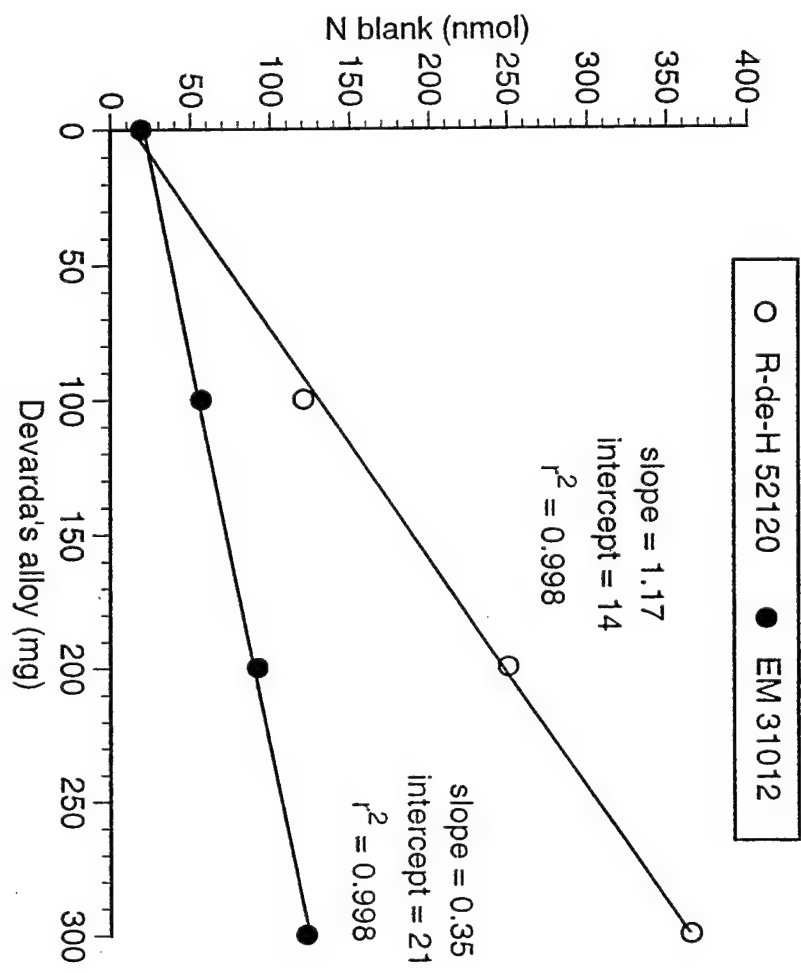


Figure 9

An experiment to check the effect of the Devarda's alloy blank on the measured nitrate $\delta^{15}\text{N}$. Replicate 100 ml sample of Woods Hole seawater with nitrate added to $20\text{ }\mu\text{M}$ were incubated with a size series of Devarda's alloy. We used a batch of Devarda's alloy (Reidel-de-Haen 50510) which has a high N blank (120 nmol/100 mg), so as to produce a significant isotopic effect.

estimating the $\delta^{15}\text{N}$ of the Devarda's Alloy blank

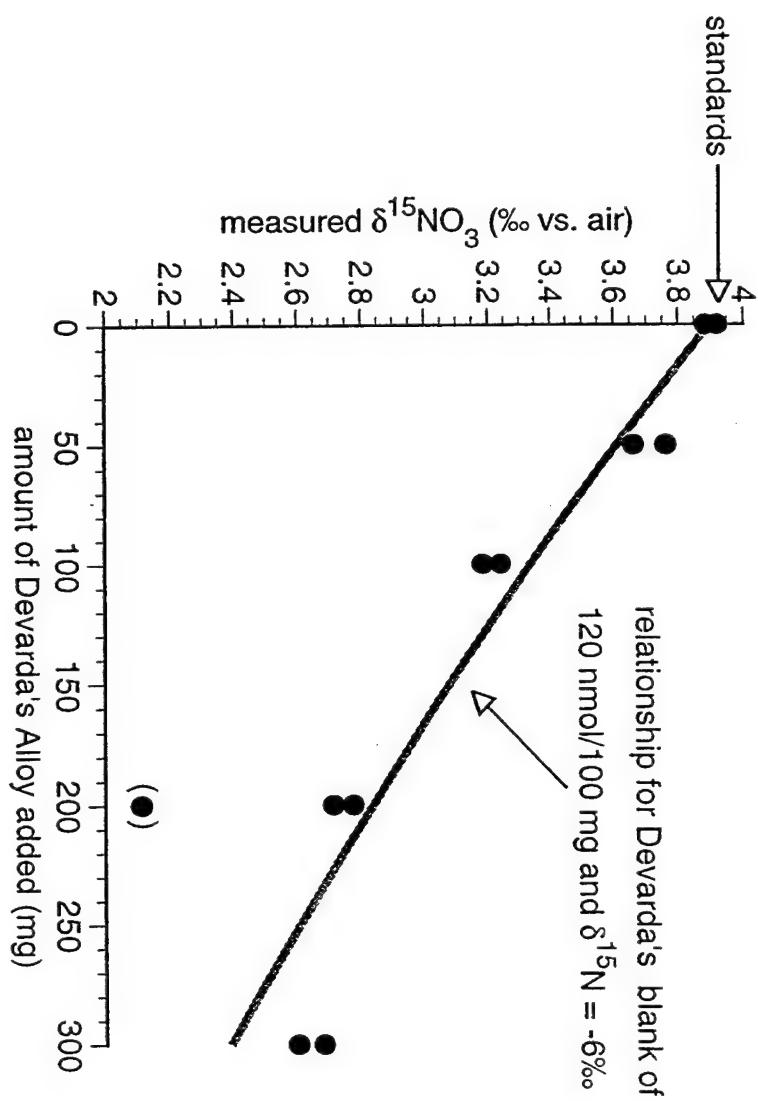


Figure 10

Calculated offset between the true $\delta^{15}\text{N}$ of nitrate and the measured $\delta^{15}\text{N}$ due to the N blank of Devarda's alloy, for two different blank sizes. The true $\delta^{15}\text{N}$ of the nitrate is assumed to be 5‰, and the $\delta^{15}\text{N}$ of the Devarda's alloy blank is assumed to be -6‰. The calculation is made assuming that 75 mg of Devarda's alloy is added per 100 ml of seawater.

theoretical effect of the Devarda's Alloy blank on the measured $\delta^{15}\text{NO}_3$

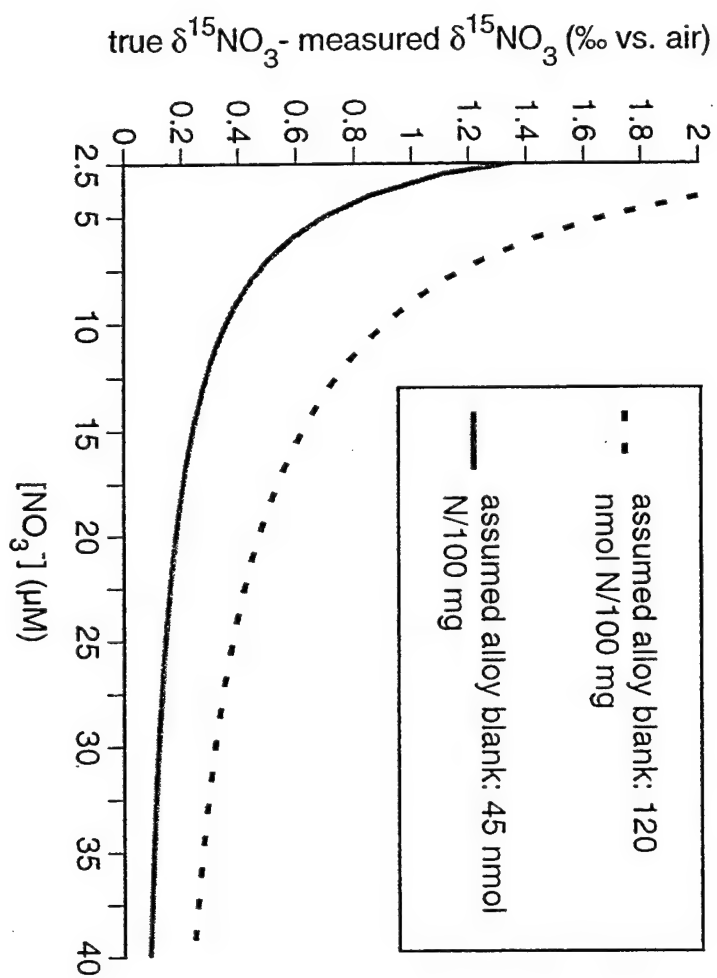


Figure 11

A depth profile of nitrate $\delta^{15}\text{N}$ from WOCE I9 station 108 in the Antarctic region of east Indian Ocean. The error bars are $\pm 0.2\text{‰}$, which is an upper limit for the standard deviation of analyses done on Woods Hole seawater with $>10\text{ }\mu\text{M}$ added nitrate (Table 4). Nitrate concentration data were generated by the WOCE I9 science crew.

WOCE 19 Stn. 108 (53.2°S, 115°E)

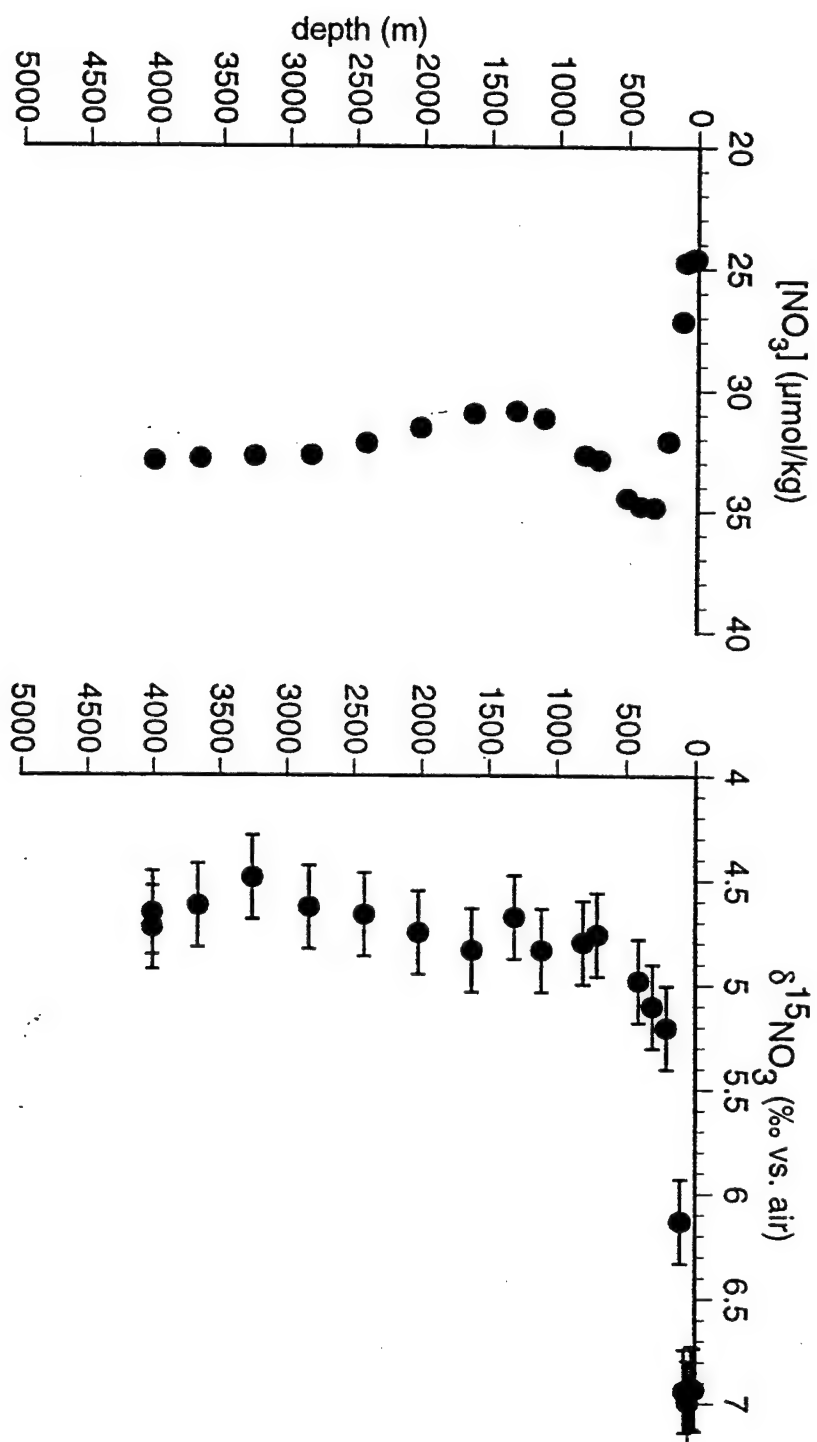


Figure 12

A depth profile of nitrate $\delta^{15}\text{N}$ from WOCE I9 station 119 in the Subantarctic region of east Indian Ocean. Nitrate concentration data, shown with connected open circles, were generated by the WOCE I9 science crew.

WOCE 19 Stn. 119 (47.5°S, 115°E)

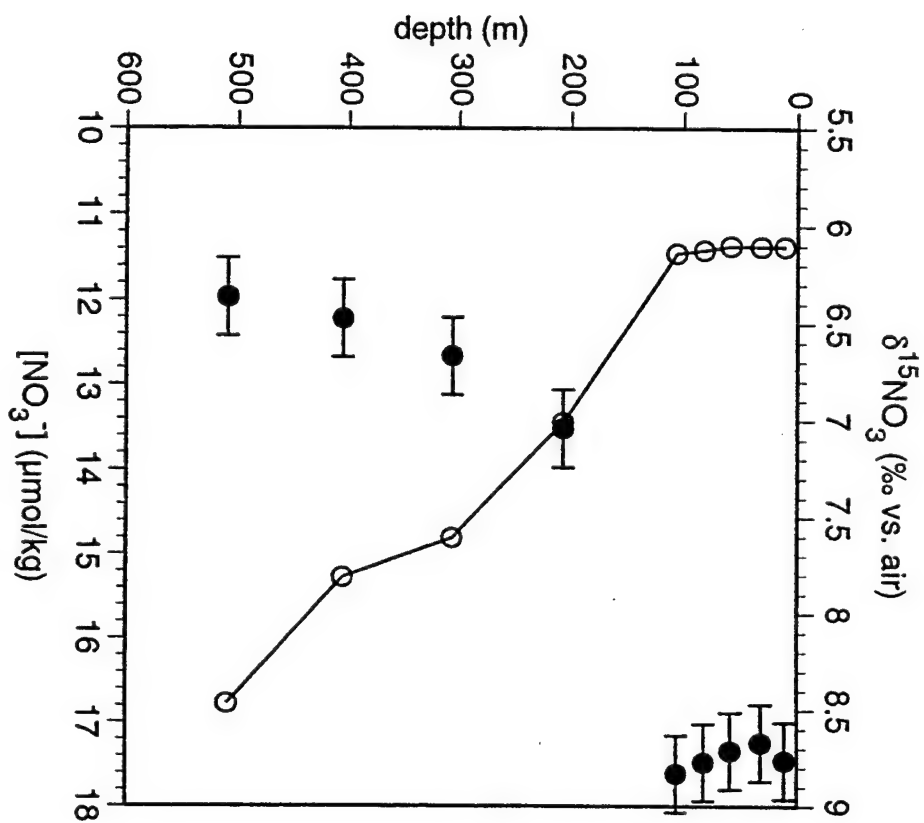
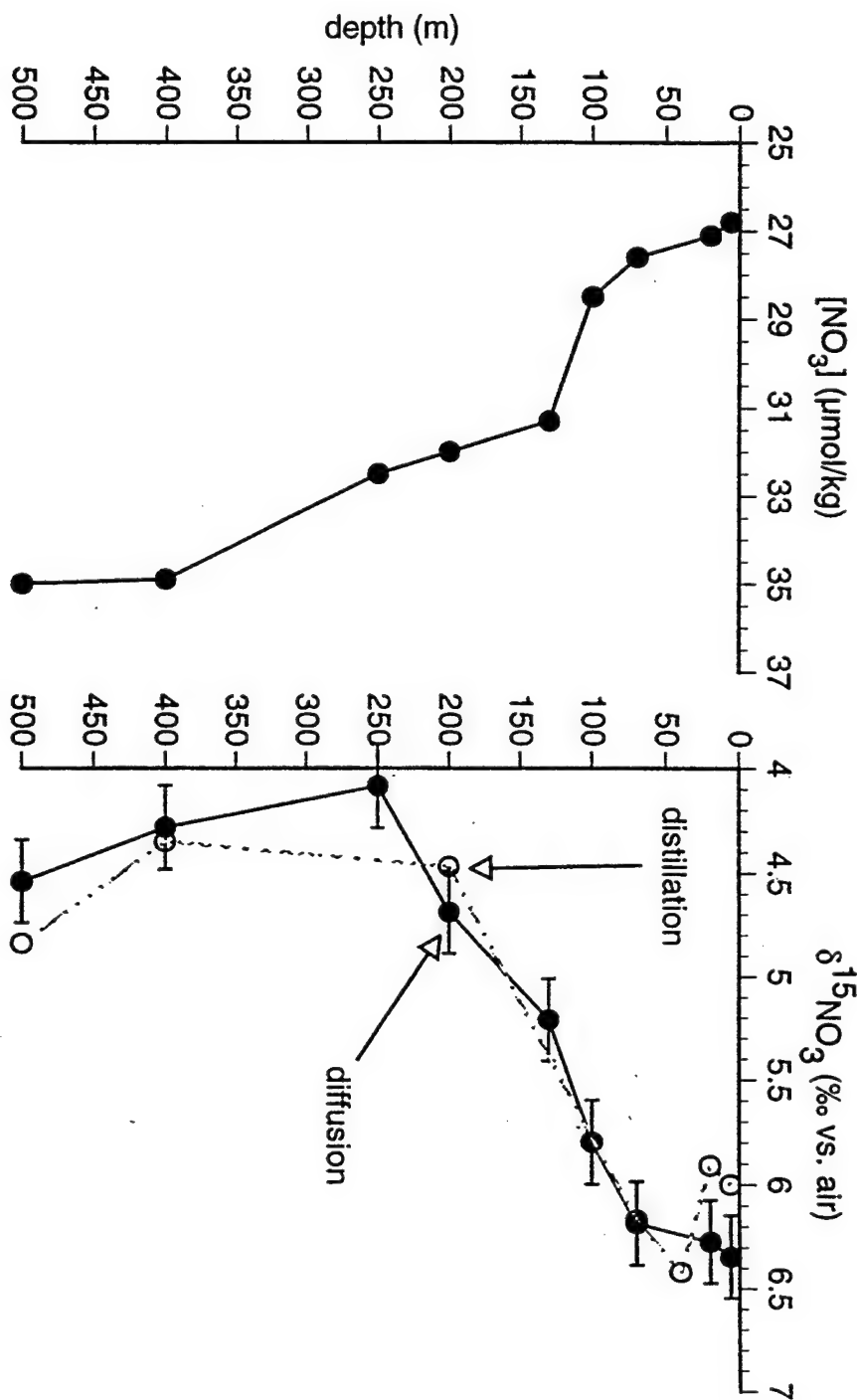


Figure 13

A profile of nitrate $\delta^{15}\text{N}$ from the Antarctic region of the Indian Ocean (near Kerguelen Island), as measured by (1) our passive diffusion method and (2) the previously published distillation method of Cline and Kaplan (1975). The distillations were done by J. Donaghue at WHOI.

MD-91 Stn. A (~50°S, ~70°E)



Chapter 4:
The Nitrogen Isotopic Composition of Nitrate
in the Southern Ocean

D.M. Sigman^{1*}, M.A. Altabet³, D.C. McCorkle¹, R. Francois², G. Fischer⁴

¹Department of Marine Geology and Geophysics and ²Department of Marine Chemistry and Geochemistry, Woods Hole Oceanographic Institution, Woods Hole, MA 02543, e-mail: dsigman@whoi.edu, fax: (508)-457-2183

*corresponding author

³Center for Marine Science and Technology, University of Massachusetts, Dartmouth, North Dartmouth, MA 02747

⁴Fachbereich Geowissenschaften, University of Bremen, Germany

Abstract

We report nitrogen isotope data for latitudinal transects of hydrocast and surface samples from the eastern Indian and Pacific sectors of the Southern Ocean. These data are used to address several of the central unknowns in the link between nitrate utilization and the $\delta^{15}\text{N}$ of nitrate in this region. These include the isotopic composition of the nitrate source, the mechanisms of nitrate supply, the isotopic fractionation factor of nitrate uptake, and the applicability of the Rayleigh fraction model to nitrate utilization in the Southern Ocean surface.

In the Antarctic Zone (south of the Polar Frontal Zone), Lower Circumpolar Deep Water nitrate has a $\delta^{15}\text{N}$ of $4.7 \pm 0.2\text{‰}$, and Upper Circumpolar Deep Water is $<0.5\text{‰}$ higher than this value. Similar deep water $\delta^{15}\text{NO}_3$ values have been measured in samples from both the North Atlantic and the central Pacific. Isotopic enrichment in the Antarctic surface layer is consistent with a simple Rayleigh fractionation model of vertical nitrate supply and seasonal nitrate utilization. However, samples just below the summer mixed layer tend to fall slightly off the Rayleigh fractionation trend connecting Upper Circumpolar Deep Water to Antarctic surface water.

Estimation of the nitrate uptake fractionation factor from the Antarctic depth profile data yield values in the range of 4.6-5.7‰ in east Indian sector, and 4-5‰ in the east Pacific sector. Surface transect data from the Pacific sector Antarctic Zone yield similar values (4.0-4.8‰), although the uncertainties in these estimates are large. A fractionation factor of $5 \pm 1\text{‰}$ appears to apply generally to the Antarctic Zone.

In the Subantarctic Zone (north of the Polar Frontal Zone), the $\delta^{15}\text{NO}_3$ of Lower Circumpolar Deep Water (>2 km) is the same as that of deep water in the Antarctic Zone. However, the $\delta^{15}\text{NO}_3$ of Subantarctic Upper Circumpolar Deep Water (1.5-2.0 km) is 0.5-1.0‰ greater than that of Lower Circumpolar Deep Water. This isotopic enrichment of Subantarctic Upper Circumpolar Deep Water is probably due to denitrification in the water masses with which Upper Circumpolar Deep Water communicates. Based on $\delta^{15}\text{NO}_3$ and $[\text{NO}_3^-]$ data, Antarctic Intermediate Water could be produced by two combinations of water masses: (1) Antarctic surface water and Antarctic Upper Circumpolar Deep Water, or (2) Subantarctic thermocline water and Subantarctic Upper Circumpolar Deep Water. The Subantarctic thermocline has a very low $\delta^{15}\text{NO}_3$ for its degree of nitrate depletion. We hypothesize that this is due to mixing along isopycnals with lower latitude thermocline waters.

In the Subantarctic Zone surface waters, the nitrate supply appears to be mostly lateral, so that the Subantarctic surface operates as a single Rayleigh fractionation system. However, just north of the Polar Frontal Zone in our transects, surface waters appear to be modified by mixing with the shallow thermocline, which has a low $\delta^{15}\text{NO}_3$ for its $[\text{NO}_3^-]$. Isotopic data from across the entire latitudinal range of the Southern Ocean suggests that a fractionation factor of $\sim 4.5\text{‰}$ applies for the Subantarctic Zone, similar to the estimates for the Antarctic.

Introduction

The Southern Ocean represents the largest open ocean region in which the extraction of nitrate and phosphate by phytoplankton is incomplete. The explanation for this incomplete nutrient extraction is a topic of current research, but probably involves both high nutrient supply rates and the limitation of phytoplankton growth, by light or trace nutrients (Cullen, 1991; Martin et al., 1990; Mitchell et al., 1991). The nutrient status of Southern Ocean surface waters has an important potential effect on atmospheric CO₂, so that it has been suggested as the cause of the CO₂ changes which accompany glacial/interglacial cycles (Knox and McElroy, 1984; Sarmiento and Toggweiler, 1984; Siegenthaler and Wenk, 1984). A number of paleoceanographic proxies have been used to address this hypothesis, including planktonic foraminiferal isotopic and trace metal composition, sediment concentrations of radionuclides and other elements, and sedimentary carbon and nitrogen isotopic composition (Charles and Fairbanks, 1990; Francois et al., 1992; Francois et al., 1997; Howard, 1992; Keigwin and Boyle, 1989; Kumar et al., 1993; Mortlock et al., 1991; Rosenthal, 1994; Shemesh et al., 1993; Singer and Shemesh, 1995; Yu, 1994). However, the studies to date are limited by uncertainties in the proxies themselves.

Field and laboratory studies have demonstrated the link between nitrate utilization and the isotopic composition of particulate nitrogen in oceanic ecosystems (Altabet et al., 1991; Altabet and Francois, 1994a; Altabet and McCarthy, 1985; Farrell et al., 1995; Francois et al., 1992; Montoya, 1990; Montoya and McCarthy, 1995; Nakatsuka et al., 1992; Pennock et al., 1988; Wada, 1980; Wada and Hattori, 1978; Waser et al., 1997a; Wu et al., 1997). This link is due to the isotopic fractionation factor associated with nitrate uptake, which leads to the preferential incorporation of isotopically "light" nitrogen into phytoplankton biomass. In the case of a closed system and a constant fractionation factor, nitrate utilization acts as a Rayleigh fractionation process, whereby the nitrate pool becomes

progressively enriched in ^{15}N as nitrate is consumed, leading to an increase in the $\delta^{15}\text{N}$ of the newly formed biomass N (Figure 1).

Surface particulate N and sedimentary N in the Southern Ocean show latitudinal gradients in $\delta^{15}\text{N}$ which anticorrelate with surface $[\text{NO}_3^-]$ and appear to reflect the lateral gradient in nitrate utilization across the major fronts (Altabet and Francois, 1994b; Francois et al., 1992; Francois et al., 1997). In conjunction with data from other regions of the ocean (Altabet and Francois, 1994a), these observations suggest that N isotopes can be used as proxy for Southern Ocean nitrate utilization in the past. Downcore records of sediment $\delta^{15}\text{N}$ are consistent with higher nitrate utilization in the glacial Antarctic, suggesting that the Southern Ocean was a major driver of the glacial atmospheric CO_2 reduction (Francois et al., 1992; Francois et al., 1997). However, there are a number of uncertainties in the paleoceanographic application of the nitrate utilization/N isotope link.

Questions regarding the generation of the nitrate utilization/N isotope link largely involve the applicability of the Rayleigh fractionation model to nitrate uptake in Southern Ocean surface waters:

- 1) What is the isotopic composition of the nitrate supply to Southern Ocean ecosystems, and what are the mechanisms of this nitrate supply?
- 2) Are the isotopic data consistent with a Rayleigh fractionation process driven by nitrate uptake?
- 3) What is the fractionation factor for nitrate uptake, and what are the causes and amplitudes of variation in this parameter?

The isotopic composition of subsurface nitrate ultimately defines the initial $\delta^{15}\text{NO}_3$ from which the surface ocean evolves. Previous studies have demonstrated large regional variations in subsurface $\delta^{15}\text{NO}_3$ due to isotopic enrichment associated with water column denitrification (Brandes, 1996; Cline and Kaplan, 1975; Liu and Kaplan, 1989). However,

the general paucity of information on subsurface $\delta^{15}\text{NO}_3$ distributions has hampered nitrogen isotope studies of both the modern ocean and the paleoceanographic record.

Key aspects of nitrate supply to Southern Ocean ecosystems are poorly known. Seasonal vertical mixing is an important mechanism of nitrate supply, especially in the Antarctic Zone (i.e., south of the Polar Frontal Zone) where there is a large seasonal variation in the upper ocean density structure (Cullen, 1991). However, nitrate is also supplied by the large-scale advective circulation, composed of diffuse upwelling at the Antarctic Divergence, net equatorward flow along the surface, and subduction and surface exchange at the Polar Frontal Zone, all within the intense zonal flow of the Circumpolar Current (Jones et al., 1990). If seasonal vertical mixing is the dominant mechanism of nitrate supply in the Southern Ocean, then the Southern Ocean surface waters can be approximated as a latitudinal array of individual Rayleigh fractionation systems, and the sinking flux $\delta^{15}\text{N}$ out of the surface ocean at each latitude will follow the "accumulated product" equation (Altabet and Francois, 1994b). On the other hand, if latitudinal advection of the surface layer dominates the nitrate supply to progressively lower latitudes, the advected water mass acts as a single Rayleigh fractionation system, with the latitudinal gradient in the $\delta^{15}\text{N}$ of the sinking flux approximating the "instantaneous product" equation. As the instantaneous product $\delta^{15}\text{N}$ varies more as a function of nitrate utilization than the accumulated product $\delta^{15}\text{N}$ does, a lateral model of nitrate supply predicts a much sharper latitudinal gradient in the $\delta^{15}\text{N}$ of export production. Thus, interpretation of sinking flux and sedimentary $\delta^{15}\text{N}$ variations, for instance, to estimate the nitrate uptake fractionation factor, requires an understanding of the relative importance of vertical and lateral nitrate supply.

Phytoplankton culture studies of the nitrate uptake fractionation factor, taken together, suggest a large range of variation in this parameter, with no consensus on the factors which control it (Montoya, 1990; Montoya and McCarthy, 1995; Pennock et al.,

1988; Wada and Hattori, 1978; Waser et al., 1997a; Waser et al., 1997b). This is a major concern for paleoceanographic work, in that ecologically-driven changes in the fractionation factor represent an alternative explanation for changes in the isotopic composition of the N sinking flux. In the case of the Antarctic, the $\delta^{15}\text{N}$ shift observed in sediments, which has been interpreted as reflecting a nitrate utilization change (Francois et al., 1997), could be due to a 2.5-4‰ lower fractionation factor during the last ice age. Given the range of culture-based estimates, we must turn to field-based estimates to determine the mean value and variability of the fractionation factor in oceanic environments. Oceanic $\delta^{15}\text{NO}_3$ data are important in this regard, as suspended particulate N $\delta^{15}\text{N}$ is affected by a range of biological processes and thus may not provide an accurate estimate of the nitrate uptake fractionation factor (DeNiro and Epstein, 1981; Altabet, 1988; Rau et al., 1991).

In this study, we have used a new method for seawater nitrate extraction (Sigman et al., 1997) to generate a large, high-precision data set of nitrate $\delta^{15}\text{N}$ in the Southern Ocean. These data provide a more direct measure of the link between nitrate utilization and the N isotopes than the particulate and sedimentary N isotopic data have previously allowed.

Sample Sets and Methods

Three sample sets from the Southern Ocean were collected and analyzed (Figure 2, Table 1): (1) a latitudinal transect of hydrocast profiles from the east Indian sector (WOCE I9), (2) hydrocast profiles and two latitudinal transects of surface samples from the east Pacific sector (ANT XII/4), and (3) a latitudinal transect of surface samples from the central and east Pacific sectors (RITS '94).

Hydrocast profiles from the east Indian sector of the Southern Ocean were collected during WOCE leg I9, a latitudinal transect along 115°E from ice edge to Freemantle, Australia aboard the RV Knorr, in January, 1995. Stations were spaced ~3° apart (Table 1). The most polar station (station 97, 59°S) is just to the south of the strong latitudinal gradient in surface silicate concentration, which decreases from 65 μM at 65°S to <20 μM at 60°S (Figure 3a). The lowest-latitude station (station 141, 36°S) is within subtropical surface waters, where $[\text{NO}_3^-]$ is <1 μM , too low to be analyzed by the current method. The WOCE I9 sample set provides our most complete information on deep ocean variations in $\delta^{15}\text{NO}_3$, especially in the Subantarctic Zone.

The east Pacific samples were collected during the ANT XII/4 cruise aboard the RV Polarstern in April, 1995. Eleven shallow (≤ 600 m) profiles from the Antarctic Zone and two from the Subantarctic Zone were sampled (Figure 3b, Table 1). The five most polar stations were from within the marginal ice zone, with surface silicate concentrations reaching ~34 μM . Water was drawn from four deep hydrocasts as well. Surface samples were collected using an underway filtration system along two latitudinal transects (among the hydrocast stations), one southward starting in Subantarctic waters and extending to the marginal ice zone in the Antarctic (Figure 4c), and the second northward from the marginal ice zone to the Polar Frontal Zone (Figure 4d). Particulate N isotopic data from this filtration system are not yet available and will be reported elsewhere. The ANT XII/4 sample set provides a thorough sampling across the open water of the Antarctic Zone, as

well as Subantarctic stations and deep samples to assess the circumpolar continuity of the observations from the Indian sector.

During the RITS '94 cruise of the RV Surveyor in January, 1994, C. Zafiriou filtered and collected 1 liter surface water samples along a latitudinal transect from 40° to 70° S along ~140° E, in the central Pacific. Sample collection continued along an eastward cruise track through the summer marginal ice zone (Figure 2). These samples provide a broad surface water transect from the low-nutrient surface waters of the Subtropical Frontal Zone to ice edge in the Antarctic Zone (Figure 3c).

Surface transect samples were filtered with combusted GF/F during collection, while hydrocast samples were not. In all cases, samples were preserved by acidification with 1-2 ml of 50% (v/v) reagent grade hydrochloric acid per liter of seawater. Samples were stored frozen or refrigerated; however, our preservation tests to date indicate that acidification alone is adequate to preserve nitrate for isotopic analysis.

$\delta^{15}\text{NO}_3$ measurements:

The isotopic analyses of nitrate were performed using the "passive ammonia diffusion" method for seawater nitrate extraction (Sigman et al., 1997). This method involves nitrate reduction to ammonia using Devarda's alloy, followed by passive diffusion of the ammonia out of the alkaline seawater sample, through a sealed envelope composed of two porous Teflon membranes, and onto an acidified glass fiber filter.

This method gives highly reproducible, complete recovery of nitrate and a standard deviation for isotopic analysis of $\leq 0.2\%$ down to 5 μM nitrate. The blanks inherent in this procedure are from Devarda's alloy and seawater dissolved organic nitrogen ("DON"). An isotopic correction is made for the Devarda's alloy blank but is not currently made for the DON blank. However, the DON blank is insignificant for most of the samples in this

study, in which $[\text{NO}_3^-]$ is $\geq 7.5 \mu\text{M}$. For the few samples with $\leq 5 \mu\text{M}$ $[\text{NO}_3^-]$, there may be an underestimation in the $\delta^{15}\text{N}$ by as much as 0.3-0.4‰ due to the DON blank.

Most of the isotopic data were generated using a Europa Roboprep elemental analyzer on-line with a Finnigan MAT 251 stable isotope mass spectrometer. Isotopic values are in δ -notation versus air N_2 , in permil units:

$$\delta^{15}\text{N}(\text{‰}) = \left(\frac{\left(\frac{^{15}\text{N}}{^{14}\text{N}} \right)_{\text{sample}} - \left(\frac{^{15}\text{N}}{^{14}\text{N}} \right)_{\text{air}}}{\left(\frac{^{15}\text{N}}{^{14}\text{N}} \right)_{\text{air}}} \right) \cdot 1000 \quad \text{equation 1}$$

They are reported versus laboratory air, which is checked for consistency using several types of calibrated lab standards, including dried solutions of 6-aminocaproic acid, glycine, potassium nitrate and ammonium sulfate. Ammonium sulfate standard solution pipetted onto an acidified glass fiber disk (identical to the sample type generated by the nitrate extraction protocol) typically yields a standard deviation of $\sim 0.15\text{‰}$. Isotopic data presented for WOCE I9 stations 119 and 126 were generated at the Marine Biological Laboratory Ecosystems Center stable isotope facility, on a Finnigan Delta-S with an on-line Heraeus elemental analyzer (Fry et al., 1992). As with the MAT 251 system, acidified ammonium sulfate standards run with the samples also yielded a standard deviation of $\sim 0.15\text{‰}$.

Extractions of a nitrate standard added to nitrate-free seawater suggest a standard deviation of 0.2‰ for $\geq 5 \mu\text{M}$ $[\text{NO}_3^-]$ samples run on the same day. Duplicates of real samples typically give a similar estimate for the standard deviation. One out of every 10 to 20 samples gives an anomalously low $\delta^{15}\text{N}$ value, probably due to incomplete ammonia diffusion. Low “flyers” were reanalyzed when possible, and suspect values which could not be reproduced have been removed from the data set. With continued experience, the fraction of “flyers” from the diffusion method has dropped to below 5% of the samples processed.

Sample sets run months or years apart have on occasion shown clear offsets of up to 0.3‰. These offsets were apparent from replicate analyses and from shifts in samples from deep water masses which had previously been shown to be isotopically homogenous. In most cases, the offsets could be accounted for by a shift in acidified ammonium standards relative to other combusted standards and laboratory air injections. When this effect is evident, it is reproduced from ammonium standards acidified with either sulfuric or phosphoric acid. We hypothesize that, under some combustion conditions, the acid can have a subtle but recognizable effect on combustion and/or N₂ purification. The mechanism of this effect remains unknown. If an offset correction was made for this effect, replicate samples were analyzed to check the validity of the correction.

Nitrate concentration measurements:

The nitrate concentration ([NO₃]) data for the WOCE I9 sample set were measured on-board by the WOCE science crew, using standard colorimetric methods. Roughly a third of the [NO₃] measurements from the ANT XII/4 cruise were performed by the ANT XII/4 science crew, also using standard colorimetric methods (Gersonde et al., in prep.). The remaining [NO₃] measurements from ANT XII/4 and all [NO₃] measurements from RITS '94 were performed in our laboratory on splits from the acidified δ¹⁵NO₃ samples, by nitrate reduction to NO followed by on-line NO chemiluminescence detection (Garside, 1982). Our measurements are of nitrate plus nitrite; however, we do not resolve these two species or make any correction for the nitrite, which is typically <0.3 μM. The measurements were performed in duplicate, which gave relative standard deviations of ~1%.

The WOCE nutrient data are reported in units of μmol/kg, whereas all other nutrient data are reported here are in units of μM. These conventions are maintained, except when

WOCE results are compared with results from the Pacific sector, in which case the WOCE values are converted to μM units, assuming a constant seawater density of 1.027 kg/l.

Results

The $\delta^{15}\text{NO}_3$ in surface waters shows a geographic anticorrelation with the variations in nitrate concentration (Figure 4). This anticorrelation is most evident on the large scale: $\delta^{15}\text{NO}_3$ increases as $[\text{NO}_3^-]$ decreases toward the north, which occurs most strongly across the Subantarctic (Figure 4a,b,c). The relationship is also apparent in most of the smaller $[\text{NO}_3^-]$ variations within the Antarctic Zone, although there are cases where it does not hold (Figure 4c,d,e).

Depth profiles from all sectors and zones of the Southern Ocean show isotopic enrichment toward the surface (Figures 5, 6, 7). The nature of the vertical gradient in $\delta^{15}\text{NO}_3$ and its relationship to $[\text{NO}_3^-]$ varies consistently among the different latitudinal zones of the Southern Ocean. Most of the profiles we have analyzed are easily characterized as belonging to either the Antarctic Zone or the Subantarctic Zone. Profiles in or near the Polar Frontal Zone (the latitudinal zone between the Polar and Subantarctic Fronts, e.g., WOCE I9 station 113, ANT XII/4 stations 177, 182) are largely transitional in terms of $\delta^{15}\text{NO}_3$ and $[\text{NO}_3^-]$, so we do not separate them into a distinct group. Profiles from the Subtropical Frontal Zone are similar to the Subantarctic Zone profiles, except that $[\text{NO}_3^-]$ reaches $\sim 0 \mu\text{M}$ in the surface.

In order to describe the $\delta^{15}\text{NO}_3$ profiles in more detail, we must introduce the basic vertical structure of the Antarctic and Subantarctic Zones. In the Antarctic Zone (south of the Polar Front), high $[\text{NO}_3^-]$ deep water occurs within 500 m of the surface (Figure 8a). There is a subsurface $[\text{NO}_3^-]$ maximum ($35\text{--}37 \mu\text{M}$) at 300–500 m depth, characteristic of Upper Circumpolar Deep Water (UCDW), distinguishing it from the $31\text{--}32 \mu\text{M}$ $[\text{NO}_3^-]$ of Lower Circumpolar Deep Water (LCDW) below (as described by Orsi et al. (1995) on the basis of oxygen concentration). Above UCDW, a salinity-driven pycnocline defines the surface mixed layer, which is typically ~ 100 m deep during the summer. The summer surface mixed layer is underlain by a ~ 200 m thick temperature minimum layer (the T_{min}

layer), which is a deep portion of the winter mixed layer that has been isolated from the surface by summer warming and melting (Gordon et al., 1977). The $[\text{NO}_3^-]$ of the Tmin layer is intermediate between UCDW and the summer surface layer, typically 31-32 μM . In summary, the water column of the Antarctic Zone, from bottom to top, is composed of (1) Lower Circumpolar Deep Water (LCDW), (2) Upper Circumpolar Deep Water (UCDW), (3) the subsurface temperature minimum (Tmin) layer, and (4) the summer surface layer (Figure 8a).

$\delta^{15}\text{NO}_3$ profiles from the Antarctic Zone are characterized by relative isotopic homogeneity in the subsurface (Figures 5a, 6, 7c). LCDW has a $\delta^{15}\text{NO}_3$ value of $4.7 \pm 0.2\text{‰}$. Similar values are observed in the deep waters of the North Atlantic and the central Pacific, suggesting that the $\delta^{15}\text{N}$ of deep water nitrate is relatively constant along the paths of global deep circulation (Table 2, see Appendix 1). There is evidence in Antarctic profiles for slight ($<0.5\text{‰}$) isotopic enrichment of UCDW compared to LCDW (Figure 9b). Above UCDW, $\delta^{15}\text{NO}_3$ increases as $[\text{NO}_3^-]$ decreases through the Tmin layer and into the surface layer.

The transition from the Antarctic Zone to the Subantarctic Zone (at the Polar Frontal Zone) is marked by the development of a permanent thermocline in the Subantarctic. This change is accompanied by a deepening of the subsurface $[\text{NO}_3^-]$ maximum from 300-500 m in the Antarctic Zone to ~2000 m in the Subantarctic Zone (Figure 8b). The subsurface $[\text{NO}_3^-]$ maximum is characteristic of UCDW and thus also denotes a northward deepening of this water mass (Orsi et al., 1995). Above UCDW in the Subantarctic, $[\text{NO}_3^-]$ decreases upward through the pycnocline, in which there are two well-studied water masses, Antarctic Intermediate Water (with its core at ~1100 m) and Subantarctic Mode Water (with its core at ~400 m, Piola and Georgi, 1982). In summary, the vertical structure of the Subantarctic Zone is (1) LCDW, (2) UCDW, (3) Antarctic Intermediate Water (AAIW), (4)

the Subantarctic thermocline (occupied by Subantarctic Mode Water, SAMW), and (5) the surface layer (Figure 8b).

LCDW $\delta^{15}\text{NO}_3$ in the Subantarctic Zone is identical to that of Antarctic LCDW (Figures 6, 9b). In the Subantarctic Zone, UCDW $\delta^{15}\text{NO}_3$ is 0.5-1‰ higher than that of LCDW (figure 9b). Above UCDW, $\delta^{15}\text{NO}_3$ increases as $[\text{NO}_3^-]$ decreases upward through the Subantarctic pycnocline, with high degrees of enrichment into the surface layer.

Interpretation and Discussion

The general anticorrelation between $[\text{NO}_3^-]$ and $\delta^{15}\text{NO}_3$ indicates that there is a strong link between nitrate utilization and the N isotopes in the Southern Ocean, whereby preferential removal of $^{14}\text{NO}_3$ by phytoplankton leaves the residual nitrate pool enriched in ^{15}N . The relationship between $\delta^{15}\text{NO}_3$ and $[\text{NO}_3^-]$ in the different zones of the Southern Ocean provides quantitative information regarding this link.

Rayleigh fractionation kinetics can be used to understand the generation of the nitrate utilization/ $\delta^{15}\text{N}$ link in surface waters. If nitrate uptake occurs with a constant fractionation factor, and if the surface ocean receives no new nitrate over the course of seasonal nitrate uptake (i.e., during the spring and summer productive periods), then Rayleigh fractionation kinetics apply to the uptake process. In this case, mixed layer nitrate can be modelled using the Rayleigh fractionation equation for the substrate pool (Figure 1):

$$\delta^{15}\text{NO}_3 = \delta^{15}\text{NO}_3\text{initial} - \epsilon \cdot \ln\left(\frac{[\text{NO}_3^-]}{[\text{NO}_3^-]\text{initial}}\right) \quad \text{equation 2}$$

where $\delta^{15}\text{NO}_3\text{initial}$ is the $\delta^{15}\text{N}$ of the nitrate supply, $[\text{NO}_3^-]\text{initial}$ is the $[\text{NO}_3^-]$ of the nitrate supply, and ϵ is the fractionation factor of nitrate uptake.

This can be rewritten as

$$\delta^{15}\text{NO}_3 = \delta^{15}\text{NO}_3\text{initial} - \epsilon \cdot \left(\ln([\text{NO}_3^-]) - \ln([\text{NO}_3^-]\text{initial}) \right) \quad \text{equation 3}$$

Therefore, if the conditions of Rayleigh fractionation kinetics are fulfilled, samples fall along a straight line in $\delta^{15}\text{NO}_3/\ln([\text{NO}_3^-])$ space, and the slope of the line provides an estimate of ϵ , the fractionation factor of nitrate uptake. This relationship can also be used graphically as a test for whether and in what manner Southern Ocean nitrate uptake proceeds as a Rayleigh fractionation process.

According to equation 3, the slope of the $\delta^{15}\text{NO}_3/\ln([\text{NO}_3^-])$ relationship does not depend on the initial $[\text{NO}_3^-]$. This means that there is no explicit requirement to know the

initial $[\text{NO}_3^-]$ and $\delta^{15}\text{NO}_3$ in order to estimate the fractionation factor, as long as all of the surface samples have evolved from the same initial composition. However, there is rarely enough variation in the surface samples at a single station to yield a robust trend. For individual sites, we need to include some estimate of the $\delta^{15}\text{NO}_3$ and $[\text{NO}_3^-]$ of the source water. The differences among the possible choices may have a significant effect on the estimated fractionation factor, so that the choices must be considered carefully.

We can also use the Rayleigh fraction relationships to understand the origin of different water masses on a larger scale. If all $[\text{NO}_3^-]$ variations in the Southern Ocean were due to a single Rayleigh fractionation process, then all samples would fall on a common nitrate utilization trend in $\delta^{15}\text{NO}_3/\ln([\text{NO}_3^-])$ space. This is not the case (Figures 10, 11), and much of the following discussion involves deconvolving the non-Rayleigh fractionation processes. To aid this effort, we define a variable $\delta^{15}\text{Nnr}$, (nr for “non-Rayleigh”) which expresses the deviation of $\delta^{15}\text{NO}_3$ data from a single nitrate utilization trend (Figure 12):

$$\delta^{15}\text{Nnr} = (\delta^{15}\text{NO}_3 - \delta^{15}\text{NO}_3\text{initial}) - \varepsilon \cdot \ln\left([\text{NO}_3^-]/[\text{NO}_3^-]\text{initial}\right) \quad \text{equation 4}$$

We use a reference nitrate utilization trend that appears to apply broadly for the Antarctic Zone ($[\text{NO}_3^-]\text{initial} = 35 \mu\text{M}$, $\delta^{15}\text{NO}_3\text{initial} = 4.7\text{‰}$, $\varepsilon = 5\text{‰}$). The initial conditions are approximately those of the $[\text{NO}_3^-]$ maximum in Antarctic Zone UCDW, which appears to be the ultimate nitrate source to the surface Antarctic. We use this same reference trend for all stations, Antarctic and Subantarctic, although Rayleigh fractionation processes with different parameters will have non-zero values for $\delta^{15}\text{Nnr}$. Therefore, $\delta^{15}\text{Nnr}$ is solely a comparative tool. Typical profiles of $\delta^{15}\text{Nnr}$ in the Antarctic and Subantarctic Zones are shown in Figure 13.

Antarctic Zone

Deep Water Variations

While Antarctic UCDW $\delta^{15}\text{NO}_3$ is the same as or slightly higher than that of LCDW, UCDW is up to 6 μM higher in $[\text{NO}_3^-]$ than LCDW (Figures 5, 9). As a result, the $\delta^{15}\text{N}_{\text{nr}}$ of UCDW is higher than that of LCDW (Figure 13). The isotopic similarity of UCDW and LCDW is inconsistent with a nitrate uptake/regeneration explanation for their difference in $[\text{NO}_3^-]$, which tends to make lower $[\text{NO}_3^-]$ waters higher in $\delta^{15}\text{NO}_3$. In order to quantify the expected effect of the regeneration of particulate N back to nitrate, we calculate the isotopic composition of the nitrate that has been removed from the mixed layer, which corresponds to the isotopic composition of the N sinking flux if there are no other mechanisms of fixed N export. Using WOCE I9 station 97 as a model, the surface Antarctic has a $[\text{NO}_3^-]$ of 26 μM and a $\delta^{15}\text{NO}_3$ of 6.5‰, while the deep Antarctic has a $[\text{NO}_3^-]$ of 35.5 μM and a $\delta^{15}\text{NO}_3$ of 4.7‰, so that

$$\delta^{15}\text{N}_{\text{flux}} = \frac{(\delta^{15}\text{NO}_3_{\text{deep}} \cdot [\text{NO}_3^-]_{\text{deep}} - \delta^{15}\text{NO}_3_{\text{surface}} \cdot [\text{NO}_3^-]_{\text{surface}})}{([\text{NO}_3^-]_{\text{deep}} - [\text{NO}_3^-]_{\text{surface}})} \quad \text{equation 5}$$

$$= \frac{(35.5 \cdot 4.7\text{‰} - 26 \cdot 6.5\text{‰})}{(35.5 - 26)} = -0.2\text{‰} \quad \text{equation 6}$$

Estimates of the sinking flux $\delta^{15}\text{N}$ calculated in this way are 0-1‰ for stations from further north in the Indian sector of the Antarctic and in the east Pacific sector.

If the $\leq 6 \mu\text{M}$ subsurface $[\text{NO}_3^-]$ maximum of UCDW was solely due to remineralization of sinking particulate N with this range of $\delta^{15}\text{N}$, then there would be a $\delta^{15}\text{NO}_3$ minimum of $\sim 0.5\text{‰}$ amplitude at the depth of the $[\text{NO}_3^-]$ maximum. The absence of an isotopic minimum in association with the $[\text{NO}_3^-]$ maximum of UCDW (Figure 5a) suggests that the $[\text{NO}_3^-]$ maximum is not generated by *in situ* remineralization. Instead, we infer that it is due to exchange with a relatively high $[\text{NO}_3^-]$ water mass. Using a multiple linear regression analysis of salinity, oxygen and nitrate data, LeJehan and Treguer (1983)

reached the same conclusion. Regional oceanography also supports a circulation-based explanation for the depth variations in $[\text{NO}_3^-]$. The $[\text{NO}_3^-]$ maximum of UCDW appears to be supplied from the western Indian and eastern South Pacific (Callahan, 1972; Park et al., 1993; Warren, 1981), while the lower $[\text{NO}_3^-]$ in Lower Circumpolar Deep Water is due to the incorporation of NADW into the Circumpolar Current (Mantyla and Reid, 1983).

Rather than being a $\delta^{15}\text{NO}_3$ minimum, the UCDW $[\text{NO}_3^-]$ maximum is characterized by slight isotopic enrichment relative to LCDW (Figure 9). While this enrichment is $<0.5\text{‰}$ in the Antarctic, it is up to 1‰ in the Subantarctic. This isotopic enrichment of Subantarctic UCDW is also evident in $\delta^{15}\text{N}/\ln([\text{NO}_3^-])$ space (Figure 14). We hypothesize that the isotopic enrichment of UCDW is due to the high $\delta^{15}\text{NO}_3$ of the intermediate depth waters which enter the Subantarctic from the western Indian and eastern South Pacific, both of which are regions of water column denitrification (Brandes, 1996; Cline and Kaplan, 1975; Liu and Kaplan, 1989; Naqvi et al., 1982). A potential explanation for the lower degree of enrichment in Antarctic UCDW is that remineralization of low $\delta^{15}\text{N}$ sinking N does in fact lower the $\delta^{15}\text{NO}_3$ of Antarctic UCDW from a higher initial $\delta^{15}\text{NO}_3$ supplied by Subantarctic UCDW. However, the high $\delta^{15}\text{NO}_3$ of UCDW may simply be mixed out as UCDW thins to the South.

Upper Water Column Variations

The samples above the subsurface $[\text{NO}_3^-]$ maximum from the Antarctic Zone show an approximately linear correlation between $\delta^{15}\text{NO}_3$ and $\ln([\text{NO}_3^-])$ (Figures 10, 11). This suggests that nitrate uptake approximates Rayleigh fractionation behavior in the Antarctic zone, with nitrate supply by vertical mixing (largely during the winter) and nitrate uptake in the surface (largely during the spring and summer). We can estimate the fractionation factor for nitrate uptake from the Antarctic Zone profiles, assuming that the subsurface $[\text{NO}_3^-]$ maximum is the ultimate nitrate source (Figure 15). If instead LCDW is assumed as the

nitrate source to surface water in the Antarctic Zone, the deep water end-member would have a lower $[\text{NO}_3^-]$ (Figures 10, 11), so that the estimates of the fractionation factor would be higher by $\sim 1\%$ or more. Given this difference, it is worth evaluating the assumption that UCDW is the ultimate source of nitrate to the Antarctic surface layer.

From the perspective of the zonal average, nitrate is supplied to the surface Antarctic from below, by vertical mixing and upwelling, and from the South, by net northward advection of water which was upwelled at the Antarctic Divergence (Gordon et al., 1977). Jacques (1991) estimates that most of the nitrate supply to the surface Antarctic is by seasonal supply from below during winter mixing, with lateral advection from the Antarctic Divergence supplying only one-tenth as much nitrate. In this case, the subsurface $[\text{NO}_3^-]$ maximum of UCDW is the ultimate source of nitrate to the surface. Over the course of the winter, nitrate-rich water is entrained directly into the winter mixed layer from UCDW, replacing roughly one-third of the mixed layer volume every winter (Gordon et al., 1984; Gordon and Huber, 1990). During the rest of the year, UCDW upwells into the T_{min} layer, which then mixes with the surface layer at the onset of deep winter mixing (Gordon et al., 1977). Even if northward advection of surface waters is an important source of nitrate to the surface Antarctic at a given site, the advected surface water would probably have originated as upwelled UCDW, since its isopycnals outcrop at the southern boundary of the Antarctic Circumpolar Current (Orsi et al., 1995). Thus, whether UCDW is entrained locally or is upwelled further to the South and advected northward along the surface to the location of these profiles, UCDW appears to be the initial nitrate source for nitrate utilization in the Antarctic surface. Put another way, vertical mixing and lateral transport from the South cannot be clearly distinguished in the Antarctic Zone on the basis of N isotopes. As described in the following section, the case is different in the Subantarctic.

The fractionation factor estimates for the hydrocasts from the east Indian Antarctic Zone are between 4.6 and 5.7‰, while the east Pacific Antarctic Zone profiles yield fractionation factors between 4.0 and 5.0‰ (Figure 16). Regression of the surface transect Antarctic Zone samples give ϵ values of 4.0‰ ($r^2=0.77$) and 4.3‰ ($r^2=0.62$) in the east Pacific (ANT XII/4 southward and northward transects, respectively) and 4.8‰ ($r^2=0.97$) along the RITS '94 longitudinal transect in the Pacific sector (Figure 17). The surface transect estimates cover a smaller range in $\delta^{15}\text{NO}_3$ and $[\text{NO}_3^-]$ than do the depth profiles from the Antarctic Zone, which is probably the reason for the lower correlation coefficients. On the other hand, the fractionation factor estimates for the surface transect data do not involve an estimate of the source nitrate composition, although these estimates do assume that the source nitrate is the same for all of the surface samples used in a given regression.

The range of fractionation factor estimates, including those from profiles and surface transects (4.0-5.7‰) agree with some culture-based estimates for diatoms (and coccolithophorids, Waser et al., 1997a; Waser et al., 1997b) but appear to disagree with others (Table 3). Cultures of haptophytes, chlorophytes, and other algal types have yielded consistently lower fractionation factor estimates (Montoya and McCarthy, 1995; Waser et al., 1997b). As our understanding of species-based differences in the fractionation factor progresses, we may be able to use our field data to estimate the relative importance of different phytoplankton groups in nitrate uptake. If our fractionation factor estimates are compared only with the results of Waser et al. (1997a,b), they would suggest that diatoms are primarily responsible for nitrate uptake in the Antarctic. However, given the range in the culture-based estimates, we cannot make this inference. Our results indicate that the range of variation in the fractionation factor across the open Antarctic is within 2‰, which

is in contrast to the large range of fractionation factors observed in cultured phytoplankton (Table 3).

Compilation of upper water column Antarctic data in $\delta^{15}\text{N}/\ln([\text{NO}_3^-])$ space shows that the $\sim 1\text{‰}$ difference in the profile-based estimates from the Indian and Pacific reflects a difference in the composition of the surface samples (Figure 18). The Pacific samples are $\sim 1.5 \mu\text{M}$ lower in $[\text{NO}_3^-]$ for the same $\delta^{15}\text{NO}_3$, or $\sim 0.3\text{‰}$ lower in $\delta^{15}\text{NO}_3$ for the same $[\text{NO}_3^-]$. The cause of the $\sim 1\text{‰}$ difference between the estimates from the Indian and Pacific sectors is unknown. While the difference in the season of sampling may make a difference (WOCE I9 during January, ANT XII/4 during April), surface transect data from RITS '94, which was collected in January, tends to corroborate the 4-5‰ range of the estimates from the ANT XII/4 data (Figure 17c). In general, the agreement in the trends defined by the profile and surface transect data argues that the profile-based estimates are accurate and supports the assumption of UCDW as the nitrate source to the surface Antarctic (Figure 18).

The difference in the estimates between the Indian and Pacific sectors may involve the presence of a permanently ice-free region in the Indian sector of the Antarctic Zone and the lack of this region in the Pacific sector. The permanently open ocean Antarctic is relatively "oligotrophic", with no evidence for a strong seasonal bloom (Jacques, 1989), whereas the seasonal ice zone is characterized by strong seasonal blooms, associated with the retreat of the ice edge (Sullivan et al., 1989). In the Pacific sector, the seasonal range of sea ice occupies virtually the entire Antarctic Zone, whereas the Antarctic hydrocast stations from the east Indian sector are within the $\sim 10^\circ$ latitudinal range of the permanently open Antarctic (Treguer and Jacques, 1992).

While these ecosystem differences may well be responsible for the apparent Indian/Pacific sector difference in the fractionation factor, we cannot identify the immediate cause of this difference. Given the available information on the fractionation factor, it is

possible that species-based variations in the fractionation factor are responsible. Studies of the effects of growth rate and nitrate supply suggest that these are not potential causes of the Indian/Pacific sector difference (Montoya, 1990; N. Waser, unpublished data).

Nitrate uptake by sea ice phytoplankton may lead to a reduction in the fractionation factor. Nitrate uptake in sea ice is vulnerable to limitation by the diffusion rate of nitrate into the ice (Fritsen et al., 1994). In the case of diffusion limitation, the biological fractionation factor of nitrate uptake would not be completely expressed, because of complete nitrate extraction. As sea ice biological nitrate uptake may represent a significant fraction of the total nitrate uptake (e.g., Fritsen et al., 1994), uptake of nitrate into sea ice may lead to a lower effective fractionation factor for the entire upper ocean phytoplankton population during periods of sea ice cover. Since sea ice occurs seasonally in the Pacific sector of the Antarctic, this represents one potential cause of the Indian/Pacific sector difference. Ongoing work in the sea ice environment should help to address our hypothesis.

Phytoplankton blooms associated with the receding sea ice margin might also explain our lower fractionation factor estimates in the Pacific sector. Ice margin blooms can lead to localized nitrate depletion (Nelson and Smith, 1986). The mixing of nitrate-depleted water with higher $[\text{NO}_3^-]$ water produces a new water parcel with a $\delta^{15}\text{NO}_3/[\text{NO}_3^-]$ composition which falls below the nitrate utilization trend (Figure 19). This occurs because the higher $[\text{NO}_3^-]$ water has a proportionally larger effect on the new $\delta^{15}\text{NO}_3$, while both water parcels equally affect the new $[\text{NO}_3^-]$. If the surface layer is significantly affected by such mixing, we would expect to underestimate the fractionation factor in that region. The key question for this explanation is whether localized nitrate depletion is quantitatively important in the Antarctic Zone. While intense nitrate depletion has been observed in marginal ice zone blooms close to the Antarctic continent, it is unclear whether intense nitrate depletion is common in ice margin blooms in the open Antarctic (Whitehouse et al.,

1995). For our mixing explanation to apply, the low $[\text{NO}_3^-]$ end-member must be significantly depleted in nitrate relative to the high $[\text{NO}_3^-]$ end-member (Figure 19).

Thus, the difference in estimates between the Indian and Pacific sectors may reflect a real, albeit minor, difference in the fractionation factor associated with ecological differences, or it may reflect the influence of oceanographic processes on our method for estimating the fractionation factor. In any case, the difference in the data for the two sectors is fairly subtle (Figure 18). We overlook these small differences for now, estimating a fractionation factor for the entire Antarctic Zone of $5 \pm 1\%$.

Samples which are just below the Antarctic Zone surface layer tend to fall below the Rayleigh fractionation trend in $\delta^{15}\text{N}/\ln([\text{NO}_3^-])$ space which connects surface layer and UCDW samples (Figures 10, 11). With regard to upper ocean physical structure, these samples represent a $\delta^{15}\text{N}_{\text{nr}}$ minimum in the shallow subsurface of the Antarctic profiles (Figure 13a). The subsurface $\delta^{15}\text{N}_{\text{nr}}$ minimum in the Antarctic Zone consistently falls within the T_{min} layer, the winter-cooled layer in the Antarctic Zone (Figure 20). The T_{min} layer is absent in several of the more polar east Pacific stations, due to a very cold, fresh surface layer. However, the low $\delta^{15}\text{N}_{\text{nr}}$ values in these stations still fall below the density stratification of the surface layer at that time, where the T_{min} layer would normally have been found.

The $[\text{NO}_3^-]$ of the summer T_{min} layer is similar to the $[\text{NO}_3^-]$ of the winter mixed layer (Jacques, 1991), which is significantly higher than that of the summer surface layer ($\sim 31 \mu\text{M}$ vs. $\sim 25 \mu\text{M}$) but is not completely reset to the $[\text{NO}_3^-]$ of UCDW ($\sim 35 \mu\text{M}$). The $[\text{NO}_3^-]$ difference between the winter-time surface layer and UCDW is probably due to both dilution of the winter mixed layer with low $[\text{NO}_3^-]$ summer surface water and to nitrate uptake during the winter.

If the T_{min} layer is an unaltered reflection of the winter mixed layer, the lower $\delta^{15}\text{N}_{\text{nr}}$ values of the T_{min} layer suggest that the effective fractionation factor of winter

nitrate uptake is 0.5-1.0‰ lower than the fractionation factor of nitrate uptake during the summer. The hypothesis described above involving nitrate uptake into sea ice is also relevant to the T_{min} layer, in that sea ice cover might lead to a lower net fractionation factor for nitrate uptake during the winter.

However, the summer T_{min} layer has probably been altered in $\delta^{15}\text{NO}_3$ and $[\text{NO}_3^-]$ from its original wintertime composition. During the winter, UCDW is incorporated directly into the mixed layer (Gordon et al., 1984). During the summer, UCDW incorporation is limited to the T_{min} layer, since the surface layer above it is stabilized by melting and warming. Thus, the T_{min} layer represents a long-term mixing zone between the summer surface layer and UCDW.

Water parcel mixing is one of the potential explanations that we considered for the $\delta^{15}\text{N}_{\text{nr}}$ minimum of the shallow subsurface samples (Figure 19). In the Antarctic Zone, where typical surface and subsurface $[\text{NO}_3^-]$ values differ by only ~10 μM , the mixing of surface and subsurface waters should produce nitrate with an isotopic composition which falls less than 0.2‰ below the nitrate utilization line (Figure 19a). Thus, simple mixing does not seem to provide a complete explanation for the $\delta^{15}\text{N}_{\text{nr}}$ minimum of the T_{min} samples. As a result, we will have to look to other processes to explain the $\delta^{15}\text{N}_{\text{nr}}$ minimum of the T_{min} layer. Seasonal data will be important in this regard.

Questions regarding the T_{min} samples aside, the small potential effect of mixing in the Antarctic Zone suggests that nitrate exchange between the surface layer and subsurface during the productive summer months would not significantly shift water parcels off of the nitrate utilization trend. Thus, although summer-time mixing would formally violate the closed system assumption of Rayleigh fractionation, the supply of new nitrate from UCDW during the course of spring/summer nitrate extraction does not greatly affect the closed system assumption or our estimates of the fractionation factor. Similarly, the mixed layer need not be completely reset by UCDW entrainment for our fractionation factor estimates to

be valid. This is an important point because winter-time surface $[\text{NO}_3^-]$ in the Antarctic is not completely reset to the high $[\text{NO}_3^-]$ of UCDW.

Subantarctic Zone

Deep Water Variations

Whereas isotopic enrichment of UCDW relative to LCDW is 0.1-0.5‰ in the Antarctic, it is 0.5-1.0‰ in the Subantarctic (Figure 9). We hypothesized above that the isotopic enrichment of the UCDW $[\text{NO}_3^-]$ maximum is due to the denitrification-driven isotopic enrichment of the water masses of the east Pacific and western Indian, which contribute the high $[\text{NO}_3^-]$ water of UCDW. The available data suggest that the isotopic enrichment from denitrification decreases rapidly away from the regions of denitrification, for instance, from up to 20‰ in the intermediate-depth Eastern Tropical North Pacific to 6‰ near Hawaii (Cline and Kaplan, 1975). However, deep boundary currents may efficiently transfer high $\delta^{15}\text{NO}_3$ water to polar latitudes.

Antarctic Intermediate Water, which is marked by a salinity minimum at ~1100 m, is isotopically enriched by 0.5-1.0‰ and depleted in $[\text{NO}_3^-]$ by ~3 μM , relative to UCDW of the Antarctic Zone (Figure 9a,b). The ratio of isotope enrichment to nitrate depletion leads to $\delta^{15}\text{N}_{\text{nr}}$ values within AAIW which are similar to those of Antarctic surface water (Figure 9c). As there has been some debate regarding the importance of Subantarctic Mode Water as a source for AAIW formation (references in Piola and Gordon, 1989), it is worth considering the constraints which our data provide. Inspection of the different potential mixing end-members in $\delta^{15}\text{NO}_3/\ln([\text{NO}_3^-])$ space demonstrates that the $\delta^{15}\text{NO}_3/[\text{NO}_3^-]$ composition of AAIW could be generated by two water mass combinations (Figure 14a): (1) Antarctic surface water and Antarctic Upper Circumpolar Deep Water, or (2) Subantarctic Mode Water and Subantarctic Upper Circumpolar Deep Water. Thus, we are unable to distinguish between surface Antarctic and Subantarctic Mode Water sources to

AAIW. This is not surprising. The $[\text{NO}_3^-]$ of AAIW ($\sim 32 \mu\text{M}$) is much closer to that of UCDW ($\sim 35 \mu\text{M}$) than to that of either SAMW ($\sim 17 \mu\text{M}$) or Antarctic surface water ($\sim 25 \mu\text{M}$, Figure 8), so that the potential contribution from either of these water masses is necessarily small, and the $\delta^{15}\text{NO}_3$ data cannot resolve them.

A difference in the AAIW/UCDW relationship is observed between the Subantarctic and the Polar Frontal Zones. Going North from the Subantarctic Zone into the Polar Frontal Zone, UCDW loses much of its isotopic enrichment relative to LCDW, while AAIW does not (Figure 9b, WOCE I9 station 119). As a result, in profiles near the Polar Frontal Zone, AAIW represents the maximum in $\delta^{15}\text{N}_{\text{nr}}$ (Figures 14b, 21). This is qualitatively consistent with AAIW formation in the Polar Frontal Zone involving the incorporation of Subantarctic UCDW, leading to the partial erosion of the isotopic enrichment which characterizes Subantarctic UCDW. However, this observation does not provide a strong constraint on the identity of the low $[\text{NO}_3^-]$ water which is incorporated into AAIW.

In the Subantarctic thermocline, $\delta^{15}\text{N}_{\text{nr}}$ is strongly negative; that is, its $\delta^{15}\text{NO}_3$ is low, given its low $[\text{NO}_3^-]$ (Figure 13b). As described above, mixing between two water masses produces a new water mass with a $\delta^{15}\text{NO}_3$ which falls below the nitrate utilization trend. In the Subantarctic, the expected effect of cross-isopycnal mixing between surface and deep waters is relatively large, producing deviations from a nitrate utilization trajectory of $>1\text{‰}$ (Figure 19b). Nevertheless, simple vertical mixing is inadequate to provide a complete explanation for the very low $\delta^{15}\text{N}_{\text{nr}}$ values of the shallow thermocline samples. Vertical mixing can explain less than half of the curvature in the $\delta^{15}\text{NO}_3/\ln([\text{NO}_3^-])$ trajectory of Subantarctic station 119 (Figure 21).

Our best explanation for the low $\delta^{15}\text{N}_{\text{nr}}$ of the Subantarctic thermocline is isopycnal mixing with low $[\text{NO}_3^-]$ and/or low $\delta^{15}\text{NO}_3$ thermocline water of lower latitudes. The thermocline data from WOCE I9 show a coherent low $\delta^{15}\text{N}/\ln([\text{NO}_3^-])$ trajectory (to the left in Figure 22). This suggests a mixing end-member which has a low $[\text{NO}_3^-]$ without being

as high in $\delta^{15}\text{NO}_3$ as the Antarctic nitrate utilization trend would dictate. That is, the suggested mixing end-member has a low $\delta^{15}\text{N}_{\text{nr}}$ (Figure 22b).

The higher salinity of the shallow Subantarctic thermocline, relative to both the surface waters above and AAIW below (Figure 8b), suggests that the low- $\delta^{15}\text{N}_{\text{nr}}$ end-member which mixes with the Subantarctic thermocline originates in the high-salinity thermocline of the subtropics. Limited observations from the subtropical ocean corroborate the existence of low- $\delta^{15}\text{N}_{\text{nr}}$ subtropical thermocline water. Measurements from the Kuroshio near Taiwan suggest that $\delta^{15}\text{NO}_3$ is $<6\text{‰}$ through the entire range of the thermocline, while $[\text{NO}_3^-]$ approaches zero in shallow thermocline (Liu et al., 1996). Liu et al. argue that the low $\delta^{15}\text{NO}_3/[\text{NO}_3^-]$ relationship of the upper thermocline is due to the regeneration of newly fixed N, which has a $\delta^{15}\text{N}$ of $\sim 0\text{‰}$ (Hoering and Ford, 1960). Our profiles from the subtropical frontal zone (WOCE I9 stations 137 and 141) demonstrate the existence of low- $\delta^{15}\text{N}_{\text{nr}}$ water in the subtropics. With continued work, we will be able to determine whether it is due to mixing with a lower latitude low- $\delta^{15}\text{N}_{\text{nr}}$ end-member, or whether processes within the subtropics are responsible for the generation of the low $\delta^{15}\text{N}_{\text{nr}}$ in the thermocline.

Upper Water Column Variations

The surface water transect data show a strong correlation between the decrease in $[\text{NO}_3^-]$ and the increase in $\delta^{15}\text{NO}_3$ to the North across the Subantarctic Zone (Figure 4a,b,c). The central Pacific surface samples from RITS '94, which provide a relatively complete transect from the Antarctic Zone across the Subantarctic Zone, fall close to a common nitrate utilization trajectory, characterized by a fractionation factor of $\sim 4.5\text{‰}$ (Figure 23). Regression of the surface transect samples from the Antarctic Zone give similar fractionation factor estimates (4.0-4.8‰, Figure 17), as do the profile-based estimates from Antarctic (Figure 16). This apparent similarity in the fractionation factor

between the Antarctic and Subantarctic Zones occurs despite an important transition in phytoplankton assemblage across the Polar Frontal Zone, with diatoms dominating cell numbers in the Antarctic and monads and flagellates dominating in the Subantarctic (Kopczynska et al., 1986). Given the culture-based evidence for differences in the fractionation factors associated with these classes of phytoplankton (Table 3), our results may indicate a primary role for diatoms in nitrate uptake across the entire Southern Ocean, despite variations in relative cell abundance.

The consistency of the surface data with a single nitrate utilization trend can be explained by two possible mechanisms of nitrate supply. The first potential mechanism is lateral nitrate transport in the surface layer, whereby nitrate is advected or mixed equatorward across the Subantarctic, with progressive nitrate utilization occurring during this net northward transport. The second potential mechanism is the vertical supply of nitrate from the Subantarctic thermocline. As described below, the data argue against vertical nitrate supply, suggesting that nitrate supply in the Subantarctic is largely by equatorward transport in the surface layer.

The depth profiles from the Subantarctic zone in both the east Indian and east Pacific sectors suggest limited exchange between the surface layer and the water below. As described in the previous section, Subantarctic profiles plotted in $\delta^{15}\text{N}/\ln([\text{NO}_3^-])$ space show a concave-upward pattern, with samples in the shallow thermocline falling well below a line connecting the deeper samples with the surface samples (Figure 10, 11, 21). This is a reflection of the strongly negative $\delta^{15}\text{N}_{\text{nr}}$ of the thermocline samples (Figure 13b). The thermocline $\delta^{15}\text{N}_{\text{nr}}$ values become more negative toward the North. The Subantarctic thermocline samples from WOCE I9 have a self-consistent trend in $\delta^{15}\text{N}/\ln([\text{NO}_3^-])$ space which diverges from that of the surface samples (Figure 22). That is, the changes in thermocline $\delta^{15}\text{NO}_3$ and $[\text{NO}_3^-]$ are not along a parallel Raleigh fractionation trend to that of the surface Subantarctic samples.

As a result of the difference between the surface layer and thermocline trends in the Subantarctic, the nitrate utilization trend of the surface Subantarctic data is inconsistent with vertical nitrate supply, unless the fractionation factor is allowed to vary widely. If the shallow thermocline is assumed as the nitrate source to the Subantarctic surface layer and the shallow thermocline and surface samples are regressed to generate an estimate of the fractionation factor, very high slopes result, suggesting unrealistically high fractionation factors (7.5‰ and 13.7‰ at WOCE I9 stations 119 and 126, Figure 10; 14.2‰ and 11.3‰ at ANT XII/4 stations 14 and 21, Figure 11).

In the case of WOCE I9 station 132, $\delta^{15}\text{NO}_3$ increases into the surface layer, even though $[\text{NO}_3^-]$ does not (Figure 24a). This represents a reversal of the $\delta^{15}\text{NO}_3/[\text{NO}_3^-]$ relationship that would be caused by nitrate utilization. If the data are plotted in $\delta^{15}\text{NO}_3/\ln([\text{NO}_3^-])$ space, the trend linking the surface samples to the shallow thermocline is close to vertical, yielding a meaningless estimate of the fractionation factor (Figure 10). The presence of offsets in both $\delta^{15}\text{N}_{\text{nr}}$ and salinity between the thermocline and the surface layer at station 132 further support the inference that vertical exchange between these two levels is minimal (Figure 24b). The lower salinity of the surface layer suggests transport from the South, consistent with the supply of nitrate by net equatorward transport in the surface layer.

The concept of equatorward nitrate transport in the Subantarctic surface layer is consistent with the physical oceanography of the Southern Ocean. As winds are eastward over the Southern Ocean, Ekman transports in the surface layer are to the North. Ocean circulation models tend to produce a strong northward component in the velocity of the surface layer, leading to meridional models of surface nitrate transport in the Southern Ocean (Follows, submitted). On the other hand, there need not be a strong surface flux of water for nitrate to be transported northward at the surface. The existence of the surface $[\text{NO}_3^-]$ gradient ensures that any meridional surface water exchange across the Subantarctic

will represent a northward nitrate flux. Since the Antarctic surface samples fall on the nitrate utilization trend defined by the Subantarctic surface samples (Figure 23), Antarctic surface water is the most likely nitrate source to the Subantarctic surface. In this case, surface nitrate would most likely be mixed northward across the Polar Frontal Zone.

The surface transect from the central Pacific shows the hint of a steeper $\delta^{15}\text{N}/\ln([\text{NO}_3^-])$ trend in the more poleward Subantarctic samples (Figure 23). This steeper trend is due to lower $\delta^{15}\text{NO}_3$ values for several samples with 10-13 μM $[\text{NO}_3^-]$, which originate from just north of the Polar Frontal Zone. Overlaying the surface samples from the WOCE I9 transect shows a similar pattern among the Subantarctic surface samples from that sector, with lower $\delta^{15}\text{N}$ values at the stations closer to the Polar Frontal Zone and more northerly samples increasing toward the general trend line (crosses in Figure 23). We interpret the lower $\delta^{15}\text{NO}_3$ of the higher latitude Subantarctic samples as being due to vertical mixing with the low- $\delta^{15}\text{N}_{\text{nr}}$ water of the Subantarctic thermocline. This mixing may represent the process of Subantarctic Mode Water formation, which occurs just north of the Subantarctic Front (McCartney, 1977).

The higher $\delta^{15}\text{N}/\ln([\text{NO}_3^-])$ trend of the samples just north of the Subantarctic Front can be interpreted as suggesting that (1) the nitrate supply which is transported across Subantarctic has an initial $\delta^{15}\text{N}_{\text{nr}}$ lower than that of Antarctic surface water, and (2) that nitrate uptake in the more polar latitudes of the Subantarctic has a higher fractionation factor than the overall regression line suggests. However, the consistency of the larger scale trend with an Antarctic surface water source and a single fractionation factor makes it worthwhile to consider an alternative explanation.

To this point, we have considered the Southern Ocean largely as a zonal average. However, there are important zonal variations. Winter mixing just north of the Subantarctic Front is responsible for Subantarctic Mode Water formation (McCartney, 1977). This winter mixing penetrates to greater depths in the eastern Indian sector and the central and

eastern Pacific sectors, generating a thick SAMW layer in these sectors (McCartney, 1982). Our transects are in these regions, so it is consistent that observe an apparent input of low- $\delta^{15}\text{N}_{\text{nr}}$ thermocline nitrate into the surface layer just north of the Polar Frontal Zone in our transects. However, the nitrate which is supplied to the Subantarctic surface further north in our transects would have come from the west, due to the strong zonal circulation of Southern Ocean (Figure 25). These surface waters have originated from a more western section of the Subantarctic Front and thus would not have been as strongly modified by SAMW formation. Instead, they would reflect surface Antarctic nitrate which was advected across the Polar Frontal and Subantarctic Zones and has undergone progressive nitrate extraction. If this is true, then the more polar Subantarctic surface samples in our transect do not represent the nitrate source to the samples further north. In this picture, the nitrate source to Subantarctic surface is similar to surface Antarctic water, except near the Polar Frontal Zone at the locations of our transects, where deep winter mixing may incorporate low- $\delta^{15}\text{N}_{\text{nr}}$ Subantarctic thermocline water into the Subantarctic surface layer. Most of the surface samples, which are largely unaffected by the local process of Mode Water formation, suggest that a fractionation factor of $\sim 4.5\text{‰}$ applies in the Subantarctic (Figure 23), consistent with a fractionation factor of $5 \pm 1\text{‰}$ across the entire Southern Ocean.

Conclusions

In the Antarctic Zone, the $\delta^{15}\text{NO}_3$ of the nitrate supply to the surface layer is 4.7-5.0‰. This value is relatively invariant with depth in the Antarctic subsurface and is similar to the $\delta^{15}\text{NO}_3$ measured throughout much of the global deep ocean. A simple model of vertical nitrate supply and Rayleigh fractionation is generally applicable in the Antarctic. One deviation from this model involves samples from the subsurface minimum temperature layer, which fall slightly below the idealized nitrate utilization trend connecting surface waters with Upper Circumpolar Deep Water. The fractionation factor of nitrate uptake in the Antarctic is estimated to be 5 ± 1 ‰, with a possible ~ 1 ‰ difference between the Indian and Pacific sectors.

In the Subantarctic Zone, nitrate supply appears to be largely by lateral surface transport from the South. The Subantarctic data suggest that the $\delta^{15}\text{NO}_3/[\text{NO}_3^-]$ composition of the ultimate nitrate supply is similar to the composition of Antarctic surface waters. However, there is tentative evidence from just north of the Polar Frontal Zone for local supply of nitrate by vertical mixing with Subantarctic thermocline water, which has a distinctively low $\delta^{15}\text{NO}_3$ for its $[\text{NO}_3^-]$. The fractionation factor of nitrate uptake is estimated to be 4.5‰ in the Subantarctic, similar to the estimates from the Antarctic.

Acknowledgements

Isotopic analyses at the MBL isotope facility were performed by K. Tholke. Sample collection for the Southern Ocean profiles shown in Figures 11 and 12 was generously performed by the science crew of WOCE I9 (OCE 13167). Michael Bender, Ed Boyle, and Bill Jenkins provided important insights. The first author was supported by the NSF Graduate Research Fellowship Program and by the JOI/USSAC Ocean Drilling Graduate Research Fellowship Program.

References

- Altabet, M.A., Deuser, W.G., Honjo, S. and Stienen, C., 1991. Seasonal and depth-related changes in the source of sinking particles in the North Atlantic. *Nature*, 354: 136-139.
- Altabet, M.A. and Francois, R., 1994a. Sedimentary nitrogen isotopic ratio as a recorder for surface ocean nitrate utilization. *Global Biogeochemical Cycles*, 8(1): 103-116.
- Altabet, M.A. and Francois, R., 1994b. The use of nitrogen isotopic ratio for reconstruction of past changes in surface ocean nutrient utilization. In: R. Zahn, M. Kaminski, L. Labeyrie and T.F. Pederson (Editors), *Carbon Cycling in the Glacial Ocean: Constraints on the Ocean's Role in Global Change*. NATO ASI series. Springer Verlag, Berlin, Heidelberg, New York, pp. 281-306.
- Altabet, M.A. and McCarthy, J.J., 1985. Temporal and spatial variation in the natural abundance of ^{15}N in PON from a warm-core ring. *Deep-Sea Research*, 32: 755-772.
- Biggs, D.C., Berkowitz, S.P., Altabet, M.A., Bidigare, R.R., DeMaster, D.J., Dunbar, R.B., Leventer, A., Macko, S.A., Nittrouer, C.A. and Ondrusek, M.E., 1988. A cooperative study of upper-ocean particulate fluxes in the Weddell Sea, Proceedings of the Ocean Drilling Program - Initial Reports. N.S.F. Joint Oceanographic Institutions Inc., pp. 77-86.
- Brandes, J.A.G., 1996. Isotopic effects of denitrification in the marine environment, Ph.D. Thesis, University of Washington, Department of Oceanography, 186 pp.
- Callahan, J.E., 1972. The structure and circulation of deep water in the Antarctic. *Deep-Sea Research*, 19: 563-575.
- Charles, C.D. and Fairbanks, R.G., 1990. Glacial to interglacial changes in the isotopic gradients of southern Ocean surface water. In: U. Bleil and J. Thiede (Editors), *Geological History of the Polar Oceans: Arctic versus Antarctic*. Kluwer Academic Publishers, Netherlands, pp. 519-538.
- Cline, J.D. and Kaplan, I.R., 1975. Isotopic fractionation of dissolved nitrate during denitrification in the eastern tropical North Pacific Ocean. *Marine Chemistry*, 3: 271-299.
- Cullen, J.J., 1991. Hypotheses to explain high-nutrient conditions in the open sea. *Limnology and Oceanography*, 36(8): 1578-1599.
- DeNiro, M.J. and Epstein, S., 1981. Influence of diet on the distribution of nitrogen isotopes in animals. *Geochimica et Cosmochimica Acta*, 45: 341-351.
- Farrell, J.W., Pedersen, T.F., Calvert, S.E. and Nielsen, B., 1995. Glacial-interglacial changes in nutrient utilization in the equatorial Pacific Ocean. *Nature*, 377(6549): 514-517.
- Follows, M.J., submitted. Models of nutrient cycling and export production in the Southern Oceans. *Global Biogeochemical Cycles*.

- Francois, R., Altabet, M.A. and Burkle, L.H., 1992. Glacial to interglacial changes in surface nitrate utilization in the Indian sector of the Southern Ocean as recorded by sediment $\delta^{15}\text{N}$. *Paleoceanography*, 7: 589-606.
- Francois, R.F., Altabet, M.A., Yu, E.-F., Sigman, D.M., Bacon, M.P., Frank, M., Bohrmann, G., Bareille, G. and Labeyrie, L.D., 1997. Water column stratification in the Southern Ocean contributed to the lowering of glacial atmospheric CO_2 . *Nature*, in press.
- Fritsen, C.H., Lytle, V.I., Ackley, S.F. and Sullivan, C.W., 1994. Autumn bloom of Antarctic ice algae. *Science*, 266: 782-785.
- Fry, B., Brand, W., Mersch, F.J., Tholke, K. and Garritt, R., 1992. Automated analysis system for coupled $\delta^{13}\text{C}$ and $\delta^{15}\text{N}$ measurements. *Anal. Chem.*, 64(3): 288-291.
- Garside, C., 1982. A chemiluminescent technique for the determination of nanomolar concentrations of nitrate, nitrite, or nitrite alone in seawater. *Marine Chemistry*, 11: 159-167.
- Gersonde, R., et al., in preparation. The Expedition ANTARKTIS XII/4 of RV "Polarstern" in 1995, Reports on Polar Research, Alfred-Wegener-Institute for Polar and Marine Research.
- Goering, J., Alexander, V. and Haubensstock, N., 1990. Seasonal variability of stable carbon and nitrogen isotope ratios of organisms in a North Pacific Bay. *Estuarine and Coastal Shelf Science*, 30: 239-260.
- Gordon, A.L., Chen, C.T.A. and Metcalf, W.G., 1984. Winter mixed layer entrainment of Weddell Deep Water. *Journal of Geophysical Research*, 89(C1): 637-640.
- Gordon, A.L. and Huber, B.A., 1990. Southern Ocean winter mixed layer. *Journal of Geophysical Research*, 95(C7): 11655-11672.
- Gordon, A.L., Taylor, H.W. and Georgi, D.T., 1977. Antarctic Oceanographic Zonation. In: M.J. Dunbar (Editor), *Polar Oceans*. Arctic Institute of North America, Calgary.
- Hoering, T.C., Ford, H.T., 1960. The isotope effect in the fixation of nitrogen by *Azotobacter*. *Journal of American Chemical Society*, 82: 376-378.
- Horrigan, S.G., Montoya, J.P., Nevins, J.L. and McCarthy, J.J., 1990. Natural isotopic composition of dissolved inorganic nitrogen in the Chesapeake Bay. *Estuarine and Coastal Shelf Science*, 30: 393-410.
- Howard, W.R., 1992. Late quaternary paleoceanography of the Southern Ocean, Ph.D. Thesis, Brown University, Providence, 345 pp.
- Jacques, G., 1989. Primary production in the open Antarctic Ocean during the austral summer, a review. *Vie Milieu*, 39: 1-17.
- Jacques, G., 1991. Is the concept of new production-regenerated production valid for the Southern Ocean? *Marine Chemistry*, 35: 273-286.

- Jones, E.P., Nelson, D.M. and Treguer, P., 1990. Chemical Oceanography. In: J. W.O. Smith (Editor), *Polar Oceanography, Part B: Chemistry, Biology, and Geology*. Academic Press.
- Keigwin, L.D. and Boyle, E.A., 1989. Late quaternary paleochemistry of high-latitude surface waters. *Paleogeography, Palaeoclimatology, and Paleoecology*, 73: 85-106.
- Knox, F. and McElroy, M., 1984. Changes in atmospheric CO₂ influence of the marine biota at high latitude. *Journal of Geophysical Research*, 89: 4629-4637.
- Kopczynska, E.E., Weber, L.H. and El-Sayed, S.Z., 1986. Phytoplankton species composition and abundance in the Indian sector of the Antarctic Ocean. *Polar Biology*, 6: 161-169.
- Kumar, N., Gwiazda, R., Anderson, R.F. and Froelich, P.N., 1993. ²³¹Pa/²³⁰Th ratios in sediments as a proxy for past changes in Southern Ocean productivity. *Nature*, 362: 45-48.
- LeJehan, S. and Treguer, P., 1983. Uptake and regeneration Si/N/P ratios in the Indian sector of the Southern Ocean: originality of the biological cycle of silicon. *Polar Biology*, 2: 127-136.
- Liu, K.-K. and Kaplan, I.R., 1989. The eastern tropical Pacific as a source of ¹⁵N-enriched nitrate in seawater off southern California. *Limnology and Oceanography*, 34: 820-830.
- Liu, K.K., Su, M.J., Hsueh, C.R. and Gong, G.C., 1996. The nitrogen isotopic composition of nitrate in the Kuroshio Water northeast of Taiwan: evidence for nitrogen fixation as a source of isotopically light nitrate. *Marine Chemistry*, 54: 273-292.
- Mantyla, A.R. and Reid, J.L., 1983. Abyssal characteristics of the World Ocean waters. *Deep-Sea Research*, 30(8a): 805-833.
- Martin, J.H., Fitzwater, S.E. and Gordon, R.M., 1990. Iron deficiency limits growth in Antarctic waters. *Global Biogeochemical Cycles*, 4: 5-12.
- McCartney, M.S., 1977. Subantarctic Mode Water. *Deep-Sea Research*, G. Deacon 70th Anniversary Volume: 103-119.
- McCartney, M.S., 1982. The subtropical circulation of mode waters. *Journal of Marine Research*, 40: 427-464.
- McDougall, T.J., 1987. Neutral surfaces. *Journal of Physical Oceanography*, 17: 1950-1964.
- Mitchell, B.G., Brody, E.A., Holm-Hansen, O., McLain, C. and Bishop, J., 1991. Light limitation of phytoplankton biomass and macronutrient utilization in the Southern Ocean. *Limnology and Oceanography*, 36(8): 1662-1677.

Montoya, J.P., 1990. Natural abundance of ^{15}N in marine and estuarine plankton: studies of biological isotopic fractionation and plankton processes. Ph.D. Thesis, Harvard University, 403 pp.

Montoya, J.P., 1994. Nitrogen isotope fractionation in the modern ocean: implications for the sedimentary record. In: R. Zahn, M. Kaminski, L. Labeyrie and T.F. Pederson (Editors), *Carbon Cycling in the Glacial Ocean: Constraints on the Ocean's Role in Global Change*. NATO ASI series. Springer Verlag, Berlin, Heidelberg, New York, pp. 259-279.

Montoya, J.P. and McCarthy, J.J., 1995. Isotopic fractionation during nitrate uptake by marine phytoplankton grown in continuous culture. *Journal of Plankton Research*, 17(3): 439-464.

Mortlock, R.A., Charles, C.D., Froelich, P.N., Zibello, M.A., Saltzman, J., Hays, J.D. and Burckle, L.H., 1991. Evidence for lower productivity in the Antarctic during the last glaciation. *Nature*, 351: 220-223.

Nakatsuka, T., Handa, N., Wada, E. and Wong, C.S., 1992. The dynamic changes of stable isotope ratios of carbon and nitrogen in suspended and sedimented particulate organic matter during a phytoplankton bloom. *Journal of Marine Research*: 267-296.

Naqvi, S.W.A., Noronha, R.J. and Reddy, C.V.G., 1982. Denitrification in the Arabian Sea. *Deep-Sea Research*, 29: 459-469.

Orsi, A.H., Whitworth, T.W. and Nowlin, W.D., 1995. On the meridional extent and fronts of the Antarctic Circumpolar Current. *Deep-Sea Research*, 42: 641-73.

Park, Y.H., Gamberoni, L. and Charriaud, E., 1993. Frontal structure, water masses, and circulation in the Crozet Basin. *Journal of Geophysical Research*, 98: 12361-12385.

Pennock, J.R., Sharp, J.H., Ludlam, J., Velinsky, D.J. and Fogel, M.L., 1988. Isotopic fractionation of nitrogen during the uptake of NH_4^+ and NO_3^- by *Skeletonema costatum*. *EOS*, 69(44): 1098.

Piola, A.R. and Georgi, D.T., 1982. Circumpolar properties of Antarctic Intermediate Water and Subantarctic Mode Water. *Deep-Sea Research*, 29(6a): 687-711.

Piola, A.R. and Gordon, A.L., 1989. Intermediate waters in the southwest South Atlantic. *Deep-Sea Research*, 36: 1-16.

Rau, G.H., Sullivan, C.W. and Gordon, L.I., 1991. $\delta^{13}\text{C}$ and $\delta^{15}\text{N}$ variations in Weddell Sea particulate organic matter. *Marine Chemistry*, 35: 355-369.

Rosenthal, Y., 1994. Late quaternary paleochemistry of the Southern Ocean: evidence from Cadmium variability in sediments and foraminifera. Ph.D. Thesis, MIT/WHOI Joint Program in Oceanography.

Sarmiento, J.L. and Toggweiler, J.R., 1984. A new model for the role of the oceans in determining atmospheric pCO_2 . *Nature*, 308: 621-624.

- Shemesh, A., Macko, S.A., Charles, C.D. and Rau, G.H., 1993. Isotopic evidence for reduced productivity in the glacial southern ocean. *Science*, 262: 407-410.
- Siegenthaler, U. and Wenk, T., 1984. Rapid atmospheric CO₂ variations and ocean circulation. *Nature*, 308: 624-626.
- Sigman, D.M., Altabet, M.A., Michener, R.H., McCorkle, D.C., Fry, B. and Holmes, R.M., 1997. Natural abundance-level measurement of the Nitrogen isotopic composition of oceanic nitrate: an adaptation of the ammonia diffusion method. *Marine Chemistry*, in press.
- Singer, A.J. and Shemesh, A., 1995. Climatically linked carbon isotope variation during the past 430,000 years in Southern Ocean sediments. *Paleoceanography*, 10(2): 171-178.
- Sullivan, C.W., McClain, C.R., Comiso, J.C. and Smith, W.O.J., 1988. Phytoplankton standing crops within the Antarctic ice edge assessed by satellite remote sensing. *Journal of Geophysical Research*, 93: 12,487-12,498.
- Treguer, P. and Jacques, G., 1992. Dynamics of nutrients and phytoplankton, and fluxes of carbon, nitrogen, and silicon in the Antarctic Ocean. *Polar Biology*, 12: 149-162.
- Wada, E. and Hattori, A., 1978. Nitrogen isotope effects in the assimilation of inorganic nitrogenous compounds. *Geomicrobiology Journal*, 1: 85-101.
- Wada, E., 1980. Nitrogen isotope fractionation and its significance in biogeochemical processes occurring in marine environments. In: E. Goldberg, Y. Horibe and K. Saruhashi (Editors), *Isotope Marine Chemistry*. Uchida Rokakuho, Tokyo, pp. 375-398.
- Warren, B.A., 1981. Transindian hydrographic section at Lat. 18°S: property distributions and circulation in the South Indian Ocean. *Deep-Sea Research*, 28: 759-788.
- Waser, N.A.D., Needoba, J., Calvert, S.E. and Harrison, P.J., 1997b. Nitrogen isotope fractionation by 4 groups of marine microalgae during batch culture growth on nitrate, ASLO Aquatic Sciences Meeting, Santa Fe, NM, pp. 337.
- Waser, N.A.D., Turpin, D.H., Harrison, P.J., Nielsen, B. and Calvert, S.E., 1997a. Nitrogen isotope fractionation during the uptake and assimilation of nitrate, nitrite, and urea by a marine diatom. *Limnology and Oceanography*, in press.
- Whitehouse, M.J., Priddle, J. and Woodward, E.M.S., 1995. Spatial variability of inorganic nutrients in the marginal ice zone of the Bellingshausen Sea during the Austral spring. *Deep-Sea Research*, 42(4-5): 1047-1058.
- Wu, J., Calvert, S.E. and Wong, C.S., 1997. Nitrogen isotope variations in the subarctic Pacific northeast Pacific: relationships to nitrate utilization and trophic structure. *Deep-Sea Research*, in press.
- Yu, E.-F., 1994. Variations in the particulate flux of ²³⁰Th and ²³¹Pa and paleoceanographic applications of ²³¹Pa/²³⁰Th ratio. Ph.D. Thesis, MIT/WHOI Joint Program in Oceanography.

Table 1: station locations of hydrocast profiles
(surface sample locations given in Data Tables)

WOCE I9 (January, 1995)

station #	latitude (°S)	longitude (°E)	max. depth (m)*
97	59.20	115.00	4547
103	56.19	115.00	4560
108	53.19	115.00	4006
113	50.50	115.03	3184
119	47.51	115.00	3458
126	44.00	115.00	4380
132	40.89	115.00	4629
137	38.00	115.00	4864
141	36.00	115.00	5286

ANTARKTIS XII/4 (April, 1995)

station #	AWI #	latitude (°S)	longitude (°E)	nutrients	max. depth (m)*
14	2660-6	50.14	270.77	+	500
21	2661-5	51.41	270.66		500
47	2667-7	55.66	270.18	+	3500
80	2682-1	66.52	262.57		1000
91	2683-1	68.52	262.83	+	600
103	2684-4	69.42	264.98	+	600
104	2685-1	69.42	265.83		600
135	2686-1	68.29	270.41	+	600
138	2687-1	67.98	267.36	+	4000
141	2688-5	67.22	268.17		600
154	2692-3	65.14	269.31	+	600
162	2696-5	63.98	270.47		4000
177	2699-1	61.02	270.50		4500
182	2700-4	60.27	270.48		600

"+" = nutrients from Gersonde et al. (in prep.)

* refers to depth range of $\delta^{15}\text{NO}_3$ samples only

Table 2: **$\delta^{15}\text{NO}_3$ from other regions along the path of deep circulation**

Region	depth (m)	latitude (°N)	longitude (°E)	[NO ₃] (μM)	$\delta^{15}\text{NO}_3$ (‰ vs. air)
<u>Arctic Ocean</u>					
	1000	82	32	15.6	4.67
	1450	"	"	16.0	4.67
	2575	"	"	16.2	4.73
<u>Greenland Sea</u>					
	1000	?	?	18.8	4.53
	1500	?	?	18.5	4.48
<u>western North Atlantic (slope water just off Georges Bank)</u>					
	1000	?	?	17.9	4.43
	1500	?	?	17.5	4.61
<u>western North Atlantic</u>					
	3005	39	-70	17.8	4.73
	3009	39	-70	17.3	4.73
<u>Sargasso Sea</u>					
	1500	?	?	18.8	4.66
<u>central Pacific, 900 km northeast of Hawaii</u>					
	2500	~30	~-150	39.6	5.20
	3000	"	"	38.4	5.10
	3500	"	"	37.8	4.90
	4000	"	"	37.1	4.70

Table 3: estimates of the fractionation factor of nitrate uptake
(compiled largely from Montoya (1994), Altabet and Francois (1994b), and Waser et al. (1997))

	Method	ϵ (‰)	Reference
Field estimates:			
<u>Coastal</u>			
Auke Bay, Alaska	$\delta^{15}\text{N-PN}$ vs $\delta^{15}\text{NO}_3$	4.0	Goering et al. (1990)
Chesapeake Bay	$\delta^{15}\text{N-PN}$ vs $\delta^{15}\text{NO}_3$	7.0	Horrigan et al. (1990)
<u>Atlantic</u>			
North Atlantic	$\delta^{15}\text{N-PN}$ vs $\delta^{15}\text{NO}_3$	8-9	Altabet et al. (1991)
<u>Pacific</u>			
western North Pacific	$\delta^{15}\text{N-PN}$ vs. $[\text{NO}_3^-]$	5.0	Wada (1980)
Subarctic Pacific	$\delta^{15}\text{N-PN}$ vs $\delta^{15}\text{NO}_3$	5-6	Wu et al. (1997)
western Subarctic Pacific	$\delta^{15}\text{NO}_3$ vs. $[\text{NO}_3^-]$	9.1	Altabet and Francois (1994b)
<u>Southern Ocean</u>			
Weddell Sea	$\delta^{15}\text{N-PN}$ vs. $\delta^{15}\text{NO}_3$	8.0	Biggs et al. (1988)
Antarctic Zone, east Indian	$\delta^{15}\text{NO}_3$ vs. $[\text{NO}_3^-]$	5-6	this study
Antarctic Zone, central Pacific	" "	4-5	" "
Antarctic Zone, east Pacific	" "	4-5	" "
Subantarctic Zone, central Pacific	" "	4.5-5.3	" "
Culture estimates:			
<u>diatoms:</u>			
<i>Pheodactylum tricomutum</i>	$\delta^{15}\text{N-PN}$ vs. $[\text{NO}_3^-]$?	0.7-23.0	Wada and Hattori (1978)
<i>Chaetoceros</i> sp.	$\delta^{15}\text{N-PN}$ vs. $[\text{NO}_3^-]$?	0.9-4.5	" "
<i>Skeletonema costatum</i>	$\delta^{15}\text{N-PN}$ vs. $[\text{NO}_3^-]$?	9.8	Pennock et al. (1988)
<i>Skeletonema costatum</i>	$\delta^{15}\text{N-PN}$ (continuous)	6.4-11.9	Montoya et al. (1995)
<i>Thalassiosira weissflogii</i>	" "	9.7-15.4	" "
<i>Thalassiosira pseudonana</i>	$\delta^{15}\text{N-PN}$ vs. $[\text{NO}_3^-]$ (batch)	4.5-6.3	Waser et al. (1997)
<i>Chaetoceros simplex</i>	" "	3.0	Waser et al. (1997b)
<i>Thalassiosira pseudonana</i>	" "	5.2	" "
<u>others:</u>			
<i>Isochrysis galbana</i> (haptophyte)	$\delta^{15}\text{N-PN}$ (continuous)	2.2-4.4	Montoya et al. (1995)
<i>Pavlova lutheri</i> (haptophyte)	" "	0.3-3.9	" "
<i>Chroomonas salina</i> (cryptophyte)	" "	1.2-2.9	" "
<i>Dunaliella teriolecta</i> (chlorophyte)	" "	0.7-6.1	" "
<i>Emiliana huxleyi</i> (prymnesiophyte)	$\delta^{15}\text{N-PN}$ vs. $[\text{NO}_3^-]$ (batch)	4.2	Waser et al. (1997b)
<i>Amphidilinium carterae</i>	" "	1.9	" "
<i>Dunaliella tertiolecta</i> (chlorophyte)	" "	2.1	" "

Figure 1

A plot of the Rayleigh fractionation equations showing the theoretical link between nitrate utilization and the $\delta^{15}\text{N}$ of the different N pools. The “instantaneous product” is the N being extracted from the surface layer nitrate pool (the “substrate”) at a given degree of nitrate utilization. The fractionation factor (ϵ) of nitrate uptake defines the $\delta^{15}\text{N}$ difference between these two pools. The “accumulated product” is the entire N pool that has been drawn from the nitrate pool up to a given degree of nitrate utilization. Rayleigh fractionation applies for the case of (1) a closed system, with no resupply of nitrate during the course of nitrate uptake, and (2) a constant fractionation factor.

The nitrate utilization/ $\delta^{15}\text{N}$ relationship:

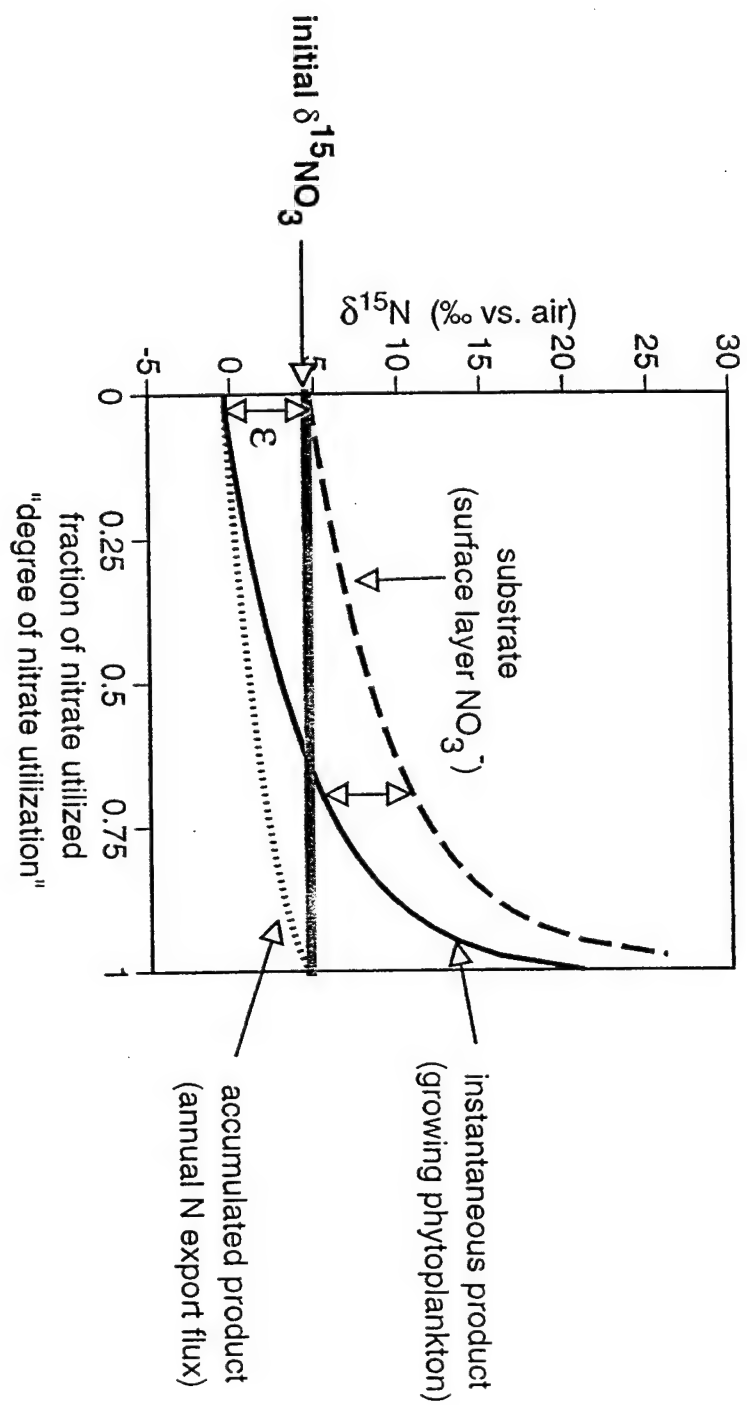


Figure 2

Locations of the three samples sets in this study: (1) the WOCE I9 transect of hydrocasts in the east Indian sector (squares), (2) the ANT XII/4 transect of hydrocasts in the east Pacific sector (circles), and (3) the RITS '94 east and central Pacific transect of surface samples (crosses). The underway surface samples of ANT XII/4 are not plotted; they are among the hydrocast stations of that cruise. The Subantarctic Front (SAF) separates the Antarctic and Polar Frontal Zones to the South from the Subantarctic Zone to the North. The Subtropical Front (STF) defines the northern boundary of the Subantarctic Zone. Frontal positions are from Orsi et al. (1995).

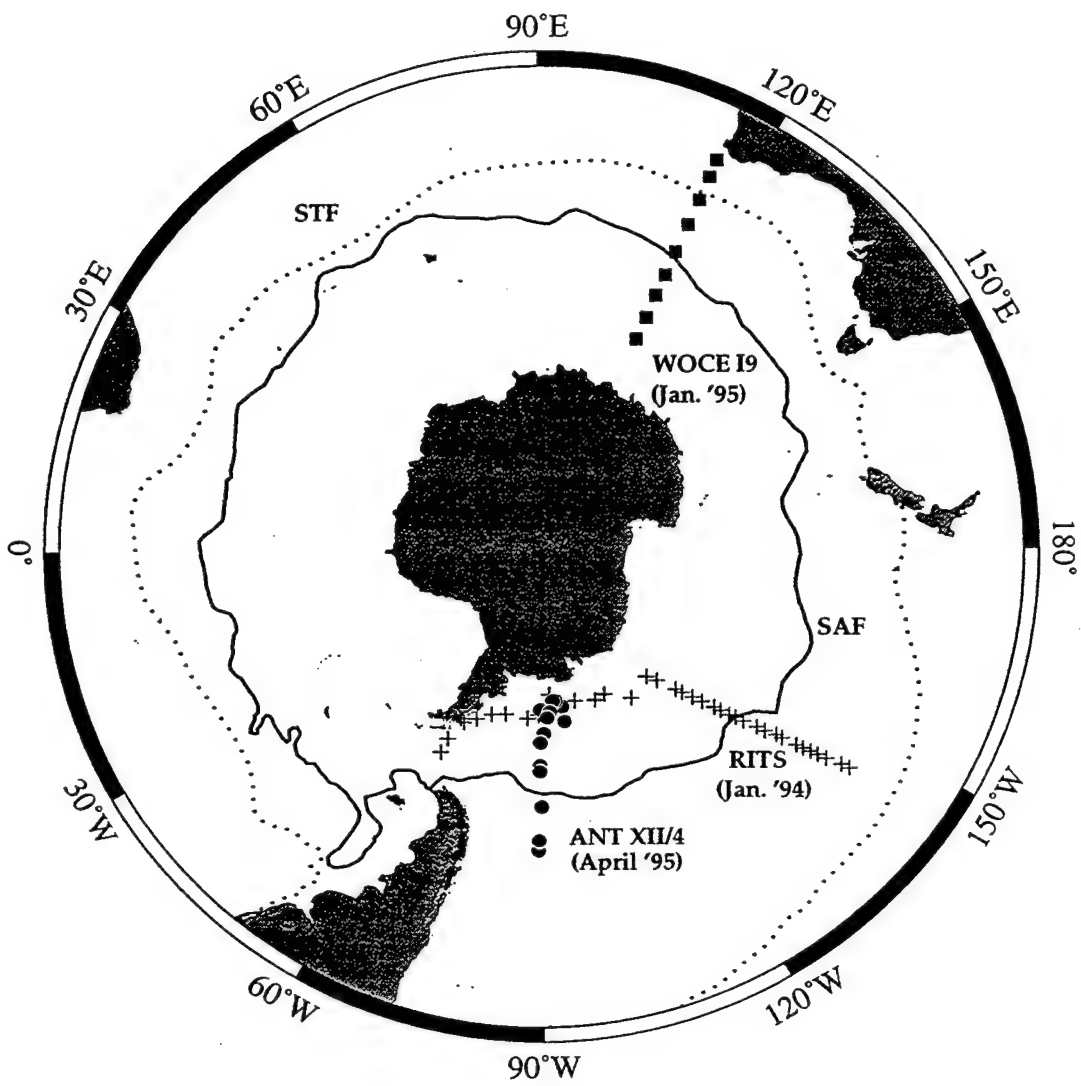


Figure 3

Surface water characteristics as a function of latitude for the three data sets reported, from (a) the east Indian sector (WOCE I9, January, 1995), (b) the central Pacific sector (RITS '94, January, 1994), and (c) the east Pacific sector (ANT XII/4, April, 1995). The eastward transect of RITS '94 through the marginal ice zone is not plotted here. Sea surface temperature is shown in the open squares, $[\text{NO}_3]$ in the filled squares, and silicate in the filled triangles. The depth profile stations for the east Indian and east Pacific cruises are shown along the upper axes of (a) and (c). The positions of the Polar, Subantarctic, and Subtropical Fronts are also indicated along this axis (PF, SAF, STF, respectively). The latitudinal range of the marginal ice zone (MIZ) is indicated if present within the transect.

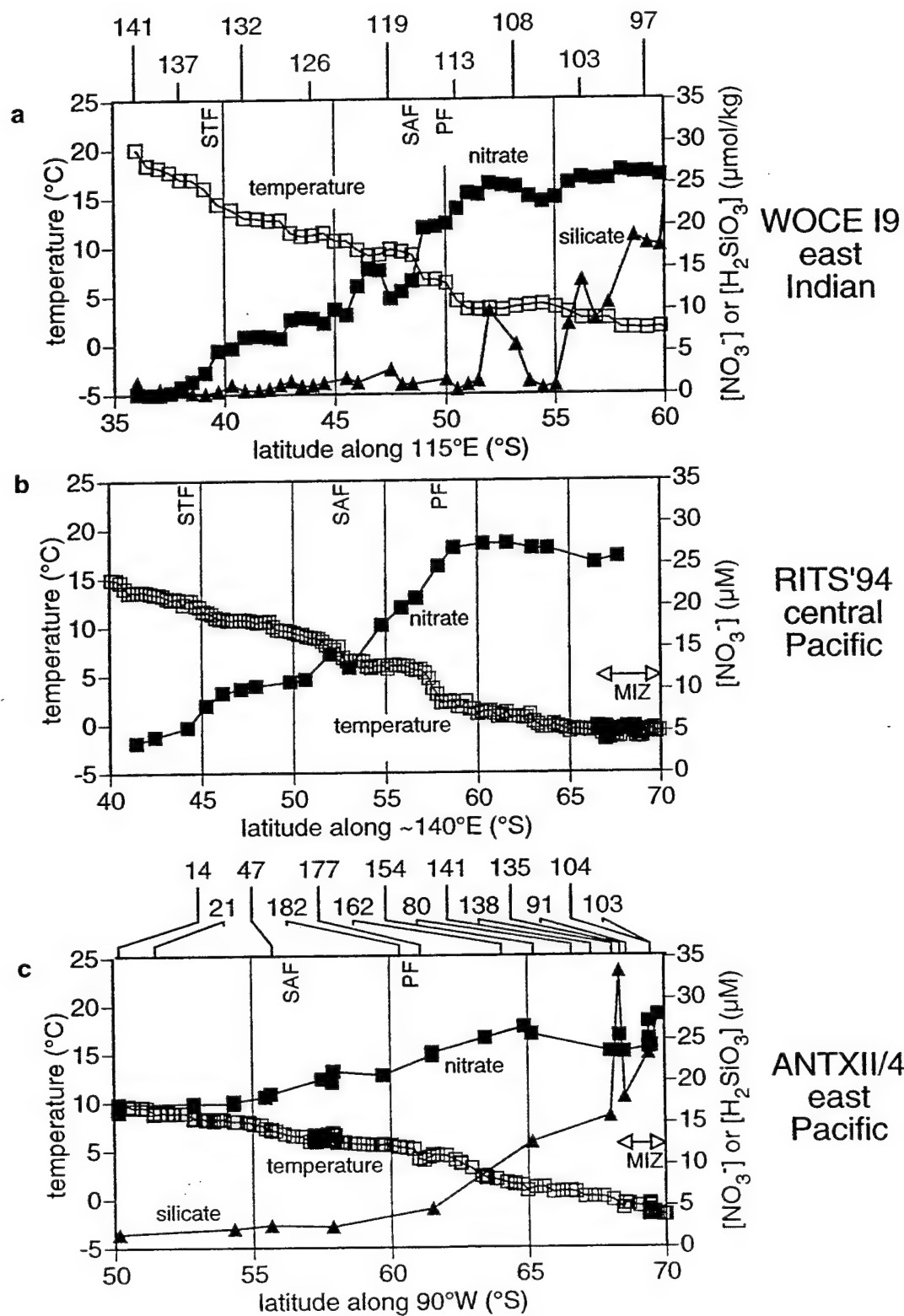


Figure 4a-c

Surface water $\delta^{15}\text{NO}_3$ (filled circles) and $[\text{NO}_3^-]$ (open circles), across the large-scale latitudinal gradient in $[\text{NO}_3^-]$ (a,b,c, this figure) and over smaller scale variations in $[\text{NO}_3^-]$ within the Antarctic (d,e, next page). Data are plotted as a function of latitude for (a) the east Indian sector (WOCE I9), (b) the central Pacific sector (RITS '94, unconnected symbols are from the longitudinal transect), (c) the east Pacific sector (ANT XII/4) southward transect, and (d) the ANT XII/4 northward transect. The longitudinal transect of RITS '94 is plotted in (e). The WOCE I9 data plotted in (a) are the shallowest samples from the depth profiles. In the ANT XII/4 plots, only the underway surface transect samples are plotted in (c) for the east Pacific sector; the shallow samples from the depth profiles are not included. Error bars indicate a typical standard deviation of 0.2‰ for nitrate extracts analyzed on the same day.

Large-scale latitudinal gradients:

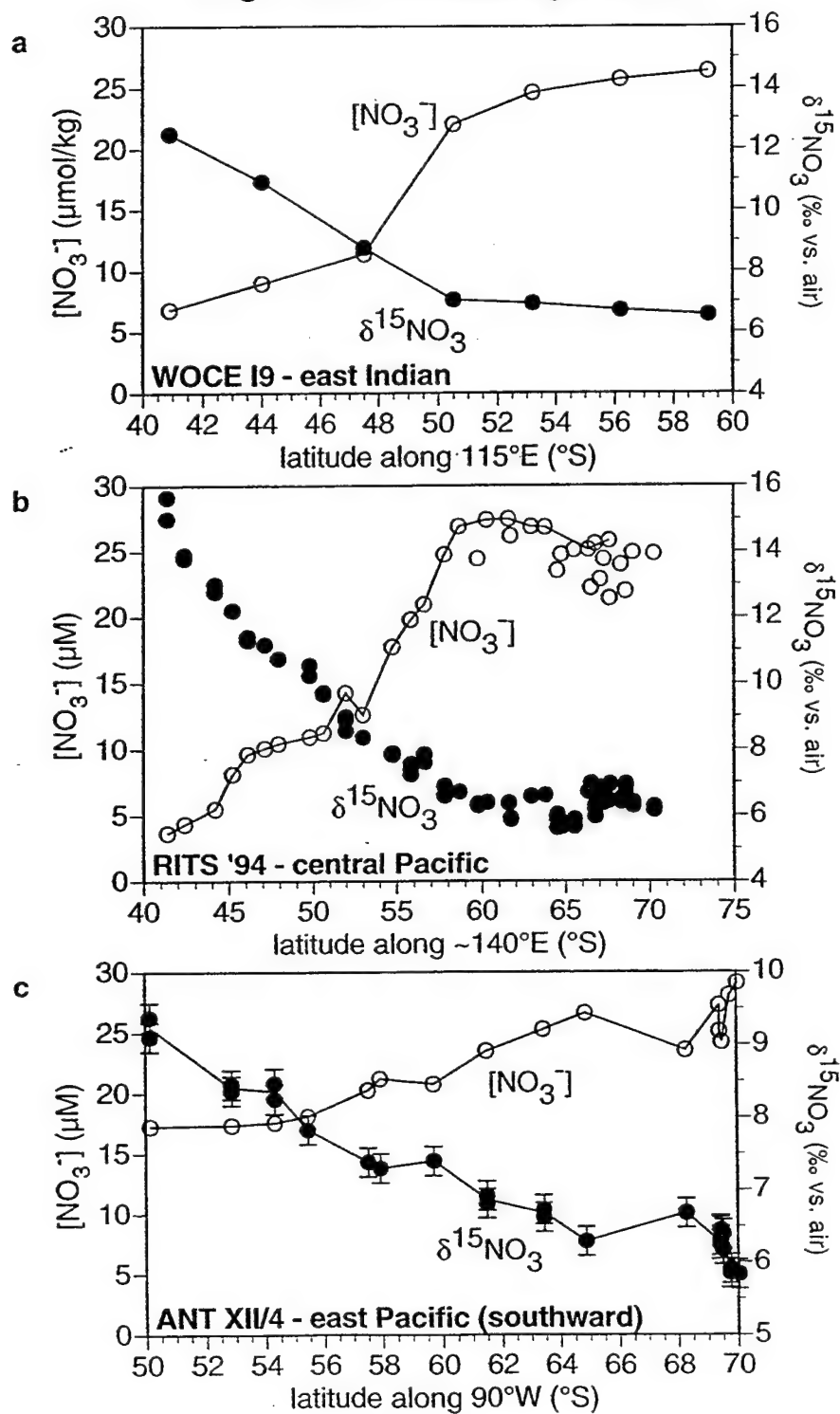


Figure 4d,e

Surface water $\delta^{15}\text{NO}_3$ (filled circles) and $[\text{NO}_3^-]$ (open circles), across the large-scale latitudinal gradient in $[\text{NO}_3^-]$ (a,b,c, previous page) and over smaller scale variations in $[\text{NO}_3^-]$ within the Antarctic (d,e, this figure). Data are plotted as a function of latitude for (a) the east Indian sector (WOCE I9), (b) the central Pacific sector (RITS '94, unconnected symbols are from the longitudinal transect), (c) the east Pacific sector (ANT XII/4) southward transect, and (d) the ANT XII/4 northward transect. The longitudinal transect of RITS '94 is plotted in (e). In the ANT XII/4 plots, only the underway surface transect samples are plotted in (c) for the east Pacific sector; the shallow samples from the depth profiles are not included. Error bars indicate a typical standard deviation of 0.2‰ for nitrate extracts analyzed on the same day.

Smaller-scale Antarctic variations:

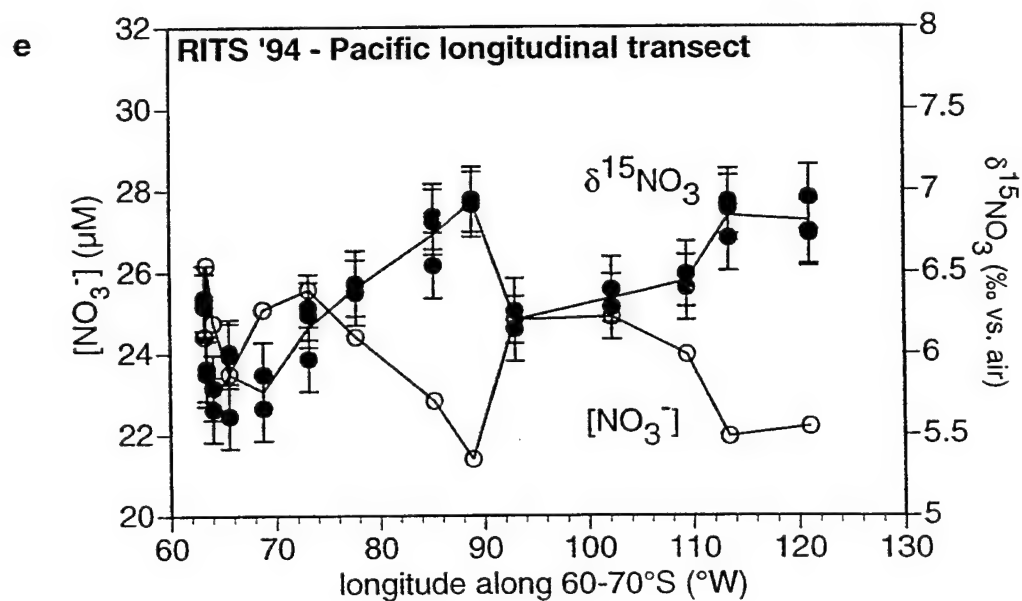
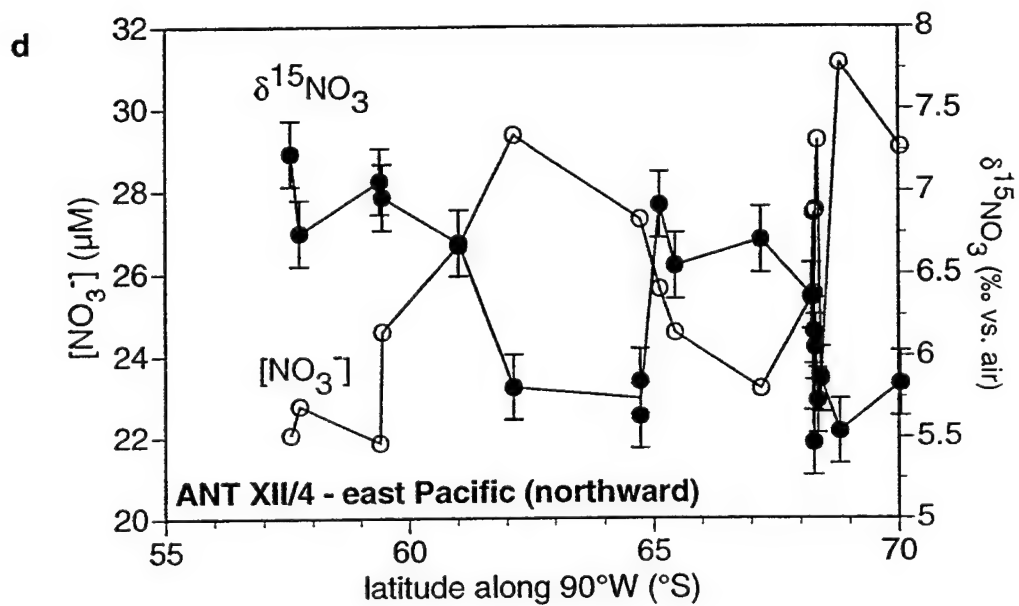


Figure 5

Depth profiles of $\delta^{15}\text{NO}_3$ (filled circles, scale on the upper axis) and $[\text{NO}_3^-]$ (open circles, scale on the lower axis) from the east Indian sector (WOCE I9). In (a), the full profiles are shown; in (b), only data in the upper 600 m are shown, to illustrate the upper water column structure. The profiles from the Antarctic Zone are in the top row, and the profiles from the Subantarctic Zone are in the bottom row, with higher latitude stations plotted toward the left in each zone. There are no $\delta^{15}\text{NO}_3$ data for the surface layer samples at stations 137 and 141, which have $<1\ \mu\text{M}$ nitrate.

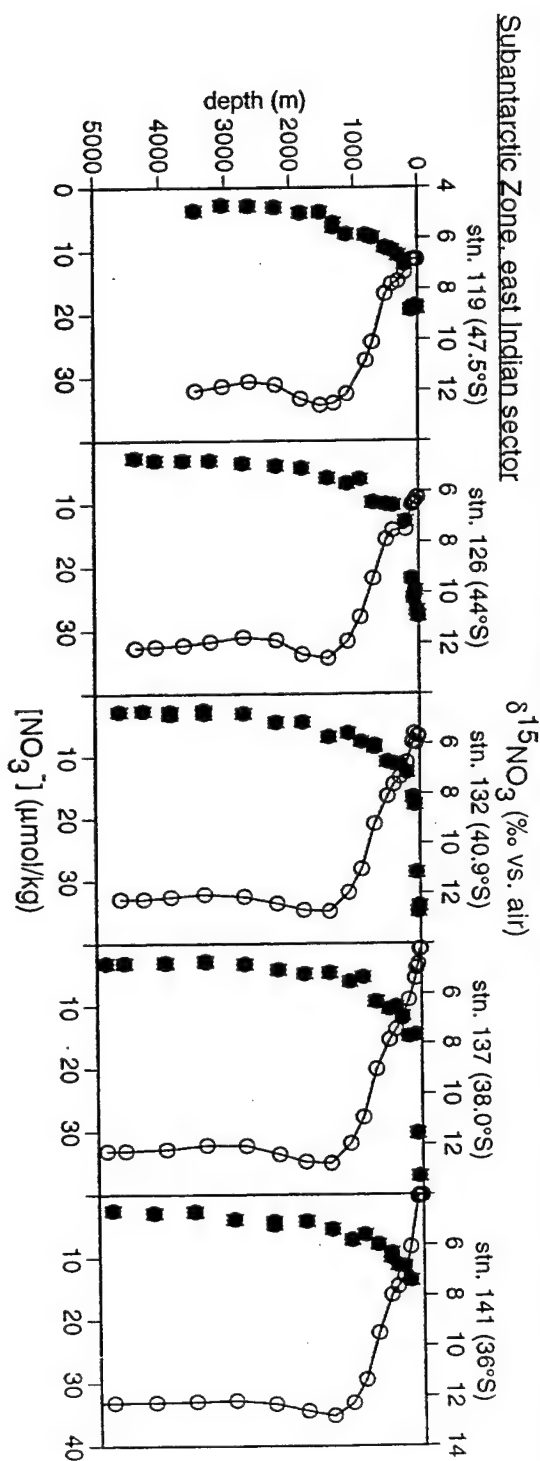
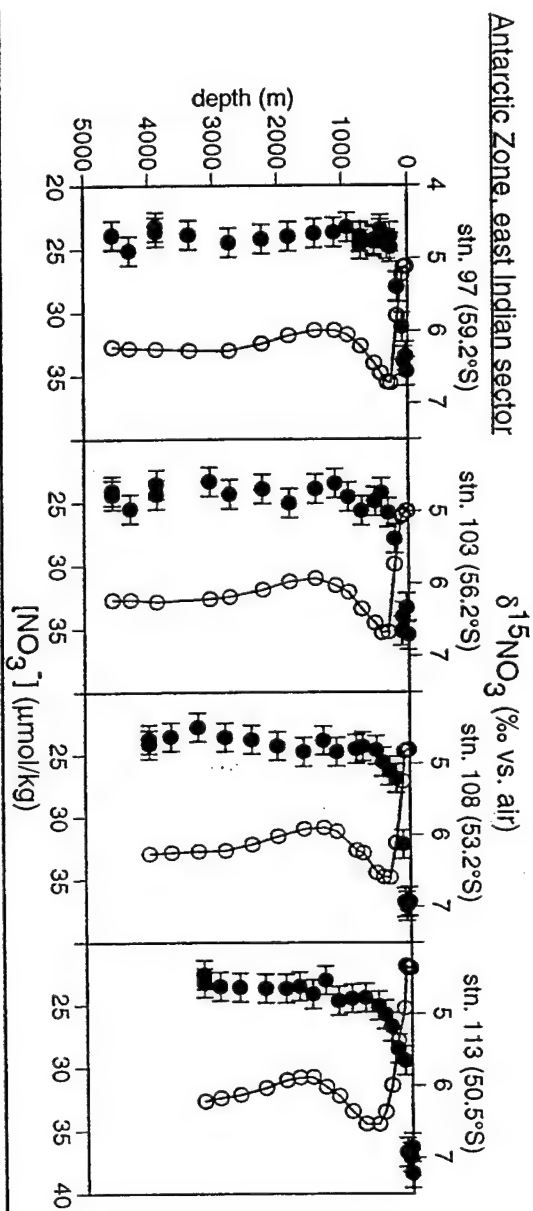


Figure 6

Compilation of the WOCE I9 profiles, for $[\text{NO}_3^-]$ and $\delta^{15}\text{NO}_3$. The values shown are analysis averages. The open and filled symbols represent profiles from the Subantarctic and Antarctic Zones, respectively.

East Indian (WOCE 19) depth profiles

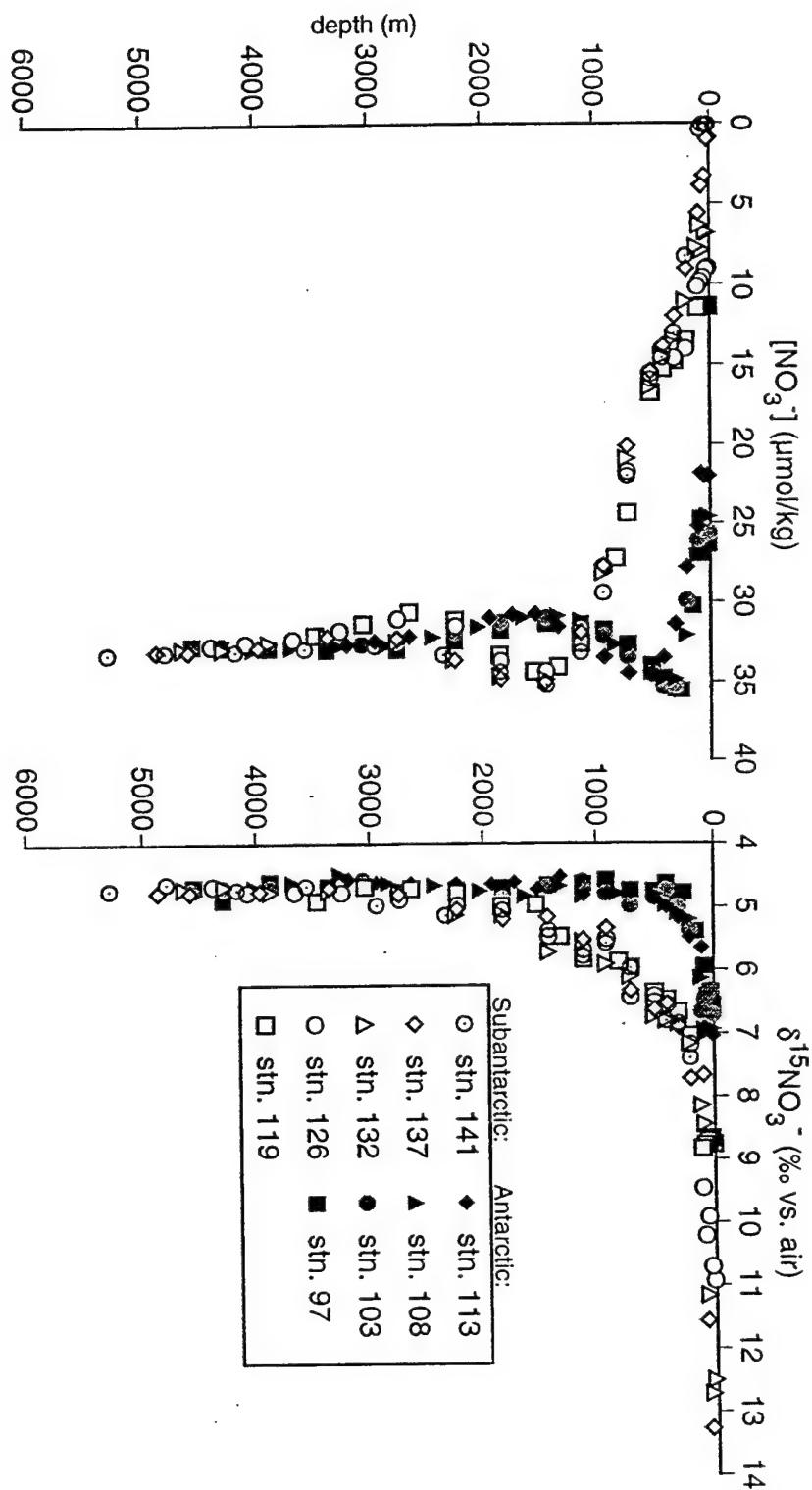


Figure 7a

Depth profiles of $\delta^{15}\text{NO}_3$ (filled circles, scale on the upper axis) and $[\text{NO}_3^-]$ (open circles, scale on the lower axis) from the east Pacific sector (ANT XII/4): (a) profiles from the Antarctic Zone, (b) profiles from the Subantarctic Zone (next page), (c) and deep profiles (next page, upper 600 m also plotted in (a) and (b)). Higher latitude stations are plotted toward the left. Symbols and axes are as described for Figure 5.

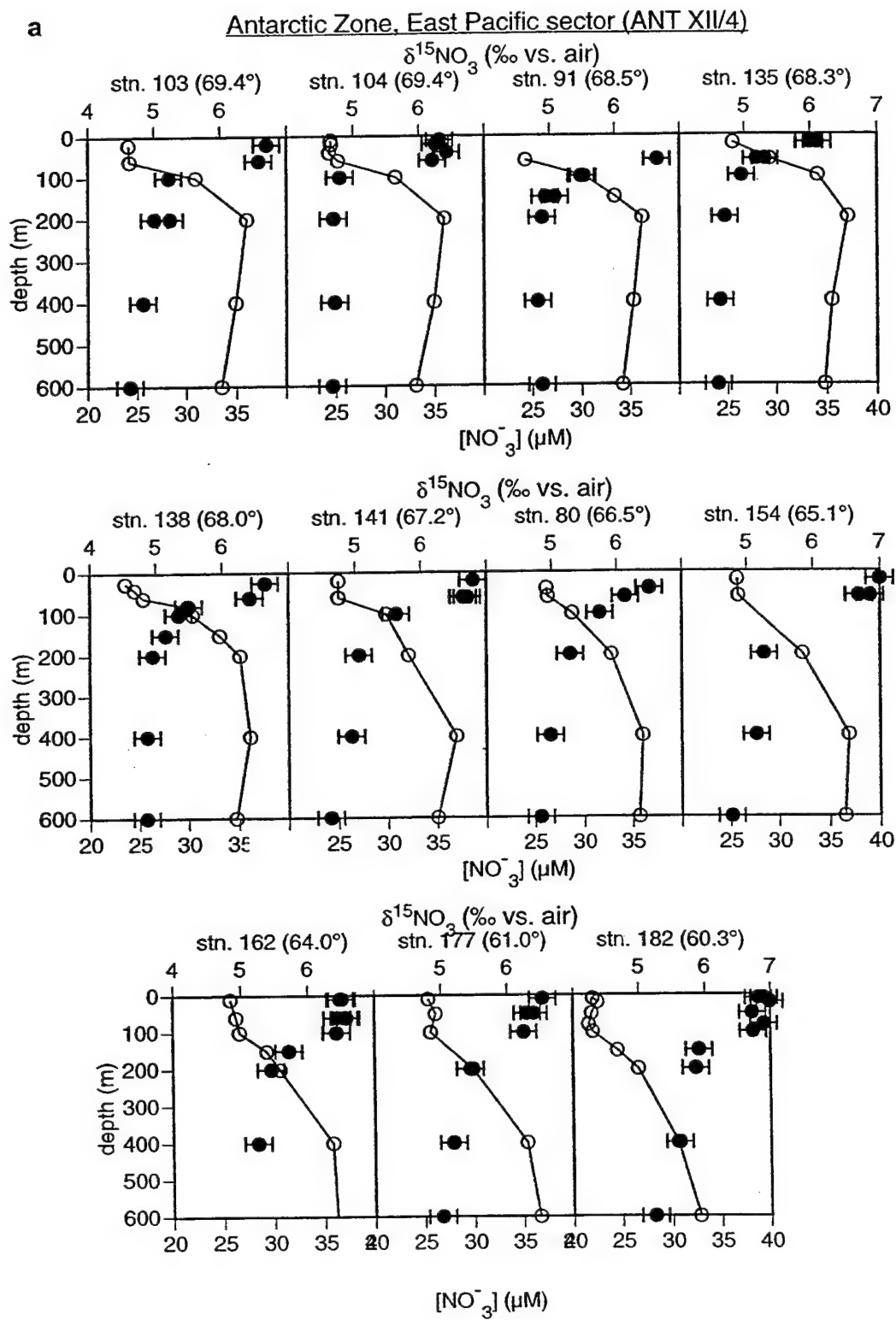
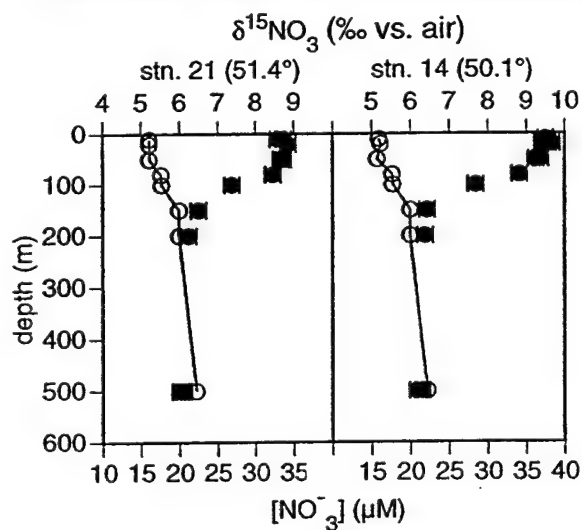


Figure 7b,c

Depth profiles of $\delta^{15}\text{NO}_3$ (filled circles, scale on the upper axis) and $[\text{NO}_3^-]$ (open circles, scale on the lower axis) from the east Pacific sector (ANT XII/4): (a) profiles from the Antarctic Zone (previous page), (b) profiles from the Subantarctic Zone, (c) and deep profiles (upper 600 m also plotted in (a) and (b)). Higher latitude stations are plotted toward the left. Symbols and axes are as described for Figure 5.

b Subantarctic Zone, east Pacific sector (ANT XII/4)



c deep profiles, east Pacific sector (ANT XII/4)

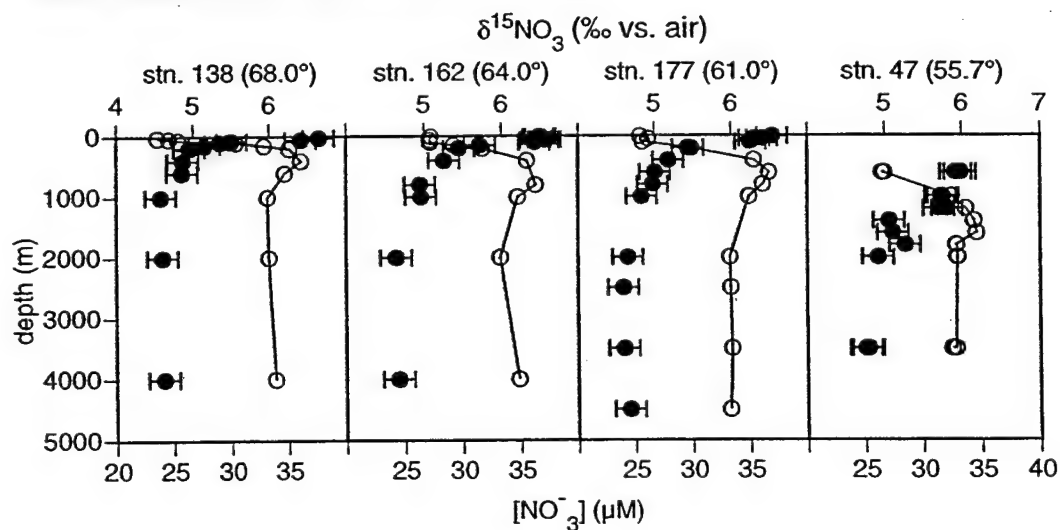


Figure 8

Depth profiles in the Antarctic (east Indian, WOCE I9 station 108, a), and the Subantarctic (station 132, b), showing the distinguishing characteristics of the water masses in these two zones. Density is shown in the thin solid line, $[\text{NO}_3^-]$ in the thick solid line, temperature in the dashed line, and salinity in the dotted line. The depths of the different water masses are indicated. Lower and Upper Circumpolar Deep Water (LCDW and UCDW) are most easily distinguished on the basis of $[\text{NO}_3^-]$. Antarctic Intermediate Water (AAIW) is evident as the salinity minimum in the Subantarctic profile. Subantarctic Mode Water (SAMW) is evident as the pycnostad within the Subantarctic thermocline. The subsurface temperature minimum (T_{min}) is evident above UCDW in the Antarctic profile.

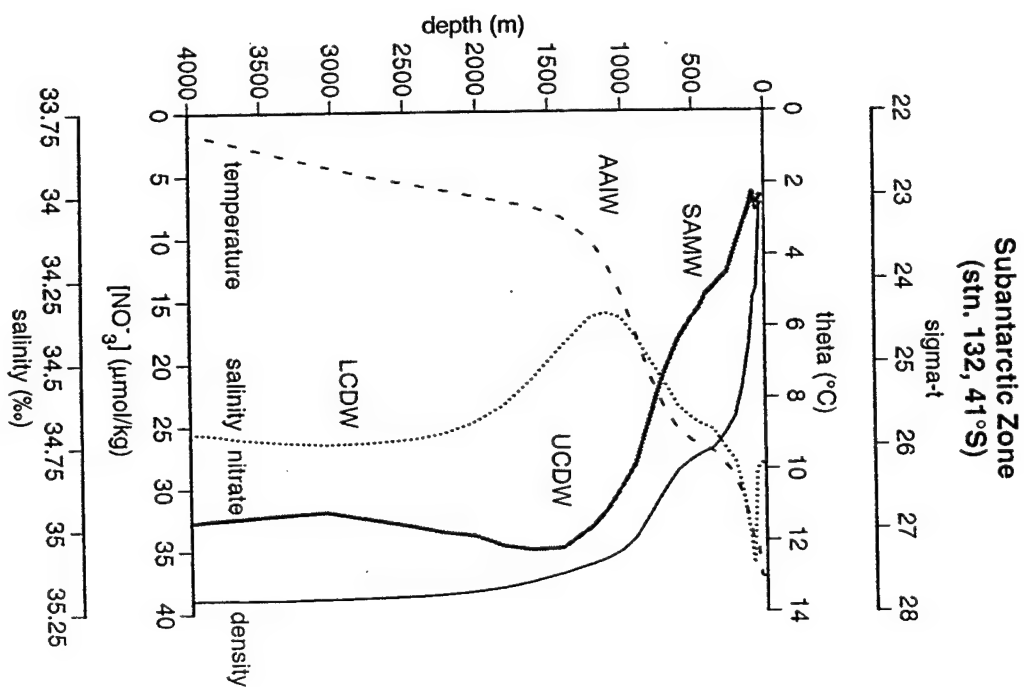
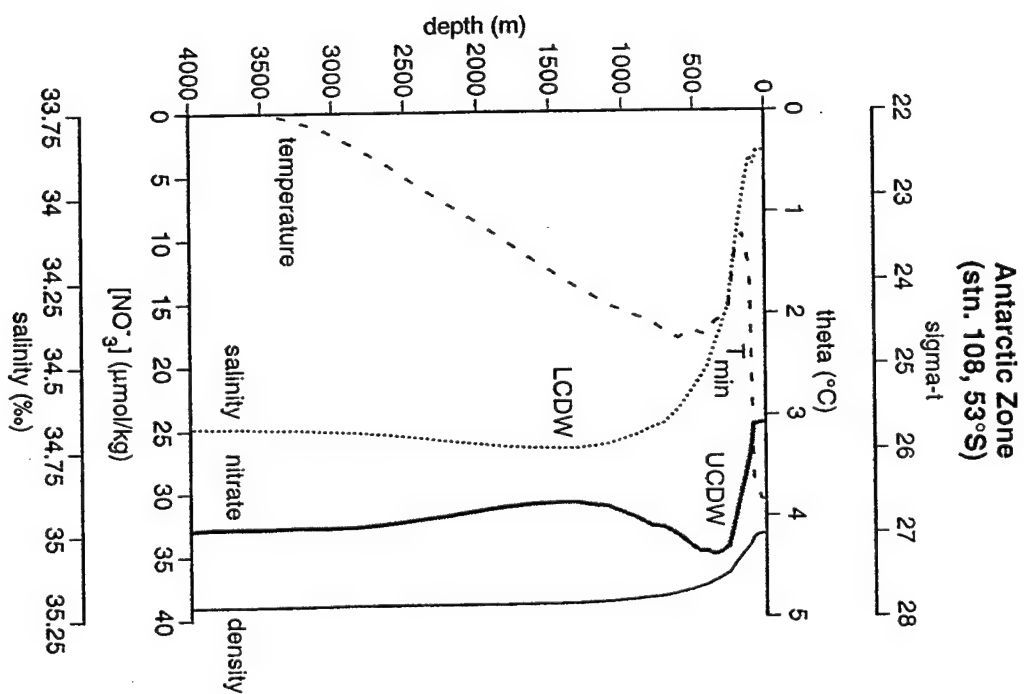


Figure 9

Latitudinal transects of water mass properties for the east Indian (WOCE I9) depth profiles. $[\text{NO}_3^-]$ is shown in (a), $\delta^{15}\text{NO}_3$ in (b), and $\delta^{15}\text{N}_{\text{nr}}$ in (c). LCDW and UCDW were picked on the basis of deep $[\text{NO}_3^-]$ minimum and maximum, respectively. The salinity minimum represents the surface layer in the Antarctic Zone and the core of AAIW in the Subantarctic Zone. Values shown are sample averages.

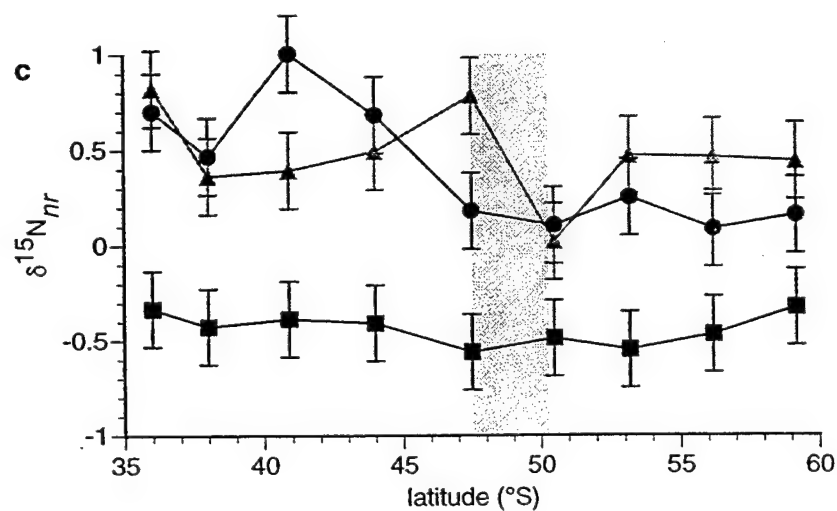
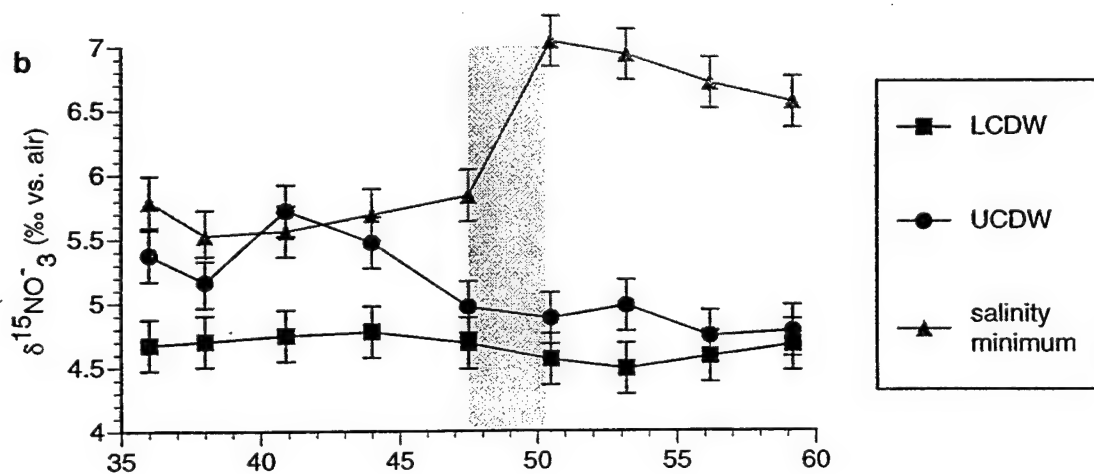
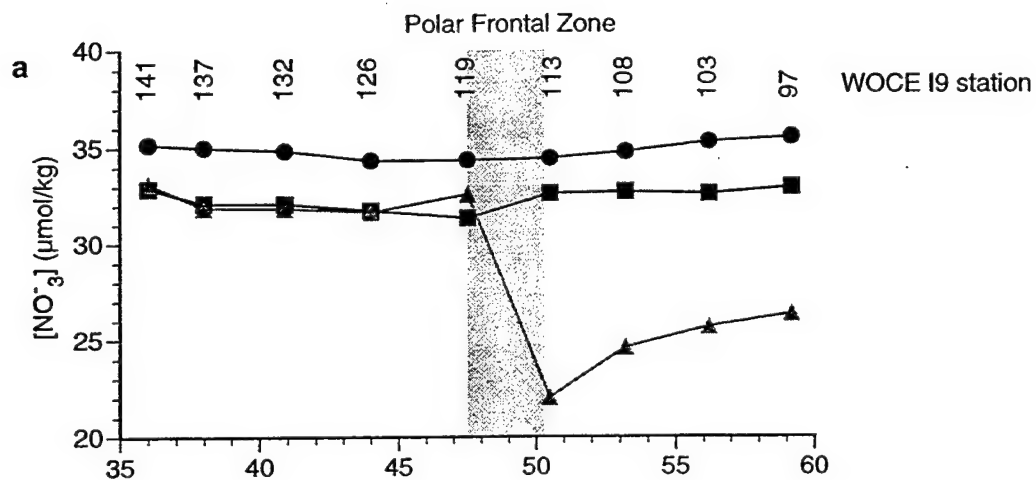
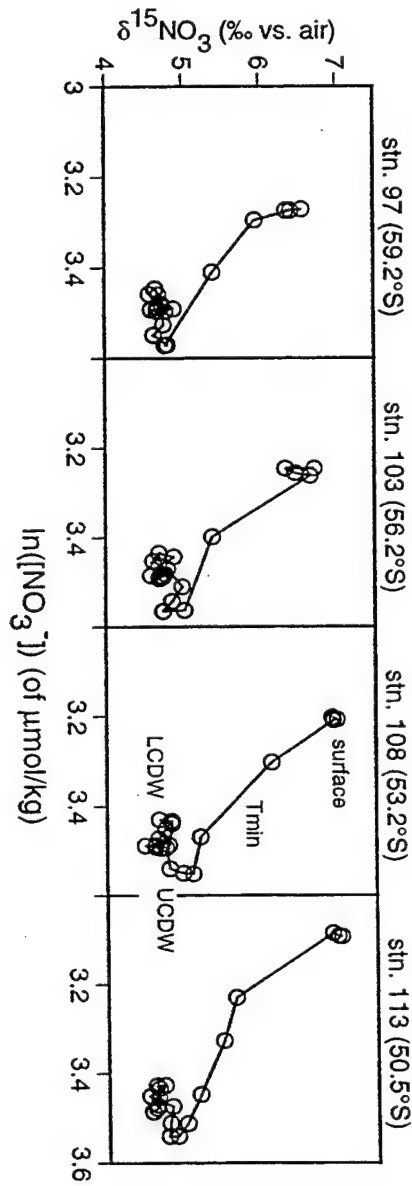


Figure 10

Plots of the east Indian (WOCE I9) profiles in $\delta^{15}\text{NO}_3/\ln([\text{NO}_3^-])$ space. Analysis averages are used, and the samples are connected according to water column depth. Water masses are labeled for stations 108 (Antarctic) and 132 (Subantarctic).

WOCE 19, east Indian sector

Antarctic Zone



Subantarctic Zone

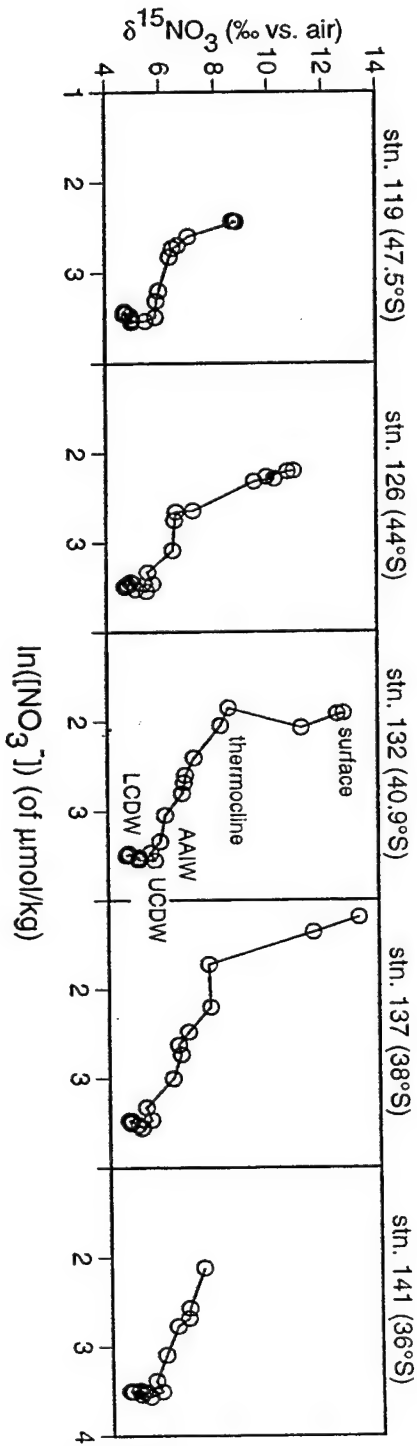
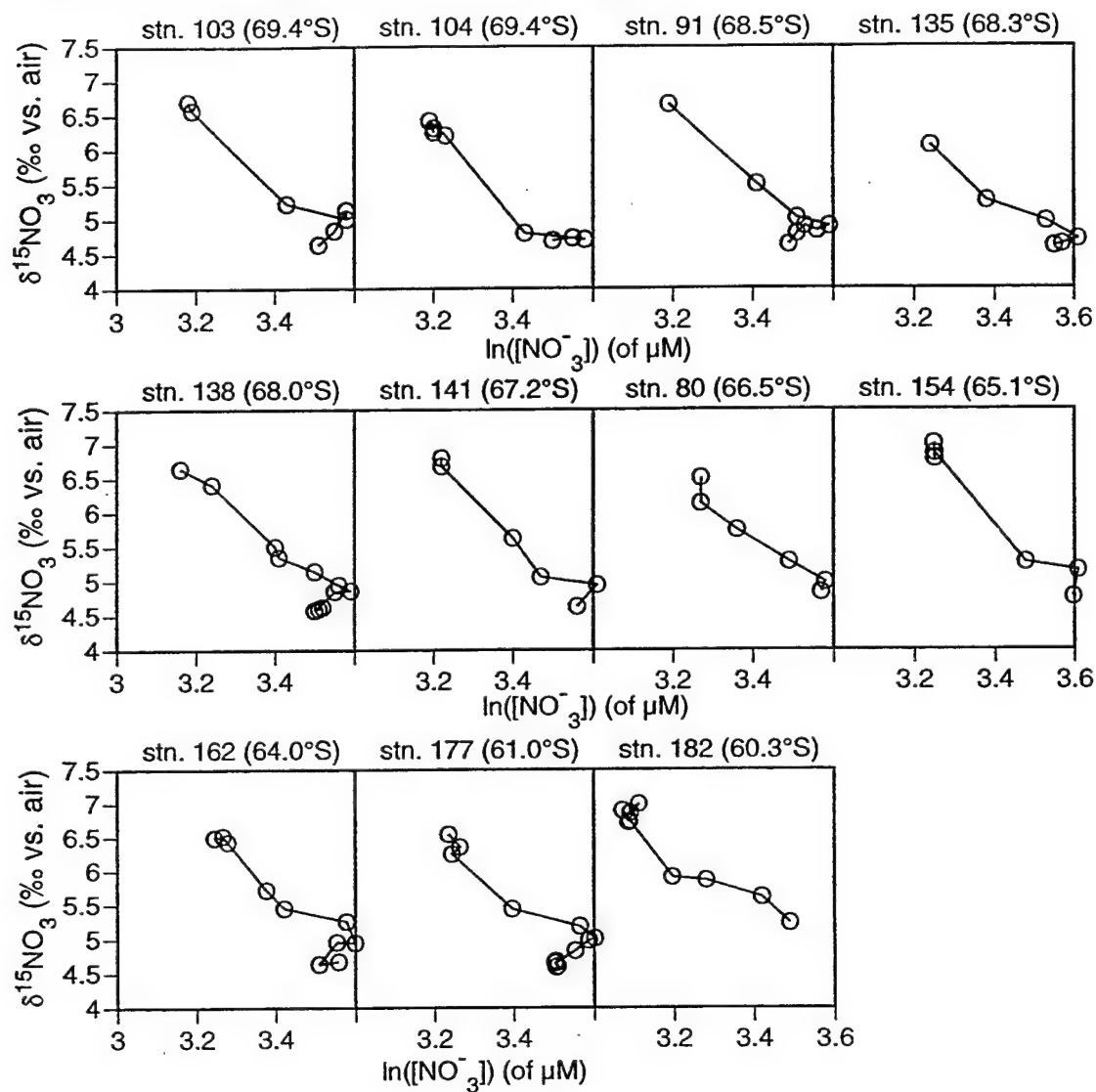


Figure 11

Plots of the east Pacific (ANT XII/4) profiles in $\delta^{15}\text{NO}_3/\ln([\text{NO}_3^-])$ space. Analysis averages are used, and the samples are connected according to water column depth. The shallow Subantarctic profiles of stations 14 (50.1°S) and 21 (51.4°S) are linked to the deep profile of station 47 (55.7°S).

Antarctic Zone, east Pacific sector (ANT XII/4)



Subantarctic Zone, east Pacific sector (ANT XII/4)

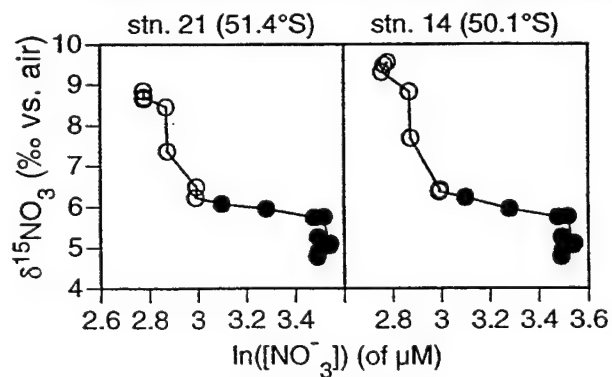


Figure 12

A graphical explanation of $\delta^{15}\text{N}_{\text{nr}}$, as defined in the text. $\delta^{15}\text{N}_{\text{nr}}$ is the difference between the actual $\delta^{15}\text{NO}_3$ of a sample and the $\delta^{15}\text{NO}_3$ it would have, based on its $[\text{NO}_3^-]$, if it followed the nitrate utilization trend which applies generally in the Antarctic Zone. If a sample falls below the utilization trend in $\delta^{15}\text{NO}_3/\ln([\text{NO}_3^-])$ space, it has a negative $\delta^{15}\text{N}_{\text{nr}}$.

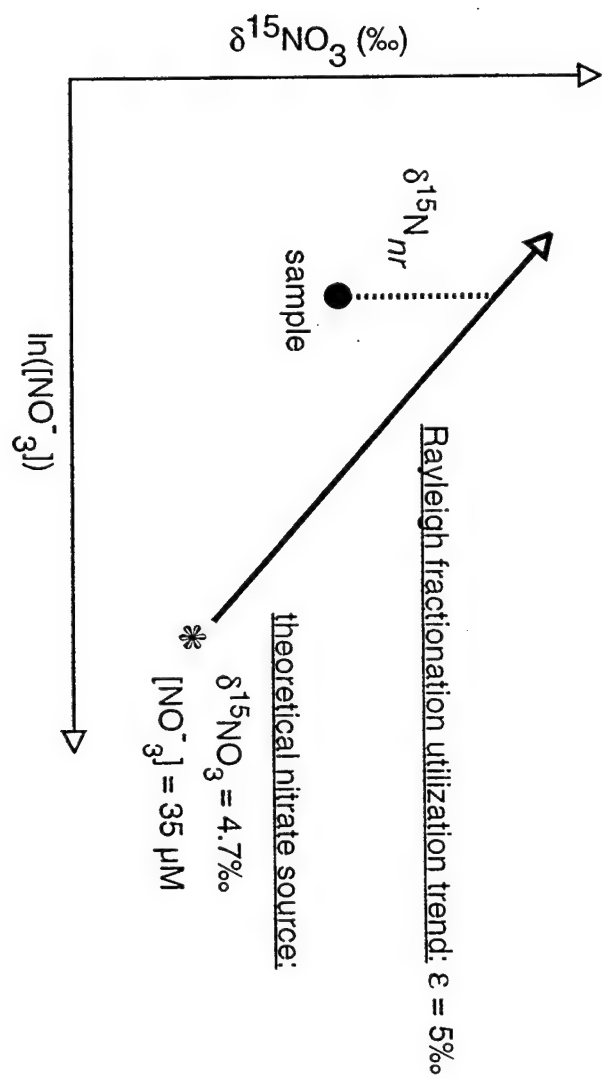


Figure 13

Depth profiles of $\delta^{15}\text{N}_{\text{nr}}$ and $[\text{NO}_3^-]$ from the Antarctic (east Indian WOCE I9 station 108, a) and the Subantarctic (station 132, b). Salinity is also plotted, showing the low salinity of the Antarctic surface and the salinity minimum of AAIW. The $\delta^{15}\text{N}_{\text{nr}}$ scale is much greater for the Subantarctic profile, to accommodate the strongly negative $\delta^{15}\text{N}_{\text{nr}}$ of the Subantarctic thermocline.

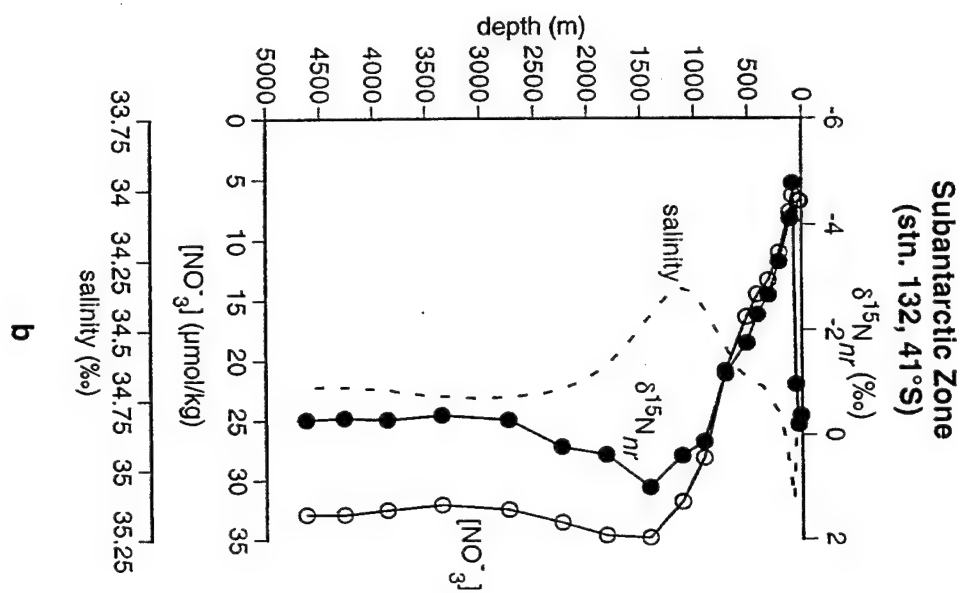
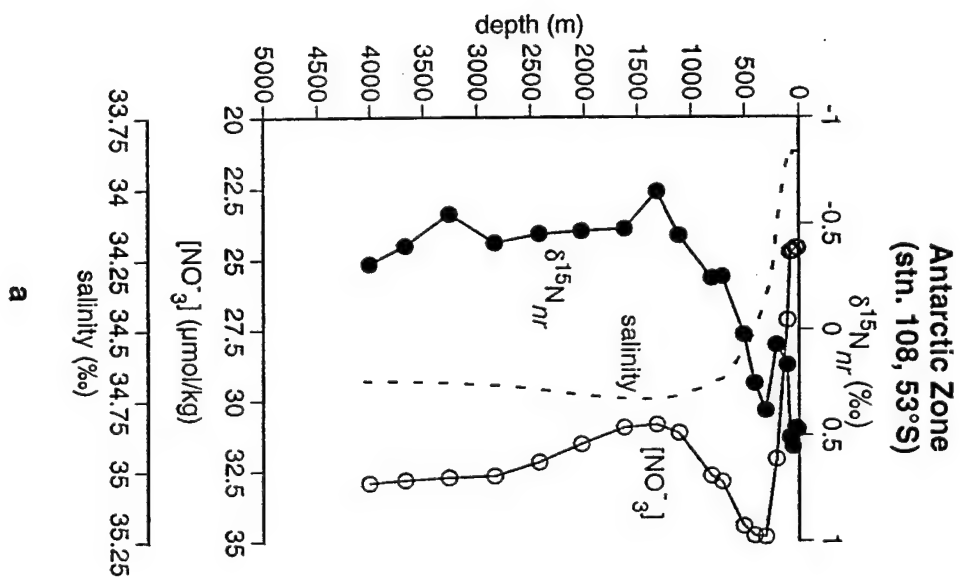
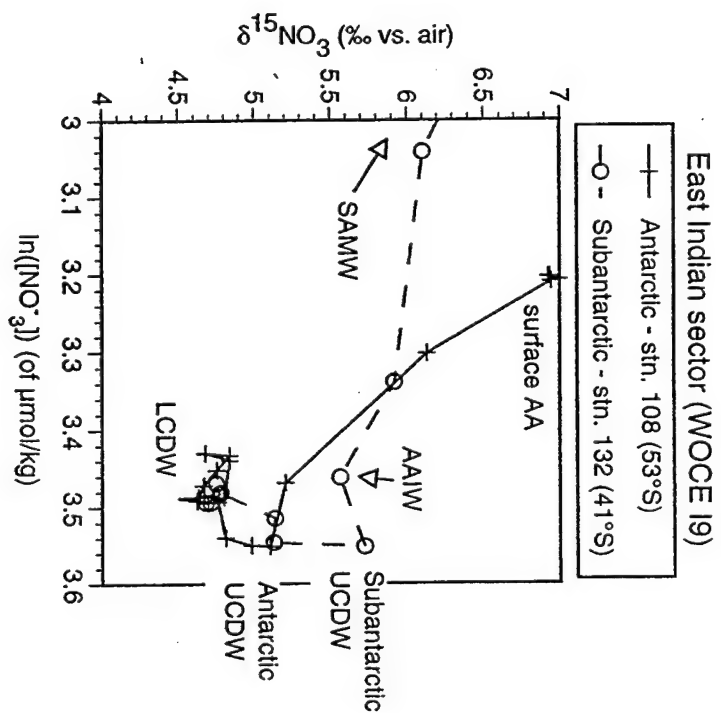
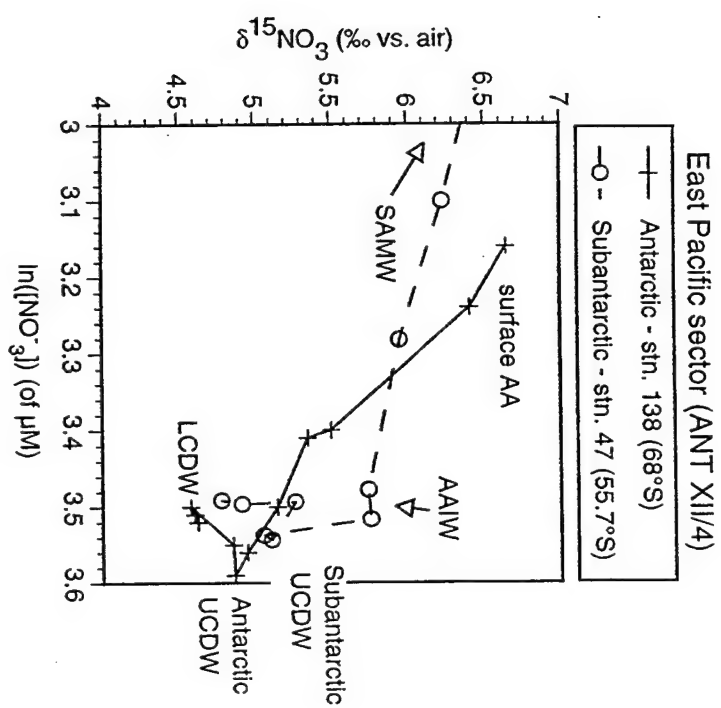


Figure 14

Comparison in $\delta^{15}\text{NO}_3/\ln([\text{NO}_3^-])$ space of Antarctic and Subantarctic profiles, in the east Indian (a) and the east Pacific (b). Subantarctic UCDW is higher in $\delta^{15}\text{NO}_3$ than Antarctic UCDW, although they have a similar $[\text{NO}_3^-]$. The $\delta^{15}\text{NO}_3/[\text{NO}_3^-]$ composition of AAIW falls roughly on mixing lines between either (1) Antarctic UCDW and Antarctic Surface Water, or (2) Subantarctic UCDW and Subantarctic Mode Water. Thus, AAIW could be formed by either of these mixing combinations. At east Pacific station 47 (b), which is located at the Subantarctic Front, AAIW is strongly enriched compared to the nitrate maximum of UCDW. This same pattern occurs at east Indian WOCE I9 station 119, which is also at the Subantarctic Front (Figure 21). This observation has not yet been explained.



a



b

Figure 15

Plots of the east Indian (WOCE I9) Antarctic Zone profiles down to 500 m in $\delta^{15}\text{NO}_3/\ln([\text{NO}_3^-])$ space. Analysis averages are used. Also shown are the regression lines which yield estimates of the fractionation factor, plotted in Figure 16. Station 113 is at the same latitude as the Polar Front (Figure 3a) and shows characteristics intermediate between those typical of the Antarctic and Subantarctic. Given that the Subantarctic profiles cannot be used to estimate the fractionation factor, the estimate at station 113 may be biased.

fractionation factor regressions for Antarctic profiles
 WOCE 19, east Indian sector

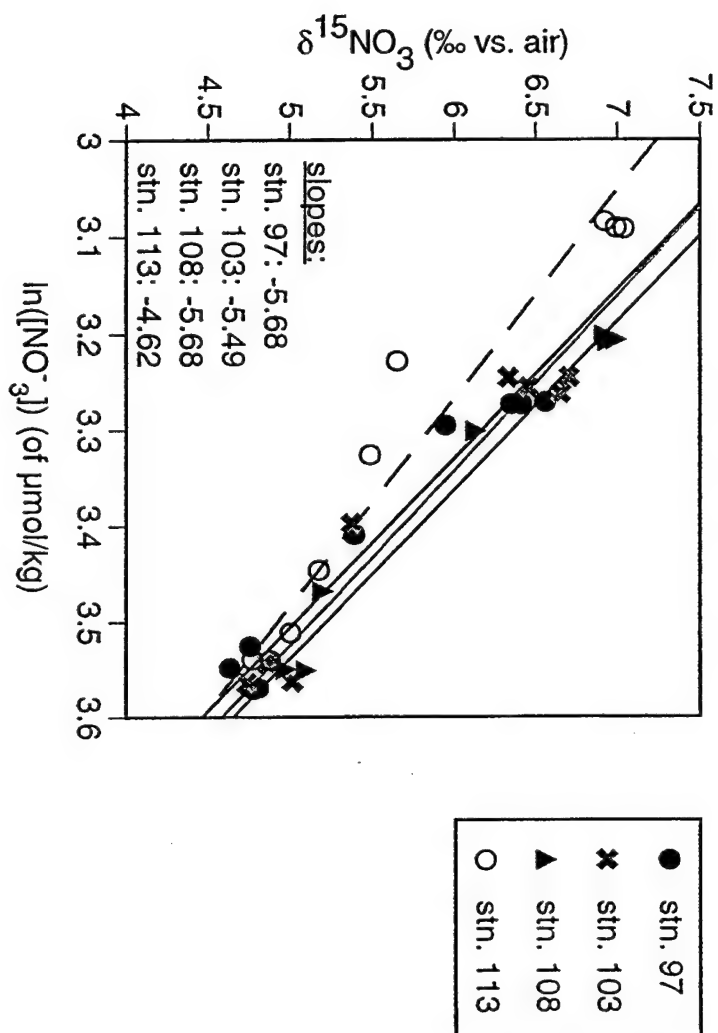


Figure 16

Estimates of the fractionation factor in the Antarctic Zone, based on depth profiles from (1) the east Indian sector (WOCE I9, filled symbols), and (2) the east Pacific sector (ANT XII/4, open symbols). Estimates from the East Indian are 4.6- 5.7‰. If station 113 is excluded (see Figure 15), the estimates are 5.5-5.7‰. Estimates from the east Pacific are 4.0-5.0‰, excepting station 135, which gives an estimate of 3.6‰. At this station, there is an isolated maximum in surface nutrients, especially silicate (Figure 3c).

profile-based estimates
of the nitrate uptake fractionation factor

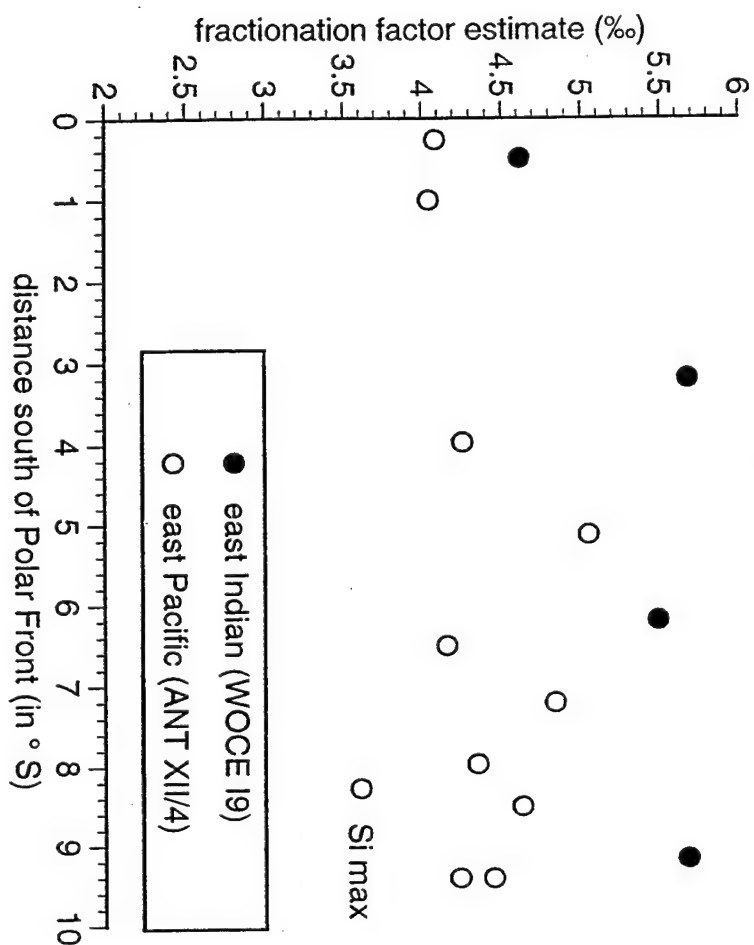


Figure 17

Estimates of the fractionation factor in the Antarctic Zone, based on underway surface samples from (a) the east Pacific sector (ANT XII/4) southward transect (open symbols are from north of the Polar Front), (b) the ANT XII/4 northward transect (only in Antarctic waters), and (c) the longitudinal transect of RITS '94. Analysis averages are used. The greater amount of scatter in (b) is not understood, but $[\text{NO}_3^-]$ varied a great deal across this transect, and there were multiple marginal ice zone front crossings (Figure 4d). Three samples fell off the trend in the RITS '94 data; these three samples are distinguished by being the shelf water of the Antarctic Peninsula (Figure 2) and have been excluded from the regression.

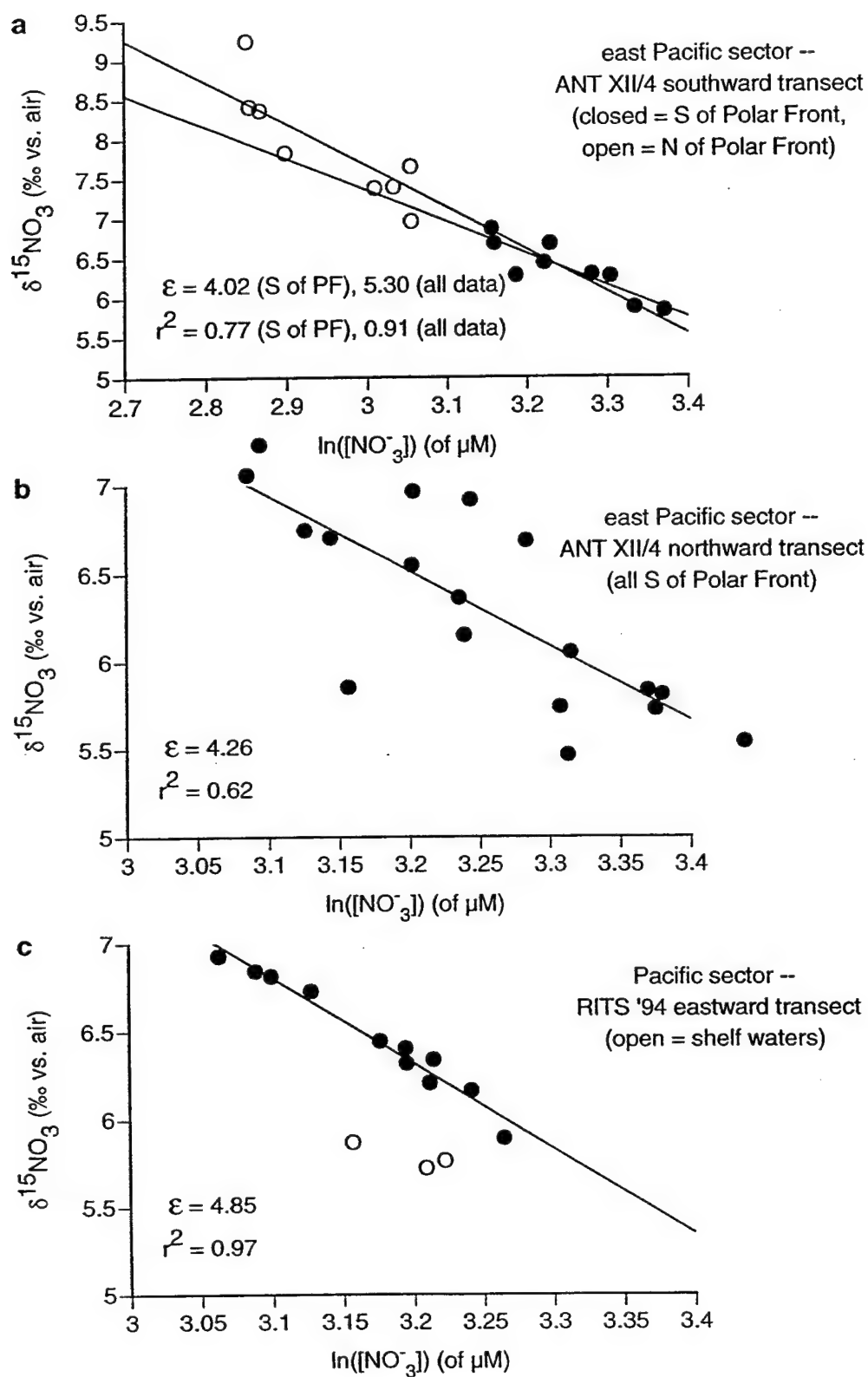


Figure 18

Comparison of east Indian and east Pacific data from the upper 500 m of the Antarctic Zone profiles, in $\delta^{15}\text{NO}_3/\ln([\text{NO}_3])$ space. Central Pacific (RITS '94) and east Pacific (ANT XII/4) surface transect data from the Antarctic Zone are also plotted for comparison, including a few values north of the Polar Front, to show the continuation of the Pacific sector trend. This comparison reveals that the difference in fractionation factors from the Indian and Pacific sectors is due largely to the surface sample composition, and that the composition of the east Pacific surface samples is consistent between two different cruises: RITS '94 (January, 1994) and ANT XII/4 (April, 1995). This is suggestive of a real, albeit small, difference in fractionation factors between the Indian and Pacific sectors.

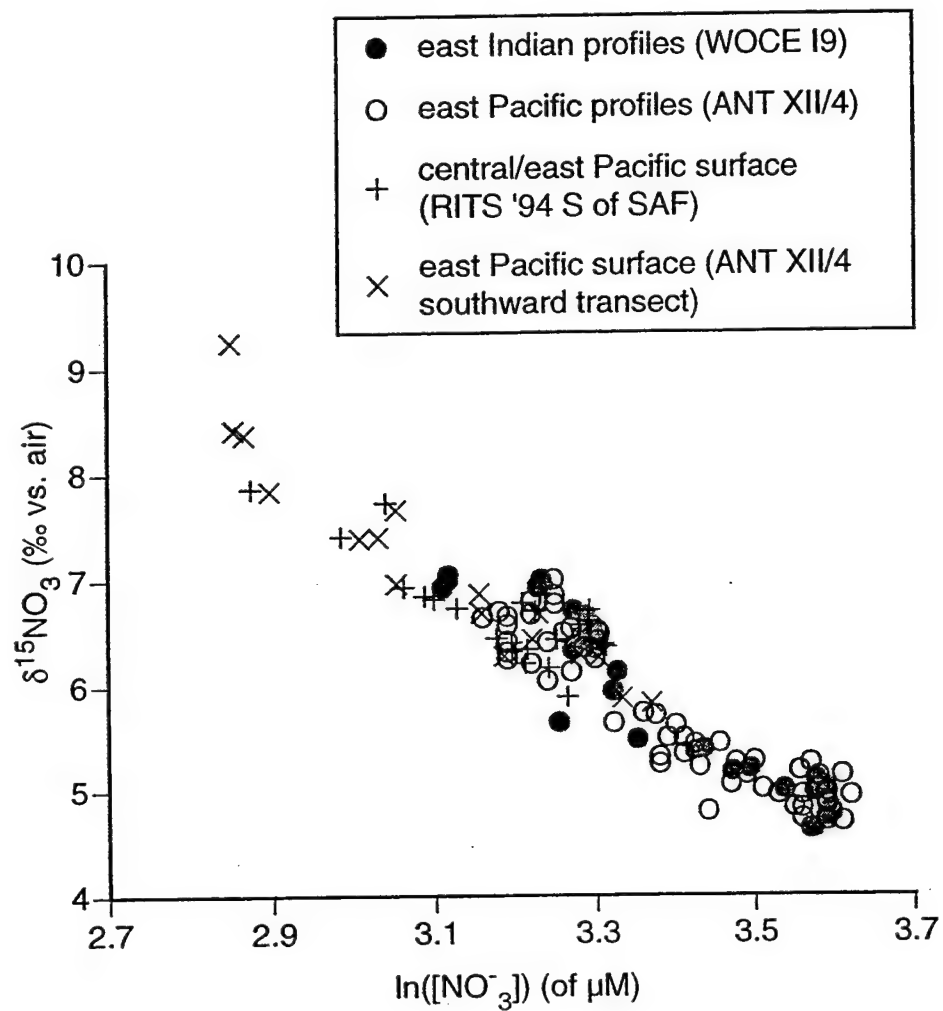


Figure 19

Calculations showing the expected effect of water mass mixing on the $\delta^{15}\text{NO}_3/\ln([\text{NO}_3^-])$ trend of water that has undergone (a) 35% nitrate extraction and (b) 70% nitrate extraction. The nitrate utilization trends (dashed lines) show the trend of a water parcel as nitrate is consumed, assuming an initial water parcel with a $[\text{NO}_3^-]$ of 35 μM , a $\delta^{15}\text{NO}_3$ of 4.7‰, and an ϵ of 5‰. The solid line then expresses the continuum of water masses that would be generated by various proportions of mixing between the new (“surface layer”) and initial (“subsurface”) water masses. The deviation of the mixing line from the Rayleigh fractionation trend increases with increasing $[\text{NO}_3^-]$ difference between the mixing end-members. The same “mixing” trends result from gradual *in situ* remineralization of the “accumulated product” N in a water parcel which has undergone nitrate utilization.

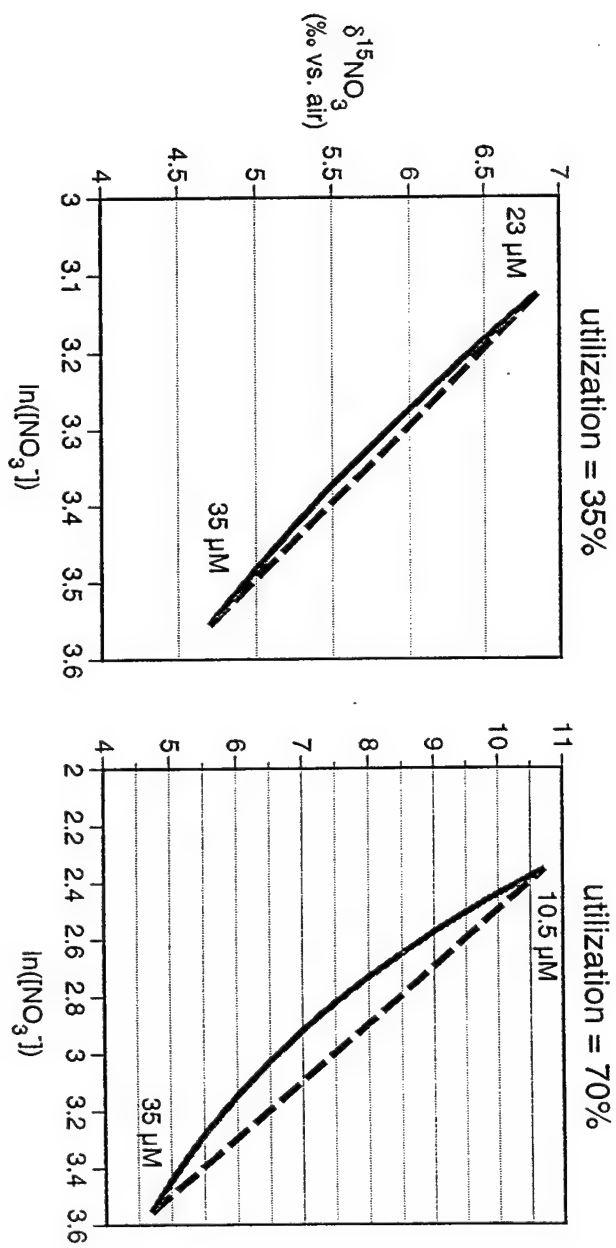
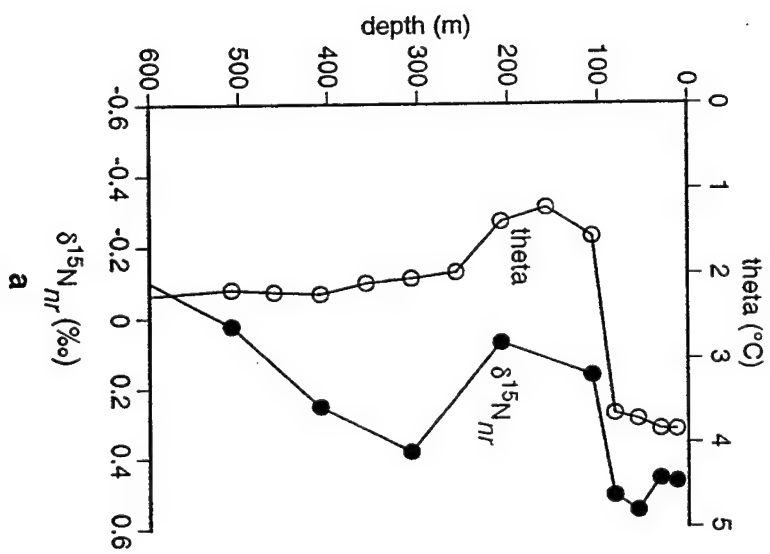


Figure 20

A comparison of the shallow depth profiles of $\delta^{15}\text{N}_{\text{nr}}$ and potential temperature in WOCE I9 station 108 from the east Indian sector (a) and ANT XII/4 station 154 from the east Pacific sector. The $\delta^{15}\text{N}_{\text{nr}}$ minimum is within the T_{min} layer, as is observed for all Antarctic stations with clear subsurface $\delta^{15}\text{N}_{\text{nr}}$ minima. The $\delta^{15}\text{N}_{\text{nr}}$ minimum is greater in (b), associated with a colder T_{min} layer. The decrease in $\delta^{15}\text{N}_{\text{nr}}$ below ~400 m is due to the lower $[\text{NO}_3^-]$ of LCDW, compared to UCDW.

east Indian sector
WOCE 19 stn. 108 (53°S, 115°E)



east Pacific sector
ANT XII/4 stn. 154 (65°S, 269°E)

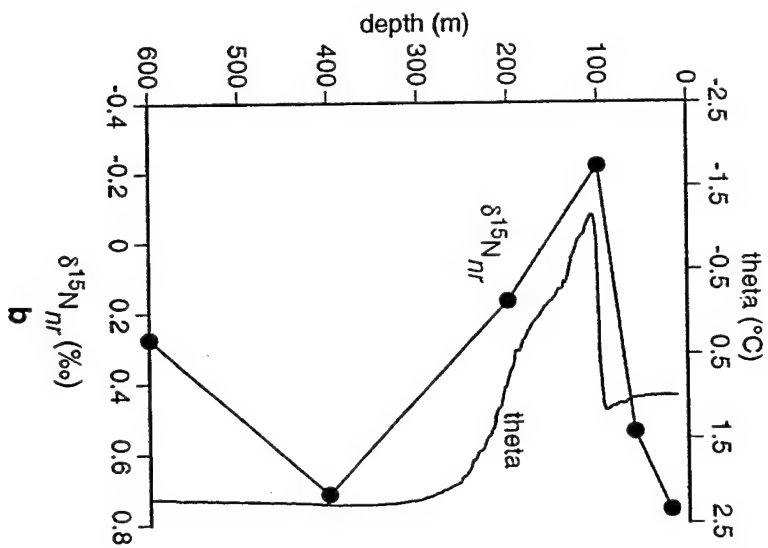


Figure 21

A plot of east Indian (WOCE I9) station 119, from just south of the Polar Front, in $\delta^{15}\text{NO}_3/\ln([\text{NO}_3^-])$ space. The gray lines show the expected values of the thermocline (Subantarctic Mode Water) samples if they were part of (a) a Rayleigh fractionation trend between Antarctic Intermediate Water and the Subantarctic surface (solid gray line), (b) a mixing trend between AAIW and the surface (dashed line), or (c) a mixing trend between the nitrate maximum (UCDW) and the surface layer. In all cases, the thermocline values are too low in $\delta^{15}\text{NO}_3$, or too low in $[\text{NO}_3^-]$ (i.e., their $\delta^{15}\text{N}_{\text{nr}}$ is too low). Thus, we infer an additional mixing component from the lower latitude thermocline.

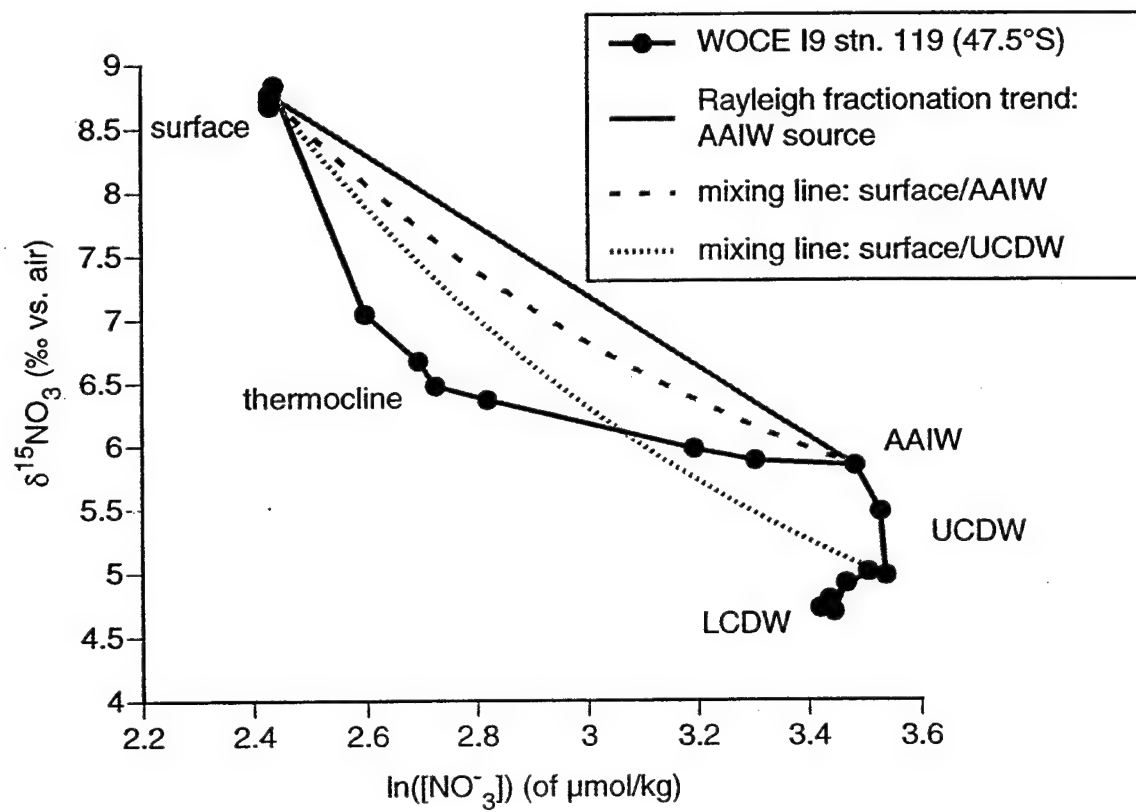


Figure 22

The entire east Indian (WOCE I9) data set plotted in $\delta^{15}\text{NO}_3/\ln([\text{NO}_3^-])$ space (a), and a cartoon to illustrate hypothesized processes (b).

(a) Antarctic and Subantarctic Zone profile data are plotted as filled and open symbols, respectively (analysis averages used). The separate trends of the mixed layer and shallow thermocline data from the Subantarctic Zone suggest that the thermocline is not the main source of nitrate to the surface layer, as this would require a very large northward increase in the fractionation factor.

(b) The hypothesized controls on the $\delta^{15}\text{NO}_3/\ln([\text{NO}_3^-])$ trend of the Subantarctic surface samples. Upper Circumpolar Deep Water is the ultimate source of nitrate to the surface Antarctic, in which nitrate utilization occurs (1). The Subantarctic surface layer acquires most of its nitrate from equatorward transfer of nitrate from the Polar Frontal Zone, either by advection or eddy transfer (2). Near the Polar Frontal Zone at the longitudes of the transects, there is significant mixing between the Subantarctic surface layer and the Subantarctic thermocline, which has a strongly negative $\delta^{15}\text{N}_{\text{nr}}$ (3). This lowers the $\delta^{15}\text{NO}_3$ of the Subantarctic Surface layer closer to the Polar Frontal Zone (stations 119, 126), steepening the overall trend of the Subantarctic surface samples. We hypothesize that the low $\delta^{15}\text{N}_{\text{nr}}$ of the Subantarctic thermocline is produced by isopycnal mixing with the low latitude thermocline.

$\delta^{15}\text{NO}_3^-$ vs. $\ln([\text{NO}_3^-])$ WOCE 19, east Indian sector

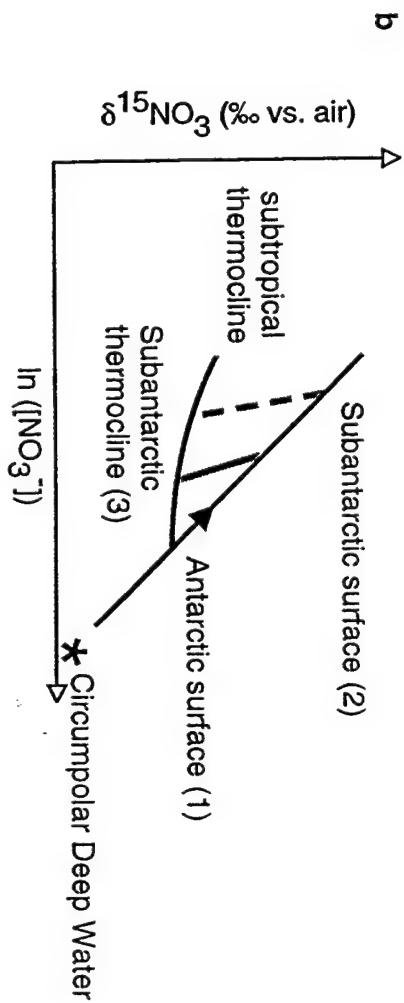
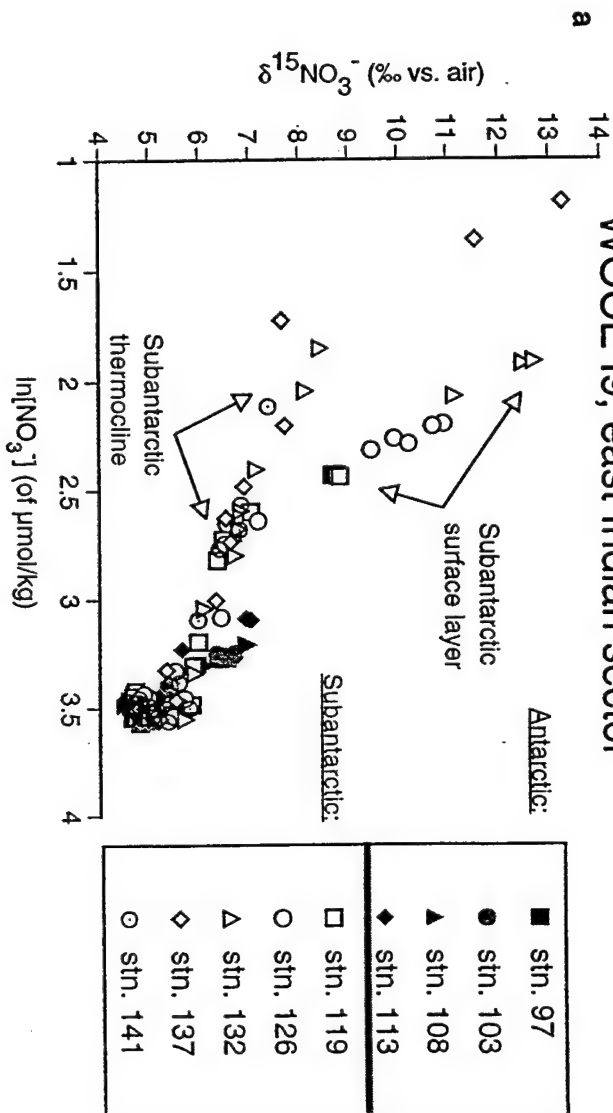


Figure 23

Surface transect data from Figures 4a-c, plotted in $\delta^{15}\text{NO}_3/\ln([\text{NO}_3^-])$ space (analysis averages used). The RITS '94 transect is shown as open squares, the ANT XII/4 southward transect as open triangles, and surface layer averages from WOCE I9 as crosses. The compiled data show a single overall trend across the Southern Ocean (a) which is similar to trends from surface Antarctic data alone (Figure 17). This suggests that nitrate is provided to Subantarctic surface largely by equatorward surface transport. A linear regression through the RITS '94 data gives a slope of 4.5‰, which can be taken as an estimate for the fractionation factor for the Subantarctic Zone if this simple picture of lateral nitrate supply is accurate.

Surface Transect Data

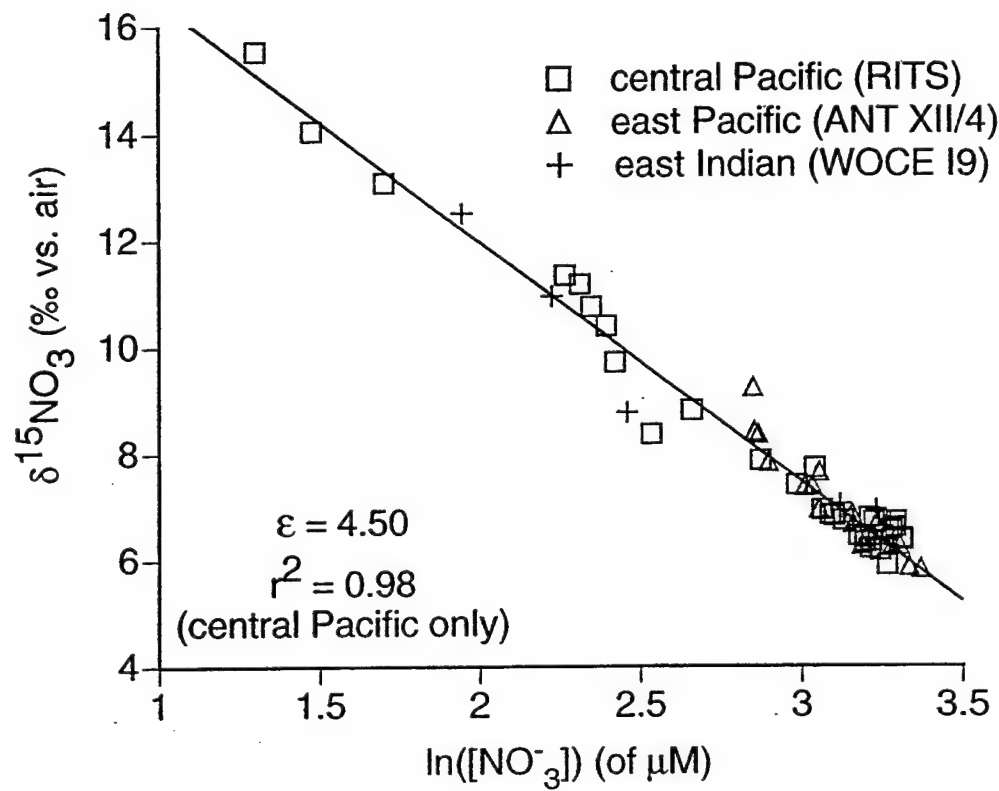


Figure 24

Depth profiles of (a) $\delta^{15}\text{NO}_3$ and $[\text{NO}_3^-]$, and (b) $\delta^{15}\text{N}_{\text{nr}}$ and salinity, for WOCE I9 station 132, in the Subantarctic. (a) While $\delta^{15}\text{NO}_3$ increases into the surface layer, $[\text{NO}_3^-]$ increases, then decreases. The $[\text{NO}_3^-]$ changes, while small, are verified by phosphate data. This is inconsistent with a model of nitrate supply from below. Estimation of the fractionation factor from this profile yields a fractionation factor with the wrong sign. (b) The discontinuities in both $\delta^{15}\text{N}_{\text{nr}}$ and salinity between the surface layer and the thermocline suggest that these layers are decoupled, with surface layer nitrate being imported laterally.

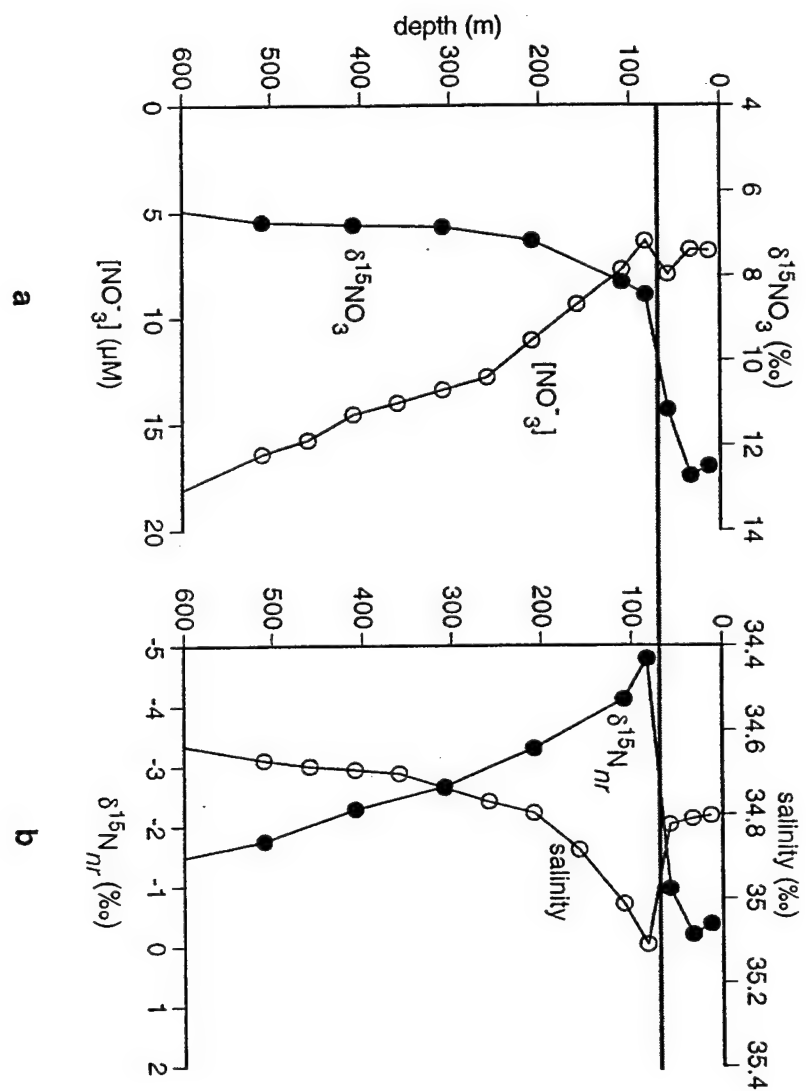
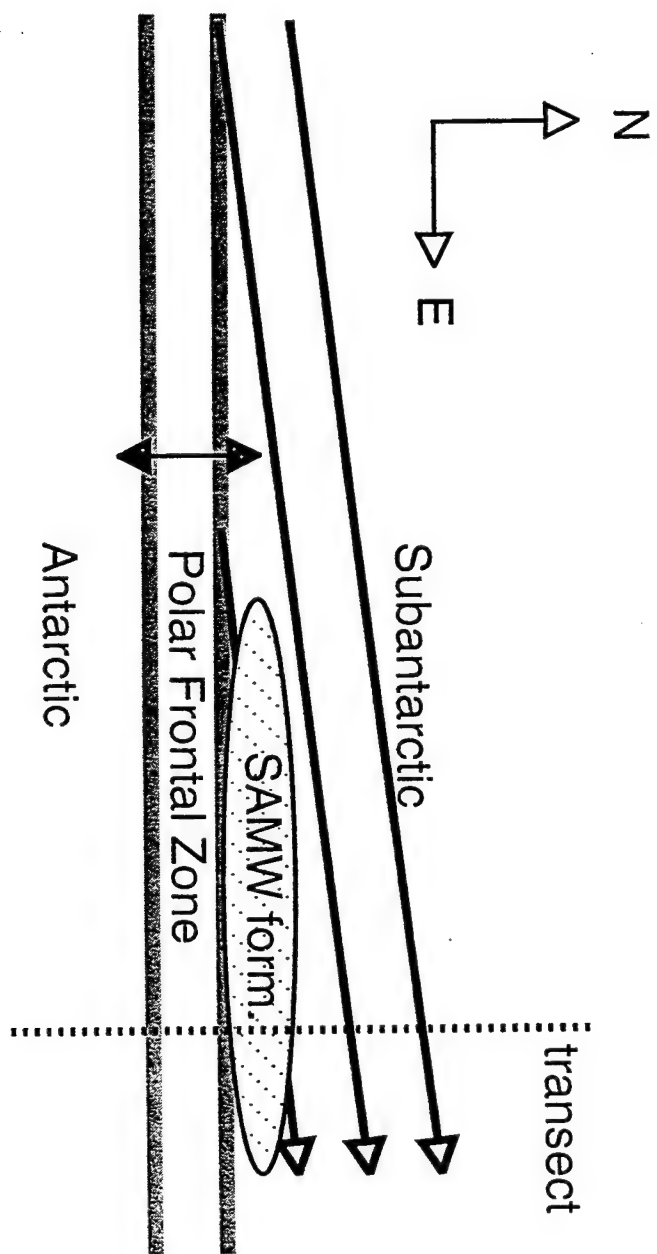


Figure 25

A map-view cartoon of our hypothesized model for nitrate supply in the Subantarctic Zone. Nitrate is supplied mostly by transfer of high- $[\text{NO}_3^-]$ water across the Polar Frontal Zone, followed by net equatorward transfer by advection or eddy processes. This explains the single Rayleigh fractionation trend suggested by the RITS '94 surface data (Figure 23). The generation of low- $\delta^{15}\text{N}_{\text{nr}}$ surface values in the more polar Subantarctic surface is suggested to be by Subantarctic Mode Water formation (i.e., vertical mixing) in this region. We hypothesize that this effect is emphasized in our data sets because our transects are in regions of deep vertical mixing (the east Indian, and the central and east Pacific, McCartney, 1977). Thus, the small number of low- $\delta^{15}\text{N}_{\text{nr}}$ Subantarctic surface samples near the Polar Front are not characteristic of the nitrate being supplied to the more northern Subantarctic.



WOCE 19 $\delta^{15}\text{NO}_3$ data

station: 97
 latitude ($^{\circ}\text{S}$): 59.20
 longitude ($^{\circ}\text{E}$): 115.00

depth (m)	WHP #*	$[\text{NO}_3^-]$ ($\mu\text{mol/kg}$)	$\delta^{15}\text{NO}_3$ (‰ vs. air)
15.6	36	26.35	6.56
30.8	35	26.41	6.35
57.2	34	26.42	6.41
82.3	33	27.00	5.95
156.1	31	30.25	5.39
156.1	31	30.25	5.40
257.7	29	35.56	4.85
257.7	29	35.56	4.71
307.0	28	35.50	4.81
406.9	26	34.76	4.60
406.9	26	34.76	4.67
507.8	24	33.98	4.75
507.8	24	33.98	4.77
709.2	22	32.63	4.71
709.2	22	32.63	4.82
709.2	22	32.63	4.70
912.4	20	31.75	4.58
1115.0	18	31.39	4.64
1420.8	16	31.39	4.66
1822.6	14	31.79	4.70
2232.3	12	32.44	4.74
2742.2	10	32.98	4.78
3361.8	8	32.97	4.67
3871.6	6	32.86	4.56
3871.6	6	32.86	4.64
4288.1	4	32.80	4.89
4547.0	2	32.68	4.68
4547.0	2	32.68	4.68

*WOCE Hydrographic Program sample #
 (for comparison with other measurements)

WOCE I9 $\delta^{15}\text{NO}_3$ data

station: 103
 latitude ($^{\circ}\text{S}$): 56.19
 longitude ($^{\circ}\text{E}$) 115.00

depth (m)	WHP #	$[\text{NO}_3^-]$ ($\mu\text{mol/kg}$)	$\delta^{15}\text{NO}_3$ (‰ vs. air)
11.2	36	25.69	6.71
31.8	35	25.69	6.33
81.8	33	25.96	6.46
106.3	32	26.12	6.66
207.4	30	29.91	5.38
307.8	28	35.26	5.02
407.9	26	35.32	4.74
508.6	24	34.56	4.86
710.6	22	33.44	4.99
912.6	20	32.12	4.80
1115.3	18	31.57	4.61
1418.3	16	31.01	4.69
1823.5	14	31.28	4.88
2233.6	12	31.90	4.69
2745.6	10	32.47	4.76
3055.4	9	32.62	4.58
3871.7	6	32.84	4.62
3871.7	6	32.84	4.77
4283.9	4	32.69	4.96
4560.4	2	32.70	4.71
4560.4	2	32.70	4.77

WOCE I9 $\delta^{15}\text{NO}_3$ data

station: 108
 latitude ($^{\circ}\text{S}$) 53.19
 longitude ($^{\circ}\text{E}$) 115.00

depth (m)	WHP #	$[\text{NO}_3^-]$ ($\mu\text{mol/kg}$)	$\delta^{15}\text{NO}_3$ (‰ vs. air)
13.3	36	24.60	6.93
31.5	35	24.60	6.93
56.9	34	24.70	6.99
82.7	33	24.75	6.94
107.4	32	27.16	6.13
208.1	30	32.09	5.20
308.0	28	34.85	5.10
409.0	26	34.80	4.98
508.7	24	34.46	4.81
711.4	22	32.88	4.76
812.5	21	32.68	4.80
1113.6	18	31.16	4.84
1316.3	16	30.86	4.68
1623.8	14	30.96	4.83
2023.9	12	31.55	4.75
2422.6	10	32.19	4.66
2836.4	8	32.68	4.63
3254.1	6	32.73	4.49
3667.0	4	32.83	4.62
4006.0	2	32.93	4.66
4006.0	2	32.94	4.73

WOCE I9 $\delta^{15}\text{NO}_3$ data

station: 113
 latitude ($^{\circ}\text{S}$) 50.50
 longitude ($^{\circ}\text{E}$) 115.03

depth (m)	WHP #	$[\text{NO}_3^-]$ ($\mu\text{mol/kg}$)	$\delta^{15}\text{NO}_3$ (‰ vs. air)
11.3	36	22.02	6.86
11.3	36	22.02	7.22
30.6	35	22.00	6.99
81.1	33	21.86	6.92
106.0	32	25.25	5.65
207.1	30	27.84	5.49
305.5	28	31.39	5.18
406.6	26	33.50	5.01
504.4	24	34.47	4.88
703.9	22	34.46	4.77
906.6	20	33.47	4.79
1108.7	18	32.24	4.82
1313.4	16	31.52	4.53
1512.4	14	30.75	4.72
1716.4	12	30.78	4.61
1920.7	10	30.99	4.64
2234.2	8	31.60	4.64
2631.0	6	32.15	4.63
2942.6	4	32.39	4.61
3184.0	2	32.64	4.56
3184.0	2	32.64	4.45

WOCE I9 $\delta^{15}\text{NO}_3$ data

station: 119
 latitude ($^{\circ}\text{S}$) 47.51
 longitude ($^{\circ}\text{E}$) 115.00

depth (m)	WHP #	$[\text{NO}_3^-]$ ($\mu\text{mol/kg}$)	$\delta^{15}\text{NO}_3$ (‰ vs. air)
11.2	36	11.38	8.76
32.1	35	11.38	8.67
58.2	34	11.37	8.71
81.4	33	11.42	8.77
106.0	32	11.46	8.83
206.6	30	13.45	7.04
305.7	28	14.81	6.67
404.8	26	15.28	6.47
508.8	24	16.78	6.36
708.6	22	24.39	5.97
808.9	20	24.39	5.87
808.9	20	27.28	5.89
1112.4	18	32.60	5.84
1312.2	16	34.07	5.56
1312.2	16	34.07	5.40
1524.1	14	34.38	4.97
1831.0	12	33.33	5.00
2227.8	9	31.11	4.79
2629.1	8	30.61	4.72
3041.1	6	31.36	4.69
3457.8	4	32.05	4.91

WOCE I9 $\delta^{15}\text{NO}_3$ data

station: 126
 latitude ($^{\circ}\text{S}$) 44.00
 longitude ($^{\circ}\text{E}$) 115.00

depth (m)	WHP #	$[\text{NO}_3^-]$ ($\mu\text{mol/kg}$)	$\delta^{15}\text{NO}_3$ (‰ vs. air)
13.1	36	9.00	10.93
32.7	35	9.09	10.71
58.2	34	9.62	9.93
83.4	33	9.86	10.22
107.2	32	10.15	9.46
208.0	30	14.03	7.18
409.1	26	14.19	6.55
509.6	24	15.58	6.51
710.7	22	21.77	6.43
910.9	20	27.87	5.52
1113.4	18	31.67	5.69
1418.1	16	34.36	5.48
1821.6	14	33.70	5.07
2224.6	12	31.50	4.98
2734.1	10	31.03	4.89
3242.3	8	31.76	4.78
3653.4	6	32.30	4.77
4071.6	4	32.55	4.78
4071.6	4	32.55	4.77
4379.8	2	32.70	4.67

WOCE I9 $\delta^{15}\text{NO}_3$ data

station: 132
latitude (°S) 40.89
longitude (°E) 115.00

depth (m)	WHP #	[NO ₃] ($\mu\text{mol/kg}$)	$\delta^{15}\text{NO}_3$ (‰ vs. air)
12.9	36	6.82	12.50
33.0	35	6.76	12.72
58.2	34	7.92	11.16
83.1	33	6.36	8.45
108.7	32	7.72	8.15
208.4	30	11.07	7.16
308.5	28	13.39	6.84
408.7	26	14.55	6.80
509.9	24	16.43	6.73
710.5	22	20.92	6.15
710.5	22	20.92	6.07
911.7	20	28.18	5.92
1113.5	18	31.87	5.56
1415.3	16	34.87	5.72
1824.1	14	34.67	5.13
2238.2	12	33.58	5.14
2738.6	10	32.50	4.78
3351.9	8	32.10	4.65
3351.9	8	32.10	4.78
3351.9	8	32.10	4.78
3351.9	8	32.10	4.78
3865.3	6	32.53	4.71
3865.3	6	32.53	4.82
4274.5	4	32.91	4.68
4629.1	2	32.90	4.71

WOCE I9 $\delta^{15}\text{NO}_3$ data

station: 137
 latitude ($^{\circ}\text{S}$) 38.00
 longitude ($^{\circ}\text{E}$) 115.00

depth (m)	WHP #	$[\text{NO}_3^-]$ ($\mu\text{mol/kg}$)	$\delta^{15}\text{NO}_3$ (‰ vs. air)
5.1	36	0.88	N
23.7	35	0.98	N
49.0	34	3.29	13.27
74.3	33	3.90	11.57
98.3	32	5.60	7.66
204.5	30	9.04	7.72
305.4	28	11.96	6.90
403.2	26	13.83	6.53
510.9	24	15.43	6.62
710.6	22	20.12	6.34
710.6	22	20.12	6.32
912.5	20	27.75	5.34
1113.8	18	31.91	5.53
1428.0	16	35.03	5.17
1822.6	14	34.81	5.20
2230.9	12	33.62	5.04
2742.3	10	32.24	4.81
3351.7	8	32.13	4.72
3351.7	8	32.13	4.68
3963.8	6	32.81	4.74
3963.8	6	32.81	4.77
4581.5	4	33.06	4.77
4864.1	2	33.04	4.77

WOCE I9 $\delta^{15}\text{NO}_3$ data

station: 141
 latitude ($^{\circ}\text{S}$) 36.00
 longitude ($^{\circ}\text{E}$) 115.00

depth (m)	WHP #	$[\text{NO}_3^-]$ ($\mu\text{mol/kg}$)	$\delta^{15}\text{NO}_3$ (‰ vs. air)
14.4	36	0.10	N
32.9	35	0.10	N
59.6	34	0.10	N
82.7	33	0.38	N
207.6	30	8.28	7.39
310.6	28	13.01	6.84
409.7	26	14.59	6.81
509.9	24	15.94	6.31
509.9	24	15.94	6.50
712.4	22	22.02	5.98
913.9	20	29.44	5.59
1114.6	18	33.15	5.79
1418.1	16	35.19	5.37
1825.4	14	34.40	5.06
2329.6	12	33.29	5.19
2329.6	12	33.29	5.08
2938.1	10	32.73	4.98
3550.2	8	32.91	4.68
3550.2	8	32.91	4.67
4163.2	6	33.05	4.73
4163.2	6	33.05	4.73
4789.1	4	33.10	4.63
5286.3	2	33.19	4.63
5286.3	2	33.19	4.74
5286.3	2	33.19	4.81

ANT XII/4 $\delta^{15}\text{NO}_3$ hydrocast data

station # 14
 AWI #* 2660-6
 latitude ($^{\circ}\text{S}$) 50.14
 longitude ($^{\circ}\text{E}$) 270.77

depth (m)	$[\text{NO}_3]$ (μM)	$\delta^{15}\text{NO}_3$ (‰ vs. air)	average $\delta^{15}\text{NO}_3$
10	15.43	9.49	9.49
10	15.43	9.42	9.55
20	15.63	9.67	
20	15.63	9.57	
50	15.25	9.24	9.31
50	15.25	9.37	
80	17.11	8.82	8.82
100	17.19	7.68	7.68
150	19.39	6.43	6.43
200	19.35	6.37	6.37
500	21.54	6.30	6.24
500	21.54	6.17	

* Alfred Wegener Institute station #

station # 21
 AWI # 2661-5
 latitude ($^{\circ}\text{S}$) 51.41
 longitude ($^{\circ}\text{E}$) 270.66

depth (m)	$[\text{NO}_3]$ (μM)	$\delta^{15}\text{NO}_3$ (‰ vs. air)	average $\delta^{15}\text{NO}_3$
10	15.61	8.73	8.65
10	15.61	8.58	
20	15.60	8.85	8.85
50	15.63	8.73	8.70
50	15.63	8.67	
80	17.11	8.46	8.46
100	17.19	7.37	7.37
150	19.39	6.49	6.49
200	19.35	6.23	6.23
500	21.54	6.10	6.08
500	21.54	6.12	
500	21.54	6.02	

ANT XII/4 $\delta^{15}\text{NO}_3$ hydrocast data

station # 47
 AWI # 2667-7
 latitude ($^{\circ}\text{S}$) 55.66
 longitude ($^{\circ}\text{E}$) 270.18

depth (m)	$[\text{NO}_3]$ (μM)	$\delta^{15}\text{NO}_3$ (‰ vs. air)	average $\delta^{15}\text{NO}_3$
600	26.63	5.98	5.95
600	26.44	5.92	
1000	32.39	5.76	5.74
1000	32.51	5.73	
1200	33.67	5.70	5.76
1200	33.66	5.81	
1400	34.38	5.06	5.06
1600	34.58	5.11	5.11
1800	32.90	5.27	5.27
2000	32.98	4.92	4.92
3500	32.83	4.79	4.78
3500	32.54	4.77	

station # 80
 AWI # 2682-1
 latitude ($^{\circ}\text{S}$) 66.52
 longitude ($^{\circ}\text{E}$) 262.57

depth (m)	$[\text{NO}_3]$ (μM)	$\delta^{15}\text{NO}_3$ (‰ vs. air)	average $\delta^{15}\text{NO}_3$
40	26.20	6.50	6.50
60	26.32	6.13	6.13
100	28.76	5.74	5.74
200	32.80	5.28	5.28
400	35.99	4.98	4.98
600	35.63	4.84	4.84

ANT XII/4 $\delta^{15}\text{NO}_3$ hydrocast data

station # 91
 AWI # 2683-1
 latitude ($^{\circ}\text{S}$) 68.52
 longitude ($^{\circ}\text{E}$) 262.83

depth (m)	$[\text{NO}_3]$ (μM)	$\delta^{15}\text{NO}_3$ (% vs. air)	average $\delta^{15}\text{NO}_3$
60	24.23	6.65	6.65
100	30.18	5.48	5.50
100	30.18	5.52	
150	33.38	5.08	5.01
150	33.38	4.94	
200	36.16	4.89	4.89
400	35.32	4.83	4.83
600	34.21	4.89	4.89
800	33.51	4.78	4.78
1000	32.95	4.63	4.63

station # 103
 AWI # 2684-4
 latitude ($^{\circ}\text{S}$) 69.42
 longitude ($^{\circ}\text{E}$) 264.98

depth (m)	$[\text{NO}_3]$ (μM)	$\delta^{15}\text{NO}_3$ (% vs. air)	average $\delta^{15}\text{NO}_3$
20	24.10	6.70	6.70
60	24.20	6.58	6.58
100	30.90	5.23	5.23
200	36.00	5.25	5.13
200	36.00	5.01	5.01
400	34.90	4.84	4.84
600	33.50	4.64	4.64

ANT XII/4 $\delta^{15}\text{NO}_3$ hydrocast data

station # 104
 AWI # 2685-1
 latitude ($^{\circ}\text{S}$) 69.42
 longitude ($^{\circ}\text{E}$) 265.83

depth (m)	$[\text{NO}_3]$ (μM)	$\delta^{15}\text{NO}_3$ (‰ vs. air)	average $\delta^{15}\text{NO}_3$
10	24.42	6.32	6.32
20	24.47	6.25	6.25
40	24.29	6.42	6.42
60	25.19	6.21	6.21
100	30.97	4.80	4.80
200	35.95	4.71	4.71
400	34.92	4.73	4.73
600	33.09	4.69	4.69

station # 135
 AWI # 2686-1
 latitude ($^{\circ}\text{S}$) 68.29
 longitude ($^{\circ}\text{E}$) 270.41

depth (m)	$[\text{NO}_3]$ (μM)	$\delta^{15}\text{NO}_3$ (‰ vs. air)	average $\delta^{15}\text{NO}_3$
20	25.50	6.11	6.05
20	25.50	5.99	
60	29.30	5.19	5.25
60	29.30	5.32	
100	34.10	4.96	4.96
200	37.10	4.70	4.70
400	35.50	4.63	4.63
600	34.80	4.60	4.60

ANT XIII/4 $\delta^{15}\text{NO}_3$ hydrocast data

station # 138
 AWI # 2687-1
 latitude ($^{\circ}\text{S}$) 67.98
 longitude ($^{\circ}\text{E}$) 267.36

depth (m)	$[\text{NO}_3]$ (μM)	$\delta^{15}\text{NO}_3$ (‰ vs. air)	average $\delta^{15}\text{NO}_3$
25	23.60	6.65	6.65
60	25.40	6.41	6.41
80	29.90	5.50	5.50
100	30.40	5.35	5.35
150	33.10	5.15	5.15
200	35.10	4.95	4.95
400	36.10	4.87	4.87
600	34.70	4.86	4.86
1000	33.20	4.58	4.58
2000	33.30	4.60	4.60
4000	33.90	4.62	4.62

station # 141
 AWI # 2688-5
 latitude ($^{\circ}\text{S}$) 67.22
 longitude ($^{\circ}\text{E}$) 268.17

depth (m)	$[\text{NO}_3]$ (μM)	$\delta^{15}\text{NO}_3$ (‰ vs. air)	average $\delta^{15}\text{NO}_3$
20	25.00	6.79	6.79
60	25.00	6.71	6.68
60	25.00	6.64	
100	29.82	5.62	5.62
200	32.10	5.06	5.06
400	36.95	4.95	4.95
600	35.04	4.63	4.63

ANT XII/4 $\delta^{15}\text{NO}_3$ hydrocast data

station # 154
AWI # 2692-3
latitude ($^{\circ}\text{S}$) 65.14
longitude ($^{\circ}\text{E}$) 269.31

depth (m)	$[\text{NO}_3]$ (μM)	$\delta^{15}\text{NO}_3$ (‰ vs. air)	average $\delta^{15}\text{NO}_3$
20	25.70	7.00	7.00
60	25.80	6.69	6.77
60	25.80	6.85	6.85
200	32.30	5.26	5.26
400	36.90	5.15	5.15
600	36.50	4.77	4.77

station # 162
AWI # 2696-5
latitude ($^{\circ}\text{S}$) 63.98
longitude ($^{\circ}\text{E}$) 270.47

depth (m)	$[\text{NO}_3]$ (μM)	$\delta^{15}\text{NO}_3$ (‰ vs. air)	average $\delta^{15}\text{NO}_3$
10	24.91	6.51	6.50
10	24.91	6.48	
60	25.44	6.55	6.52
60	25.44	6.58	
60	25.44	6.45	
100	25.76	6.43	6.43
150	28.39	5.72	5.72
200	29.69	5.45	5.45
400	34.73	5.26	5.26
800	35.48	4.95	4.95
1000	33.90	4.96	4.96
2000	32.41	4.64	4.64
4000	34.03	4.67	4.67

ANT XII/4 $\delta^{15}\text{NO}_3$ hydrocast data

station # 177
 AWI # 2699-1
 latitude ($^{\circ}\text{S}$) 61.02
 longitude ($^{\circ}\text{E}$) 270.50

depth (m)	$[\text{NO}_3]$ (μM)	$\delta^{15}\text{NO}_3$ (% vs. air)	average $\delta^{15}\text{NO}_3$
10	24.67	6.54	6.54
50	25.36	6.31	6.36
50	25.36	6.41	
100	24.87	6.25	6.25
200	28.97	5.44	5.44
400	34.29	5.18	5.18
600	35.55	5.01	5.01
800	35.04	4.98	4.98
1000	33.88	4.83	4.83
2000	32.23	4.65	4.65
2500	32.32	4.59	4.59
3500	32.42	4.60	4.60
4500	32.27	4.68	4.68

station # 182
 AWI # 2700-4
 latitude ($^{\circ}\text{S}$) 60.27
 longitude ($^{\circ}\text{E}$) 270.48

depth (m)	$[\text{NO}_3]$ (μM)	$\delta^{15}\text{NO}_3$ (% vs. air)	average $\delta^{15}\text{NO}_3$
10	22.02	6.82	6.86
10	22.02	6.90	
20	22.48	6.99	6.99
50	21.90	6.73	6.73
80	21.57	6.90	6.90
100	21.98	6.74	6.74
150	24.45	5.91	5.91
200	26.62	5.86	5.86
400	30.57	5.62	5.62
600	32.77	5.24	5.24

ANT XII/4 $\delta^{15}\text{NO}_3$ surface data

southward transect

northward transect

latitude (°S)	longitude (°W)	[NO ₃] (μM)	$\delta^{15}\text{NO}_3$ (‰ vs. air)	latitude (°S)	longitude (°W)	[NO ₃] (μM)	$\delta^{15}\text{NO}_3$ (‰ vs. air)
50.15	89.20	17.29	9.38	70.03	83.97	29.07	5.83
50.15	89.20	17.29	9.11	68.81	75.66	31.13	5.54
52.88	89.49	17.36	8.46	68.42	70.87	23.49	5.86
52.88	89.49	17.36	8.37	68.35	75.94	29.23	5.73
54.33	89.64	17.58	8.48	68.31	85.83	27.53	6.05
54.33	89.64	17.58	8.26	68.28	89.53	25.51	6.15
55.46	89.76	18.13	7.83	68.28	91.54	27.47	5.47
57.52	91.09	20.27	7.38	68.23	94.46	25.42	6.36
57.93	90.44	21.20	7.30	67.21	91.83	23.20	6.70
59.72	96.03	20.74	7.40	65.45	90.64	24.57	6.55
61.50	97.68	23.47	6.82	65.13	90.71	25.63	6.92
61.50	97.68	23.47	6.92	64.73	93.91	27.32	5.63
63.45	98.00	25.25	6.62	64.73	93.91	27.32	5.85
63.45	98.00	25.25	6.73	62.14	89.50	29.36	5.81
64.88	97.71	26.59	6.29	62.14	89.50	29.36	5.81
64.88	97.71	26.59	6.29	61.02	89.50	26.68	6.69
68.28	97.17	23.54	6.69	59.45	89.50	24.60	6.96
68.28	97.17	23.54	6.68	59.40	89.53	21.87	7.06
69.42	92.41	27.22	6.29	57.73	90.01	22.78	6.75
69.42	92.41	27.22	6.24	57.55	91.12	22.07	7.23
69.43	97.35	25.07	6.43				
69.43	97.35	25.07	6.45				
69.50	94.77	24.20	6.39				
69.50	94.77	24.20	6.17				
69.76	91.99	28.04	5.91				
69.76	91.99	28.04	5.85				
70.03	83.97	29.09	5.83				

RITS '94 $\delta^{15}\text{NO}_3$ surface transect data
southward transect

latitude (°S)	longitude(°W)	[NO ₃] (μM)	$\delta^{15}\text{NO}_3$ (‰ vs. air)
41.40	144.36	3.67	15.66
41.40	144.36	3.67	15.00
42.40	144.08	4.37	13.90
42.40	144.08	4.37	13.79
44.20	143.54	5.49	12.98
44.20	143.54	5.49	12.77
45.23	143.23	8.13	12.20
46.12	142.93	9.63	11.29
46.12	142.93	9.63	11.30
46.12	142.93	9.63	11.40
47.11	142.58	10.08	11.16
47.92	142.32	10.44	10.74
49.80	141.69	10.95	10.54
49.80	141.69	10.95	10.23
50.62	141.54	11.24	9.72
50.62	141.54	11.24	9.67
51.97	140.74	14.27	8.87
51.97	140.74	14.27	8.56
51.97	140.74	14.27	8.98
53.00	140.30	12.62	8.36
54.77	139.46	17.72	7.89
54.77	139.46	17.72	7.83
55.84	138.92	19.80	7.24
55.84	138.92	19.80	7.41
55.84	138.92	19.80	7.56
56.62	138.53	20.93	7.84
56.62	138.53	20.93	7.60
57.81	137.85	24.76	6.58
57.81	137.85	24.76	6.89
57.81	137.85	24.76	6.86
58.66	137.35	26.91	6.71
60.30	136.34	27.40	6.39
61.60	135.41	27.48	6.37
62.97	134.37	26.90	6.57
63.81	133.67	26.85	6.60
66.38	131.25	25.14	6.70
67.62	129.55	25.83	6.44

RITS '94 $\delta^{15}\text{NO}_3$ surface transect data
eastward transect

latitude (°S)	longitude(°W)	$[\text{NO}_3^-]$ (μM)	$\delta^{15}\text{NO}_3$ (‰ vs. air)
66.53	121.05	22.20	6.96
66.53	121.05	22.20	6.74
66.53	121.05	22.20	6.75
68.58	113.45	21.95	6.71
68.58	113.45	21.95	6.93
68.58	113.45	21.95	6.89
68.32	109.42	23.97	6.49
68.32	109.42	23.97	6.40
69.02	102.25	24.90	6.29
69.02	102.25	24.90	6.39
70.28	93.00	24.83	6.26
70.28	93.00	24.83	6.15
67.63	88.90	21.40	6.94
67.63	88.90	21.40	6.91
67.07	85.22	22.83	6.54
67.07	85.22	22.83	6.81
67.07	85.22	22.83	6.84
67.30	77.73	24.41	6.43
67.30	77.73	24.41	6.38
66.78	73.13	25.58	6.29
66.78	73.13	25.58	5.97
66.78	73.13	25.58	6.24
65.53	68.82	25.09	5.66
65.53	68.82	25.09	5.87
64.53	65.60	23.50	5.99
64.53	65.60	23.50	5.62
64.53	65.60	23.50	6.01
64.78	64.08	24.76	5.79
64.78	64.08	24.76	5.66
61.73	63.47	26.18	5.91
61.73	63.47	26.18	5.88
59.77	63.28	24.42	6.29
59.77	63.28	24.42	6.34

Chapter 5:

The Isotopic Composition of Diatom Microfossil-Bound Organic Nitrogen in Southern Ocean Sediments

D.M. Sigman^{1*}, M.A. Altabet², R. Francois³, D.C. McCorkle¹, J-F. Gaillard⁴

¹Department of Marine Geology and Geophysics, Woods Hole Oceanographic Institution,
Woods Hole, MA 02543, e-mail: dsigman@whoi.edu, fax: (508)-457-2183

*corresponding author

²Center for Marine Science and Technology, University of Massachusetts, Dartmouth,
North Dartmouth, MA 02747

³Department of Marine Chemistry and Geochemistry, Woods Hole Oceanographic
Institution, Woods Hole, MA 02543

⁴Department of Civil Engineering, Northwestern University, 2415 Sheridan Road,
Evanston, IL 60208-3109

Abstract

Nitrogen isotope records of bulk sediment in the Southern Ocean suggest that nitrate utilization was higher during the last ice age than it is today. However, the glacial/interglacial bulk sediment N isotope difference may be of diagenetic origin, rather than recording a change in the N isotopic composition of the sinking flux. To address this possibility, we investigate the isotopic composition of diatom microfossil-bound N from Southern Ocean sediments. To target diatom microfossil-bound N, we isolate the diatomaceous fraction from bulk sediment and oxidize this fraction with perchloric acid at 70°C, similar to the methodology of Shemesh et al. (1993).

The perchloric acid treatment of diatom microfossils leaves a N fraction which is 0-4‰ lower in $\delta^{15}\text{N}$ than the bulk sediment, typically 3‰ lower in recent diatom oozes from the Antarctic region. Fluorescence microscopy demonstrates that the surviving organic matter is associated with the microfossils and not visibly altered by the oxidation step. Pyrolysis/gas chromatography/mass spectrometry suggests that the isolated organic matter is composed largely of proteinaceous material, consistent with its C/N molar ratio of ~6. The results are consistent with a diatom-native origin for diatom-bound N, but they do not absolutely preclude the possibility of absorption of organic N from the sedimentary environment.

A detailed depth profile through the top 15 cm of a multicore from the west Pacific sector of the Southern Ocean shows that early diagenetic changes in bulk sediment N content and $\delta^{15}\text{N}$ are not reflected in diatom-bound N, suggesting that the diatom-bound N is insensitive to early diagenesis. Data from a latitudinal transect of multicores from the Indian sector indicate that the $\delta^{15}\text{N}$ of diatom-bound N varies with nitrate utilization in the overlying surface waters, as has been demonstrated previously for bulk sedimentary N.

We find that the $\delta^{15}\text{N}$ of diatom-bound N is 3-4‰ higher in glacial sediments than in Holocene sediments. These results support the hypothesis, previously based on bulk sediment $\delta^{15}\text{N}$, that nitrate utilization in the surface Antarctic was higher during the last ice age.

Introduction

Southern Ocean sediment cores from south of the modern Polar Frontal Zone record a change in bulk sediment $\delta^{15}\text{N}$ at the last glacial/interglacial transition, with last glacial sediments being higher than Holocene sediments by 2-4‰ (Francois et al., 1992; Francois et al., 1997). Field and laboratory studies show that a Rayleigh fractionation process links the degree of nitrate utilization by phytoplankton to the isotopic composition of nitrate, suspended particulate N, and the sinking N flux, with the $\delta^{15}\text{N}$ of each of the N pools increasing as the degree of nitrate utilization increases (Altabet et al., 1991; Altabet and Francois, 1994a; Altabet and McCarthy, 1985; Francois et al., 1992; Montoya, 1990; Montoya and McCarthy, 1995; Nakatsuka et al., 1992; Pennock et al., 1988; Sigman et al., 1996; Wada, 1980; Wada and Hattori, 1978; Waser et al., 1997; Wu et al., 1997). Sediment trap and surface sediment data have demonstrated that this nitrate utilization/ $\delta^{15}\text{N}$ link is recorded in seafloor sediments, although apparently with a 3-5‰ diagenetic increase during incorporation into the sediment record (Altabet and Francois, 1994a; Farrell et al., 1995). On this basis, the glacial/interglacial bulk sediment $\delta^{15}\text{N}$ change in Antarctic sediments has been hypothesized to reflect a higher degree of nitrate utilization in Antarctic surface waters during the last ice age (Francois et al., 1992; Francois et al., 1997).

One concern about this interpretation involves the potential effects of diagenetic and sedimentary processes on bulk sediment $\delta^{15}\text{N}$. Given the significant isotopic increase associated with the incorporation of sinking organic N into surface sediments (Altabet and Francois, 1994a) and evidence for variability in this isotopic enrichment as a function of the degree of preservation (Sachs, 1996), diagenetic or other sedimentary changes may be responsible for the isotopic difference between glacial and Holocene sediments in Antarctic sediment cores. The impact of diagenetic effects on paleoceanographic records can be assessed (or avoided) by isolating organic materials in sediments which are either protected from diagenesis or are not isotopically affected by it (Hayes et al., 1989; Sachs, 1996).

Shemesh et al. (1993) pioneered a diatom microfossil-based approach to overcome the uncertainties of bulk sediment carbon and nitrogen isotopic composition. The premise of this approach is that organic matter resides within the hydrated silica matrix of diatoms, that this organic matter was incorporated into the microfossil by the living phytoplankton, and that the organic matter is physically protected by the opal matrix from bacterial decomposition, both within the water column and at the sea floor. In their analytical procedure, "diatom-bound" organic matter is isolated by physical separation of the diatom microfossil fraction from the other components in the sediments, followed by wet chemical oxidation to remove any organic matter on the microfossil surface. The remaining organic matter, presumably within the microfossils, is converted to gas for mass spectrometry by combustion of the surface-oxidized diatom microfossil material.

Southern Ocean diatom-bound organic carbon isotopic records generated in this way show a similar pattern to bulk sediment $\delta^{13}\text{C}_{\text{org}}$ records, with lower $\delta^{13}\text{C}$ values during ice ages (Singer and Shemesh, 1995). However, published nitrogen isotopic data from this diatom-bound organic matter show a trend which is opposite to that observed in bulk sediment N isotopic composition: the diatom-bound $\delta^{15}\text{N}$ data suggest that the sinking flux was lower in $\delta^{15}\text{N}$ during the last ice age (Shemesh et al., 1993). The results of Shemesh et al. (1993) indicate that diatom $\delta^{15}\text{N}$ is 9-11‰ in Holocene sediments, which is ~5‰ higher than bulk sediment $\delta^{15}\text{N}$ and $\geq 8\%$ higher than the estimated $\delta^{15}\text{N}$ of the N sinking flux (Chapter 4).

In this study, we report N isotope results for diatom-bound N from recent and glacial-age Southern Ocean sediments, as well as supporting organic geochemical and microscopic analyses. These results support the use of diatom-bound N as a paleoceanographic tool. In contrast to the downcore results of Shemesh et al. (1993), we find that the $\delta^{15}\text{N}$ of diatom-bound organic N is 3-4‰ higher in glacial sediments than in Holocene sediments, in qualitative agreement with the N isotope change which occurs in

bulk sediment N (Francois et al., 1992, 1997).

Materials and Methods

We have studied: (1) a multicore profile from the Antarctic Zone (i.e., south of the Polar Front), in the west Pacific sector, (2) a latitudinal transect of multicore profiles from the central Indian sector, and (3) two Antarctic paleoceanographic-scale cores, one from the Atlantic sector and one from the central Indian sector (Figure 1, Table 1).

The multicore profile (NBP 96-4-2 MC 4) from the Antarctic Zone of the west Pacific sector (64°S, 170°E) is used to study the relationship between bulk sediment and diatom microfossil-bound N during the course of early diagenesis. This core was collected during the Southern Ocean JGOFS site survey cruise of the RV Nathaniel B. Palmer, in September, 1996. The sediment is a nearly pure diatom ooze, with <3% CaCO₃ and no visible clay. Information on accumulation rate is not yet available.

The latitudinal transect of multicores from the Indian sector was collected during the ANTARES 1 cruise of the RV Marion Dufresne, in March-May, 1993 (Gaillard, 1997). We use this transect to test for the existence of a latitudinal gradient in diatom $\delta^{15}\text{N}$. The cores from below the Polar Frontal Zone (48-50°S in this region) show evidence of winnowing, such as abundant large clastics in the tops of some cores, and core recovery was inconsistent in this region. While no direct information on deposition rates is yet available for these cores, our data are consistent with very low sedimentation rates (<1 cm/ky).

Two cores, gravity core AII 107 22 GGC from the Atlantic sector, and piston core MD 84-552 from the Indian, have been studied to address the record of diatom $\delta^{15}\text{N}$ across the last glacial/interglacial transition. Both cores are from the modern Antarctic Zone and have oxygen isotope stratigraphies (Keigwin and Boyle, 1989, L.D. Labeyrie, pers. comm.). Holocene accumulation rates are higher in MD 84-552, in which the last glacial maximum occurs at ~170 cm depth, compared to ~65 cm depth in AII 107-22 GGC.

Four homogenized sediment samples were used during method development, two with a small percentage of clay (from CH 115 26PG and 34PC) and two with significant clay (from AII 107 11PG and 14PC, Table 1). These large samples were taken from cores which have not been used for intensive paleoceanographic studies, so little information is available for these sediments.

To isolate diatom-bound N, we use: (1) physical separation steps to isolate the diatom microfossil fraction from other sedimentary materials, and (2) chemical oxidation of the diatom microfossil fraction, to remove labile organic matter on the exterior of the microfossils.

The physical separation methods largely follow those published by Shemesh et al. (1988), with the addition of two steps: (1) a 10 μm sieving step to aid with clay removal, and (2) a heavy liquids step to remove detrital grains and clays.

We use a similar oxidation procedure to that of (Shemesh et al., 1993; Singer and Shemesh, 1995), which involves an oxidizing acid at 70°C. We use concentrated perchloric acid, rather the nitric acid/perchloric acid mixture used by Shemesh et al. (1993), since the nitric acid represents a potential source of contamination for nitrogen isotopic work.

Protocol For the Isolation of Diatom-Bound N

1) The sediment samples are decarbonated using 25% hydrochloric acid. If this does not adequately disaggregate sample, then the acid is decanted and replaced with deionized water, and the sediments are sonicated using an ultrasonic probe (medium power, 3 minutes).

2) The samples are washed through a 150 μm sieve to remove large radiolaria and detrital material.

Notes: A significant fraction of the diatoms in sediments are >63 μm in diameter, so that sieving at 63 μm typically yields a >63 μm size fraction which is predominantly diatoms.

For samples with an adequate amount of the $>63\ \mu\text{m}$ fraction, we have carried out the perchloric acid treatment and measured its $\delta^{15}\text{N}$, which is similar to the “diatom” size fraction (Figure 10). In order to reduce the required sample size and the time invested in the sieving step, we switched to a $150\ \mu\text{m}$ mesh size.

3) The samples are transferred into 250 ml beakers and the volume is brought up to 200 ml with distilled water. The samples are stirred and left to settle for 1.5 hour, at which time the supernatant (which contains clays and some diatoms) is decanted down to $\sim 30\ \text{ml}$ and saved in a 2 liter plastic container. This is repeated 5 times.

4) The supernatant is run through a $10\ \mu\text{m}$ nylon “mesh sock” to recapture diatoms lost during the settling step. During filtering, a squirt bottle of distilled water is used to keep material from clogging on the mesh. In high-clay sediments, this step is too slow to be practical, so that this step is skipped or a larger pore mesh is used ($20\ \mu\text{m}$). The material remaining on the mesh is transferred back to the sample, using a squirt bottle.

Notes: The “mesh sock” is a 40 cm diameter circle of $10\ \mu\text{m}$ nylon mesh, with its edges clamped over a small piece of core liner. This conical filtering surface reduces clogging by larger particles, which settle to the bottom of the sock. Skipping this step simply reduces the amount of diatoms recovered from a given sediment sample. Isotopic comparison of the $>10\ \mu\text{m}$ and $<10\ \mu\text{m}$ size fractions from a diatomaceous ooze has shown no size dependence of diatom $\delta^{15}\text{N}$.

5) The sample is dried down completely at 65°C in a glass beaker, scraped off the bottom of the beaker, and left to drying is continued for ~ 2 hours. The sample is then transferred to a polypropylene test tube.

6) Sodium polytungstate solution, adjusted to a specific gravity of 2.15, is added to reach a 40 ml volume. The sample is disaggregated using a sonic probe (medium power, 3 minutes). The sample is then centrifuged at $\sim 3000\ \text{rpm}$ for 20 minutes. After centrifugation, the layer of opal-rich material is removed from the top of the polytungstate

solution. If there are concerns regarding remaining clays and aluminosilicates, the centrifugation can be repeated in a new aliquot of sodium polytungstate. In this case, sediment transfers should use the adjusted polytungstate solution.

7) The sample is filtered onto a polycarbonate filter and rinsed several times with DI to remove traces of sodium polytungstate. The sample is then transferred back into a polypropylene centrifuge tube.

8) In a suitable fume hood, 72% perchloric acid is added to each sample up to the 45 ml mark of the centrifuge tube. The sample is placed in a water bath at 70°C overnight. The centrifuge tubes are then removed from the water bath and allowed to cool.

9) The samples are centrifuged, the perchloric acid is decanted, and ~50 ml distilled water is added. The sample is poured into a filter holder with a 47 mm polycarbonate filter. The sample is vacuum-filtered until no liquid remains. 300 mls of distilled water are added and vacuum-filtration is repeated. The filter sides and sediment are rinsed with distilled water using a squirt bottle, while vacuum filtering. The sample is then transferred to a glass vial and dried at 65°C.

Notes: Centrifugation and decanting alone must be repeated >5 times to remove all traces of the acid, causing us to adopt the filtration step. If any acid remains in the dried sediment when samples are packed into tin cups for automated combustion, the tin corrodes quickly and the sediment pellet is lost.

10) If combustion is by elemental analyzer, 10-20 mg of tin powder should be added to the sample to aid in combustion. This can be done by dropping the tin powder into the center of the sediment within the tin capsule and tapping the capsule several times before sealing. This causes the tin powder to sink into the center of the sample pellet.

Isotopic and N Content Analyses

The isotopic and N content analyses were performed on a Europa Roboprep elemental analyzer on-line with a Finnigan MAT 251 stable isotope mass spectrometer. Isotopic values are in permil (‰) units versus laboratory air, which is checked for consistency using several types of calibrated lab standards, including dried solutions of 6-aminocaproic acid, glycine, potassium nitrate and ammonium sulfate. Ammonium sulfate standard solution pipetted onto an acidified glass fiber disk typically yields a standard deviation of 0.15‰. Isotopic measurements of diatom-bound N are less precise because they have a low N content and are bulky, making combustion less intense. The standard deviation for this type of sample is typically 0.3‰ for analysis within a single instrument run, although performance is sometimes significantly better. Our long term precision is somewhat worse, probably because of changes in the sediment combustion conditions (see below), with a standard deviation of ~0.5‰. N content, measured by integration of the mass spectrometer ion peaks, have a typical relative standard deviation of 5-10% for diatom-bound N samples over multiple runs. The sample combustion tube is typically filled to above the “hot zone” by 15 samples, leading subsequent samples to be erroneously low in $\delta^{15}\text{N}$. Therefore, without any adaptation of the elemental analyzer for this sample type, samples must be run in small sets, with several diatom-bound standard samples included to check the quality of combustion throughout the run.

Sample sets run months apart have on occasion shown clear offsets of up to 0.5‰; these offsets were apparent from replicate analyses of a perchloric-treated opal standard. If an offset correction was made, replicate samples were analyzed to check the validity of the correction. This problem has a number of potential sources, such as subtle problems in combustion/reduction conditions or the effect of instrument non-linearity on the integration of the relatively broad sample gas peaks which arise from the combustion of perchloric-treated opal.

We have investigated the option of HF previous to digestion, in order to avoid problems with the combustion of bulky opal samples. While several samples run in this way gave excellent precision, subsequent attempts were unsuccessful because reactions of Fluorine with several of the elemental analyzer reagents. In the future, we will assess several options for the scavenging of fluorine during combustion.

Results

The results of this study are presented in four sections. The order of these sections reflects the general progression of method development, proxy testing, and paleoceanographic application. In the first section, "Characteristics of the diatom microfossil-bound N fraction", we present results on the characteristics of the sedimentary N fraction that is isolated by our method and by similar treatments. In the second section, "Depth variations in the $\delta^{15}\text{N}$ of diatom-bound and bulk sedimentary N", we compare the responses of diatom microfossil-bound N and bulk sedimentary N to early diagenesis. In the third section, "Latitudinal variations in the $\delta^{15}\text{N}$ of diatom-bound N and bulk sedimentary N," we test for a latitudinal gradient in diatom-bound $\delta^{15}\text{N}$ as an indication of its dependence on nitrate utilization in the surface waters above. In the fourth section, "Paleoceanographic records of diatom-bound and bulk sedimentary $\delta^{15}\text{N}$ ", we compare these two potential proxies of sinking flux $\delta^{15}\text{N}$ through the last glacial/interglacial transition.

1. Characteristics of the diatom microfossil-bound N fraction

The progress of the perchloric acid oxidation step provides insight into the nature of the diatom-bound N fraction. Subsamples of a diatomaceous sediment standard (NBP 96-4-3 MC 6, 14-20 cm, 62°S, 170°E) were oxidized with perchloric acid at 70°C for different lengths of time (1 hour, 6 hours, and 20 hours). Because the sediment is a very pure diatomaceous ooze, the physical separation step was not necessary to purify the diatom fraction (as verified by the physical separation and treatment of one subsample). After one hour of oxidation, the diatom microfossil material shows a 3‰ decrease in $\delta^{15}\text{N}$ and a decrease in N content of 5 $\mu\text{mol N/g}$ sediment (Figure 2a). Continued oxidation (with new additions of perchloric acid) have no further effect on either N content or $\delta^{15}\text{N}$. The reproducibility of the isolated N fraction through 20 hours of perchloric acid treatment

suggests either that the surviving N is physically isolated within the diatom microfossils, or that its chemical structure makes it recalcitrant to the chemical oxidant over tens of hours. Physical protection seems more likely, since one would expect a spectrum of reactivities for surviving N that is accessible to the oxidant, which would lead to gradual changes in N content and $\delta^{15}\text{N}$ over the course of the experiment.

The N content results are useful in comparing oxidation treatments. However, there is some uncertainty in the quantitative interpretation of these results, because of a $\leq 25\%$ weight loss which occurs during the perchloric oxidation treatment. This weight loss cannot be attributed to the dissolution of calcite, which is $< 3\%$ of the sediment weight. Opal dissolution and dehydration are two possible mechanisms for this weight loss. While diatom opal is typically $\sim 10\%$ water by weight (Mortlock and Froelich, 1989), water content can be as high as 20%. In addition, the bulk sediments contain a small amount of salt from the sedimentary porewater, as well as other coatings. This appears to increase the hygroscopic nature of the opal, making the bulk sediment noticeably denser than the perchloric-treated sediment, which has been cleaned of these coatings. The weight loss resulting from perchloric acid treatment was recognized late in the course of this study. The determination of its exact cause has been left for future work.

We have also carried out an oxidation time course experiment using bleach as the oxidant (Figure 2b). These results show a continued decrease in N content throughout the experiment, with lower values than observed with perchloric acid, and the $\delta^{15}\text{N}$ of the remaining N also varies with oxidation time. We suspect that the isotopic variations and continued N loss are due to the loss of diatom-bound N during progressive etching and leaching of the microfossils over the course of the treatment, because of the alkaline nature of bleach ($\text{pH} = 11.6$). As with the perchloric acid oxidation, the treatment with bleach causes a $\sim 20\%$ loss in sediment weight. Despite the isotopic variations, which make bleach

a poor choice for the chemical oxidant, the diatom-bound $\delta^{15}\text{N}$ values are within $\sim 1\text{‰}$ of the value which results from perchloric acid treatment.

Other oxidative treatments show roughly similar isotopic results (Table 2).

Treatment with a 1/1 30% H_2O_2 /50% HCl mixture yields a $\delta^{15}\text{N}$ value which is $\sim 0.5\text{‰}$ higher than results from the standard perchloric treatment. Carrying out both the perchloric and peroxide oxidation treatments (in either order) yield similar $\delta^{15}\text{N}$ values to the standard perchloric treatment alone. This suggests that the perchloric acid treatment cleans the diatom surfaces more completely than does the H_2O_2 /HCl solution. Oxidation using either boiling or fuming perchloric acid yield $\delta^{15}\text{N}$ values which are $\sim 0.5\text{‰}$ lower than in the standard perchloric acid treatment, which is at 70°C . In addition, these hotter perchloric acid treatments yield a lower N content for the oxidized opal. These results may indicate that perchloric treatment at 70°C fails to remove a small remaining fraction of the physically vulnerable N which is isotopically enriched due to diagenesis. This suggestion will be tested in the future. However, all further results presented here use the perchloric/ 70°C cleaning procedure described in the protocol. The decrease in $\delta^{15}\text{N}$ which occurs for all of these oxidative treatments is in contrast to the very high $\delta^{15}\text{N}$ values (9-12‰) which resulted from the oxidation of Holocene diatomaceous sediments in the study of Shemesh et al. (1993), although no direct bulk/diatom $\delta^{15}\text{N}$ comparison was presented in that study. We will return to this important discrepancy in a later section.

The clay fraction in marine sediments can contain a similar or higher concentration of organic N after oxidation than does the diatom fraction. The isotopic effect of this fraction has been tested by oxidation of clay-bearing sediments, with and without previous removal of the clay fraction (Table 3). The N content of sediments after perchloric acid treatment alone is similar to or higher on a per-gram basis than that of the sample after both clay removal and perchloric acid treatment, suggesting that clays protect as much or more N than the cleaned diatoms (far-right columns in Table 3). The clays generally appear to

contribute N with a higher $\delta^{15}\text{N}$ than the diatom fraction (middle columns in Table 3), which indicates the need to remove the clay fraction in order to make reliable isotopic measurements of the diatom-bound organic N fraction.

Stevenson and Cheng (1970) noted low recovery of amino acids from clay-rich sediments using 6 N HCl extraction alone. Addition of an HF pretreatment increased recoveries, suggesting the protection of amino acids by clays. These authors concluded that amino acids are "keyed" into hexagonal holes on the interlamellar surfaces of expanding-lattice clays. The existence of a clay-bound N fraction which survives the oxidation step and which is present at per-gram concentrations similar to diatom N raises the concern that the diatom-bound organic N fraction may have been irreversibly absorbed from the sediments, rather than being native to the diatoms. While the chemical mechanism of absorption would be different from that of clays, protection of organic matter by diverse mineral surfaces is recognized as an important process (Mayer, 1994). To address this concern, we have undertaken microscopic and pyrolysis/gas chromatography/mass spectrometry investigations of the diatom-bound organic matter. As described below, the results argue against an absorptive origin for diatom-bound N, but they do not absolutely preclude it.

Both transmitted and reflected light microscopy reveal disseminated, amorphous organic matter in unoxidized diatomaceous sediment (Figure 3a). The perchloric acid step completely removes all of this microscopically visible organic matter (Figure 3b). The organic matter surviving the oxidation step is either internal to the microfossils or adsorbed onto their surfaces.

When excited with 450-490 nm light, the diatom microfossils in both perchloric-treated and untreated sediment fluoresce an intense yellow-green, indicating the presence of relatively unaltered organic matter (Figure 3c, Senftle et al., 1993). The distribution of this fluorescence does not correspond to the disseminated organic matter that is visible under

white light in untreated sediments, suggesting that this disseminated organic matter is not related to the fluorescent organic matter associated with the microfossils. Neither the intensity nor the color of the microfossil fluorescence is noticeably altered by the perchloric oxidation step, suggesting that the oxidation step does not degrade or alter the fluorescent organic matter. Since only the microfossils fluoresce in both untreated and oxidized sediments, the fluorescent organic matter within the microfossil fraction has probably not been absorbed from the sedimentary environment.

We have used HF digestion to isolate the organic material surviving the perchloric acid treatment. HF addition causes quantitative digestion of the opal, yielding a tan-colored solution. Evaporation to dryness under a heat lamp leaves a dark brown residue. Pyrolysis/gas chromatography/mass spectrometry of this residue yields N-rich pyrolysis products, dominated by pyridines, pyrroles, and aromatic nitriles, consistent with a protein source (Figure 4a, Table 4a, Irwin, 1982; Tsuge and Matsubara, 1985). The molar C/N of the diatom-bound organic matter tends to range between 5 and 7 (Table 5), also consistent with protein. Swift and Wheeler (1992) report that an oxidative treatment of cultured diatom microfossils yields a compositionally distinct proteinaceous material which is apparently internal to the microfossils, supporting a diatom-native origin for our isolated organic matter. Free amino acids are scarce in the sedimentary environment (Whelan, 1977), so their absorption cannot account for diatom-bound N. Peptide absorption from the sediments into the microfossil matrix remains a possibility, albeit a remote one.

Pyrolysis products of sugars are relatively unimportant (Figure 4b, Table 4b, Helleur, 1987), despite the abundance of this material in marine particulates (Alldredge and Silver, 1988). While sugars are an important component of diatom cell walls, temporal studies of diatom cell wall composition indicate that protein provides the template for silicification (Volcani, 1982; Blank et al., 1986), consistent with its dominance in diatom microfossils from sediments. Swift and Wheeler (1992) find that carbohydrates are about

one-third as abundant (by weight) as protein in the bleach-treated microfossils of cultured diatoms. These authors also observe significant levels of phosphate, suggestive of protein phosphorylation. This observation is interesting in light of the fact that we have observed phosphoric acid as a pyrolysis product from our isolated diatom-bound organic matter.

Alkane/alkene doublets from long-chain fatty acids, observed in the pyrolysis of bulk algal biomass (e.g., Peulve, 1995), are absent in the cleaned diatom sample. However, the pyrolysis products of a number of short-chain mono-, di-, and tricarboxylic fatty acids were recognized (Figure 4c, Table 4c). These compounds probably come from triglycerides, and their chemistry is suggestive of a role in silicification (J. Whelan, pers. comm.). The lack of long-chain fatty acids argues against permeation of the microfossil matrix by organic matter from the sedimentary diagenetic environment.

The evidence for protein, the paucity of polysaccharides, and the absence of long-chain fatty acids are all consistent with the notion that the isolated organic N was incorporated into the microfossils during silicification (Hecky et al., 1973; Volcani, 1982; Blank et al., 1986; Swift and Wheeler, 1992), but they do not absolutely preclude the possibility of some absorption from the sedimentary environment. Future work will focus on a compositional comparison of the organic matter in cleaned and uncleaned sedimentary diatom microfossils, to provide a clear picture of the N functionalities both within the microfossils and in the sedimentary environment. In order to assess the possibility of N absorption more directly, we will analyze both treated and untreated microfossils for the non-protein amino acids β -alanine and γ -aminobutyric acid, which are of microbial origin and have been used as indicators of early diagenesis (Cowie and Hedges, 1994; Henrichs et al., 1984; Lee and Cronin, 1982; Schroeder, 1975). In any case, the data in hand are highly suggestive that diatom-bound organic N, as isolated from sediments, is native to diatoms.

2. Depth variations in the $\delta^{15}\text{N}$ of diatom-bound and bulk sedimentary N

To investigate the effect of diagenesis on bulk sedimentary N and diatom-bound N, we measured a 0.5-1.0 cm scale depth profile of N content and $\delta^{15}\text{N}$ before and after treatment with perchloric acid in a multicore taken in diatom ooze from the Antarctic Zone in Pacific sector of the Southern Ocean (NBP 96-4-2 MC 4, Figure 5). These sediments are almost entirely diatomaceous, with a small percentage of radiolaria and $<3\%$ CaCO_3 (with the carbonate being dissolved upon perchloric acid addition). As a result, there was no need to carry out the physical separation on these sediments. To confirm this, a subsample of the 13-14 cm depth interval was treated with perchloric acid both with and without prior physical separation steps, with no measurable difference in $\delta^{15}\text{N}$ or N content.

Bulk sediment N content decreases with depth (Figure 5b), as is commonly observed in surface sediments. However, the concentration of organic N which survives the perchloric oxidation is constant with depth. In the deeper part of the core, the N content of the untreated sediment converges on the N content of the oxidized sediment, implying that physical protection plays an important role in sedimentary N preservation.

The bulk sediment $\delta^{15}\text{N}$ is 3-5‰, which is ~4‰ higher than the estimated sinking flux $\delta^{15}\text{N}$ in the Antarctic Zone, based on nitrate isotopic data (0-1‰, see Chapter 4). This sinking flux/bulk sediment $\delta^{15}\text{N}$ offset is consistent with comparisons of sediment trap and surface sediment $\delta^{15}\text{N}$ from other open ocean regions, which have revealed a “diagenetic offset” of 3-5‰ (Altabet and Francois, 1994a).

The oxidized sediment $\delta^{15}\text{N}$ is 0.8-2.0‰, ~3‰ lower than that of bulk sediment and therefore closer to the expected $\delta^{15}\text{N}$ of integrated sinking flux. Holocene diatom-bound $\delta^{15}\text{N}$ from all other Antarctic sites in this study are similarly between 0.5 and 2.0‰. The ~3‰ difference between diatom-bound and bulk sediment $\delta^{15}\text{N}$ is qualitatively consistent with a direct surface ocean source for diatom-bound N, as it would not have undergone the 3-5‰ increase in $\delta^{15}\text{N}$ associated with diagenesis on the seafloor.

The $\delta^{15}\text{N}$ of bulk sediment in MC 4 shows several depth variations which coincide with changes in N content. The uppermost section of the core, which contains a "fluff layer," is characterized by a high bulk sediment N content and a $\sim 1\text{‰}$ lower $\delta^{15}\text{N}$ than the underlying sediment. Similar patterns have been observed for bulk sediment profiles from the equatorial Pacific and appear to reflect the incorporation of the recent biogenic rain into the sediment column (M. Altabet, unpublished). Another shift in bulk sediment $\delta^{15}\text{N}$ occurs at 8-12 cm depth and coincides with a downcore decrease in bulk sediment N content. The depth variations in bulk sediment $\delta^{15}\text{N}$ are not matched by variations in oxidized sediment $\delta^{15}\text{N}$. This suggests that the bulk sediment variations are diagenetic and that these diagenetic changes do not affect the diatom-bound organic N. Both bulk and diatom-bound N show gradual $\sim 1\text{‰}$ decreases in $\delta^{15}\text{N}$ with depth. This change may reflect a longer time scale diagenetic effect on the diatom-bound organic N or may represent a long term change in the isotopic composition of the sinking flux reaching the seafloor.

The $\delta^{15}\text{N}$ offset between bulk and diatom-bound N is roughly constant down the entire multicore profile, while the difference in N content decreases to low levels in the deeper part of the core (Figure 5). This implies that the $\delta^{15}\text{N}$ of the organic N removed by chemical oxidation increases with depth, becoming enriched as the size of the labile organic N pool decreases. While isotopic enrichment is expected for the bacterial consumption of a sedimentary N pool (Macko et al., 1993), the degree of enrichment must be verified as reasonable.

The amount of N removed during perchloric treatment and its $\delta^{15}\text{N}$ can be estimated by a mass balance calculation using N content and $\delta^{15}\text{N}$ data. However, our estimates are complicated by the $\leq 25\%$ loss of mass which occurs during the perchloric acid step (see previous section). If we assume that the mass loss causes no loss of opal-bound N (i.e., we make the maximum weight loss correction), then the amount of N removed by the oxidation is $\geq 8 \mu\text{mol}$ per gram of microfossils (Figure 6a). If we assume that diatom-

bound N is lost in equal proportion to the apparent opal weight loss during the perchloric acid step (i.e., we make no weight loss correction), then the calculated amount of N removed by the oxidation is $\geq 2.75 \mu\text{mol}$ per gram of microfossils (Figure 6b). The calculated $\delta^{15}\text{N}$ of the N removed is higher for the second case, in which the observed $\delta^{15}\text{N}$ change between treated and untreated microfossils must be accounted for by a smaller amount of N loss. The $\delta^{15}\text{N}$ of N lost during oxidation is $\leq 13\text{‰}$ in the first case and $\leq 35\text{‰}$ in the second case (Figure 6). The $\delta^{15}\text{N}$ of this removed N is high, especially in the case of no mass loss correction. If the case of no mass loss correction were taken as appropriate, the apparently extreme isotopic enrichment of the removed N would raise the concern that the perchloric acid step somehow alters the isotopic composition of the surviving organic matter, rather than removing an isotopically distinct N pool.

Several points argue against this possibility. First, the use of other oxidants typically yield similar isotopic values. Although 0.5-1‰ differences have been noted for different oxidants, the oxidized fraction is always significantly lighter than the unoxidized sediment, regardless of the oxidant used (Table 2). Second, the $\delta^{15}\text{N}$ depth profile for oxidized sediment is simpler than the profile of unoxidized sediment, so that diatom-bound $\delta^{15}\text{N}$ does not behave as bulk sediment $\delta^{15}\text{N}$ with an isotopic offset. This same observation can be made from many of the results in this study. Third, barring a major contribution from contaminant N in all of the cleaning methods, for which there is no evidence, it is unavoidable that the oxidation step removes a high $\delta^{15}\text{N}$ fraction of the sedimentary N. The isotopic change occurs upon the first hour of perchloric acid treatment but does not continue to occur for longer periods of treatment (Figure 2a). If isotopic alteration of the entire N pool was responsible for the $\delta^{15}\text{N}$ change, it would need to occur quickly and then cease altogether, which seem unlikely. Given these observations, the removal of an isotopically enriched pool is the best explanation for the $\delta^{15}\text{N}$ change upon perchloric acid treatment, although the removed N is probably not as high in $\delta^{15}\text{N}$ as suggested by the “no

weight loss correction" case (Figure 6). Thus, these profile data suggest that diatom-bound N is (1) an important fraction of sedimentary N in diatomaceous sediments, (2) unaltered by early diagenesis, and (3) isotopically distinct from the diagenetically vulnerable N pool, which undergoes isotopic enrichment as it is degraded.

3. Latitudinal variations in the $\delta^{15}\text{N}$ of diatom-bound and bulk sedimentary N

Once we are confident that the N fraction we are isolating is protected from early diagenesis, we need to address whether the $\delta^{15}\text{N}$ of the diatom-bound N varies with nitrate utilization. We attempt to link the $\delta^{15}\text{N}$ of the diatom-bound N to nitrate utilization by using the latitudinal gradient in nitrate utilization in Southern Ocean surface waters, as done for bulk sediments by Francois et al. (1992) and Altabet and Francois (1994a). The sediments used for this purpose are from the ANTARES 1 multicores collected along a latitudinal transect in the Indian sector of the Southern Ocean, between the islands of Kerguelen and Crozet in the Indian sector (Figure 1, Table 1).

$\delta^{15}\text{N}$ and N content were measured for both bulk sediment and the diatom-bound N fraction at a number of depths in the ANTARES 1 cores (Figure 7). The bulk sediment $\delta^{15}\text{N}$ decreases to the South. A similar decrease in bulk sediment $\delta^{15}\text{N}$ observed in the east Indian sector has been interpreted as being due to a latitudinal gradient in nitrate utilization (Francois et al., 1992). The bulk $\delta^{15}\text{N}$ gradient across the transect of cores used in this study is only 2-3‰ (Figure 7a). Surface sediments further to the North increase to 7.5‰, yielding a total bulk $\delta^{15}\text{N}$ latitudinal gradient of ~3.5‰. Nevertheless, this gradient is lower than the 6-8‰ latitudinal gradient observed in the eastern Indian sector (Francois et al., 1992) and is mostly associated with the $\delta^{15}\text{N}$ decrease into the high-opal Antarctic sediments south of 50°S. Downcore changes in both bulk sediment and diatom-bound $\delta^{15}\text{N}$ are also evident in the different multicores. As described below, these depth variations

probably represent glacial/interglacial stratigraphy in these cores, due to low overall sedimentation rates.

The diatom-bound $\delta^{15}\text{N}$ shows a larger latitudinal gradient, with a decrease of about 4‰ toward the South. This gradient suggests that diatom-bound $\delta^{15}\text{N}$ is related to the $\delta^{15}\text{N}$ of the integrated N sinking flux or, by extension, to nitrate utilization. Without these results, we could not have assumed a link between diatom-bound $\delta^{15}\text{N}$ and nitrate utilization. While the integrated flux $\delta^{15}\text{N}$ is linked to nitrate utilization by mass balance, any specific N pool is not similarly constrained (Altabet, 1988). For instance, surface suspended particulate N $\delta^{15}\text{N}$ variation is controlled by a number of processes, including the incorporation of isotopically light recycled nitrogen (Checkley and Entzeroth, 1985). Surface PN from the Southern Ocean is frequently lower in $\delta^{15}\text{N}$ than it would be if it simply reflected the incorporation of nitrate by phytoplankton (Altabet and Francois, 1994b, M. Altabet, unpublished). However, the covariation of diatom $\delta^{15}\text{N}$ with the latitudinal gradient in nitrate utilization would suggest that the diatoms are tracking the nitrate cycle, at least to the first order. This is consistent with recent suggestions that diatoms are the primary consumers of nitrate in the Southern Ocean, with other phytoplankton predominantly using recycled N (R. Dugdale, unpublished; see Chapter 4).

If we assume a simple model of vertical nitrate supply to the surface in this region, then we can use the Rayleigh fractionation integrated product equation to model the variation of diatom-bound $\delta^{15}\text{N}$ as a function of nitrate utilization in the overlying surface waters. If we assume that the southern end underlies Antarctic surface waters in which nitrate utilization is 20% (typical for the Antarctic zone), and that the northern end represents nearly complete nitrate utilization, then the ~4‰ $\delta^{15}\text{N}$ increase from South to North, associated with a 80% change in nitrate utilization, indicates a fractionation factor for nitrate uptake of ~5‰. This fractionation factor value is similar to that estimated from water column $\delta^{15}\text{NO}_3$ data (see Chapter 4).

However, there are important caveats regarding this calculation, involving the expected gradient in the sinking flux $\delta^{15}\text{N}$ from 52 to 46°S in this region. The first is that nitrate is probably not completely consumed in the surface waters overlying KTB 21, the multicore at 46°S, which is classified by Park and Gamberoni (1997) as being in the Polar Frontal Zone (Figure 7). The second caveat is that the hydrography in this region is not comparable to that in other sectors of the Southern Ocean, in particular, in the breadth of the Polar Frontal Zone (Figure 7) and the narrowness of the Subantarctic (Figure 1). As a result, it is difficult to generalize from other data (Chapter 4) as to the isotopic composition of the nitrate supply and the mechanism of nitrate transport, both of which affect the applicability of the Rayleigh fractionation integrated product equation to model the $\delta^{15}\text{N}$ of the export flux. Last, sediment transport below the Southern Ocean fronts appears to control sediment deposition in this region, so that the expectation of an exact latitudinal correspondence between surface conditions and the underlying sediments may not be reasonable. These data provide confirmation that diatom-bound N varies with nitrate utilization in the surface ocean. However, until the uncertainties described above are addressed, we cannot provide a robust quantification of the link between diatom $\delta^{15}\text{N}$ and nitrate utilization.

Below 10 cm depth in the intermediate latitude ANTARES 1 multicores (KTB11, 49°S and KTB 13, 50°S), there are high values for both bulk $\delta^{15}\text{N}$ and diatom-bound $\delta^{15}\text{N}$, which are inconsistent with a simple latitudinal gradient in nitrate utilization (Figure 7a). A depth profile of KTB 13 shows that diatom-bound $\delta^{15}\text{N}$ increases below 10 cm (Figure 8a). At this same depth, sedimentary Ba decreases downward, while Al increases (Figure 8c). KTB 13 most likely represents a condensed stratigraphic section, with the last glacial/interglacial transition occurring at a depth of only ~14 cm. The $\delta^{15}\text{N}$, Ba, and Al data are all consistent with this interpretation (Francois et al., 1997). The occurrence of the glacial/interglacial transition at ~14 cm suggests a low sedimentation rate of <1 cm/ky.

Observations of low sedimentation rate, winnowing, and scouring are common under the Polar Frontal Zone, where current speeds are typically highest (Heezen and Hollister, 1971). Thus, while the low $\delta^{15}\text{N}$ values observed near the surface are appropriate for the low degree of nitrate utilization in the surface waters overlying the site today, sediments below ~10 cm depth do not correspond to Holocene conditions.

The diatom-bound N content is not correlated with latitudinal variations in bulk sediment N content (Figure 7b). This decoupling is consistent with the results from the multicore profile MC 4 discussed above, reinforcing the interpretation that diatom-bound N does not vary due to early diagenetic or sedimentary processes. If there is a latitudinal trend in the diatom-bound N content data, it is of higher values in the more southern sediments, which are diatom oozes. In these sediments, diatom-bound N content is very close to that of bulk sediment, while the $\delta^{15}\text{N}$ differences between diatom-bound N and bulk sediment are largest in these cores (2-4‰, Figure 7a). As with the profile from MC 4, these results require that the small fraction of organic N removed from the opal-rich sediments during the perchloric acid step is isotopically enriched.

By contrast, in the clay-rich northernmost multicores (KTB 19, KTB 21), bulk sediment and diatom-bound $\delta^{15}\text{N}$ are only ~1‰ different (Figure 7a). Thus, there is a northward decrease in the $\delta^{15}\text{N}$ difference between bulk sediment and diatom-bound N (Figure 7a), despite a northward increase in the amount of N being removed by the diatom separation and oxidation steps (Figure 7b). This suggests that the $\delta^{15}\text{N}$ of the diagenetically vulnerable N increases as the size of this N pool decreases, as would result from isotopic fractionation during microbial and geochemical decomposition (references in Macko et al., 1993). Increasing $\delta^{15}\text{N}$ with decreasing N pool size was also inferred for the diagenetically vulnerable N in the depth profile of MC4 from the Antarctic Zone of the Pacific sector (previous section). Alternatively, one could attempt to explain the latitudinal change in the diatom/sediment $\delta^{15}\text{N}$ difference as being due to a latitudinal change in the relationship

between diatom-bound $\delta^{15}\text{N}$ and the N sinking flux. However, the similarity of N content and C/N ratios suggest no large compositional change in this material, arguing against this type of explanation (Figure 7b, Table 5). Future work will attempt to address this concern more directly, by both isotopic and organic geochemical analysis of diatom-bound organic matter. Nevertheless, given the other results in this study, it seems far more likely that diagenetically-driven differences in bulk sediment $\delta^{15}\text{N}$ are responsible for the latitudinal gradient in the diatom/bulk sediment $\delta^{15}\text{N}$ offset.

Diatom-bound N content in these multicores appears to decrease with depth in cores KTB 6 (52°S) and KTB 13 (50°S), and KTB 11 (49°S) (Figure 7b, Figure 8b). In the paleoceanographic profiles described below, there is evidence for a similar gradual decrease in diatom-bound N content with age. This decrease is probably apparent in the ANTARES 1 multicores because of their low inferred sedimentation rates. This suggests that diatom-bound N is vulnerable to diagenesis on a time scale of ≥ 10 kyrs, which will be a concern for longer time scale paleoceanographic work.

4. Paleoceanographic records of the $\delta^{15}\text{N}$ of diatom-bound and bulk sedimentary N

We have generated N isotopic data on both cleaned diatom material and bulk sediment from two long cores from the Antarctic Zone: gravity core AII 107-22 GGC from the Atlantic sector (55°S, 3°W, 2768 m), and piston core MD 84-552 from the Indian sector (55°S, 74°E, 2230 m).

Both cores show the glacial/interglacial bulk sediment $\delta^{15}\text{N}$ change which has been recognized throughout the Antarctic Zone (Figures 9, 10, Francois et al., 1997). The higher $\delta^{15}\text{N}$ values of the glacial-age sediment have been interpreted as reflecting a higher degree of nitrate utilization in the Antarctic during the last ice age. However, the bulk $\delta^{15}\text{N}$ records from these two cores differ substantially. In AII 107-22 GGC, the maximum glacial/interglacial difference in bulk $\delta^{15}\text{N}$ is the $\sim 2\text{‰}$ shift at 50 cm, but bulk $\delta^{15}\text{N}$

increases back to higher values near the top of the core. In MD 84-552, the glacial sediments are up to 5‰ higher in $\delta^{15}\text{N}$ than the Holocene sediments, and the Holocene section does not show a significant increase toward the top of the core. If these changes are interpreted strictly in terms of nitrate utilization, they imply very different histories of nitrate utilization for these two regions since the last ice age. Specifically, bulk sediment data from AII 107 22 GGC (in the Atlantic sector) would imply roughly half the amount of nitrate utilization change suggested by MD 84-552 (in the central Indian sector). For the most part, the differences between these two cores involve the Holocene portion of the record. Holocene bulk sediment $\delta^{15}\text{N}$ is $\geq 4\text{‰}$ in 22 GGC, as opposed to 2-3.5‰ in 84-552, and it increases to 5-6‰ toward the surface in the Holocene section of 22 GGC. This would imply higher nitrate utilization in the Holocene Atlantic sector, with utilization increasing over the course of the Holocene back to near-glacial levels.

The cleaned diatom $\delta^{15}\text{N}$ records show the same sense of glacial/interglacial change as the bulk sediment $\delta^{15}\text{N}$ records, with higher values in the glacial section (Figures 9, 10). These results suggest that the glacial/interglacial bulk sediment $\delta^{15}\text{N}$ change was not solely due to diagenetic processes; both the bulk sediment and diatom-bound N data suggest that the $\delta^{15}\text{N}$ of the N sinking flux out of the surface ocean was higher during the last ice age. Given our understanding of the Southern Ocean N isotope dynamics, a change in nitrate utilization in surface waters is the simplest explanation for this sinking flux change (Altabet and Francois, 1994b; see Chapter 4).

While the amplitude of the glacial/interglacial change differs significantly for the two bulk sediment records, the diatom $\delta^{15}\text{N}$ records are more similar to one another. Although the depth resolution of the diatom $\delta^{15}\text{N}$ samples are too sparse to allow for a rigorous comparison, the glacial/interglacial amplitude for both cores is 3-4‰. Based on these diatom $\delta^{15}\text{N}$ data, we conclude that the glacial/interglacial change in the $\delta^{15}\text{N}$ of the sinking flux was similar in the Atlantic and Indian sectors of the Southern Ocean, as would

be expected based on the continuity of zonal circulation in these sectors of the Southern Ocean.

The main difference in the two diatom records is that the Holocene section in AII 107-22 GGC is 0.5-1‰ higher than in MD 84-552. If this difference in the Holocene sections reflects real differences in sinking flux $\delta^{15}\text{N}$ between these two regions, they suggest a difference in nitrate utilization of 15-30% (that is, 20% utilization at the site of MD 84-552 compared with 35-50% utilization at AII 107-22 GGC). However, this isotopic difference approaches the long term precision of the measurement ($\sim 0.5\text{‰}$) and thus should not be overinterpreted. The greater consistency between the two diatom $\delta^{15}\text{N}$ records may indicate that they provide a more reliable record of sinking flux changes than do the bulk sediment records. For instance, the diatom $\delta^{15}\text{N}$ record from 22 GGC suggests that the bulk sediment $\delta^{15}\text{N}$ increase in the top 30 cm of 22 GGC could be interpreted as a diagenetic change, associated with the loss of sedimentary N with depth (Figure 9b).

AII 107 22 GGC (55°S, 3°W, 2768 m) is from the same region as RC 13-271 (52°S, 5°E, 3634 m) and RC 13-256 (53°S, 0°E, 3243 m), the cores studied by Shemesh et al. (1993). These authors observed diatom $\delta^{15}\text{N}$ values of about 5‰ in sediments of glacial age (similar to our glacial values) but saw an increase to values between 9 and 12‰ in Holocene sediments (different from our Holocene values of $\sim 1\text{--}2\text{‰}$ at 22 GGC). This change would imply a decrease in nitrate utilization during the last glacial, the opposite conclusion to the one reached here.

Several aspects of the Shemesh et al. data are puzzling. First, the amplitude of the glacial $\delta^{15}\text{N}$ decrease is significantly greater than we would expect from a nitrate utilization control on diatom $\delta^{15}\text{N}$. Even assuming a very high fractionation factor, the glacial/interglacial $\delta^{15}\text{N}$ difference would correspond to a physically impossible "negative" degree of nutrient utilization during the last ice age. Second, the core-top diatom $\delta^{15}\text{N}$ of Shemesh et al. is $\sim 10\text{‰}$ higher than that of the sinking flux in the Antarctic (estimated from

nitrate isotopic data, Chapter 4) and of typical surface sediments in that region. While this isotopic enrichment of diatom bound $\delta^{15}\text{N}$ is possible, it seems unlikely.

We have consistently observed diatom $\delta^{15}\text{N}$ values between 0.5 and 2.0‰ for Holocene Antarctic sediments from the Atlantic, Indian, and Pacific sectors. These diatom $\delta^{15}\text{N}$ values, which are lower than bulk sediment $\delta^{15}\text{N}$ by 2-4‰, are consistent with the observation of a 3-5‰ diagenetic increase in bulk sedimentary N relative to the N sinking flux (Altabet and Francois, 1994a). In addition, we have observed similarly low diatom $\delta^{15}\text{N}$ values from a range of chemical cleaning methods (Table 2). Given these results on Southern Ocean surface sediments, we are confident that Holocene diatom-bound $\delta^{15}\text{N}$ from the Antarctic is lower, not higher, than bulk sediment $\delta^{15}\text{N}$.

We do not know the origin of the difference between our results and those of Shemesh et al. (1993). One explanation for the difference is that the use of nitric acid in the oxidative cleaning step of Shemesh et al. resulted in contamination of the diatom-bound N, leading to erroneous isotopic results. However, this does not explain the similarity of their glacial-age diatom $\delta^{15}\text{N}$ values to our results for glacial-age Antarctic sediments. Ongoing work is aimed at evaluating this and other possible causes for the disagreement between the results of Shemesh et al. and those reported here.

Our diatom N results support the conclusion, reached previously from the bulk sediment $\delta^{15}\text{N}$ data, that the sinking flux $\delta^{15}\text{N}$ out of the surface Antarctic was higher during the last glacial. While the latitudinal transect results demonstrate a qualitative link between sinking flux $\delta^{15}\text{N}$ and diatom $\delta^{15}\text{N}$, the quantitative aspects of the sinking flux/diatom $\delta^{15}\text{N}$ link must be understood before diatom $\delta^{15}\text{N}$ can be used confidently as a quantitative proxy for sinking flux $\delta^{15}\text{N}$. Assuming for the time-being that diatom-bound $\delta^{15}\text{N}$ variations reflect the same amplitude of sinking flux variations, and using a nitrate uptake fractionation factor of 5‰ (Chapter 4), the glacial/interglacial change in Antarctic

nitrate utilization suggested by the 3-4‰ change in diatom-bound $\delta^{15}\text{N}$ is roughly 70-80%, that is, 90-100% in the glacial compared to ~20% in the modern Antarctic.

Complete nutrient utilization in surface Antarctic during the last ice age seems unlikely and suggests that some aspect of our Rayleigh fractionation-based calculation is inaccurate. Under the hypothesized glacial conditions of increased stratification and higher nitrate utilization, much about the N isotope dynamics of the Antarctic might have been different (Francois et al., 1997). There are reasonable mechanisms by which these changes could have lead to changes in either the isotopic composition of the nitrate supply or the fractionation factor of nitrate uptake, which are central parameters in the nitrate utilization/N isotope relationship. A discussion of these potential changes is beyond the scope of this paper. However, consideration of the possibilities is a more valuable exercise now that we are more confident that a glacial/interglacial change in sinking flux $\delta^{15}\text{N}$ has occurred.

Conclusions

Diatom-bound organic N appears to be unaltered by early bacterial diagenesis, although its concentration decreases gradually in paleoceanographic records. This organic N appears to be proteinaceous, suggesting that it survives early diagenesis due to physical protection within the opal matrix, rather than because of chemical resistance. Our results are most consistent with a diatom-native origin for diatom-bound N, but they do not absolutely preclude the possibility that organic N is scavenged from sediments.

Our downcore results on diatom microfossil-bound organic N suggest that the $\delta^{15}\text{N}$ of the sinking flux was 3-4‰ higher during the last glacial, supporting the interpretation that the previously reported glacial/interglacial change in bulk sediment $\delta^{15}\text{N}$ had its origins in the upper ocean, rather than being due to diagenetic or sedimentary processes. The simplest explanation for such an upper ocean change in the N isotopes is that surface Antarctic nitrate utilization was higher during the last ice age.

Acknowledgements

Jean Whelan and Lorraine Eglinton both helped generously with the pyr/gc/ms and microscopic studies. Thanks are also owed to Jim Broda and Eben Franks for their help in the lab. The first author was supported by the NSF Graduate Research Fellowship Program and by the JOI/USSAC Ocean Drilling Graduate Research Fellowship Program.

References

- Allredge, A.L. and Silver, M.W., 1988. Characteristics, dynamics, and significance of marine snow. *Progress in Oceanography*, 20: 41-82.
- Altabet, M.A., 1988. Variations in nitrogen isotopic composition between sinking and suspended particles: implications for nitrogen cycling and particle transformation in the open ocean. *Deep-Sea Research*, 35: 535-554.
- Altabet, M.A., Deuser, W.G., Honjo, S. and Stienen, C., 1991. Seasonal and depth-related changes in the source of sinking particles in the North Atlantic. *Nature*, 354: 136-139.
- Altabet, M.A. and Francois, R., 1994a. Sedimentary nitrogen isotopic ratio as a recorder for surface ocean nitrate utilization. *Global Biogeochemical Cycles*, 8(1): 103-116.
- Altabet, M.A. and Francois, R., 1994b. The use of nitrogen isotopic ratio for reconstruction of past changes in surface ocean nutrient utilization. In: R. Zahn, M. Kaminski, L. Labeyrie and T.F. Pederson (Editors), *Carbon Cycling in the Glacial Ocean: Constraints on the Ocean's Role in Global Change*. NATO ASI series. Springer Verlag, Berlin, Heidelberg, New York, pp. 281-306.
- Altabet, M.A. and McCarthy, J.J., 1985. Temporal and spatial variation in the natural abundance of ^{15}N in PON from a warm-core ring. *Deep-Sea Research*, 32: 755-772.
- Blank, G.S., Robinson, D.H. and Sullivan, C.W., 1986. Diatom mineralization of silicic acid. VIII. Metabolic requirements and the timing of protein synthesis. *Journal of Phycology*, 22: 238-239.
- Checkley and Entzeroth, 1985. Elemental and isotopic fractionation of carbon and nitrogen by marine, planktonic copepods and implications to the marine nitrogen cycle. *Journal of Plankton Research*, 7: 553-568.
- Cowie, G.L. and Hedges, J.I., 1994. Biochemical indicators of diagenetic alteration in natural organic matter mixtures. *Nature*, 369: 304-307.
- Francois, R., Altabet, M.A. and Burkle, L.H., 1992. Glacial to interglacial changes in surface nitrate utilization in the Indian sector of the Southern Ocean as recorded by sediment $\delta^{15}\text{N}$. *Paleoceanography*, 7: 589-606.
- Francois, R.F., Altabet, M.A., Yu, E.-F., Sigman, D.M., Bacon, M.P., Frank, M., Bohrmann, G., Bareille, G. and Labeyrie, L.D., 1997. Water column stratification in the Southern Ocean contributed to the lowering of glacial atmospheric CO_2 . *Nature*, in press.
- Gaillard, J.-F., 1997. ANTARES-1: a biogeochemical study of the Indian sector of the Southern Ocean. *Deep-Sea Research*, 44(5): 951-962.
- Hayes, J.M., Popp, B.N., Takigiku, R. and Johnson, M.W., 1989. An isotopic study of biogeochemical relationships between carbonates and organic carbon in the Greenhorn Formation. *Geochimica et Cosmochimica Acta*, 53: 2961-2972.

- Hecky, R.E., Mopper, K., Kilham, P. and Degens, E.T., 1973. The amino acid and sugar composition of diatom cell-walls. *Marine Biology*, 19: 323-331.
- Heezen, B.C. and Hollister, C.D., 1971. *The Face of the Deep*. Oxford University Press, New York, 657 pp.
- Helleur, R.J., 1987. Characterization of the saccharide composition of heteropolysaccharides by pyrolysis-capillary gas chromatography-mass spectrometry. *Journal of Analytical and Applied Pyrolysis*, 11: 297-311.
- Henrichs, S.M., Farrington, J.W. and Lee, C., 1984. Peru upwelling region sediments near 15°S. 2. Dissolved free and total hydrolyzable amino acids. *Limnology and Oceanography*, 29(1): 20-34.
- Irwin, W.J., 1982. Analytical Pyrolysis. *Chromatographic Science*, 22. Marcel Dekker, New York, 577 pp.
- Keigwin, L.D. and Boyle, E.A., 1989. Late quaternary paleochemistry of high-latitude surface waters. *Paleogeogr. Palaeoclim. Paleoecol.*, 73: 85-106.
- Lee, C. and Cronin, C., 1982. Particulate amino acids in the sea: Effect of primary productivity and biological decomposition. *Journal of Marine Research*, 40: 1075-1079.
- Macko, S.A., Engel, M.H. and Parker, P.L., 1993. Early diagenesis of organic matter in sediments: assessment of mechanisms and preservation by the use of isotopic molecular approaches. In: M.H. Engel and S.A. Macko (Editors), *Organic Geochemistry: Principles and Applications*. Plenum Press, New York, pp. 185-210.
- Mayer, L., 1994. Surface area control of organic carbon accumulation in continental shelf sediments. *Geochimica et Cosmochimica Acta*, 58(4): 1271-1284.
- Montoya, J.P., 1990. Natural abundance of ^{15}N in marine and estuarine plankton: studies of biological isotopic fractionation and plankton processes. Ph.D. Thesis, Harvard University, 403 pp.
- Montoya, J.P., 1994. Nitrogen isotope fractionation in the modern ocean: implications for the sedimentary record. In: R. Zahn, M. Kaminski, L. Labeyrie and T.F. Pederson (Editors), *Carbon Cycling in the Glacial Ocean: Constraints on the Ocean's Role in Global Change*. NATO ASI series. Springer Verlag, Berlin, Heidelberg, New York, pp. 259-279.
- Montoya, J.P. and McCarthy, J.J., 1995. Isotopic fractionation during nitrate uptake by marine phytoplankton grown in continuous culture. *Journal of Plankton Research*, 17(3): 439-464.
- Mortlock, R.A. and Froelich, P.N., 1989. A simple method for the rapid determination of biogenic opal in pelagic marine sediments. *Deep-Sea Research*, 36(9A): 1415-1426.

- Nakatsuka, T., Handa, N., Wada, E. and Wong, C.S., 1992. The dynamic changes of stable isotope ratios of carbon and nitrogen in suspended and sedimented particulate organic matter during a phytoplankton bloom. *Journal of Marine Research*: 267-296.
- Park, Y.-H. and Geroni, L., 1997. Cross-frontal exchange of Antarctic Intermediate Water and Antarctic Bottom Water in the Crozet Basin. *Deep-Sea Research*, 44(5): 987-1004.
- Pennock, J.R., Sharp, J.H., Ludlam, J., Velinsky, D.J. and Fogel, M.L., 1988. Isotopic fractionation of nitrogen during the uptake of NH_4^+ and NO_3^- by *Skeletonema costatum*. *EOS*, 69(44): 1098.
- Peulve, S., 1995. Biogéochimie de la matière organique macromoléculaire dans les environnements marins récents. Ph.D. Thesis, L'Université Paris 6, Paris, 151 pp.
- Sachs, J.P., 1996. Nitrogen isotopes in chlorophyll and the origin of the eastern Mediterranean sapropels, MIT/WHOI Joint Program in Oceanography.
- Senftle, J.T., Landis, C.R. and McLaughlin, R., 1993. Organic petrographic approach to kerogen characterization. In: M.H. Engel and S.A. Macko (Editors), *Organic Geochemistry: Principles and Applications*. Plenum Press, New York, pp. 355-376.
- Schroeder, R.A., 1975. Absence of β -alanine and γ -aminobutyric acid in cleaned foraminiferal shells: Implications for use as a chemical criterion to indicate removal of non-indigenous amino acid contaminants. *Earth and Planetary Science Letters*, 25: 274-278.
- Shemesh, A., Mortlock, R.A., Smith, R.J. and Froelich, P.N., 1988. Determination of Ge/Si in marine siliceous microfossils: separation, cleaning and dissolution of diatoms and radiolaria. *Marine Chemistry*, 25: 305-323.
- Shemesh, A., Macko, S.A., Charles, C.D. and Rau, G.H., 1993. Isotopic evidence for reduced productivity in the glacial southern ocean. *Science*, 262: 407-410.
- Sigman, D.M., M.A. Altabet, R. Michener, D.C. McCorkle, B. Fry, R. Francois, and J. Donaghue, A new method for the nitrogen isotopic analysis of oceanic nitrate and first results from the Southern Ocean. *EOS*, 1996. 76(3): p. 143.
- Singer, A.J. and Shemesh, A., 1995. Climatically linked carbon isotope variation during the past 430,000 years in Southern Ocean sediments. *Paleoceanography*, 10(2): 171-178.
- Stevenson, F.J. and Cheng, C.-N., 1970. Amino acids in sediments: recovery by acid hydrolysis and quantitative estimation by colorimetric procedure. *Geochimica et Cosmochimica Acta*, 34: 77-78.
- Swift, D.M. and Wheeler, A.P., 1992. Evidence of an organic matrix from diatom biosilica. *Journal of Phycology*, 28: 202-209.
- Tsuge, S. and Matsubara, H., 1985. High-resolution pyrolysis-gas chromatography of proteins and related materials. *Journal of Analytical and Applied Pyrolysis*, 8: 49-64.

Volcani, B.E., 1982. Cell wall formation in diatoms: morphogenesis and biochemistry. In: T.L. Simpson and B.E. Volcani (Editors), *Silicon and Siliceous Structures in Biological Systems*. Springer-Verlag, New York, pp. 157-200.

Wada, E. and Hattori, A., 1978. Nitrogen isotope effects in the assimilation of inorganic nitrogenous compounds. *Geomicrobiology Journal*, 1: 85-101.

Wada, E., 1980. Nitrogen isotope fractionation and its significance in biogeochemical processes occurring in marine environments. In: E. Goldberg, Y. Horibe and K. Saruhashi (Editors), *Isotope Marine Chemistry*. Uchida Rokakuho, Tokyo, pp. 375-398.

Waser, N.A.D., Turpin, D.H., Harrison, P.J., Nielsen, B. and Calvert, S.E., 1997. Nitrogen isotope fractionation during the uptake and assimilation of nitrate, nitrite, and urea by a marine diatom. *Limnology and Oceanography*, in press.

Whelan, J.K., 1977. Amino acids in a surface sediment core of the Atlantic abyssal plain. *Geochimica et Cosmochimica Acta*, 41: 803-810.

Wu, J., Calvert, S.E. and Wong, C.S., 1997. Nitrogen isotope variations in the subarctic Pacific northeast Pacific: relationships to nitrate utilization and trophic structure. *Deep-Sea Research*, in press.

Table 1: sample locations

site name	purpose in this study	location
NBP 96-4-2 multicore 4	cm-scale profile in recent sediments	64°S, 170°E
ANTARES 1 multicores:	latitudinal transect of recent sediments	
KTB 5	"	55°S, 72°E
KTB 6	"	52°S, 61°E
KTB 13	"	50°S, 58°E
KTB 11	"	49°S, 58°E
KTB 16	"	48°S, 56°E
KTB 19	"	47°S, 58°E
KTB 21	"	46°S, 56°E
AII 107-22GGC	paleoceanographic record	55°S, 3°W
MD 84-552	"	55°S, 74°E

Table 2: treatments of NBP96-4-3 MC6 (14-20 cm), diatom ooze

treatment	$\delta^{15}\text{N}$ (‰ vs. air)	N content* ($\mu\text{mol N/g}$)
untreated sediment (diatom ooze)	4.0	34.1
72% H_4ClO_4 , 70°C	1.0	27.6
1/1 30% H_2O_2 /50% HCl , 70°C**	1.6	30.4
1) 1/1 30% H_2O_2 /50% HCl , 70°C 2) 72% H_4ClO_4 , 70°C	1.1	22.3
1) 72% H_4ClO_4 , 70°C 2) 1/1 30% H_2O_2 /50% HCl , 70°C	0.9	22.8
36% H_4ClO_4 (initial), boiled 2 hrs	0.5	20.5
36% H_4ClO_4 (initial), boiled to fuming, fuming 1 hr	0.4	20.5
bleach, 70°C, 1 hr	0.2	24.0
bleach, 70°C, 6 hr	-0.2	20.6
bleach, 70°C, 20 hr	1.4	17.8

* No correction is made here for the weight losses which occur during these treatments (see text).

** The 1/1 30% H_2O_2 /50% HCl treatment was carried out for an hour past the time when the peroxide was consumed (when bubbling stopped).

Table 3: results for Southern Ocean sediment standards

			$\delta^{15}\text{N}$ (‰ vs. air)		N content ($\mu\text{mol N/g}$)			
sediment	location	% clay*	bulk	bulk, acid-treated	diatoms, acid-treated	bulk	bulk, acid-treated	diatoms, acid-treated
NBP 96-4-3, MC6 14-20 cm	62°S, 170°E	<5	4.2	1.0	1.1	34.0	27.5	26.5
CH 115 26PG 44-61 cm	54°S, 0°E	15.0	3.2	1.2	0.9	21.3	16.3	17.5
CH 115 34 PC 799-832 cm	54°S, 2°E	15.0	2.9	2.7	2.5	34.7	21.5	20.8
ANTARES 1 KTB 16 21-22 cm	48°S, 56°E	30.0	5.3	4.7	4.2	25.6	22.9	20.6
ANTARES 1 KTB 13 19-20 cm	50°S, 58°E	40.0	6.8	5.5	4.9	31.0	21.7	18.5
All 107 11PG 80-101 cm	56°S, 33°W	60.0	3.7	4.0	2.7	57.9	29.8	19.2
All 107 14PC 719-740 cm	55°S, 22°W	75.0	5.0	4.5	4.6	23.1	18.9	15.7

* % clay values are estimates from smear slides.

Table 4a: m/e = 115, 117, 118, 119

peaks identified from mass scans aimed at recognizing N-bearing compounds

peak #	identification
1	pyrimidinone, methyl
2	furanone, heptyldihydro
3	benzofuranone
4	indole, dihydro
5	aminostyrene
6	carbamothioic acid, o-isopropyl ester
7	benzoxazole
8	benzene, 1-propenyl
9	furandione, dimethyl
10	pyridine, chloromethyl
11	indene
12	pyridine acetonitrile
13	indole, dihydro
14	methyl phenol
15	benzoic acid, aminohexylester
16	pyridine acetonitrile
17	methylbenzonitrile
18	methylbenzonitrile
19	pyrrolopyridine
20	pyrrolopyridine
21	methylbenzonitrile
22	pyridine acetonitrile
23	pyridine acetonitrile
24	benzene acetonitrile
25	pyrazolopyridine, methyl
26	phenolmethylamino ethyl ether
27	pyrrolopyridine
28	pyrrolopyridine
29	pyridine carboxylic acid ester
30	isoquinoline

Table 4b: m/e = 68, 82, 96, 98, 110, 126

peaks identified from mass scans aimed at recognizing sugar pyrolysates

peak #	identification
1	furandione, methyl
2	pyrimidinone, methyl
3	pyrimidinone, aminomethyl
4	furandione, dimethyl
5	benzene, 1,3-dimethyl-butyl
6	furandione, methyl
7	pyrimidinone, aminomethyl
8	pyrimidinone, aminomethyl
9	furan
10	methoxyformanilide
11	methoxyformanilide

Table 4c: total ion current, with methylation

peaks identified from pyrolysis with a methylating reagent, aimed at identifying carboxylic acids

peak #	identification
1	trimethylamine
2	butaneamine, N-methyl, N-nitroso
3	alkane
4	hexanoic acid, methyl ester
5	phosphoric acid, trimethyl ester
6	butandioic acid, dimethyl ester
7	methylbutanoic acid, dimethyl ester
8	trimethylamine
9	methylenebutanoic acid, dimethyl ester
10	dimethylethyldienemalonate
11	trimethylurea
12	nonanoic acid, methyl ester
13	heterocyclic oxygen-bearing compound
14	dimethoxydodecane
15	triazinetriene
16	?
17	trimethylpropane-1,2,3-tricarboxylate
18	2,4,4-trimethyl-1-pentanol
19	pentane, 2,3,3-trimethyl
20	hexadecanoic acid, methyl ester

Table 5: C/N molar ratios for diatom microfossil-bound organic matter

sediment	location	C/N
NBP 96-4-2, MC4	64°S, 170°E	
4.25 cm		6.2
8.5 cm		6.3
9.5 cm		6.3
ANTARES 1 KTB 5 9-10 cm	55°S, 72°E	6.9
ANTARES 1 KTB 6 9-10 cm	52°S, 61°E	5.6
ANTARES 1 KTB 13 9-10 cm	50°S, 58°E	5.8
ANTARES 1 KTB 3 9-10 cm	49°S, 58°E	6.5
ANTARES 1 KTB 11 9-10 cm	49°S, 58°E	6.8
ANTARES 1 KTB 16 9-10 cm	48°S, 56°E	6.4, 6.1
ANTARES 1 KTB 19 9-10 cm	47°S, 58°E	5.0
ANTARES 1 KTB 21 9-10 cm	46°S, 56°E	6.2

Figure 1

Map view of the Southern Ocean cores used in this study. NBP 96-4-2 MC 4 is a multicore in diatom ooze from the Antarctic Zone, east Pacific sector, from which we generate a cm-scale depth profile (filled square). The ANTARES 1 multicores from the central Indian provide a latitudinal transect across the Polar Frontal Zone (filled circles). AII 107-22GGC, from the Atlantic sector of the Antarctic Zone, and MD 84-552, from the Indian sector of the Antarctic Zone, are used to generate diatom-bound $\delta^{15}\text{N}$ records back to the Last Glacial Maximum (filled triangles).

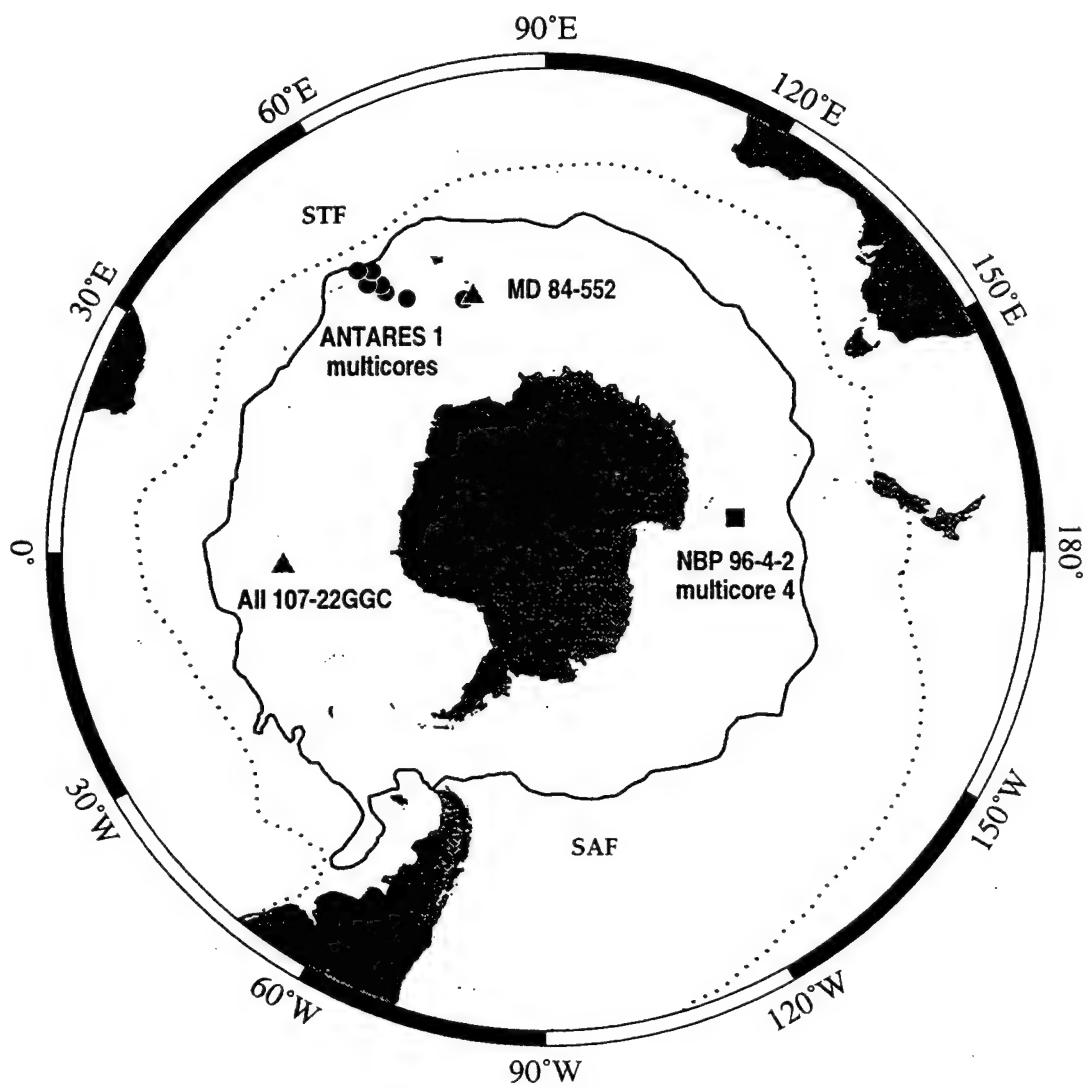


Figure 2

Time course of $\delta^{15}\text{N}$ (filled circles) and N content (open circles) in a diatom ooze sediment standard (NBP 96-4-3 MC 6, 62°S, 170°E), for treatment with (a) perchloric acid at 70°C (as in the protocol) and (b) bleach at 70°C. Replicate analyses are shown, and solid lines connect the analysis means.

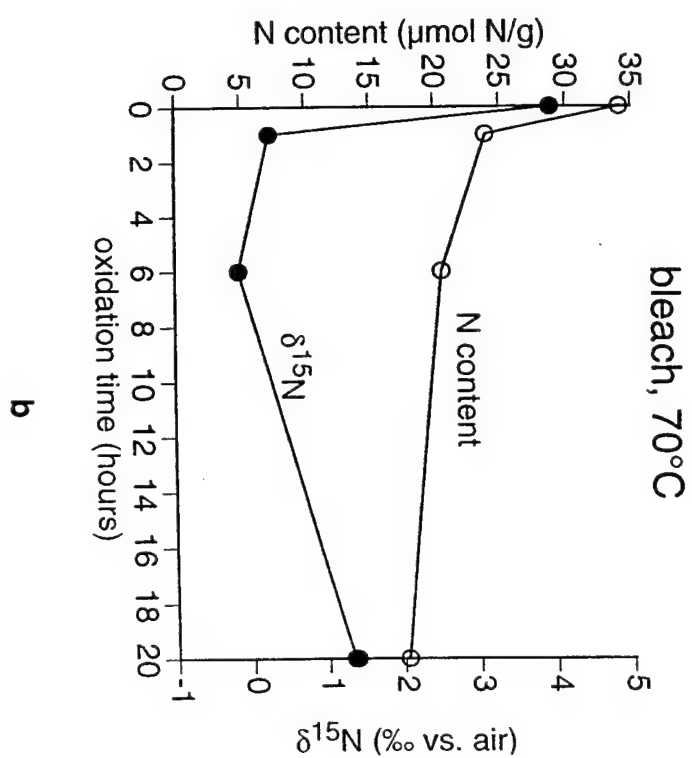
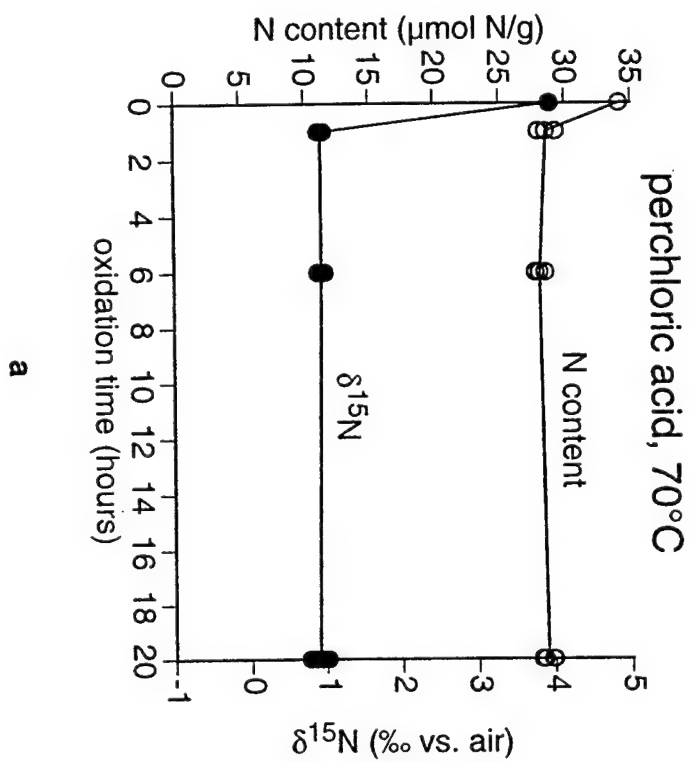


Figure 3

Microscopic images of a diatom ooze sediment standard (NBP 96-4-3 MC 6, 62°S, 170°E). (a) Untreated diatom ooze under visible light, using phase contrast to better visualize the microfossils. Note the brown material, which is amorphous organic matter (L. Eglinton, pers. comm.). Under 450–490 nm light, this material does not fluoresce. (b) Diatom ooze that has undergone perchloric acid treatment lacks this amorphous organic matter. (c) The same field as (b), but excited with 450–490 nm light (emission >520 nm). The fluorescent organic matter is associated with the diatom microfossils. The intensity and color of the fluorescence is characteristic of relatively fresh organic matter, suggesting that the diatom-bound organic material was not greatly altered during the perchloric acid treatment.

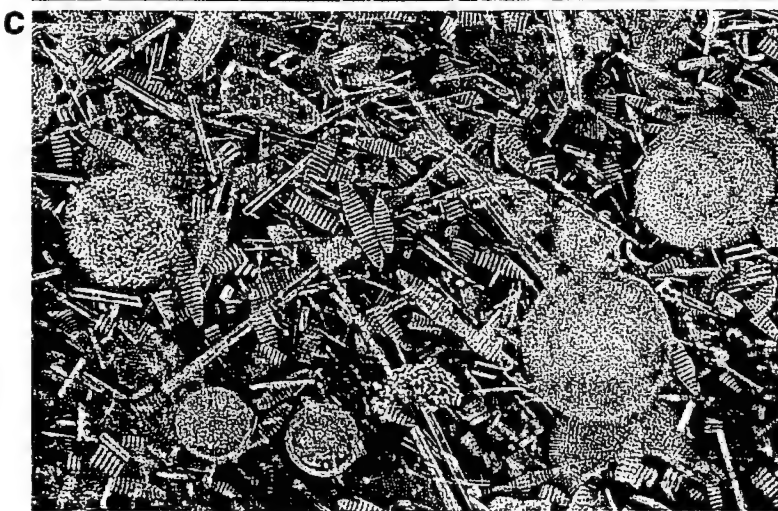
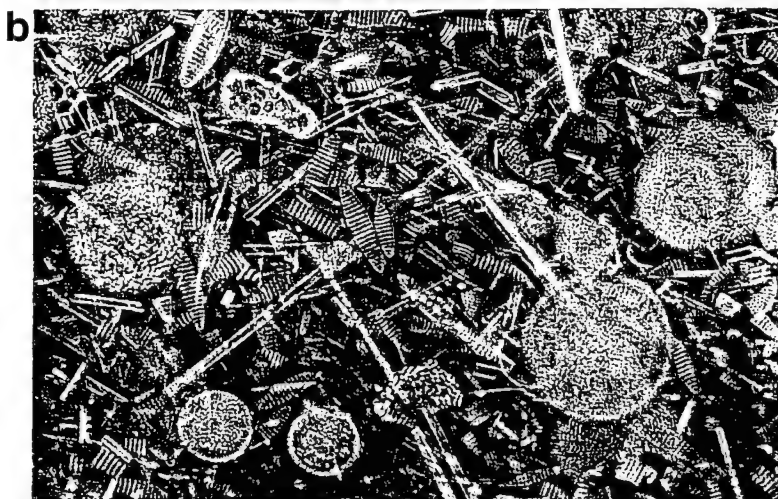
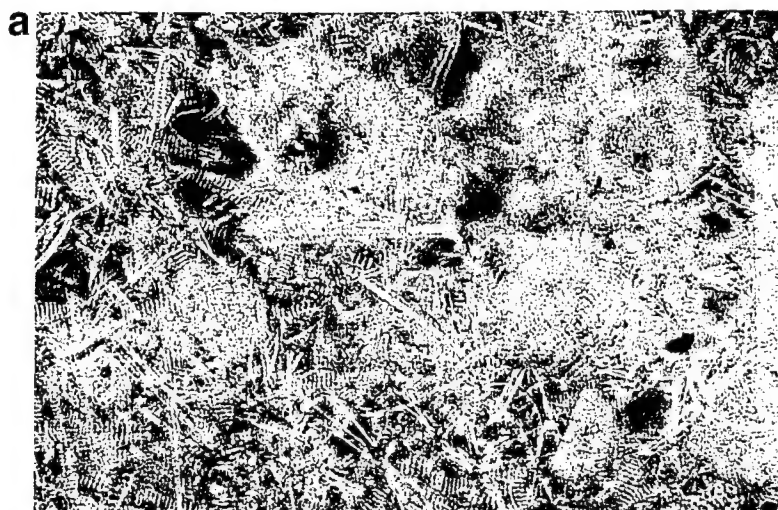


Figure 4

Chromatograms of Curie-point pyrolysis/gas chromatography/mass spectrometry performed on the organic residue from the HF digestion of a diatom ooze sediment standard (NBP 96-4-3 MC 6, 62°S, 170°E), that has undergone perchloric acid treatment. Pyrolysis was carried out using 610°C Curie-point wires. The x-axis is time of elution (~15-35 minutes for (a) and (b), ~15-60 minutes for (c)), while the y-axis is the mass spectrometric signal. (a) The superimposed ion chromatograms for masses 115, 117, 118, and 119, which tend to pick up nitrogenous compounds (J. Whelan, pers. comm.). (b) The superimposed ion chromatograms for masses 68, 82, 96, 98, 110, and 126, which are useful in doing a preliminary analysis for sugar pyrolysis products (J. Whelan, pers. comm.). (c) The total ion current chromatogram of the organic residue with tetra-methyl ammonium hydroxide, a reagent which methylates the carboxylic acids prior to gas chromatography, in order to resolve the compounds with carboxylic acid groups, such as fatty acids. Peaks of N-bearing compounds are labeled with a "+". In (c), most of the N-bearing compounds are from the methylating reagent. Identifications of the numbered peaks are listed in Table 4.

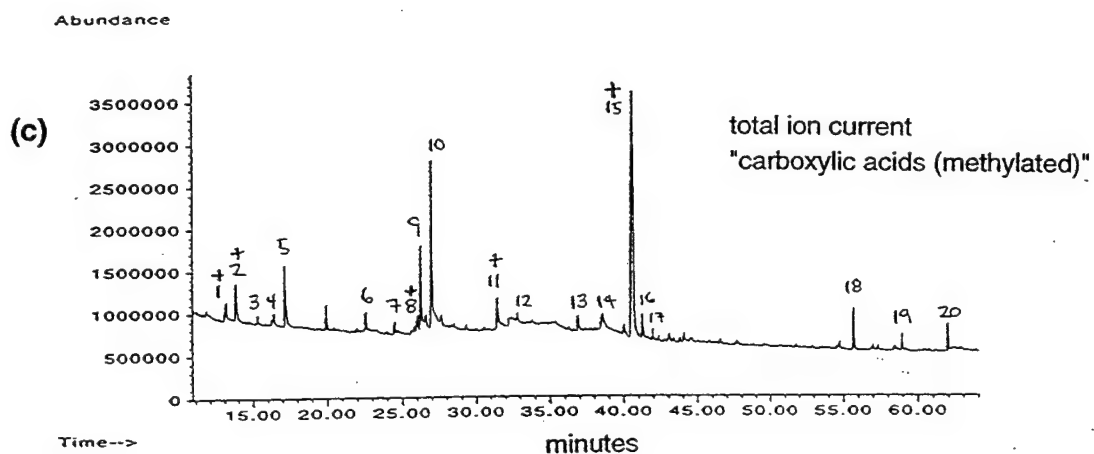
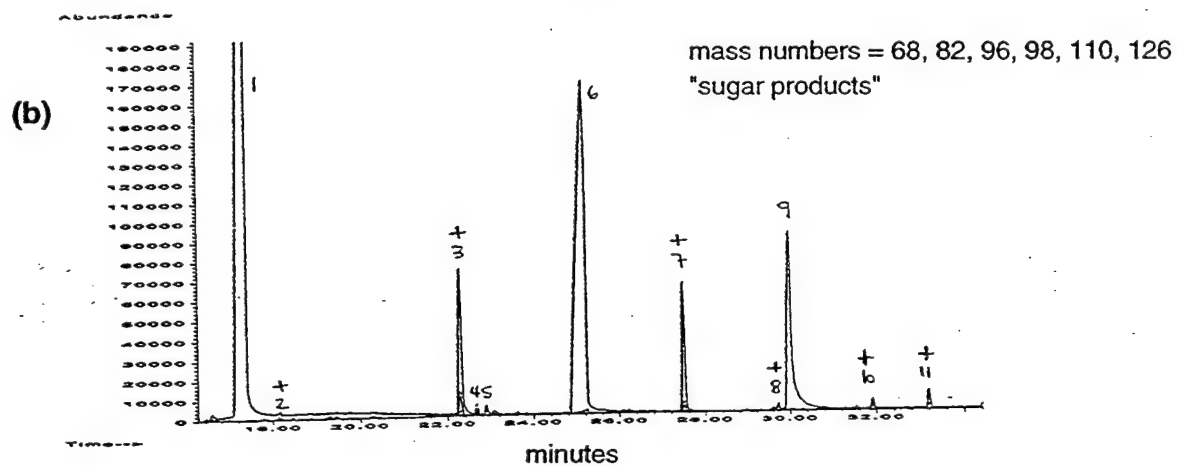
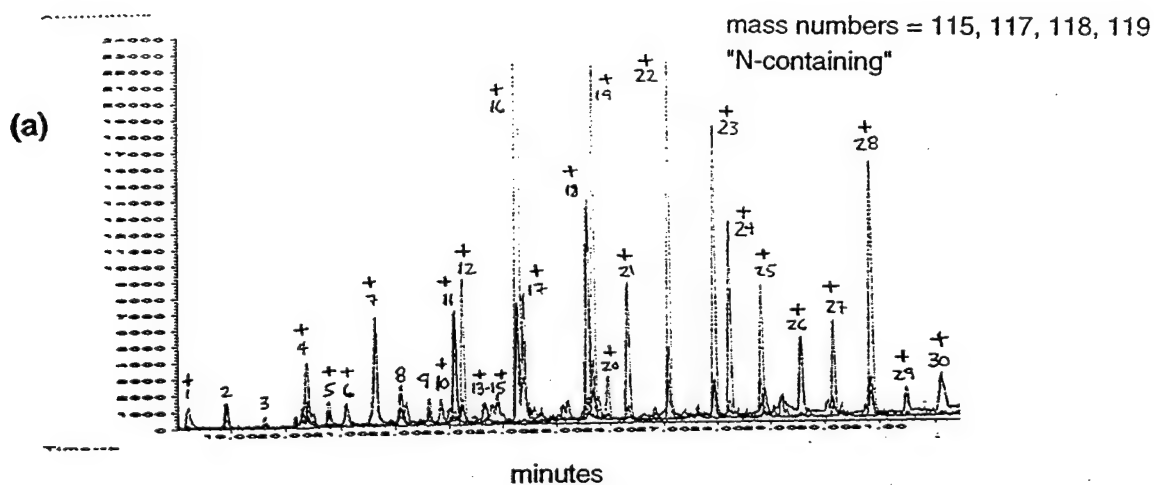


Figure 5

Depth profiles in a multicore in diatom ooze (NBP 96-4-2 MC 4, Antarctic Zone, east Pacific sector, 64°S, 170°E) of the (a) N content and (b) $\delta^{15}\text{N}$ for the bulk sediment before (open symbols) and after (closed symbols) treatment with perchloric acid. Replicate analyses are shown, and solid lines connect the means of the bulk sediment analyses. The arrow on the $\delta^{15}\text{N}$ axis indicates the sinking flux $\delta^{15}\text{N}$ estimated for the Antarctic Zone from $\delta^{15}\text{NO}_3$ data (see Chapter 4). These sediments are almost entirely diatomaceous, so no physical separation steps were necessary.

NBP 96-4-2 MC4(64°S, 170°E): multicore in diatom ooze

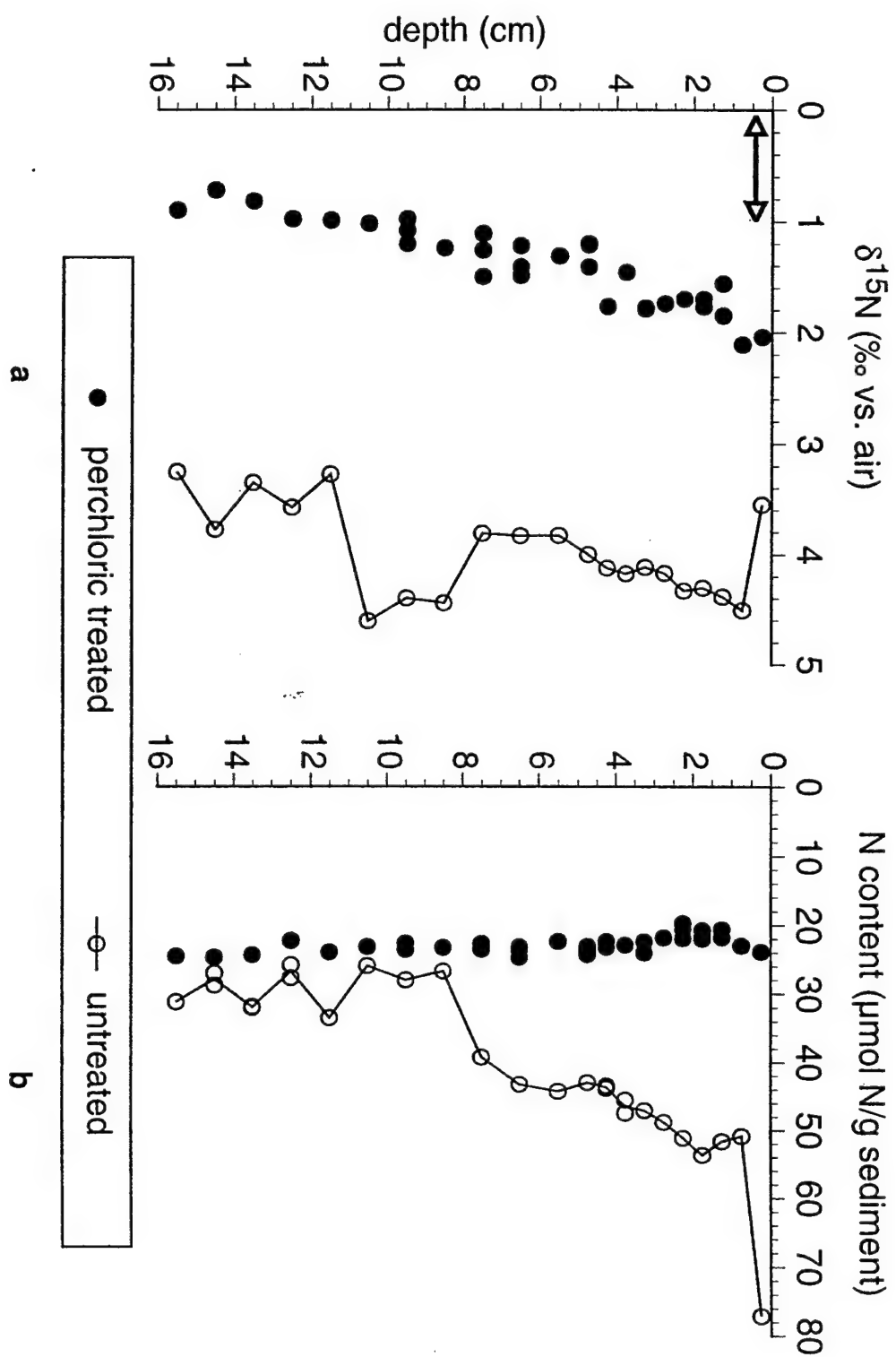


Figure 6

Depth profiles in NBP 96-4-2 MC 4 of (a) the estimated fraction of N lost from the sediments during oxidation, and (b) the estimated $\delta^{15}\text{N}$ of this fraction, based on the N content and $\delta^{15}\text{N}$ data for the bulk sediment and perchloric acid-treated sediment. The estimation is made with two different assumptions regarding the opal mass lost during the perchloric acid treatment, one with the maximum possible correction for the mass loss (closed circles), and the other without a correction for the mass loss (open circles, see text). The error bars for the second case show the effect of 5% uncertainties in the N content measurements on the isotopic estimates.

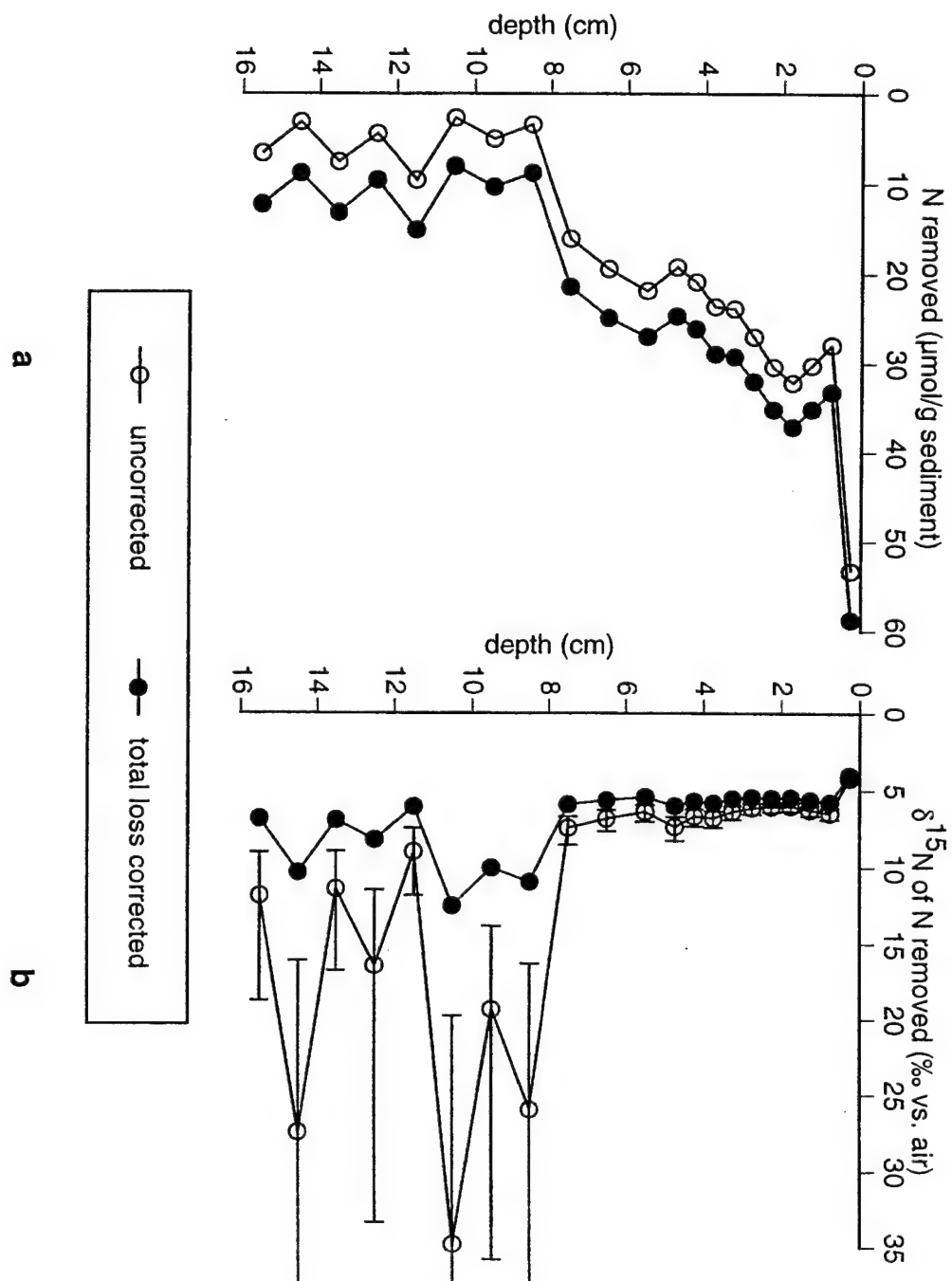


Figure 7

$\delta^{15}\text{N}$ (a) and N content (b) vs. latitude for bulk sediment (open symbols) and the diatom-bound N fraction (filled symbols), at several depths in the latitudinal transect of multicores from ANTARES 1. Plotted values are the means of at least duplicate analyses. The approximate locations of the Subantarctic Front (SAF) and Polar Front (PF) are shown (Park and Gamberoni, 1997).

ANTARES 1 transect (~58°E)

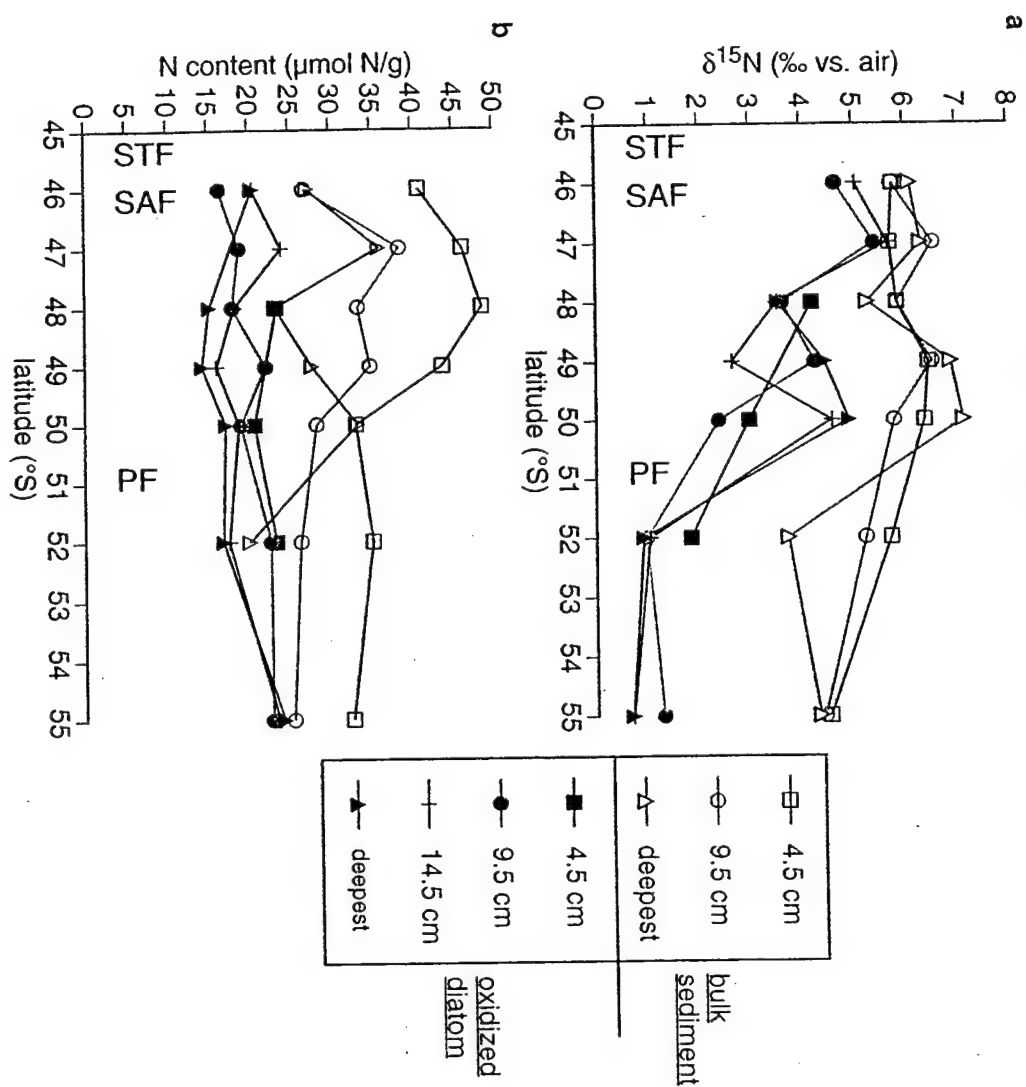


Figure 8

Depth profiles in core KTB 13 (50°S) of $\delta^{15}\text{N}$ (a) and N content (b) for both bulk N and diatom N. Replicate analyses are shown, with solid lines connecting the mean values.

Depth profiles of sedimentary Ba and Al content (c) are shown to demonstrate the stratigraphic change at ~12 cm depth.

ANTARES 1--KTB 13 (50°S, 58°E)

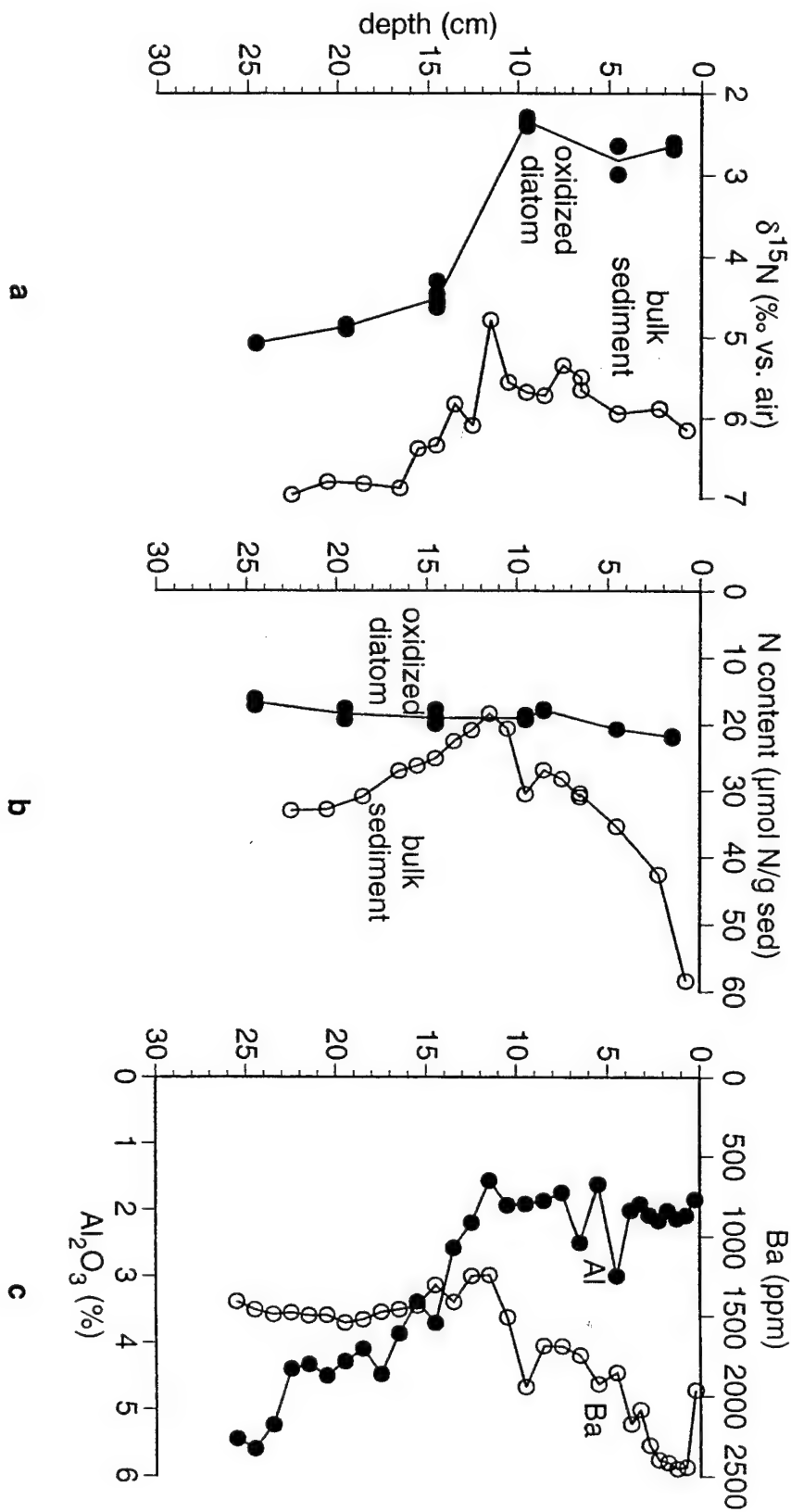


Figure 9

Depth profiles in AII 107-22 GGC (Antarctic Zone, Atlantic Sector, 55°S, 3°W, 2768 m) of $\delta^{15}\text{N}$ (a) and N content (b) for bulk N (open circles), diatom N (filled circles), and the perchloric acid-treated >63 μm fraction (crosses), which is composed of large diatoms, radiolaria, and some detrital grains. Replicate analyses are shown for the cleaned diatom and >63 μm fractions, with solid lines connecting the mean values for the diatom N analyses. N content for the bulk sediment is in some cases lower than for the cleaned diatom fraction because of the presence of dense detrital grains in the bulk sediment. The planktonic $\delta^{18}\text{O}$ stratigraphy suggests that sediment from the Last Glacial Maximum is at 65 cm depth (Keigwin and Boyle, 1989).

All 107-22GGC: Antarctic zone, Atlantic sector (55°S, 3°W)

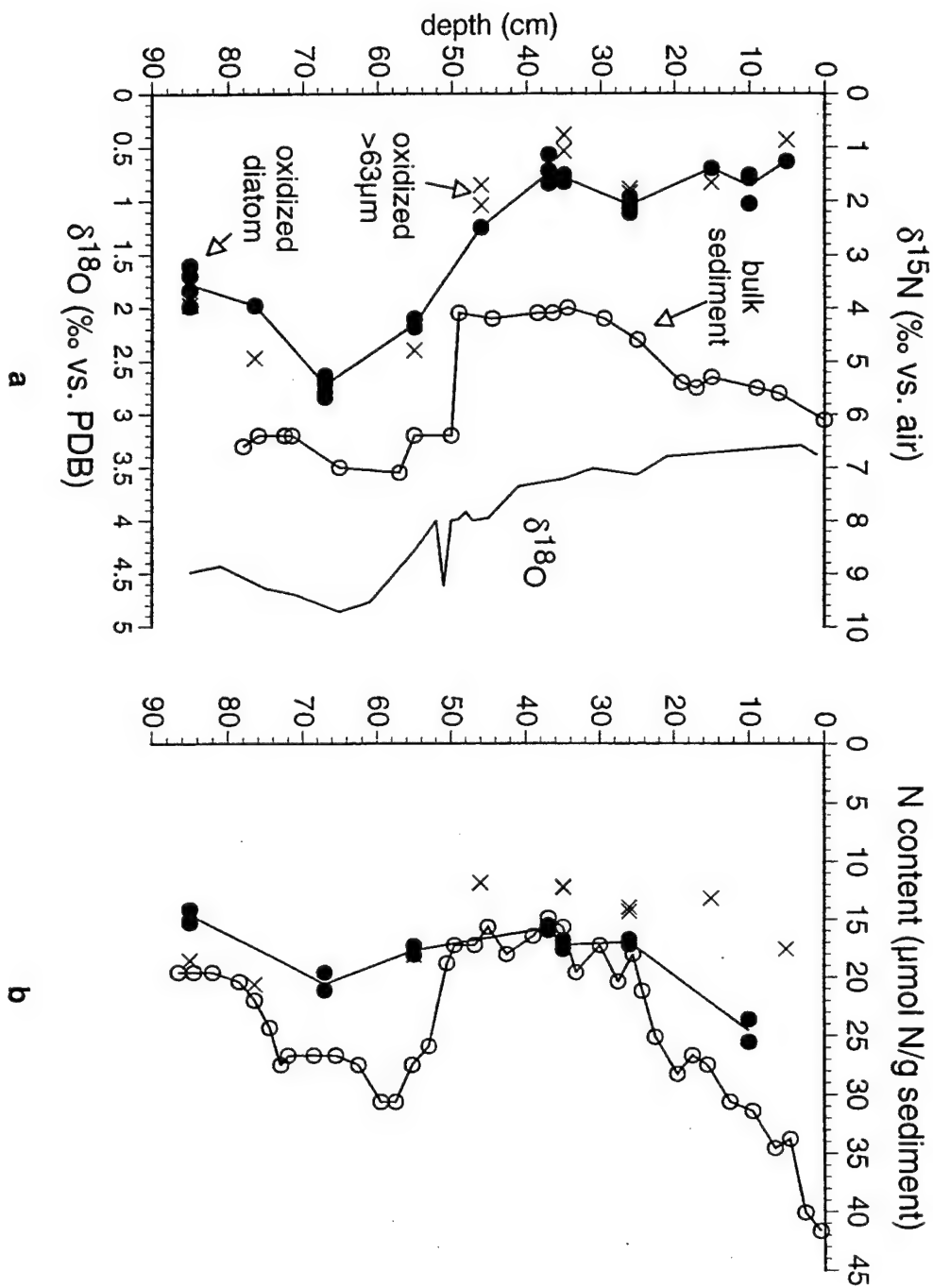
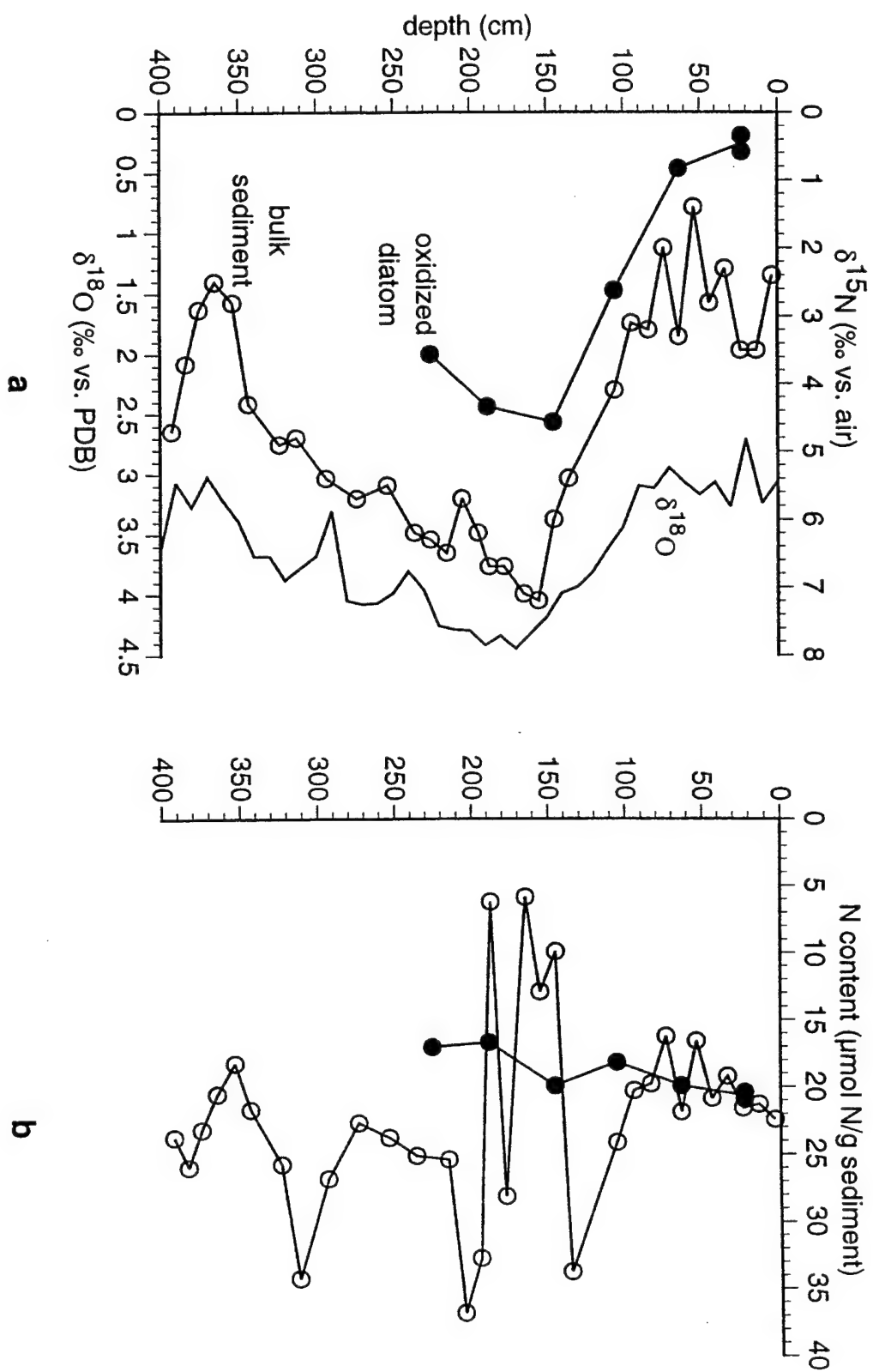


Figure 10

Depth profiles in MD 84-552 (Antarctic Zone, Indian Sector, 55°S, 74°E, 2230 m) of $\delta^{15}\text{N}$ (a) and N content (b) for bulk sediment N (open circles) and diatom N (filled circles). Replicate analyses are shown for the cleaned diatom fraction, with solid lines connecting the mean values. The $\delta^{18}\text{O}$ stratigraphy for this core in (a) suggests that sediment from the Last Glacial Maximum is at 170 cm depth (L.D. Labeyrie, pers. comm.). As in 22 GGC, N content for the bulk sediment is strongly affected by the presence of detrital grains, especially in the glacial section.

MD 84-552: Antarctic Zone, Indian sector (55°S, 74°E)



NBP 96-4-2, MC 4 DATA: 1

$\delta^{15}\text{N}$ data

diatom-bound N		bulk sedimentary N	
depth (cm)	$\delta^{15}\text{N}$ (‰ vs. air)	depth (cm)	$\delta^{15}\text{N}$ (‰ vs. air)
0.25	2.04	0.25	3.55
0.75	2.11	0.75	4.51
1.25	1.56	1.25	4.38
1.25	1.85	1.75	4.30
1.75	1.7	2.25	4.33
1.75	1.77	2.75	4.17
2.25	1.7	3.25	4.12
2.75	1.74	3.75	4.17
3.25	1.78	4.25	4.12
3.25	1.79	4.75	4.00
3.75	1.46	5.5	3.83
4.25	1.77	6.5	3.83
4.75	1.2	7.5	3.81
4.75	1.21	8.5	4.44
4.75	1.41	9.5	4.40
5.5	1.31	10.5	4.61
6.5	1.41	11.5	3.28
6.5	1.22	12.5	3.58
6.5	1.49	13.5	3.35
7.5	1.5	14.5	3.78
7.5	1.26	15.5	3.25
7.5	1.11		
8.5	1.24		
9.5	1.08		
9.5	1.2		
9.5	0.98		
10.5	1.02		
11.5	0.99		
12.5	0.98		
13.5	0.82		
14.5	0.72		
15.5	0.9		

NBP 96-4-2, MC 4 DATA: 2

N content data

diatom-bound N		bulk sedimentary N	
depth (cm)	μmol N/g sed	depth (cm)	μmolN/g sed
0.25	23.83	0.25	77.08
0.75	22.98	0.75	50.91
1.25	21.77	1.25	51.65
1.25	20.65	1.75	53.67
1.25	21.79	2.25	51.16
1.75	22.01	2.75	48.84
1.75	20.76	3.25	47.11
1.75	21.70	3.75	47.53
2.25	21.93	3.75	45.56
2.25	19.75	4.25	43.50
2.25	20.57	4.25	43.85
2.75	21.83	4.75	43.00
3.25	22.43	5.50	44.26
3.25	24.05	6.50	43.28
3.75	22.91	7.50	39.28
4.25	23.26	8.50	26.74
4.25	22.37	9.50	28.04
4.75	23.10	10.50	25.94
4.75	23.61	11.50	33.53
4.75	24.01	12.50	25.81
4.75	24.31	12.50	27.70
5.50	22.39	13.50	31.87
6.50	24.70	13.50	32.01
6.50	23.66	14.50	28.79
6.50	23.16	14.50	27.02
7.50	23.36	15.50	31.19
7.50	22.72		
7.50	23.53		
8.50	23.28		
9.50	22.64		
9.50	23.60		
9.50	22.64		
10.50	23.19		
11.50	23.95		
12.50	22.28		
13.50	24.32		
14.50	24.72		
15.50	24.51		

ANTARES-1 MULTICORE DATA: 1

diatom microfossil-bound N: N content ($\delta^{15}\text{N}$ (‰ vs. air))

core #	latitude (°S)	4.5 cm	9.5 cm	14.5 cm	deepest
KTB 21	46	N	4.67	5.06	N
KTB 19	47	N	5.42	5.68	N
KTB 16	48	4.21	3.63	3.53	3.56
KTB 11	49	N	4.27	2.66	4.46
KTB 13	50	2.99	2.40	4.59	4.92
KTB 6	52	1.84	0.98	1.04	0.92
KTB 5	55	N	1.29	0.69	0.69

diatom microfossil-bound N: N content ($\mu\text{mol N/g frustules}$)

core #	latitude (°S)	4.5 cm	9.5 cm	14.5 cm	deepest
KTB 21	46	N	16.5	20.5	20.5
KTB 19	47	N	18.9	24.0	N
KTB 16	48	23.4	18.1	18.3	15.2
KTB 11	49	N	22.1	16.1	14.3
KTB 13	50	20.7	19.1	18.8	17.2
KTB 6	52	23.3	22.7	17.6	16.9
KTB 5	55	N	22.8	23.6	24.2

ANTARES-1 MULTICORE DATA: 2

bulk sedimentary N: $\delta^{15}\text{N}$ (‰ vs. air)

core #	latitude (°S)	0-2 cm	4.5 cm	9.5 cm	19-20 cm	deepest
KTB 21	46	5.19	5.78	5.76	N	6.12
KTB 19	47	4.91	5.72	6.55	5.98	6.33
KTB 16	48	5.73	5.86	5.86	4.78	5.29
KTB 11	49	6.16	6.46	6.53	5.73	6.89
KTB 13	50	6.49	6.39	5.80	7.00	7.14
KTB 6	52	5.72	5.74	5.24	3.54	3.75
KTB 5	55	5.09	4.53	4.43	N	4.35

bulk sedimentary N: N content ($\mu\text{mol N/g}$ sediment)

core #	latitude (°S)	0-2 cm	4-5 cm	9-10 cm	19-20 cm	deepest
KTB 21	46	64.6	40.9	26.8	N	27.3
KTB 19	47	76.8	46.2	38.5	34.3	36.0
KTB 16	48	62.6	48.6	33.4	25.6	23.2
KTB 11	49	71.0	43.7	34.9	16.8	27.8
KTB 13	50	56.4	33.1	28.3	31.0	33.3
KTB 6	52	60.9	35.2	26.4	18.2	20.1
KTB 5	55	55.9	32.6	25.4	N	N

ANTARES-1 MULTICORE DATA: 3

KTB 13 depth profile data: 1

diatom microfossil-bound N

depth (cm)	$\delta^{15}\text{N}$ (‰ vs. air)	N content ($\mu\text{mol N/g}$ frustules)
1.5	2.68, 2.60	22.00, 21.71
4.5	2.99, 2.64	20.73, 20.72
9.5	2.40, 2.29, 2.33	18.60, 19.34, 19.28, 19.02
14.5	4.62, 4.54, 4.57, 4.63, 4.30, 4.46	17.78, 19.96, 18.97, 19.47
19.5	4.90, 4.84	19.29, 17.63
24.5	5.07, 5.08	17.21, 16.13

bulk sedimentary N

depth (cm)	$\delta^{15}\text{N}$ (‰ vs. air)	N content ($\mu\text{mol N/g}$ frustules)
0.75	6.15	58.40
2.25	5.89	42.66
4.5	5.95	35.41
6.5	5.65	30.44
6.5	5.50	30.99
7.5	5.35	28.24
8.5	5.73	26.94
9.5	5.68	30.58
10.5	5.56	20.64
11.5	4.79	18.40
12.5	6.09	20.91
13.5	5.83	22.57
14.5	6.34	25.20
15.5	6.38	26.30
16.5	6.88	27.09
18.5	6.83	30.96
20.5	6.80	32.88
22.5	6.96	33.02

AII-107 22GGC DATA:1

$\delta^{15}\text{N}$ data

diatom-bound N		bulk sedimentary N		cleaned >63 μm fraction N	
depth (cm)	$\delta^{15}\text{N}$ (‰ vs. air)	depth (cm)	$\delta^{15}\text{N}$ (‰ vs. air)	depth (cm)	$\delta^{15}\text{N}$ (‰ vs. air)
5	1.26	0.5	6.1	5	0.87
10	2.05	6.5	5.6	15	1.67
10	1.58	9.5	5.5	26	1.86
10	1.52	15.5	5.3	26	1.78
15	1.40	17.5	5.5	35	1.07
26	2.08	19.5	5.4	35	0.77
26	2.01	25.5	4.6	46	2.09
26	2.23	30	4.2	46	1.71
26	2.13	35	4	55	4.80
26	1.94	37	4.1	76.5	4.94
35	1.51	39	4.1	85	3.94
35	1.65	45	4.2		
35	1.54	49.5	4.1		
37	1.14	50.5	6.4		
37	1.67	55.5	6.4		
37	1.68	57.5	7.1		
37	1.44	65.5	7		
46	2.49	72	6.4		
55	4.36	73	6.4		
55	4.36	76.5	6.4		
55	4.20	78.5	6.6		
67	5.68				
67	5.58				
67	5.38				
67	5.26				
67	5.42				
67	5.30				
76.5	3.95				
85	3.67				
85	3.39				
85	3.97				
85	3.20				

AII-107 22GGC DATA:2

N content data

diatom-bound N		bulk sedimentary N		cleaned >63 μ m fraction N	
depth (cm)	μ molN/g opal	depth (cm)	μ molN/g sed	depth (cm)	μ molN/g sed
10	25.57	0.5	41.64	5	17.61
10	23.64	2.5	40.07	15	13.22
26	17.24	4.5	33.79	26	14.00
26	16.79	6.5	34.57	26	14.37
35	17.28	9.5	31.43	35	12.34
35	17.65	12.5	30.64	35	12.22
35	16.86	15.5	27.50	46	11.93
37	16.03	17.5	26.71	46	11.88
37	15.58	19.5	28.29	55	18.17
55	17.34	22.5	25.14	76.5	20.68
55	18.11	24.25	21.21	85	18.62
67	21.14	25.5	18.07		
67	21.17	27.5	20.43		
67	19.66	30	17.29		
85	15.35	33.25	19.64		
85	15.16	35	15.71		
85	14.17	37	14.93		
		39	16.50		
		42.5	18.07		
		45	15.71		
		46.75	17.29		
		49.5	17.29		
		50.5	18.86		
		53	25.93		
		55.25	27.50		
		57.5	30.64		
		59.5	30.64		
		62.5	27.50		
		65.5	26.71		
		68.5	26.71		
		72	26.71		
		73	27.50		
		74.5	24.36		
		76.5	22.00		
		78.5	20.43		
		82	19.64		
		84.5	19.64		
		86.5	19.64		

MD84-552 DATA: 1

$\delta^{15}\text{N}$ data

diatom-bound N		bulk sedimentary N	
depth (cm)	$\delta^{15}\text{N}$ (‰ vs. air)	depth (cm)	$\delta^{15}\text{N}$ (‰ vs. air)
22.5	0.58	3.5	2.4
22.5	0.34	13.5	3.5
63.5	0.83	23.5	3.5
105.5	2.62	33.5	2.3
145.5	4.57	43.5	2.8
188.5	4.34	53.5	1.4
225.5	3.56	63.5	3.3
		73.5	2
		83.5	3.2
		94.5	3.1
		105.5	4.1
		135.5	5.4
		145	6
		155	7.2
		164.5	7.1
		177.5	6.7
		187.5	6.7
		194.5	6.2
		205	5.7
		215	6.5
		236	6.2
		253.5	5.5
		273.5	5.7
		293.5	5.4
		312.5	4.8
		323.5	4.9
		343.5	4.3
		353.5	2.8
		365	2.5
		375	2.9
		383.5	3.7
		392.5	4.7

MD84-552 DATA: 2

N content data

diatom-bound N		bulk sedimentary N	
depth (cm)	μmolN/g opal	depth (cm)	μmolN/g sed
22.5	20.91	3.5	22.43
22.5	20.41	13.5	21.29
63.5	19.91	23.5	21.57
105.5	18.18	33.5	19.21
145.5	19.94	43.5	20.86
188.5	16.68	53.5	16.57
225.5	17.04	63.5	21.86
		73.5	16.21
		83.5	19.79
		94.5	20.29
		105.5	24.14
		135.5	33.79
		145	9.93
		155	12.93
		164.5	5.86
		177.5	28.14
		187.5	6.21
		194.5	32.79
		205	36.86
		215	25.43
		236	25.14
		253.5	23.79
		273.5	22.71
		293.5	26.86
		312.5	34.29
		323.5	25.79
		343.5	21.71
		353.5	18.29
		365	20.57
		375	23.21
		383.5	26.00
		392.5	23.79

Appendix:

The Isotopic Homogeneity of Deep Ocean Nitrate: a Comparison with Dissolved Inorganic Carbon

Nutrient concentrations in the deep ocean increase from the North Atlantic, through the Southern Ocean, and into the deep Indo-Pacific (Bainbridge, 1975; Bainbridge, 1976). This is largely due to the paths of deep circulation, in particular, that of North Atlantic Deep Water, which is formed in the North Atlantic and flows into the Indian and Pacific basins, accumulating the regeneration products of the biological pump during its residence in the deep ocean (Broecker and Peng, 1982).

Nitrogen isotopic measurements of nitrate from the Antarctic have demonstrated that Lower Circumpolar Deep Water has a $\delta^{15}\text{NO}_3$ of $4.7 \pm 0.2\text{‰}$, while that of Upper Circumpolar Deep Water is less than 0.5‰ higher than this value (Chapter 4). We have measured very similar isotopic values in deep water samples from the North Atlantic, the Arctic Ocean and the central Pacific (Table A-1, Sigman, Altabet, and Sheehan, unpublished data). This isotopic homogeneity among the deep basins is in contrast to the distribution of $\delta^{13}\text{C}$ of dissolved inorganic carbon (DIC), which decreases by more than 1‰ from the deep Atlantic to the deep Pacific (Kroopnick, 1985). The C isotopes of DIC and N isotopes of nitrate are both fractionated during uptake by phytoplankton. One can then ask why nitrate does not show an isotopic decrease from the deep Atlantic to the deep Southern Ocean and Pacific, as DIC does.

The fractionation factor for nitrate uptake is $\sim 25\%$ of the amplitude of the fractionation factor for CO_2 uptake, in their relative units ($\sim 5\text{‰}$ vs. $20\text{--}25\text{‰}$, see Chapter 4; Montoya and McCarthy, 1995; Sackett et al., 1965; Waser et al., 1997). However, $[\text{NO}_3^-]$ increases by roughly a factor of two from the deep Atlantic to the deep central Pacific,

whereas organic C-derived DIC concentrations increase by less than 10%. If we assume that variations in nitrate and DIC concentration in the deep ocean reflect simply the uptake of these constituents with their respective fractionation factors in the surface ocean and the subsequent remineralization of this material at depth, then Rayleigh fractionation approximates the ranges of variation in $\delta^{15}\text{NO}_3$ and $\delta^{13}\text{C}$ of DIC that we should observe in the deep ocean (Figure A-1). On this basis, we would expect $\delta^{15}\text{NO}_3$ to vary by $\sim 4\text{‰}$ and $\delta^{13}\text{C}$ to vary by $\sim 1.5\text{‰}$ from the deep North Atlantic ($\sim 17 \mu\text{M} [\text{NO}_3^-]$) to the deep Indo-Pacific ($35\text{--}40 \mu\text{M}$). The superposition of deep ocean data shows that, while the prediction works well for $\delta^{13}\text{C}$, it clearly does not for $\delta^{15}\text{NO}_3$.

The lack of a $\delta^{15}\text{NO}_3$ gradient along the path of deep circulation stems fundamentally from the fact that, while DIC uptake in surface waters is never more than 15% of the surface DIC pool, nitrate is completely consumed in most of the global surface ocean (the Southern Ocean being the most important exception). This high degree of nitrate consumption (relative to DIC) encourages deep ocean $\delta^{15}\text{NO}_3$ homogeneity in two ways.

First, because essentially all nitrate is consumed in surface waters, the integrated isotopic composition of sinking particulate organic N (PON) converges on that of the nitrate supply. Therefore, the $\delta^{15}\text{N}$ of the PON rain out of the surface ocean is similar to that of subsurface nitrate. For instance, Altabet (1988) observed a $\delta^{15}\text{N}$ of 3.7‰ for the annually integrated sinking flux out of the Sargasso Sea, compared with a thermocline $\delta^{15}\text{NO}_3$ value of $3.5\text{--}4.0\text{‰}$. As a result, the $\delta^{15}\text{NO}_3$ of a subsurface water parcel is only subtly altered by the regeneration of this organic N, even if that regeneration causes a significant increase in the $[\text{NO}_3^-]$ of the water parcel. By contrast, the $\delta^{13}\text{C}$ of POC does not converge on the $\delta^{13}\text{C}$ of oceanic DIC (Rau et al., 1989), because only a small portion of upwelled DIC is converted to POC. Therefore, when POC is remineralized, it has a significant effect on the $\delta^{13}\text{C}$ of deep ocean DIC.

Second, water masses which have undergone nitrate extraction do not contribute significantly to the $\delta^{15}\text{NO}_3$ of newly formed deep waters, because of their low $[\text{NO}_3^-]$. North Atlantic Deep Water can be thought of as an overturning cell with two upper limbs, one which enters the region of water mass formation at the surface and one which enters at intermediate depth (Figure A-2, Stuiver et al., 1983). The surface limb forming NADW has a very low $[\text{NO}_3^-]$, due to essentially complete nitrate extraction at lower latitudes. Regardless of the $\delta^{15}\text{NO}_3$ in the surface limb, the $\delta^{15}\text{NO}_3$ of the NADW formed by mixing these two water types will be nearly identical to that of the subsurface limb (Figure A-3). This occurs because the higher $[\text{NO}_3^-]$ of the subsurface limb leads to a proportionally larger effect of the subsurface limb on the new $\delta^{15}\text{NO}_3$, while both water masses equally affect the new $[\text{NO}_3^-]$. Because the DIC content of surface waters is only ~10% lower than that of intermediate waters, the surface and intermediate limbs contribute to the new $\delta^{13}\text{C}$ in essentially the same proportion as they contribute to the new DIC concentration.

There are other processes which also work against the generation of a deep sea utilization/generation gradient for N isotopes. Water column denitrification is probably the most important of these. Denitrification preferentially consumes isotopically light nitrate, causing isotopic enrichment of the residual nitrate pool (Figure A-4, Cline and Kaplan, 1975). Because water column denitrification only occurs in low O_2 environments, it is restricted to poorly ventilated, high- $[\text{NO}_3^-]$ water masses. This isotopic enrichment in "old", nutrient-rich waters works against the nitrate utilization/regeneration trend (Figure A-1), which would tend to cause isotopic depletion in these waters. Indeed, the effect of denitrification dominates at intermediate depths, resulting in $\delta^{15}\text{NO}_3$ values of ~6‰ in the central Pacific, with values reaching as high as 20‰ in the eastern Pacific (Brandes, 1996; Cline and Kaplan, 1975; Liu and Kaplan, 1989). This isotopic enrichment also appears to penetrate into the deep Pacific, causing the $\delta^{15}\text{NO}_3$ of the deep central Pacific to be $\leq 0.5\text{‰}$ higher than North Atlantic Deep Water (Figure A-1).

A second possible process, which has not yet been fully demonstrated, is the addition of isotopically light nitrate to the low- $[\text{NO}_3^-]$ upper water column by N fixation in low latitude surface waters. Liu et al. (1996) observe low $\delta^{15}\text{NO}_3$ in the thermocline of the western Pacific and hypothesize that N fixation is its source. Initial results from the Sargasso Sea suggest that Atlantic thermocline waters are isotopically depleted as well (M. Altabet, unpublished). Brandes et al. (submitted) also recognize a contribution of low $\delta^{15}\text{NO}_3$ nitrate to the shallow subsurface waters of the eastern tropical North Pacific and the Arabian Sea (Figure A-4). Thus, it appears that low $\delta^{15}\text{NO}_3$ nitrate is generated in those environments that would otherwise be isotopically enriched by the fractionation associated with nitrate utilization, providing yet another mechanism to counteract the utilization/remineralization trend for $\delta^{15}\text{NO}_3$.

References

- Altabet, M.A., 1988. Variations in nitrogen isotopic composition between sinking and suspended particles: implications for nitrogen cycling and particle transformation in the open ocean. *Deep-Sea Research*, 35: 535-554.
- Bainbridge, A.E., 1975. GEOSECS Atlantic Ocean: final hydrographic data report, GEOSECS Operations Group/National Science Foundation, Washington D.C.
- Bainbridge, A.E., 1976. GEOSECS Pacific Ocean: final hydrographic data report, GEOSECS Operations Group/National Science Foundation, Washington D.C.
- Brandes, J.A.G., 1996. Isotopic effects of denitrification in the marine environment, Ph.D. Thesis, University of Washington, Department of Oceanography, 186 pp.
- Brandes, J.A.G., Devol, A.H., Yoshinari, T., Jayakumar, D.A., Naqvi, S.W.A., submitted, Isotopic composition of nitrate in the central Arabian Sea and eastern tropical North Pacific: a tracer for mixing and nitrogen cycles. *Limnology and Oceanography*.
- Broecker, W.S. and Peng, T.-H., 1982. *Tracers in the Sea*. Lamont-Doherty Geological Observatory, Columbia University, Palisades, NY, 690 pp.
- Cline, J.D. and Kaplan, I.R., 1975. Isotopic fractionation of dissolved nitrate during denitrification in the eastern tropical North Pacific Ocean. *Marine Chemistry*, 3: 271-299.
- Gruber, N. and Sarmiento, J.L., 1997. Global patterns of marine nitrogen fixation and denitrification. *Global Biogeochemical Cycles*, 11: 235-266.
- Kroopnick, P.M., 1985. The distribution of ^{13}C of TCO_2 in the world oceans. *Deep-Sea Research*, 32: 57-84.
- Liu, K.-K. and Kaplan, I.R., 1989. The eastern tropical Pacific as a source of ^{15}N -enriched nitrate in seawater off southern California. *Limnology and Oceanography*, 34: 820-830.
- Liu, K.K., Su, M.J., Hsueh, C.R. and Gong, G.C., 1996. The nitrogen isotopic composition of nitrate in the Kuroshio Water northeast of Taiwan: evidence for nitrogen fixation as a source of isotopically light nitrate. *Marine Chemistry*, 54: 273-292.
- Lynch-Stieglitz, J. and Fairbanks, R.G., 1994. A conservative tracer for glacial ocean circulation from carbon isotope and palaeonutrient measurements in benthic foraminifera. *Nature*, 369: 308-310.
- Montoya, J.P. and McCarthy, J.J., 1995. Isotopic fractionation during nitrate uptake by marine phytoplankton grown in continuous culture. *Journal of Plankton Research*, 17(3): 439-464.
- Ostlund, H.G., Craig, H., Broecker, W.S. and Spencer, D., 1987. GEOSECS Atlantic, Pacific, and Indian Ocean Expeditions -- Volume 7, Shorebased Data and Graphics. National Science Foundation, Washington, D.C.

Rau, G.H., Takahashi, T. and Des Marais, D.J., 1989. Latitudinal variations in plankton $\delta^{13}\text{C}$: implications for CO_2 and productivity in past oceans. *Nature*, 341: 516-518.

Redfield, A.C., Ketchum, B.H. and Richards, F.A., 1963. The Influence of Organisms on the Composition of Seawater. In: M.N. Hill (Editor), *The Sea*, Vol. 2. Interscience, New York, pp. 26-77.

Sackett, W.M., Eckelmann, W.R., Bender, M.L. and Bé, A.W.H., 1965. Temperature dependence of carbon isotope composition in marine plankton and sediments. *Science*, 148: 235-237.

Stuiver, M., Quay, P.D. and Ostlund, H.G., 1983. Abyssal water carbon-14 and age of the world oceans. *Science*, 219: 849-851.

Waser, N.A.D., Turpin, D.H., Harrison, P.J., Nielsen, B. and Calvert, S.E., 1997. Nitrogen isotope fractionation during the uptake and assimilation of nitrate, nitrite, and urea by a marine diatom. *Limnology and Oceanography*, in press.

Table A-1: $\delta^{15}\text{NO}_3$ along the path of deep circulation

Region	depth (m)	latitude (°N)	longitude (°E)	[NO ₃] (μM)	$\delta^{15}\text{NO}_3$ (‰ vs. air)
<u>Arctic Ocean</u>					
	1000	82	32	15.6	4.67
	1450	"	"	16.0	4.67
	2575	"	"	16.2	4.73
<u>Greenland Sea</u>					
	1000	?	?	18.8	4.53
	1500	?	?	18.5	4.48
<u>western North Atlantic (slope water just off Georges Bank)</u>					
	1000	?	?	17.9	4.43
	1500	?	?	17.5	4.61
<u>western North Atlantic</u>					
	3005	39	-70	17.8	4.73
	3009	39	-70	17.3	4.73
<u>Sargasso Sea</u>					
	1500	?	?	18.8	4.66
<u>Southern Ocean, east Indian sector</u>					
	1114	-53	115	31.2	4.84
	1316	"	"	30.9	4.68
	1624	"	"	31.0	4.83
	2024	"	"	31.6	4.75
	2423	"	"	32.2	4.66
	2836	"	"	32.7	4.63
	3254	"	"	32.7	4.49
	3667	"	"	32.8	4.62
	4006	"	"	32.9	4.69
<u>Southern Ocean, east Pacific sector</u>					
	2000	-61	-90	32.9	4.65
	2500	"	"	33.1	4.59
	3500	"	"	33.3	4.60
	4500	"	"	33.3	4.68
<u>central Pacific, 900 km northeast of Hawaii</u>					
	2500	~30	~150	39.6	5.20
	3000	"	"	38.4	5.10
	3500	"	"	37.8	4.90
	4000	"	"	37.1	4.70

Figure A-1

A plot of the expected variations in deep water $\delta^{15}\text{NO}_3$ and $\delta^{13}\text{C}_{\text{dic}}$ as a function of $[\text{NO}_3^-]$ if the isotopic variations of nitrate and DIC vary with their respective concentrations according to Rayleigh fractionation kinetics, with relevant data overlain. Rayleigh fractionation trends are not strictly correct for a system which includes remineralization; however, they show the approximate trends which would be expected due to uptake and remineralization in a simple system. The $\delta^{15}\text{NO}_3$ curve was generated assuming (1) a fractionation factor of 5‰, and (2) a $\delta^{15}\text{NO}_3$ of 4.7‰ at 35 μM (see Chapter 4). The $\delta^{13}\text{C}_{\text{dic}}$ curve was generated assuming (1) a fractionation factor of -25‰, (2) a $\delta^{13}\text{C}_{\text{dic}}$ of 0‰ at 2200 μM DIC, and (3) DIC/nitrate uptake and regeneration ratios according to Redfield et al. (1963). The $\delta^{15}\text{NO}_3$ data taken from the Atlantic and Southern Ocean are from below 1 km, while the Pacific data are from below 2.5 km, to avoid the depth range of intense denitrification. There is no significant nitrogen isotopic difference between the North Atlantic and the Southern Ocean deep waters, while central Pacific deep water is $\leq 0.5\text{‰}$ enriched relative to these. The $\delta^{13}\text{C}$ data are from taken from GEOSECS stations 1, 30, and 53 in the Atlantic, station 438 from the Indian, and station 343 from the Pacific (Ostlund et al., 1987). The $\delta^{13}\text{C}$ data in the North Atlantic fall slightly below the trend, probably for three reasons: (1) a higher effective temperature of atmospheric exchange compared to the Antarctic (Lynch-Stieglitz and Fairbanks, 1994), (2) the penetration of fossil fuel $\delta^{13}\text{C}$ into the Atlantic (Kroopnick, 1985), and (3) the assumption of 25‰ for the CO_2 uptake fractionation factor, which may be $\sim 10\%$ too high on a global basis.

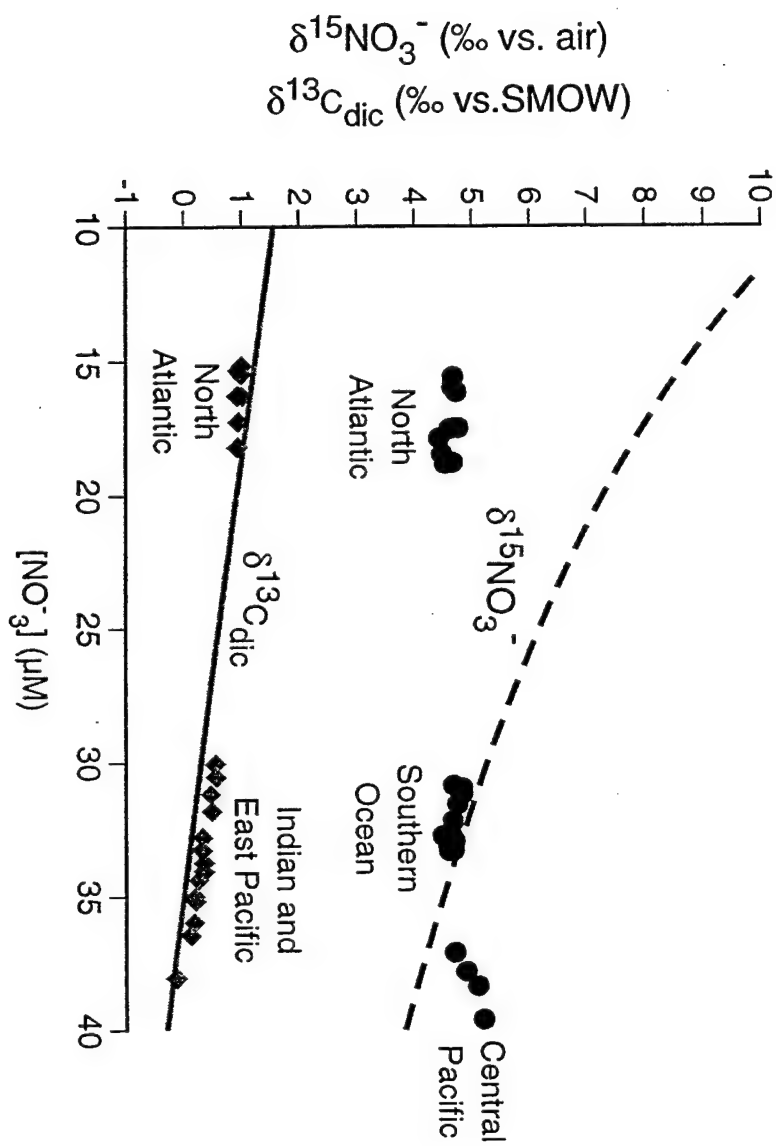


Figure A-2

A cartoon of NADW formation, pointing out that deep water forms from both surface and intermediate-depth water masses, which are mixed at the site of deep water formation. Assigned nitrate concentrations are rough estimates; choosing values for the upper two limbs is complicated by the fact that the mixing of these two water masses occurs once these water masses reach high northern latitudes, prior to deep water formation.

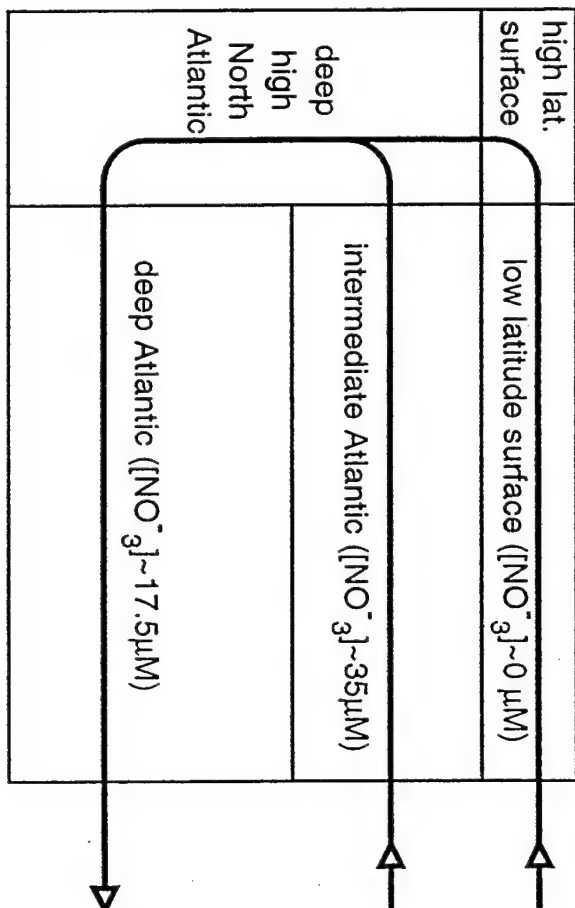


Figure A-3

Expected deviations from Rayleigh fraction behavior because of mixing, for both $\delta^{15}\text{NO}_3$ and $\delta^{13}\text{C}_{\text{dic}}$. The Rayleigh fractionation trends are shown in thick lines. The thin lines show the composition of water parcels generated by mixing $35\ \mu\text{M}\ [\text{NO}_3^-]$ (and its equivalent in DIC, assumed to be $2200\ \mu\text{M}$) with water parcels who have had nitrate and DIC depleted to different degrees by phytoplankton production. For nitrate, three curves are shown, showing mixing of the high $[\text{NO}_3^-]$ water with water depleted to 0.2 , 1 , and $5\ \mu\text{M}\ [\text{NO}_3^-]$. For DIC, only the first is shown, as the mixing trends are indistinguishable from the Rayleigh fractionation trend. The vertical shaded bar indicates the approximate $[\text{NO}_3^-]$ of newly formed NADW ($17.5\ \mu\text{M}$). If NADW is generated by $1/1$ mixing of $35\ \mu\text{M}\ [\text{NO}_3^-]$ intermediate depth water and $0.2\ \mu\text{M}\ [\text{NO}_3^-]$ surface water, even with the extreme enrichment of the depleted water mass, the resultant water parcel $\delta^{15}\text{NO}_3$ will be indistinguishable from that of the original intermediate water parcel. The assumptions are the same as in Figure A-1.

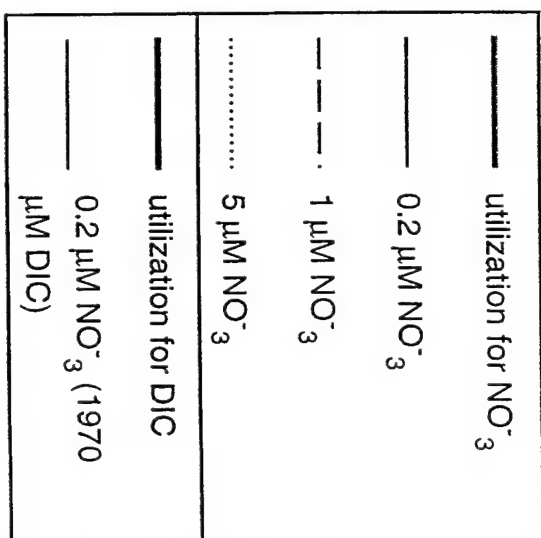
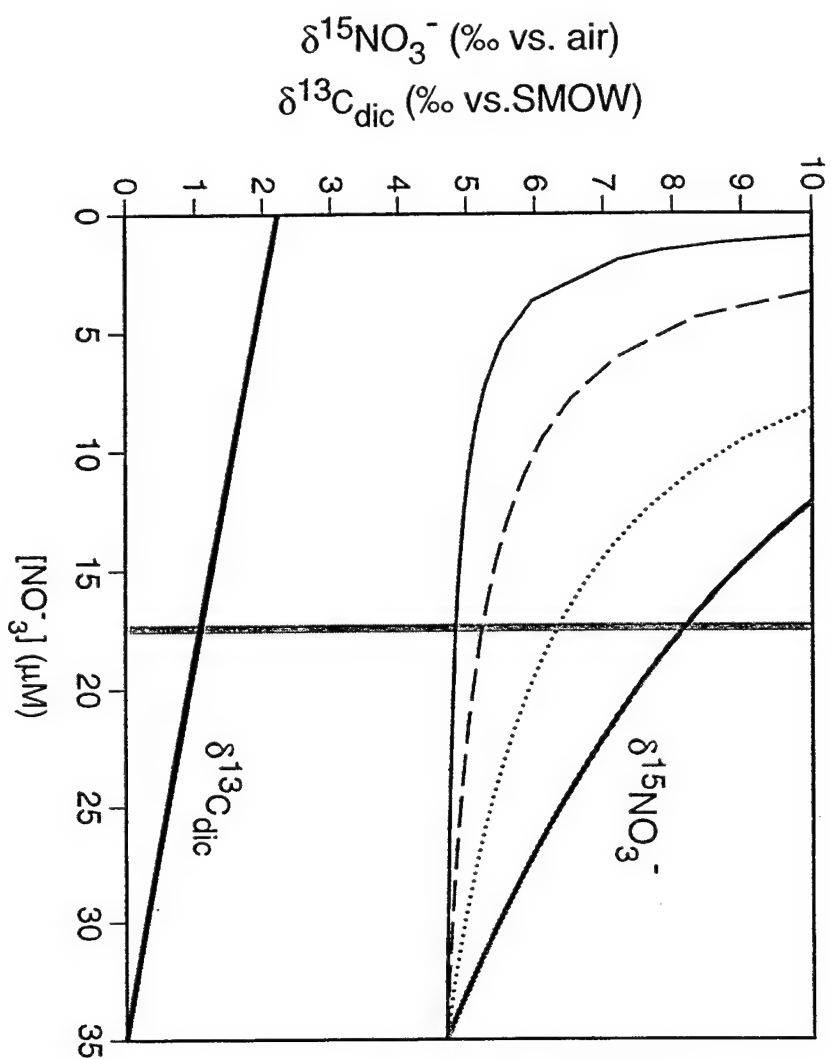
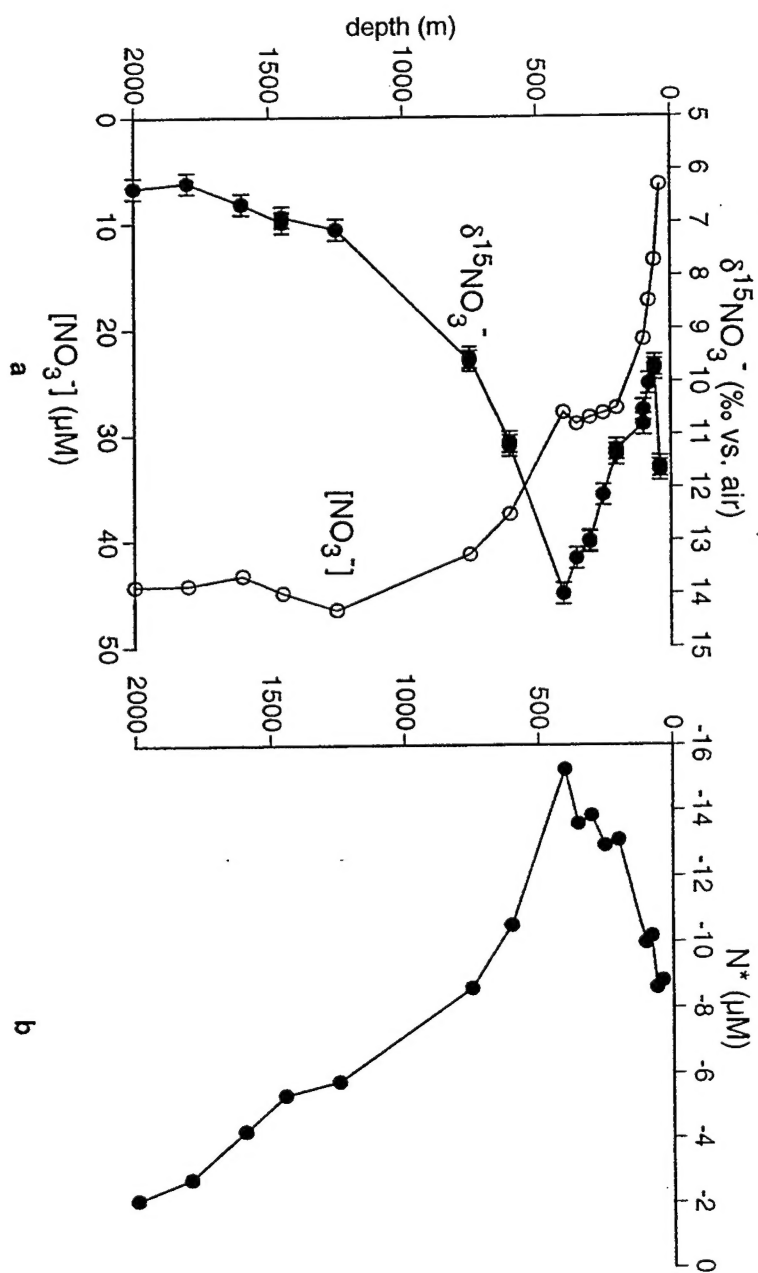


Figure A-4

(a) $\delta^{15}\text{NO}_3$ and $[\text{NO}_3^-]$ profiles from a station in the Guaymas Basin, Gulf of California.

(b) Isotopic enrichment in the thermocline is associated with strongly negative N^* , a measure of the nitrate deficit based on phosphate data which indicates denitrification in the oxygen minimum zone of the eastern tropical North Pacific ($\text{N}^* = [\text{N} - 16 \cdot \text{P} + 2.9 \mu\text{mol/kg}] \cdot 0.87$, Gruber and Sarmiento, 1997). The lower $\delta^{15}\text{NO}_3$ values above the N^* minimum, which have also been observed in depth profiles from the open eastern tropical North Pacific, have been attributed to the addition of low $\delta^{15}\text{NO}_3$ nitrate from the remineralization of newly fixed N (Brandes et al., submitted). The isotopic enrichment in the shallowest sample probably reflects isotope fractionation during nitrate uptake by phytoplankton.

Guaymas Basin Station A, Gulf of California



DOCUMENT LIBRARY

Distribution List for Technical Report Exchange – February 1996

University of California, San Diego
SIO Library 0175C
9500 Gilman Drive
La Jolla, CA 92093-0175

Hancock Library of Biology & Oceanography
Alan Hancock Laboratory
University of Southern California
University Park
Los Angeles, CA 90089-0371

Gifts & Exchanges
Library
Bedford Institute of Oceanography
P.O. Box 1006
Dartmouth, NS, B2Y 4A2, CANADA

NOAA/EDIS Miami Library Center
4301 Rickenbacker Causeway
Miami, FL 33149

Research Library
U.S. Army Corps of Engineers
Waterways Experiment Station
3909 Halls Ferry Road
Vicksburg, MS 39180-6199

Institute of Geophysics
University of Hawaii
Library Room 252
2525 Correa Road
Honolulu, HI 96822

Marine Resources Information Center
Building E38-320
MIT
Cambridge, MA 02139

Library
Lamont-Doherty Geological Observatory
Columbia University
Palisades, NY 10964

Library
Serials Department
Oregon State University
Corvallis, OR 97331

Pell Marine Science Library
University of Rhode Island
Narragansett Bay Campus
Narragansett, RI 02882

Working Collection
Texas A&M University
Dept. of Oceanography
College Station, TX 77843

Fisheries-Oceanography Library
151 Oceanography Teaching Bldg.
University of Washington
Seattle, WA 98195

Library
R.S.M.A.S.
University of Miami
4600 Rickenbacker Causeway
Miami, FL 33149

Maury Oceanographic Library
Naval Oceanographic Office
Building 1003 South
1002 Balch Blvd.
Stennis Space Center, MS, 39522-5001

Library
Institute of Ocean Sciences
P.O. Box 6000
Sidney, B.C. V8L 4B2
CANADA

National Oceanographic Library
Southampton Oceanography Centre
European Way
Southampton SO14 3ZH
UK

The Librarian
CSIRO Marine Laboratories
G.P.O. Box 1538
Hobart, Tasmania
AUSTRALIA 7001

Library
Proudman Oceanographic Laboratory
Bidston Observatory
Birkenhead
Merseyside L43 7 RA
UNITED KINGDOM

IFREMER
Centre de Brest
Service Documentation - Publications
BP 70 29280 PLOUZANE
FRANCE

REPORT DOCUMENTATION PAGE	1. REPORT NO. MIT/WHOI 97-28	2.	3. Recipient's Accession No.
4. Title and Subtitle The Role of Biological Production in Pleistocene Atmospheric Carbon Dioxide Variations and the Nitrogen Isotope Dynamics of the Southern Ocean			5. Report Date September 1997
7. Author(s) Daniel M. Sigman			6.
9. Performing Organization Name and Address MIT/WHOI Joint Program in Oceanography/Applied Ocean Science & Engineering			8. Performing Organization Rept. No.
			10. Project/Task/Work Unit No. MIT/WHOI 97-28
			11. Contract(C) or Grant(G) No. (C) OCE-9201286 (G)
12. Sponsoring Organization Name and Address National Science Foundations and its Graduate Fellowship Program and the JOI/USSAC Ocean Drilling Graduate Fellowship Program			13. Type of Report & Period Covered Ph.D. Thesis
			14.
15. Supplementary Notes This thesis should be cited as: Daniel M. Sigman, 1997. The Role of Biological Production in Pleistocene Atmospheric Carbon Dioxide Variations and the Nitrogen Isotope Dynamics of the Southern Ocean. Ph.D. Thesis. MIT/WHOI, 97-28.			
16. Abstract (Limit: 200 words) <p>This dissertation contributes to the search for a cause of glacial/interglacial variations in atmospheric carbon dioxide. A modelling exercise demonstrates that the paleoceanographic record of calcite preservation places constraints on hypothesized changes in low latitude biological production, indicating very few mechanisms by which low latitude production could have driven Pleistocene carbon dioxide variations.</p> <p>The use of N isotopes as a paleoceanographic proxy for nitrate utilization in Southern Ocean was investigated. In order to examine the generation of the link between nitrate utilization and N isotopes in the surface ocean, the isotopic composition of nitrate was studied. A new method to measure the isotopic composition of nitrate was developed. Results from the Southern Ocean support the use of N isotopes as a proxy for nitrate utilization in the Antarctic.</p> <p>A study of diatom microfossil-bound N in sediments suggests that this N is native to the diatoms, that it is protected from early diagenesis, and that its isotopic composition varies with that of the sinking flux. Paleoceanographic records of diatom-bound N isotopic composition corroborate the conclusion, previously based on bulk sediment isotopic data, that nitrate utilization was elevated in the glacial Antarctic, representing a major cause of lower glacial atmospheric carbon dioxide levels.</p>			
17. Document Analysis			
a. Descriptors nitrogen stable isotope paleoceanography			
b. Identifiers/Open-Ended Terms			
c. COSATI Field/Group			
18. Availability Statement Approved for publication; distribution unlimited.	19. Security Class (This Report) UNCLASSIFIED		21. No. of Pages 392
	20. Security Class (This Page)		22. Price